



HAL
open science

N-heterocyclic carbenes coated nanocrystals and supracrystals

Xiang Ling

► **To cite this version:**

Xiang Ling. N-heterocyclic carbenes coated nanocrystals and supracrystals. Chemical Physics [physics.chem-ph]. Université Pierre et Marie Curie - Paris VI, 2015. English. NNT : 2015PA066334 . tel-01559825

HAL Id: tel-01559825

<https://theses.hal.science/tel-01559825>

Submitted on 11 Jul 2017

HAL is a multi-disciplinary open access archive for the deposit and dissemination of scientific research documents, whether they are published or not. The documents may come from teaching and research institutions in France or abroad, or from public or private research centers.

L'archive ouverte pluridisciplinaire **HAL**, est destinée au dépôt et à la diffusion de documents scientifiques de niveau recherche, publiés ou non, émanant des établissements d'enseignement et de recherche français ou étrangers, des laboratoires publics ou privés.

THÈSE

DE DOCTORAT DE L'UNIVERSITÉ PIERRE ET MARIE CURIE (PARIS VI)

ECOLE DOCTORALE DE CHIMIE-PHYSIQUE ET CHIMIE ANALYTIQUE DE PARIS
CENTRE

SPÉCIALITÉ «CHIMIE-PHYSIQUE»

présentée par

XIANG LING

pour obtenir le grade de

DOCTEUR DE L'UNIVERSITÉ PIERRE ET MARIE
CURIE

Sujet de la thèse

N-HETEROCYCLIC CARBENES COATED NANOCRYSTALS AND SUPRACRYSTALS

Thèse soutenue le 10 Juillet 2015 devant le jury composé de:

Pr. DIDIER ASTRUC	Rapporteur
Pr. PIERO BAGLIONI	Examineur
Pr. HÉLÈNE GÉRARD	Président du jury
Pr. MIR WAIS HOSSEINI	Rapporteur
Pr. MARIE-PAULE PILENI	Directrice de thèse
Dr. SYLVAIN ROLAND	Examineur

Acknowledgement

Abstract

Nanomaterials have received extraordinary attention owing to their unique properties, strongly associated to their nanoscale dimensions. In particular, noble metal (Au, Ag) nanoparticles (NPs) exhibit particular mechanical, electronic, optical and magnetic properties and present a high potential for developing applications in many domains with important societal impacts. Due to their higher stability by comparison with other metal-based nanoparticles, Au NPs have been extensively investigated for research in nanotechnology. In the last decades, N-Heterocyclic carbenes (NHCs) have emerged as an essential class of neutral ligands in organometallic chemistry. NHCs are characterized by their high synthetic flexibility, their specific geometry, and a very strong metal–C_{carbene} bond in metal complexes. All these properties have been widely studied and exploited for applications in homogeneous catalysis and for the development of biologically active complexes. By comparison, the use of NHCs in nanomaterials remains largely unexplored.

In this work, the potential of NHC ligands in the field of nanomaterials, as coating agents for gold nanocrystals synthesis, stabilization and self-assembly into supracrystals has been explored. First, well-defined silver and gold–NHC complexes with different well-known NHC ligands are investigated for their relevance to generate stable nanocrystals (NCs) under reductive conditions with a good control of nanocrystals size. We demonstrate that both Au and Ag NCs can be formed by reduction of metal-NHC complexes with amine-boranes. The efficiency of the process and the average size and size distribution of the nanocrystals markedly depends on the structure of the NHC ligand. However, we demonstrate in this part that different pathways are involved to generate nanocrystals from Au or Ag precursors, as a specific reaction is observed between Ag-NHCs and thiols leading to the formation of silver thiolates whereas the corresponding Au-NHCs remain unchanged.

In the second part, a new series of NHCs is designed with the aim of forming Au nanocrystals that can self-assemble in 3D organized superstructures (Au supracrystals). We demonstrate that the average size of the Au NCs and their ability to self-assemble are dependent on the length, orientation, and number of alkyl chains on the NHCs. Here, the geometry of both the C_{carbene}–Au bond and N–C bonds, induce a specific orientation of the alkyl chains in the NHCs, different from that of alkylthiols. We assume that the long alkyl chains may be both involved in Au surface covering and in stabilizing interdigitation

N-Heterocyclic Carbenes coated Nanocrystals and Supracrystals

phenomena. This is demonstrated by the edge-edge distances in the supracrystals suggesting that the supracrystals are stabilized by interdigitation of neighboring nanocrystals alkyl chains, whose terminal part must point outward with the appropriate geometry.

Finally, NHC-based Au nanocrystals are submitted to oxygen plasma to evaluate their stability under oxidative conditions to compare with the typical used thiol-based Au nanocrystals. The impact of the synthetic method to produce Au nanocrystals and the size of Au nanocrystals are studied. The stability of the dodecanethiol-stabilized Au nanocrystals is independent of the sizes of Au nanocrystals and the methods to generate the nanocrystals. We demonstrate that NHC-coated Au Nanocrystals are considerably more resistant to oxygen plasma than thiol-coated Au Nanocrystals. In addition, we demonstrate that NHC ligands bound to the surface of Au NCs are significantly more resistant to oxygen-induced transformations than dodecanethiol.

Résumé

Les nanomatériaux ont beaucoup captivé l'attention pour leur propriétés uniques, fortement associées à leurs dimensions nanoscopiques. En particulier, les nanoparticules (NP) à base de métaux nobles (Au, Ag) présentent des propriétés mécaniques, électroniques, optiques et magnétiques particulières intéressantes pour le développement d'applications dans de nombreux domaines à fort impact sociétal. En raison de leur stabilité élevée par rapport aux autres nano-particules métalliques, les nanoparticules d'or ont été abondamment explorées pour les nanotechnologies. Ces dernières décennies, les NHC ont émergé en tant que classe essentielle de ligands neutres en chimie organométallique. Les NHC sont caractérisés par leur flexibilité synthétique élevée, leur géométrie spécifique, et une liaison métal-C_{carbène} très forte dans les complexes métalliques. Toutes ces propriétés ont été largement étudiées et exploitées pour les applications en catalyse homogène et pour le développement de complexes biologiquement actifs. Par comparaison, l'utilisation des NHC dans les matériaux reste largement peu explorée.

Dans ce travail, le potentiel de ligands NHC dans le domaine des nanomatériaux, comme des agents de revêtement pour le produit nanocristaux de synthèse de l'or (et l'argent), la produit de stabilisation et de l'auto-assemblage dans supracrystals ont été explorés. Tout d'abord, des complexes d'argent et d'or-NHC qui sont bien définies avec différents ligands qui sont connus comme le NHC, sont étudiés pour leur pertinence afin de générer des stable nanocristaux (NCs) dans des conditions réductrices avec un bon contrôle de la taille des nanocristaux. Nous démontrons que le Au et le Ag NCs peuvent tous être formés par la réduction des complexes métal-NHC avec les amine-boranes. L'efficacité du procédé, la taille moyenne et la taille de la répartition des nanocristaux dépendent fortement de la structure du ligand NHC. Cependant, nous démontrons dans cette partie que les différentes voies sont impliqués à générer des nanocristaux par Au ou Ag précurseurs, comme une spécifique réaction observée entre Ag-NHC et thiols conduisant à la formation de thiolates argent alors que le Au-NHC correspondant reste inchangé.

Dans la deuxième partie, une nouvelle série de NHCs est conçu avec des Au nanocristaux dans le but d'être capable de se auto-assembler en 3D superstructures organisés (Au supracrystals). Nous démontrons que la taille moyenne de l' Au CN et leur capacité à auto-assembler sont dépend de la longueur, de l'orientation, et du nombre des chaînes alkyle

sur le NHC. Ici, la géométrie à la fois de la liaison $C_{\text{carbene}}-\text{Au}$ et des liaisons $\text{N}-\text{C}$, s'induisent une spécifique orientation des chaînes alkyles dans le NHC, qui est différente de celle des alkylthiols. Nous supposons que les longues chaînes alkyle peuvent être à la fois impliqués dans Au revêtement et dans les phénomènes stabilisés de interdigitation. Cela est démontré par les distances de bord pointe dans les supracrystals suggérant où les supracrystals sont stabilisées par l'interdigitation des chaînes alkyle des nanocristaux voisins, dont la partie terminale doit pointer vers l'extérieur avec la géométrie appropriée.

Enfin, les Au nanocristaux en basant de NHC sont soumis à un plasma d'oxygène pour évaluer leur stabilité sous les conditions oxydantes à comparer avec les nanocristaux de Au qui sont typiquement utilisés. L'impact de la méthode de synthèse pour produire les nanocristaux de Au et la taille de Au nanocristaux sont étudiés. La stabilité des DDT stabilisée de Au nanocristaux est indépendante de la taille des nanocristaux de Au et des méthodes pour générer les nanocristaux. Nous démontrons que NHC revêtu de Au nanocristaux sont considérablement plus résistants à plasma d'oxygène que les thiols revêtu de Au nanocristaux. De plus, nous avons démontré que les ligands NHC liés à la surface de Au NCs sont nettement plus résistants à l'oxygène induite par des transformations que le dodécane-thiol.

Abbreviations

NHC	N-Heterocyclic Carbene
2/3D	two/three dimension or dimensional
Au	gold
bcc	body centered cubic lattice
fcc	face centered cubic lattice
FFT	fast fourier transform
HRSEM	high resolution scanning electron microscopy
hcp	hexagonal close packed lattice
MPC	monolayer protected cluster
NP	nanoparticle
NC	nanocrystal
SAM	self-assembled monolayer
SAXRD	small angle X-ray diffraction
SEM	Scanning electron microscopy
TEM	transmission electron microscope/microscopy
NMR	nuclear magnetic resonance
HRMS	high resolution mass spectrometry
Mp	melting point
XPS	X-ray photoelectron spectroscopy

Contents

Acknowledgement	I
Abstract	III
Résumé	V
Abbreviations	VII
Contents	IX
Introduction	1
Chapter 1 State of the Art	5
1.1 History of gold nanoparticles	5
1.2 Ligands for gold nanoparticles synthesis	5
1.2.1 Citrate ligands	6
1.2.2 Sulfur ligands	8
1.2.3 Phosphine ligands.....	10
1.2.4 Oxygen-based ligands	11
1.2.5 Nitrogen-based ligands.....	12
1.2.6 Carbon-based ligands	13
1.2.7 Polymer ligands.....	14
1.2.8 Dendrimer ligands	16
1.3 N-Heterocyclic Carbenes in surface chemistry	17
1.3.1 Properties of N-Heterocyclic Carbenes.....	17
1.3.2 N-Heterocyclic Carbenes as ligands for SAMs stabilization and functionalization.....	19
1.3.3 N-Heterocyclic Carbenes as ligand for nanoparticles synthesis and stabilization	19
1.4 Stability of gold nanoparticles.....	24
1.4.1 Thermal stability.....	25
1.4.2 Chemical stability.....	26
1.5 Self-assembly of nanoparticles.....	27
1.5.1 Self-assembly in two dimensions	28
1.5.2 Self-assembly in three dimensions	29
Chapter 2 Well-defined Ag and Au-NHC complexes as precursors for one-phase	

synthesis of nanocrystals.....	31
2.1 Abstract.....	31
2.2 Nanocrystals: Why Do Silver and Gold N-Heterocyclic Carbene Precursors Behave Differently?	31
Chapter 3 Supracrystals of N-Heterocyclic Carbene-coated Au Nanocrystals	49
3.1 Abstract.....	49
3.2 Supracrystals of N-heterocyclic Carbene-coated Au Nanocrystals.....	49
Chapter 4 Superior Oxygen Stability of N-Heterocyclic Carbene-coated Au Nanocrystals - Comparison with Thiol-coated Analogues.....	74
4.1 Abstract.....	74
4.2 Articles: Superior Oxygen Stability of N-Heterocyclic Carbene-coated Au Nanocrystals – Comparison with Thiol-coated Analogues	74
Conclusions and Perspectives.....	97
Appendices	99
Bibliography	117
List of publications.....	131

Introduction

Nanomaterials are nanostructured materials, characterized by a well-defined grain size or a dimension from several nanometers to several dozen nanometers (< 50 nm). Nanomaterials can be classified according to the dimensionality resulting from the spatial arrangement of the structural elements. Zero-dimensional (0D) nanomaterials include nanoclusters, *nanocrystals* (NCs) or nanodispersions (isolated nanoparticles). Nanofibers, nanorods, and other nanotubular materials with fibers, are one-dimensional (1D) materials. Two-dimensional (2D) materials are films (coatings) with nanometer thickness. Three-dimensional (3D) materials result from the 3D arrangement of nanometer-sized grains to give 3D superlattices or supracrystals. The chemical and physical properties of a material are mainly due to the atoms at the surface. A decrease in the dimension (size) and dimensionality of nanomaterials induces a decrease in the number of bulk atoms and an increase of the number of atoms at the surface. Therefore, changes in the dimensionality and size induce marked changes in the material properties. In addition, nanoentities of same dimension(alitie)s and made of the same structural units, can adopt a range of different well-defined shapes (cylinders, rods, disks, cubes, etc.) that can also be associated with different properties. Furthermore, at very low sizes, quantic properties erase. Supracrystals that present a new level or hierarchy, may also be associated with unique collective properties, different from those of discrete NCs.

The concept of using nanocrystals as building blocks for the generation of larger colloidal structures has attracted great attention from scientists. Assemblies of nanocrystals of higher dimensionality are expected to exhibit unique properties resulting from the combination of both single nanocrystals properties and of collective properties resulting from the interactions between proximal NCs, either aligned along one direction (1D), self-ordered in close-packed networks (2D) or in 3D superlattices. Self-assembly is one of the most promising way to drive individual particles into highly ordered superstructures in a controlled way. A major challenge in nanosciences is to develop flexible, efficient and reproducible methods to control the assembly of nanocrystal building blocks. Here again, an important prerequisite is to produce NCs with a narrow size distribution. Simulations showed that a polydispersity exceeding 10 – 12% could impede crystallization (self-assembly). For this reason, thiolate-coated AuNCs that can be obtained as nearly monodisperse NCs, have been identified as model systems. Supracrystals can be obtained by slow evaporation of colloidal solutions of monodisperse NCs in organic solvents. Many fundamental aspects of the phenomena involved in this

process remain to be investigated. Here, the ligand and the solvent likely play an essential role in controlling the formation (crystalline structure and shape) and the different properties of the as-formed supracrystals.

Surface ligands play a very important role for nanoparticles, by controlling their size and shape during synthesis, preventing metal leaching into the surrounding solution, protecting from oxidation or even boosting properties such as the photoluminescent yield of semiconductor nanocrystals or the relaxivity of magnetic nanoparticles. NCs are usually coated with a layer of surfactant dispersed in a carrying solvent. The molecules of surfactant link through various modes of binding including covalent, dative, ionic bonds or physical adsorption to the metallic surface, preventing coalescence, and providing solubility and desired surface properties. During NC growth in solution, the organic surfactants adsorb to the NCs surface, providing a dynamic organic shell (capping layer) that stabilizes the NCs and mediates their growth. So far, a lot of surface ligands have been used for nanoparticles capping, such as citrate ligands, sulfur-based ligands (thiols or thiolates), phosphorus ligands, oxygen-based ligands, nitrogen-based ligands, polymers, dendrimers and surfactant (e.g. cetyltrimethylammonium bromide CTAB). The introduction of a specific capping agent may alter the way in which the final nanocrystal may be driven to adopt a specific shape. It was shown that selective chemisorption of molecular species onto the metal nanoparticle surface can have a profound effect on the shape displayed by a NC and may cause drastic morphological changes. Despite the importance of surface capping in controlling the shape of a nanocrystal, little is known about its explicit roles and the mechanisms are far from being fully elucidated. Surface ligands also act as templates for NCs 3D assembly to form supracrystals. Here, the nature/structure of the ligand (coating agent) and its properties (e.g. grafting density, mode of bonding with the nanocrystal surface, solubility) have a great influence on the ability of the nanocrystals to self-assemble in high-dimensional organized structures. The surface ligands play also an essential role for functionalizing nanoparticles and surfaces. It enables the direct or post-introduction of many different functionalities for various applications. The ability of the ligand to be functionalized and its synthetic flexibility are essential parameters to be considered for the design of future materials, which are particularly important for biomedical applications.

The introduction of new ligands associated with different spatial structures, more flexible synthetic routes, and different binding properties is also of great interest to investigate the self-assembly of NCs to control supracrystals formation as well as their properties. Many fundamental aspects in this field remain to be investigated. This prompted us to explore the

use of *N*-heterocyclic carbene (NHC) ligands which are C–ligands associated with particular electronic and structural properties, for the preparation and stabilization of AuNCs and their self-assembly into 3D superstructures.

Chapter 1

State of the Art

Gold nanoparticles (AuNPs), also called gold colloids, are metal nanoparticles of particular interest. Because of the quantum size effect resulting in specific electronic structures, metal nanoparticles have been considered to have unique physical and chemical properties different from those of the bulk state or atoms.¹⁻³ AuNPs are the most outstanding members of the metal NP groups.^{4,5} They have attracted a lot of attention in many aspects, related to the behavior of individual particles, their assembly of multiple types, their size-related optical, electronic and magnetic properties,⁶⁻⁸ and their applications in catalysis⁹⁻¹⁴ and biology.¹⁵⁻¹⁸

1.1 History of gold nanoparticles

Gold has been used in a variety of forms throughout human history. The extraction of gold could date back to the 5th millennium B.C. near Varna, and reached 10 tons per year in Egypt around 1200-1300 B.C. In ancient time, materials were used in an ecological sense for aesthetic and curative purposes. Colloidal gold, was used to make ruby glass and for coloring ceramics. These applications are still used in recent period. In 1850s, M. Faraday conjectured that gold exists in solution in a “finely divided metallic state”.¹⁹ Thus, the preparation of AuNPs with controlled sizes and shapes has raised increased attention, and a lot of breakthroughs have been made. Firstly, in 1951, Turkevich et al. reported the citrate method.²⁰ Then Frens et al. in 1973 improved this method.²¹ Secondly, Schmid et al. reported a phosphine-stabilized Au₅₅ cluster in 1981. Later in 1993, P. Mulvaney et al. reported the first synthesis of AuNPs stabilized by thiolates. Finally in 1994, Schiffrin et al. reported the Brust-Schiffrin biphasic method for synthesizing AuNPs stabilized by thiols.⁴ The importance of Au in nanotechnology, chiefly stems from its unique stability compared to most other metals under ambient conditions. Hence, AuNPs have been a preferred choice for research in nanotechnological applications.

1.2 Ligands for gold nanoparticles synthesis

AuNPs can be prepared by two different ways: the “top-down” or “bottom-up” strategy.²² The mechanical fragmentation of bulk materials into nano-sized debris is used in the

top-down method. Here, bulk state Au is systematically broken down to generate AuNPs in the corresponding nanoscale dimensions. However, the resulting fragments always have a broad size distribution. The bottom-up method starts from molecular precursors, such as organometallic compounds or salts, which are decomposed to generate individual metal atoms by chemical reduction or thermal/optical excitation. Then, the metals nucleate to form nanoparticles with a much narrower size distribution.²³ In a typical bottom-up system for colloidal nanoparticles preparation, there are four components: the precursor, the reducing agent, surface ligands, and solvents. All these four components, especially surface ligands, play an important role in controlling the size and shape of the nanoparticles. Many kinds of surface ligands have been used in the synthesis of AuNPs, such as trisodium citrate dehydrate, sulfur ligands, phosphorus ligands, oxygen-based ligands, nitrogen-based ligands, carbon-based ligands, polymers, and dendrimers. However, compared with other ligands, carbon-based ligands have rarely been explored.

1.2.1 Citrate ligands

In 1940, Hauser and Lynn proposed the first synthesis of gold nanoparticles by citrate reduction of aqueous gold ions. Then in 1951, this method was studied and promoted by Turkevich et al.²⁰ Addition of a sodium citrate solution quickly to a boiling HAuCl₄ solution was shown to give (**Figure 1**), after a few minutes, a wine-red colloid was obtained with the AuNPs size of 20 ± 1.5 nm. In this procedure, the resulting spherical gold nanoparticles are stabilized electrostatically by surface-bound citrate ions. Since then, AuNPs stabilized by citrate have been the most popular one among AuNPs obtained by reduction of HAuCl₄. In 1973, Frens et al.²¹ modified the Turkevich method by controlling the ratio of trisodium citrate to Au. They obtained different sizes of AuNPs varying from 16 nm to 150 nm. The average particle size and size distribution could be determined accurately from electron micrographs.

Since then, the Turkevich-Frens method to generate citrate-stabilized AuNPs has been continuously studied and optimized. Especially, the mechanism of AuNPs formation in this method has been studied in details recently.²⁴⁻²⁸ Due to Turkevich's report on the presence of a very small percentage of triangular particles in citrate-reduced gold solution, in 2005, M. Sastry et al. reinvestigated the citrate reduction procedure in detail for gold nanotriangle formation.²⁸ They found that the temperature of the reaction is a crucial parameter and that slowing down the reduction rate of gold ions by progressive temperature decrease leads to the

growth of gold nanotriangles. Furthermore, they observed that the presence of halide ions in solution during gold ion reduction critically affects the morphology of the particles. Br⁻ and I⁻ ions distort the morphology and lead to the formation of spherical particles, while Cl⁻ ions promote the formation of gold nanotriangles. In the following year, A. Plech et al. found that a general relation exists between the gold-to-reductant ratio and the final size of the particles.²⁴ They indicated that low gold concentration favors longer time stable AuNPs of smaller sizes, while high gold concentration leads to unstable AuNPs of larger sizes. The limit for the production of long time stable AuNPs is below 2mM. Then in 2007, J. Y. Lee et al. focused on the particle growth process in the citrate reduction and found that the growth process is different from the commonly accepted LaMer nucleation growth model.²⁵ They indicated that small Au particles of about 5 nm in diameter coalesce to form an extensive network of nanowires during the initial stage of the reaction, which fragments into spherical particles later. Subsequently, in the same year, S. Kumar et al.²⁹ developed a model to study the mechanism of the citrate process of synthesis of Au nanoparticles in multiple steps, as follows: reduction of Au³⁺ in solution, disproportionation of Au⁺ to gold atoms and their nucleation, growth by disproportionation on particle surface, and coagulation. The oxidation of citrate forms dicarboxy acetone, which aids nucleation but also decomposes into side products. In 2007, X. Peng et al. studied growth kinetics and temporal size/shape evolution of gold nanocrystals by citrate reduction in detail.²⁷ They found that the solution pH which was controlled by the concentration of sodium citrate influences the size variation and overall reaction mechanism. Based on this result, by varying the pH of the solution, monodispersed AuNPs with an average size ranging from 20-40 nm have been synthesized.³⁰⁻³³ In addition, there are some other improvements of the citrate method which have been done involving reaction temperature adjustment,³⁴ introduction of fluorescent light irradiation,³⁵ and use of high-power ultrasound.³⁶ Because of the modest reducing ability of trisodium citrate, the size of AuNPs stabilized by citrate is always larger than 10 nm. However, in 2010, Puentes et al. obtained smaller sized AuNPs (5.3 nm) with the citrate method by using D₂O as the solvent instead of H₂O.³⁷ This indicated that the presence of deuterium increases the reducing strength of the citrate molecule.

In these cases described above, citrate acts as both stabilizing and reducing agent. The wide use of citrate as stabilizing agent is limited by its weak reducing ability, implying relatively high temperature to prepare AuNPs. To decrease the temperature of the reaction, in 1985, tannic acid was used by Geuze et al. as a reducing agent to assist citrate. They obtained

AuNPs at 60 °C. Then in 1996, M. J. Natan et al. made a significant progress by using NaBH₄ as reducing agent to obtain citrate stabilized AuNPs at room temperature.³⁸ Compared with the AuNPs larger than 10 nm using traditional citrate method, 6 nm AuNPs were obtained by using this method.

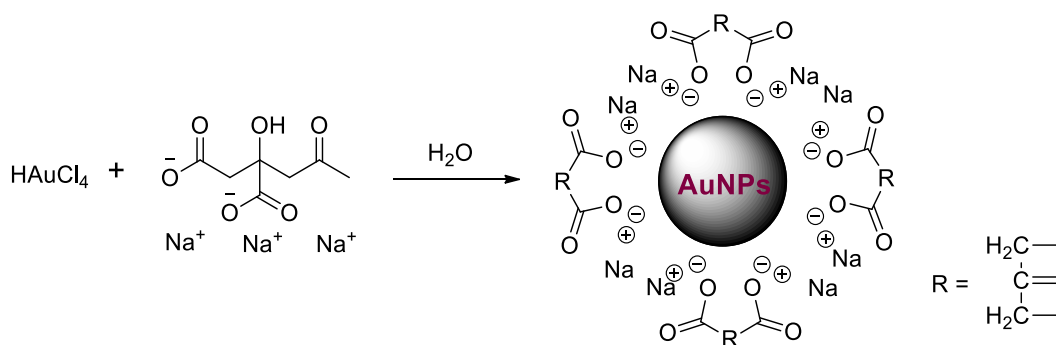


Figure 1. AuNPs synthesis using the Turkevich method

1.2.2 Sulfur ligands

Since 1988, Whiteside et al. have demonstrated that a wide variety of alkanethiols form well-defined monolayers on gold metal surfaces.³⁹ On this basis, then, in 1993 P. Mulvaney et al. firstly reported AuNPs stabilized with alkylthiols through ligand exchange.⁴⁰ They demonstrated that it is possible to use alkylthiols of various chain length to stabilize AuNPs and that the alkylthiol-capped AuNPs can produce ordered two-dimensional arrays. Combining the two-phase approach introduced by Faraday¹⁹ and the technique of ion extraction and alkanethiols self-assembly to well-defined monolayers on gold metal surfaces, in 1994, M. Brust et al. described the first one-step method for preparation of thiol-stabilized AuNPs.⁴¹ They used two-phase (water-toluene) reduction of AuCl₄⁻ by sodium borohydride in the presence of alkanethiol to obtain gold particles. The average sizes of AuNPs bearing a surface coating of thiol are in the range 1-3 nm, and the shapes of AuNPs are cuboctahedral and icosahedral. The particles prepared in this way are more stable. They can be precipitated, redissolved, and isolated without any apparent change in their properties. Based on the results obtained by Brust et al., it was indicated that larger thiol/gold molar ratio give smaller average core sizes, and fast reductant addition and cooled solutions produced smaller, more monodisperse particles due to the nucleation-growth-passivation process.⁴² Quenching the reaction immediately following reduction or the use of sterically bulky ligands leads to form higher portion of very small NPs.⁴³ Following the Brust-schiffirin two-phase method, in 1995, R. W. Murray et al. obtained AuNPs stabilized by alkanethiols of various chain length (8, 12,

and 16 carbons).⁴⁴ In 1998, R. W. Murray et al. succeeded to adjust the mean size of dodecanethiolate-stabilized AuNPs varying between 1.5 and 5.2 nm by tuning the Au/dodecanethiol ratio and the temperature and the rate of reductant addition.⁴² To functionalize AuNPs, in 1998, S.D. Evans et al. used small aromatic thiol molecules HS-C₆H₄-X, where X=OH, COOH, NH₂, and CH₃.⁴⁵ They found that the physical properties of the surfactant-coated nanoparticles, both in solution and as thin films, were dependent upon the nature of the functional group X. Particularly, the particles bearing COOH and NH₂ functionalities were prone to significant aggregation through hydrogen bond formation. T. R. Lee et al. also reported AuNPs functionalized with *n*-octadecyl disulfide in the same year.⁴⁶ Very recently, the Brust-Schiffrin method is still much in use for the preparation and application on the thiolate stabilized AuNPs,⁴⁷⁻⁵⁰ such as stable gold nanoparticles stabilized by different mono- and bi-functional arenethiols, namely, benzylthiol and 1,4-benzenedimethanethiol, as reported by Floriana Vitale et al. in 2011.⁴⁷

In 1995, M. Brust et al. extended the two-phase method. They reported the synthesis of stable gold nanoparticles stabilized by a bifunctional thiol ligand, which was *p*-mercaptophenol. The *p*-mercaptophenol AuNPs were synthesized in a one-phase system in order to avoid the phase-transfer agent TAOB, which introduced impurities. Then, in the following years, the formation of these functional thiol stabilized AuNPs by using the one-phase method has attracted a lot of attention. In 2002, M. Brust et al. synthesized water-soluble gold nanoparticles of two different size ranges (2-4 and 5-8 nm) by using monohydroxy (1-mercaptoundec-11-yl) tetraethylene glycol as a novel capping agent, which do not aggregate or lose stability under any conditions likely to be encountered in bio-analytical applications.⁵¹ For the biological interest, nonspecific binding between nanoparticles and biomolecules is one of the major barriers. Based on the results obtained by M. Brust, X. Huang et al. reported in 2004 a new approach to eliminate nonspecific interactions between nanoparticles and biological molecules by shielding the nanoparticle with a monolayer of ethylene glycol, as di-, tri-, and tetra(ethylene glycol)-protected gold nanoparticles.⁵² Very recently, AuNPs stabilized by thiolates were synthesized by this one-phase method, such as ω -functionalized alkylthiolates,⁵³ bifunctional alkanethiolates,^{54,55} arenethiolates⁵⁶⁻⁵⁸ and other functional thiolates (**Figure 2**) from the corresponding thiols.⁵⁹

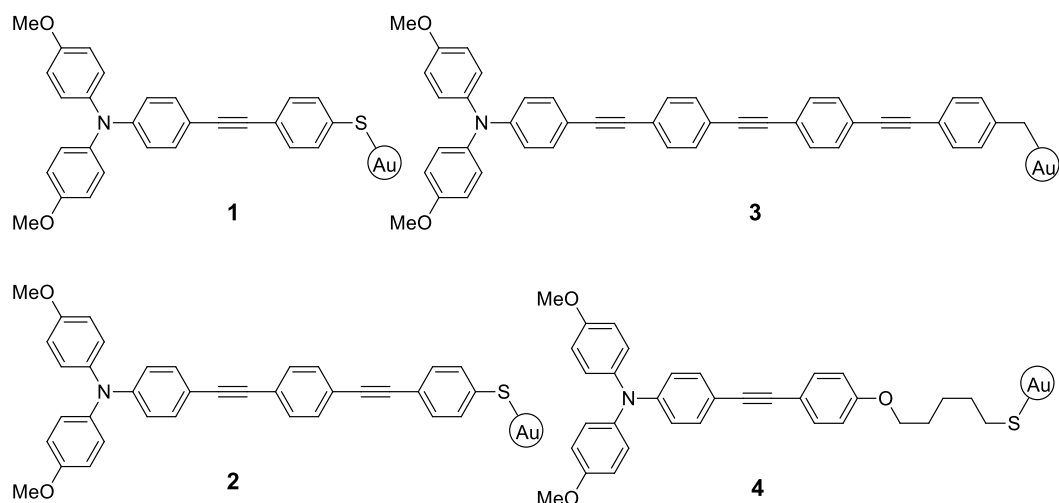


Figure 2. Functional thiolate stabilized AuNPs

In addition, a lot of other kinds of sulfur ligands have also been used in the synthesis of AuNPs by the Brust-Schiffrin two-phase method or ligand exchange, such as disulfides,⁶⁰⁻⁶⁴ xanthates,⁶⁵ thioacetates,⁶⁶ dithiocarbamates,⁶⁷ trithiolates,⁶⁸ benzenesulfonate (SDBS),⁶⁹ and thiocetic acid.⁷⁰ The binding strength of these ligands bind with the AuNP cores of AuNPs might be weaker than that of the thiolates.^{71,72} However, sulfur ligands-stabilized AuNPs as the bioprobes have a broad used in DNA or protein detection and other bio-applications because of the abundance of sulfur ligand in DNA or other proteins.⁶⁰

However, the AuNPs prepared by Brust-Schiffrin two-phase method and its variations typically have a continuous and broad size distribution in the range of 1-3 nm. In 2006, G. D. Stucky et al. reported a facile one-step one-phase method to prepare AuNPs stabilized by dodecanethiol with a narrow distribution on gram scale.⁷³ They used Au(PPh₃)Cl as precursor through reduction by amine-borane complexes in the presence of dodecanethiol to obtain the AuNPs. The sizes of AuNPs were in the range of 2-8 nm, which were controlled by varying the reaction temperature and solvent. This method was revised in the SUPRANANO group.⁷⁴ The AuNPs in the range of 5-8 nm were prepared in toluene at 100 °C by varying the concentration of the capping agent dodecanethiol and the reducing agent t-butylamine-borane complex.

1.2.3 Phosphine ligands

Phosphine stabilized gold nanoparticles have been found broad application in imaging, catalysis, nanoscale electronic development, sensing and drug delivery platforms.⁷⁵⁻⁷⁷ They also can act as starting materials for the production of nanoparticles functionalized by other

ligands, such as thiols, amines and other phosphines, as they can readily be replaced through ligand exchange reactions.^{78,79} In 1981, G. Schmid et al. prepared Au₅₅ cluster stabilized by triphenyl-phosphine with a narrow size distribution (1.4 ± 0.4 nm). This Au cluster defined as [Au₅₅(PPh₃)₁₂Cl₆], was characterized by X-ray crystal structure. It also firstly showed the properties of a quantum-dot particle.⁸⁰ In recent years, some papers reported improvements of the Schmid method. Particularly, in 2009, J. S. Shumaker-Parry et al. reported a simple method to synthesize triphenylphosphine stabilized AuNPs varying from 1.2 to 2.8 nm (**Figure 3**).⁷⁶ The size of the triphenylphosphine stabilized AuNPs can be tuned by controlling the temperature during synthesis. These AuNPs display size-dependent optical properties. Triphenylphosphine (PPh₃) is commonly assigned a passive role as a chemical placeholder, electron balancing species, or surfactant. However, in 2011, J. W. Hudgens et al. reported the first direct evidence that PPh₃ is a proactive etching agent that promotes the formation of specific closed-shell cluster sizes.⁸¹ In 2009 and 2010, A. Katz et al. reported the synthesis and characterization of gold nanoparticles stabilized by calix[6]arene- and calix[4]arene-phosphine ligand.⁸² The calixarene-bound particles were demonstrated to have high level of accessibility for binding molecules to gold nanoparticles, which could be used for catalysis.

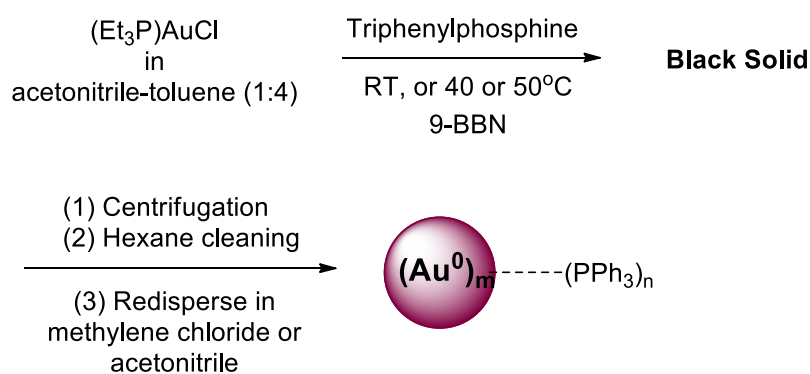


Figure 3. Synthetic pathway for TPP-stabilized AuNPs.

1.2.4 Oxygen-based ligands

The oxygen-based ligands, which are able to stabilize AuNPs, contain carbonyl, alcohol, and phenol groups. Among the oxygen-based ligands, phenol and carboxyl derivatives are well-known as stabilizing ligands for AuNPs. In 2007, C. R. Raj et al. synthesized gold nanoflowers by a one-pot synthesis using N-2-hydroxyethylpiperazine-N-2-ethanesulphonic acid (HEPES, **Figure 4**) as a reducing/stabilizing agent.⁸³ In 2009, E. Wang et al. reported the

N-Heterocyclic Carbenes coated nanocrystals and supracrystals

first example of using folic acid (**Figure 4**), to directly reduce a gold precursor salt (HAuCl_4) for producing AuNPs, that also acts as a stabilizing agent for AuNPs via a carboxyl group.⁸⁴ The folic acid stabilized AuNPs could be taken up by HeLa cells, which are known to overexpress folic acid receptors. Thus, it is useful for nanomedicinal applications. Later on in the same year, Y. Xia et al. described a protocol that generates Au icosahedra in high yields by simply mixing aqueous solutions of HAuCl_4 and N-vinyl pyrrolidone.⁸⁵ Their mechanistic study indicated that water plays an important role in this synthesis. As a nucleophile, it induces the generation of an alcohol-based Au^{I} intermediate by attacking the gold-vinyl complex. Then this intermediate undergoes a redox reaction in which Au^{I} is reduced to Au^{0} , leading to the formation of a carboxylic acid stabilized Au icosahedra of about 18 nm in size.

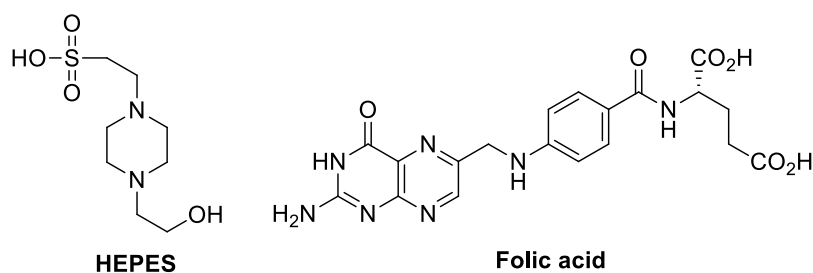


Figure 4. The structures of HEPES and folic acid

1.2.5 Nitrogen-based ligands

Nitrogen-containing derivatives are a particularly important and attractive class of reducing and stabilizing agents because of their universal presence in biological and environmental systems. Both neutral and cationic nitrogen-based ligands act as stabilizing agents for AuNPs. In the case of neutral ligands, 4-(*N,N*-dimethylamino) pyridine (DMAP) is the most common ligand for AuNPs. It can be used to cap AuNPs as well as acting as an organic-aqueous transfer agent. DMAP is proposed to bind to AuNPs as a zwitterion through the nitrogen atom of the pyridine bearing a negative charge. In 2001, F. Caruso et al. firstly reported DMAP stabilized AuNPs.⁸⁶ Their preparation method relies on the exchange of tetraoctylammonium bromide (TOAB) with DMAP, followed by spontaneous phase transfer of the DMAP stabilized nanoparticles from toluene to water. DMAP, acting as a zwitterion, is shown to be an excellent ligand for stabilizing water-soluble gold nanoparticles. Then in 2005, R. B. Lennox et al. prepared water-soluble, positively charged, and fairly monodispersed (6.2 ± 0.9 nm) DMAP-protected gold nanoparticles.⁸⁷ They found that the DMAP-stabilized AuNPs are soluble and stable over a wide pH range (5.0 – 12.8), and that excess of DMAP is necessary for both the preparation and the stability of the DMAP-stabilized AuNPs. In 2011, H. Lange

et al. synthesized stable 4-methoxypyridine colloidal solutions of AuNPs by a transfer method.⁸⁸ They demonstrated by SERS measurements and periodic DFT calculations that 4-methoxypyridine adsorbs in a flat binding mode on the gold surface via π -electrons of the pyridine ring, a mode of binding different from that of DMAP and unsubstituted pyridines. Except for DMAP, other kinds of neutral amine ligands have been used. In 2001, M. Sastry et al. synthesized octadecylamine (ODA)-stabilized AuNPs by phase transfer method.⁸⁹ The fatty amine-capped AuNPs are very stable, could be easily precipitated out of solution and redissolved in different organic solvents without significant change in the particle size. Later in 2003, M. Sastry et al. also reported AuNPs stabilized by laurylamine (LAM).⁹⁰ They found that the surface bound alkylamine monolayer may be place-exchanged with other amine derivatives in a manner similar to that observed for alkanethiols. In 2008, C. R. Suri et al. reported the synthesis and capping of stable gold nanoparticles by using glutamic acid which is an amino acid.⁹¹ They showed that the AuNPs can be prepared in water directly by complexation with the glutamic acid molecules. The amino acid acted as a reducing agent, as well as a stabilizing agent where the amino groups were bound to AuNPs.

In the case of cationic ligands, tetraalkylammonium salts have a variety of applications in the synthesis and stabilization of nanoparticles, especially tetraoctylammonium bromide (TOAB) and cetyltrimethylammonium bromide (CTAB). The TOAB stabilized AuNPs are prepared by the Brust-Schiffrin two-phase method without adding other stabilizing agents, which are colloidally stable for two weeks without further functionalization.⁴¹ The TOAB protected AuNPs are starting materials for the production of nanoparticles functionalized by other ligands, especially neutral amine ligands which have been described above. In the case of CTAB, in 2001, M. A. El-Sayed et al. synthesized CTAB stabilized AuNPs with an average size of 12 nm.⁹² Then in 2003, E. Wang et al. reported the first synthesis of CTAB-capped gold nanoparticles in a two-phase liquid/liquid system using CTAB as a phase-transfer catalyst and a stabilizer simultaneously.⁹³ They demonstrated that the alkyl chains in the 3D surface-bound CTAB monolayer on a gold cluster are in the disorder liquid state.

1.2.6 Carbon-based ligands

Carbon-based ligands, which have been used to stabilize AuNPs, mainly through carbon-gold covalent bonds. So far, carbon-based ligands stabilizing AuNPs have contained aryl or alkyne groups. However, more recently, neutral N-Heterocyclic Carbenes have been introduced (see section 1.3). In the case of aryl ligands, the synthesis of AuNPs involves

attachment of aryl radicals to perform or grow AuNPs. The aryl radicals are produced by reduction of diazonium salts. In 2006, F. Mirkhalaf et al. synthesized 4-decylbenzene-protected AuNPs with a size of 8.1 nm.⁹⁴ The corresponding diazonium derivative of the capping ligand decylbenzene were prepared and reduced together with HAuCl₄ by aqueous NaBH₄ to generate AuNPs stabilized by decylbenzene. The AuNPs protected by decylbenzene are very stable due to the strong metal-ligand covalent bond. In the case of terminal alkynes ligands, terminal alkynes have become a new type of protective ligand of Au clusters / nanoparticles in recent years.⁹⁵⁻¹⁰⁰ In 2007, C. B. Gorman et al. synthesized dodecyne-capped AuNPs with a two size ranges (4.5 and 2.6 nm) which were made in the presence of dodecyne by reducing HAuCl₄ in toluene/water containing 6 mM dodecyne. It was concluded that terminal acetylenes form self-assembled monolayers on gold substrates and nanoparticles that are relatively densely packed and stable. In 2011, T. Tsukuda et al. reported the first synthesis of phenylacetylene-protected Au clusters by using a biphasic ligand exchange of preformed polyvinylpyrrolidone-stabilized Au clusters (diameter < 2 nm).⁹⁶ Then in the following year, they also succeeded in synthesizing a magic cluster, Au₅₄(phenylacetylene)₂₆ selectively by reacting polymer-stabilized Au clusters (1.2 nm) with excess phenylacetylene in chloroform.⁹⁷ To investigate the fundamental information about the interfacial structures between the terminal alkynes and Au clusters and their formation process, gold clusters protected by terminal alkynes (1-octyne, phenylacetylene and 9-ethynyl-phenanthrene) were prepared by T. Tsukuda et al. through the ligand exchange of small Au clusters stabilized by polyvinylpyrrolidone.⁹⁸ The binding motif of these alkynes on Au clusters was investigated using various spectroscopic methods. It was revealed that the terminal hydrogen is lost during the ligand exchange and that the C≡C bond of the alkynyl group is weakened upon attachment to the Au clusters. Also, EXAFS analysis suggests that the alkynyl carbon is bound to bridge and/or hollow sites of the Au cluster surfaces.

1.2.7 Polymer ligands

In general, polymer ligands have large molecular weights, and easily fold up to form 3-dimensional network structures. Polymer ligands which contain functional groups such as NH₂, SH and CN at the end or in the middle of polymers, can stabilize Au nanoparticles and prevent them from aggregating. Using polymers as stabilizing agents can enhance long-term stability of AuNPs and adjust the solubility and amphiphilicity of AuNPs. They also can tailor the properties of AuNPs.¹⁰¹ Various polymers have been used to stabilize AuNPs from

aggregation via either physisorption or chemisorption on Au nano-cores. Among these polymers, most of polymers used to protect AuNPs through chemisorption contain sulfur groups which possess strong affinities to gold. The synthesis routes which have widely been studied toward polymer stabilized AuNPs through covalent binding include the “grafting to” and “grafting from” techniques.

In 1998, R. W. Murray et al. reported the synthesis of poly(ethylene glycol)-functionalized gold nanoparticles (PEG-Au) using a “grafting to” method.¹⁰² In 2004, R. B. Lennox et al. prepared AuNPs stabilized by thiol-terminated polystyrene (PS) ligands.¹⁰³ The polymer ligands were found to form dense brushes on the faceted gold nanoparticle surfaces. In 2005, D. J. Pine et al. synthesized PS- and poly(vinyl pyridine) (PVP)-coated gold particles by standard reduction of HAuCl_4 in THF or two phase toluene/water utilizing thiol-terminated PS and PVP stabilizing ligands, respectively.¹⁰⁴ H. Tenhu et al. have for the first time successfully prepared amphiphilic gold nanoparticles grafted with a mixture of hydrophilic poly(N-isopropylacrylamide (PNIPAM) and hydrophobic PS chains by using the “grafting-to” technique in a homogeneous THF phase.¹⁰⁵ N. Higashi et al. described the preparation of polypeptide (poly(γ -benzyl-L-glutamate)) monolayer-covered gold nanoparticles (PBLG(n)SS–Au).¹⁰⁶ Two types of PBLG(n)SS having a PBLG segment length of $n = 20$ and 50 were synthesized and successfully attached to the gold nanoparticle surface using the Brust–Schifferin method. M. Brust et al. reported a single-step method which leads to near monodisperse gold nanoparticles stabilized by a water-soluble alkyl thioether end-functionalized poly(methacrylic acid) in the 1-4 nm size range.¹⁰⁷ The size of AuNPs is controlled precisely by the ratio of polymer to Au, and the particles are readily available in both aqueous and nonaqueous solutions. In 2006, J. F. Gohy et al. reported on the formation of quite monodisperse AuNPs of improved stability against aggregation, prepared by using poly(ethylene glycol)-block-poly(ϵ -caprolactone) (PEG-b-PCL) five-arm star block copolymers.¹⁰⁸ Those AuNPs were templated by the PEG core of the star block copolymers, and their stability was directly related to the length of the PCL chains acting as stabilizing groups against aggregation. In 2008, L. Pasquato et al. succeeded in synthesizing the first example of water-soluble gold nanoparticles protected by a monolayer of fluorinated amphiphilic thiols (MPC-F8-PEG).¹⁰⁹ The solubility properties of the nanoparticles in connection with the intrinsic features of perfluorinated amphiphiles opens the way to possible applications in the medical field such as antioxidant carriers. In 2011, some other kinds of polymers were used for stabilizing AuNPs, such as poly(ethylenimine) (PEI) with amine

groups,^{23,110} thioether-functionalized polymer ligands (DDT-PVAc and PTMP-PVAc),¹¹⁰ ionic polymers,¹¹¹ and *O*-ethyl-*s*-(1-methoxycarbonyl)ethyl dithiocarbonate functionalized poly(*N*-vinyl caprolactam) (PVCL) (**Figure 5**).¹¹² However, some polymers such as PS and PAAPHA not only act as stabilizing agents but also as reducing agents. Therefore, AuNPs were formed without any additional reducing agents. But these AuNPs formed by such weak reducing agent were much larger than those using additional stronger reducing agents such as NaBH₄.

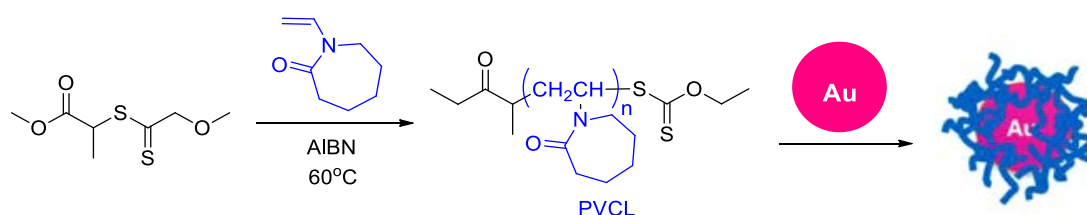


Figure 5. Synthesis of PVCL and coating of AuNPs

1.2.8 Dendrimer ligands

Dendrimers are macromolecules with a regular and highly branched three-dimensional architecture and a well-defined chemical structure.¹¹³ The way of dendrimers to stabilize nanoparticles is through adsorption on the coordinately unsaturated surface atoms or by incorporating the particles into their interior pores. Various dendrimer molecules have been used to stabilize gold nanoparticles. Among these, polyamidoamine (PAMAM) dendrimers are the most frequent one. In 1998, K. Esumi et al. prepared Au colloids by reduction of HAuCl₄ with UV irradiation in the presence of dendrimers, where PAMAM dendrimers with surface amino groups for generations 0-5 have been used. It was demonstrated that the average sizes decreased while the concentration of surface amino group of dendrimers increased. In 1999, R. M. Crooks et al. reported the first example of dendrimer-encapsulated AuNPs in the 2-3 nm size range using PAMAM dendrimers as stabilizing agent.¹¹⁴ AuNPs were prepared by in situ reduction of HAuCl₄ in the presence of PAMAM. The dendrimers stabilize the colloids by sorbing to their exterior. Solutions of these materials are stable for periods of weeks. The average size of dendrimer-stabilized AuNPs depends on the dendrimer-to-Au ratio and dendrimer generation.¹¹⁵⁻¹¹⁷ When the generation of the dendrimers increases, particle growth would be prevented by threedimensional structure of the dendrimer, resulting in a smaller particle size. PAMAM dendrimers, can easily be modified on their terminal groups, so that many derivatives of PAMAM dendrimers containing sulfur, nitrogen,

phosphorous and oxygen functional groups have been synthesized. In 1999, R. M. Crooks et al. reported the synthesis of fourth-generation PAMAM dendrimers possessing terminal thiol groups.¹¹⁸ Thiol-modified dendrimers acted as efficient stabilizers for Au nanoparticles. Then in 2005, gold–silver binary nanoparticles, which feed atomic ratios of gold to silver were 3:1, 1:1, and 1:3, were prepared by K. Esumi et al.¹¹⁹ These particles were stabilized by amine-terminated (generation (G) 3.0 and 5.0) and carboxyl-terminated (G 3.5 and 5.5) PAMAM dendrimers in water. In 2010, F. Mazzei et al. synthesized bifunctional hydroxyl/thiol-functionalized fourth-generation of PAMAM dendrimer-encapsulated Au nanoparticle. In 2011, J. Ji et al. prepared phosphorylcholine (PC)-functionalized PAMAM dendrimers and used it as both reducing and stabilizing agents for synthesis of highly stable and reactive gold nanoparticles.¹²⁰ The obtained AuNPs were shown to be spherical, with particle diameters ranging from 5 to 12 nm. The sizes and growth kinetics of AuNPs could be tuned by changing the pH and the initial molar ratio of dendrimers to gold as indicated by transmission electron microscopy (TEM) and UV–Vis data.

There are other kinds of dendrimers which have been used to stabilize AuNPs, such as polyphenylene dendrimers¹²¹, poly(benzyl ether) alcohol dendrons¹²², 4-pyridone-based dendrons¹²³, thiophene dendrimers¹²⁴, thioether dendrimers¹²⁵, L-Lysine-based dendrimers¹¹⁶, citric acid-based dendrimers¹²⁶, and PEGylated dendrimers^{127,128}.

1.3 N-Heterocyclic Carbenes in surface chemistry

1.3.1 Properties of N-Heterocyclic Carbenes

N-Heterocyclic Carbenes (NHCs) are singlet carbenes, in which the divalent carbonic center is directly connected to at least one nitrogen atom within the heterocycle.^{129,130} The most common subclasses of NHCs are shown in **Figure 6**. In the early 1960s, Wanzlick et al. originally reported their existence and proposed a practical way to generate them. This early finding paved the way to their use as ligands in organometallic chemistry. However, the original chemists' perception of nucleophilic carbenes as elusive odd laboratory curiosities changed only in 1988, as Bertrand et al. reported the first stable (phosphine)(silyl)carbene. Arduengo et al. in 1991¹³¹ reported the isolation and full characterization of the stable, free NHC 1,3-di(adamantly)imidazole-2-ylidene (IAd), obtained by deprotonation of its imidazolium precursor.

N-Heterocyclic Carbenes coated nanocrystals and supracrystals

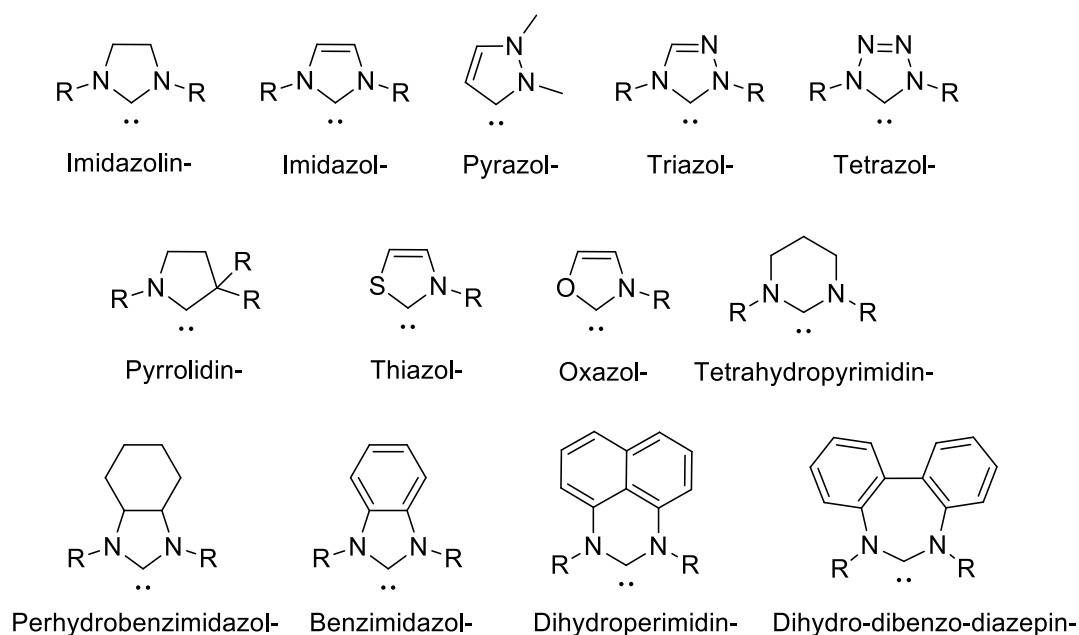


Figure 6. Structures of the most common NHC subclasses

N-heterocyclic carbenes are electron-rich nucleophilic species in which carbene center benefits from the stabilization associated with both the σ -electron withdrawing and π -electron donating character of the nitrogen centers. Because of their strong σ -electron donating properties, NHC ligands form stronger bonds with metal centers than most classical ligands such as phosphines, thus giving transition metal complexes that are generally resistant to decomposition and can be used as precatalysts without an excess of ligand.¹³²⁻¹³⁴ A better steric protection of the active site within the inner metal coordination sphere gives a further advantage in catalysis, as the exocyclic nitrogen substituents of the NHC shield the metal center in a fence- or fan-like fashion, more efficiently than a tertiary phosphine. These beneficial features make NHCs to become firstly an essential class of ligands in organometallic chemistry,¹³⁵ as evidenced by numerous applications ranging from homogeneous catalysis to material and medical sciences,¹³⁶⁻¹⁴⁰ and secondly, an excellent nucleophilic organocatalyst.^{141,142} For the same reason, and because of NHCs exhibiting a particular geometry associated with a flexible structure allowing fine-tuning of their steric properties, NHCs are expected to be highly promising ligands for the development of functionalized materials. Furthermore, the strength of the Au–NHC bond in metal complexes is estimated to be 90 kJ mol^{-1} higher than the corresponding Au–phosphine bond and double that of the sulfide-metal bond.¹⁴³

1.3.2 N-Heterocyclic Carbenes as ligands for SAMs stabilization and functionalization

NHC-based self-assembled monolayers (SAMs) on Au surfaces were recently reported as well as their high stability in various conditions and their relevance for modifying Au surfaces properties by chemical post-functionalization.¹⁴⁴ The bond strength in NHC–Au surfaces was estimated at 150 KJ.mol^{-1} , 25 KJ.mol^{-1} higher than the thiolate–Au bond.

More recently, NHC ligands have been rarely been explored for stabilizing or modifying nanoparticles. So far, three general methods have been employed to generate structurally defined NHC-stabilized metal NPs, involving: (i) a ligand exchange approach by using free NHCs to replaced thioethers on the surface of metal-NPs,¹⁴⁴⁻¹⁴⁷ (ii) the selective reduction of the corresponding metal-NHC complexes,¹⁴⁸⁻¹⁵² and (iii) the reduction of metal salts and the deprotonation of imidazolium salts.¹⁵³

1.3.3 N-Heterocyclic Carbenes as ligand for nanoparticles synthesis and stabilization

a) Ligand exchange by using free NHCs to replace thioethers

The first example of structurally defined NHC stabilized metal NPs was reported by V. Chechik et al. in 2009.¹⁴⁵ They have prepared NHC-coated Au and Pd nanoparticles by ligand exchange. Bis-tert-butylimidazol-2-ylidene was synthesized by the deprotonation of the corresponding imidazolium salt by KO^tBu. This ligand was then reacted with the Au nanoparticles protected by thioethers and Pd nanoparticles coated with trioctylphosphine to get the corresponding NHC-coated Au and Pd nanoparticles (**Figure 7**). However, these nanoparticles have as limited stability in solution. A spontaneous irreversible aggregation of nanoparticles was observed along with the release of NHC-metal complexes. These observations suggest that NHC-coated nanoparticles might leach mononuclear NHC-metal species in catalytic process.

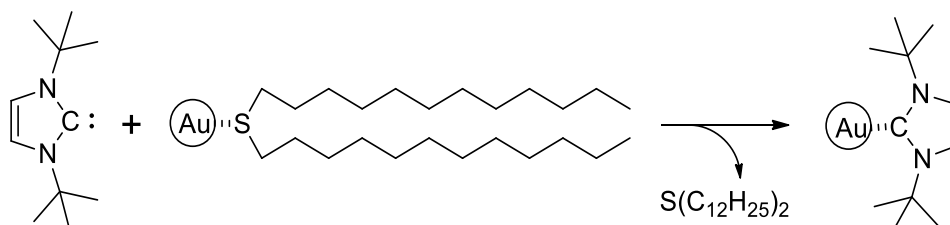


Figure 7. Synthesis of NHC-protected Au Nanoparticles through ligand exchange

As a matter of fact, it was found that the stability of NHC-coated NPs obtained by ligand

exchange reactions is surprisingly low, despite the formation of strong NHC-metal bonds. Therefore, in a recent study by F. Glorius et al. in 2014,¹⁴⁶ they report a novel class of NHC ligands bearing long alkyl chains at their backbone, which allow for the first time the synthesis of stable NHC-modified NPs via a ligand exchange approach. They chose small N-methyl substituents NHC with long aliphatic chains at positions 4 and 5 of the heterocycle to react with PdNPs with weak thioether ligands as the leaving group to generate NHC coated PdNPs (**Figure 8**). Furthermore, they demonstrate that the modification by NHCs influences the activity and selectivity of PdNPs in the hydrogenations of olefins. S. Richeter et al. investigated the mostly the reactivity of benzimidazol-2-ylidene ligands towards AuNPs. They showed how the reaction between these ligands and the Au surface leads to the formation of structurally well-defined Au (I) complexes.

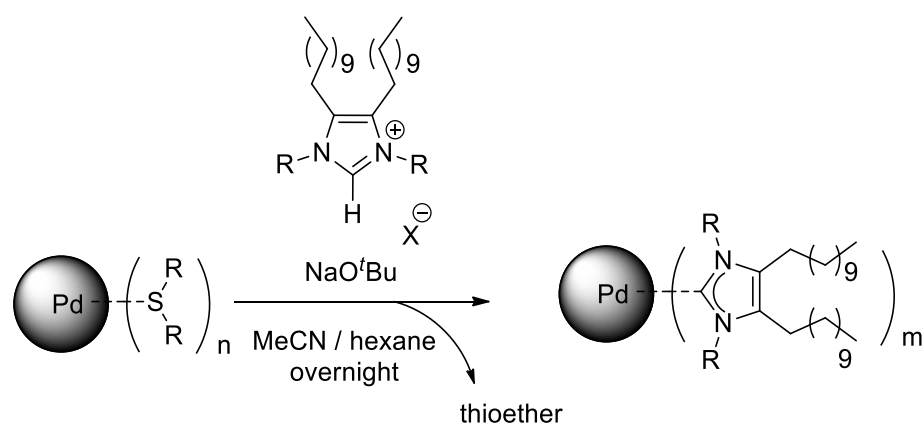


Figure 8. Ligand exchange reaction on thioether stabilized Pd-NP with NHCs. Cite the source from ref. 146. Copyright from 2014 ACS publishing group.

b) Selective reduction of metal-NHC complexes

As we described above, Stucky's group reported a facile one-step one-phase synthetic route to achieve a variety of noble-metallic NPs by reduction of metal salts or organometallic precursors.⁷³ Therefore, the use of organometallic complexes bearing organic ligands makes it possible, by changing the ability of the ligands to give electrons to the metal center and the bulkiness of the ligand or reducing agent, to tune kinetics of metal reduction which in turn enables control of nanocrystal size.

T. D. Tilley et al.¹⁴⁸ reported the first example of a facile, one-phase synthesis of AuNPs coated with NHC ligands based on reduction of single source NHC-AuCl complexes (**Figure 9**). They found that the nature of the substituent on the NHC ligand allows for the control of NP size, with NPs of more or less 2 nm in diameter being obtained with bulky and rigid

isopropyl substituents on the NHC ligand, while 6-7 nm NPs are formed with flexible, long linear alkyl chains on the NHC. The self-assembly of AuNPs coated by NHCs into thin 3D superlattices, made of three NHCs layers, without the requirement of a post-treatment procedure for narrowing the size distribution has been described in Tilley's paper.

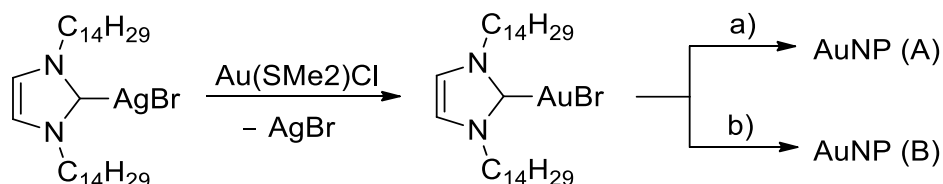


Figure 9. Synthesis of complex and its reduction with (a) KBEt₃H, THF and (b) 9-BBN, Et₂O (9-BBN = 9-borabicyclo [3.3.1]nonane)

Ultrasmall gold nanoparticles (Au UNPs) ranging in size from 1 to 2 nm represent a unique class of nanomaterials due their specific ultrasmall size-related optical, magnetic, electronic and chemical properties. Au UNPs require a compact ligand or polymer shell for their stabilization. M. Monge et al.¹⁵² developed an organometallic approach to synthesis of Au UNPs stabilized with the C₁₈H₃₇-NHC ligand by the solvent free thermolysis of [RMIM] [Au(C₆F₅)₂] or [Au(C₆F₅)-(RNHC)] (with R = C₁₈H₃₇-), by controlling the reactivity of pentafluorophenyl ligands as deprotonating or reductive elimination agents (**Figure 10**). Pentafluorophenyl Au^I complexes are synthesized from the corresponding ionic and neutral precursors. The presence of long alkyl chain imidazolium or carbene species in the complexes makes them to behave as isotropic liquids at moderate temperatures. NMR spectroscopy both in solution and in the solid state confirms the mechanism of formation and the surface state of the Au UNPs.

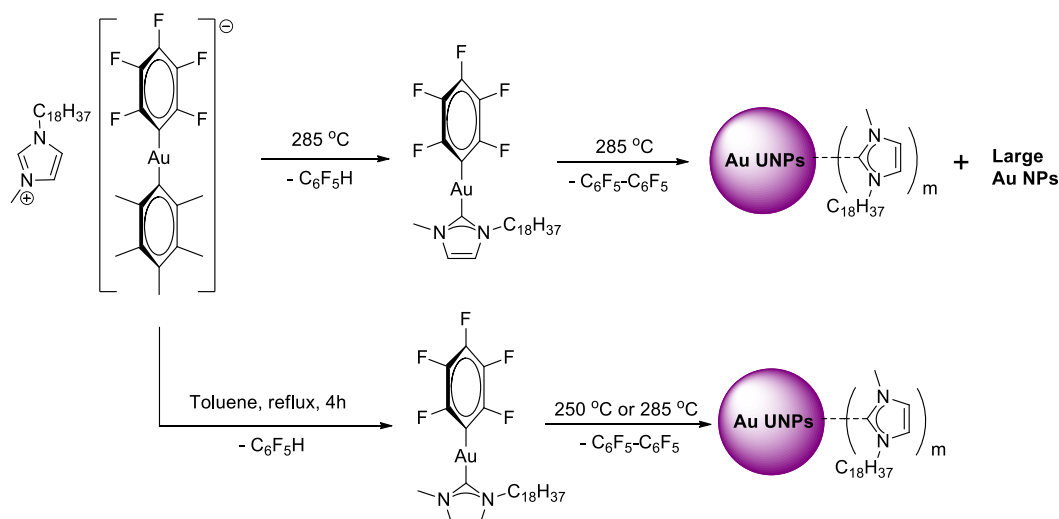


Figure 10. Synthesis of organometallic precursors [RMIM] [Au(C₆F₅)₂] or [Au(C₆F₅)-(RNHC)] (with R = C₁₈H₃₇-) and Au UNPs

Because of the NHC strong binding ability to metal ions, NHC-incorporated conducting polymers would have strong interaction with metal nanoparticles, furnishing well-dispersed polymer-nanoparticle hybrids. C. Song et al.¹⁵⁴ reported the synthesis of conducting polymer/Au nanoparticle hybrids based on bithiophene-functionalized NHC-Au (I) complexes (**Figure 11**). The NHC was incorporated into the polythiophene derivative to increase polymer-nanoparticle interactions. They demonstrated that the NHC played an important role in furnishing well-dispersed NHC-CP/AuNPs hybrids.



Figure 11. Schematic representation of NHC-CP / AuNPs. Cite the source from ref 145.

Copyright from 2014 ACS publishing group.

Controlling the synthesis of stable metal nanoparticle in water is a current challenge in nanochemistry. In 2014, B. Chaudret et al.¹⁵¹ presented the first example of highly stable water-soluble platinum nanoparticles stabilized by hydrophilic NHCs (**Figure 12**). They use sulfonated NHC ligands to stabilize platinum nanoparticles in water, under air, for an

indefinite time period. The particles were prepared by thermal decomposition of a preformed molecular Pt complex containing the NHC ligand and were then purified by dialysis. Solution NMR spectroscopy studies, including diffusion measurements, revealed that the high stability and solubility of these MNPs in water was a consequence of the strong and insert coordination of the hydrophilic NHC ligand to Pt surface.

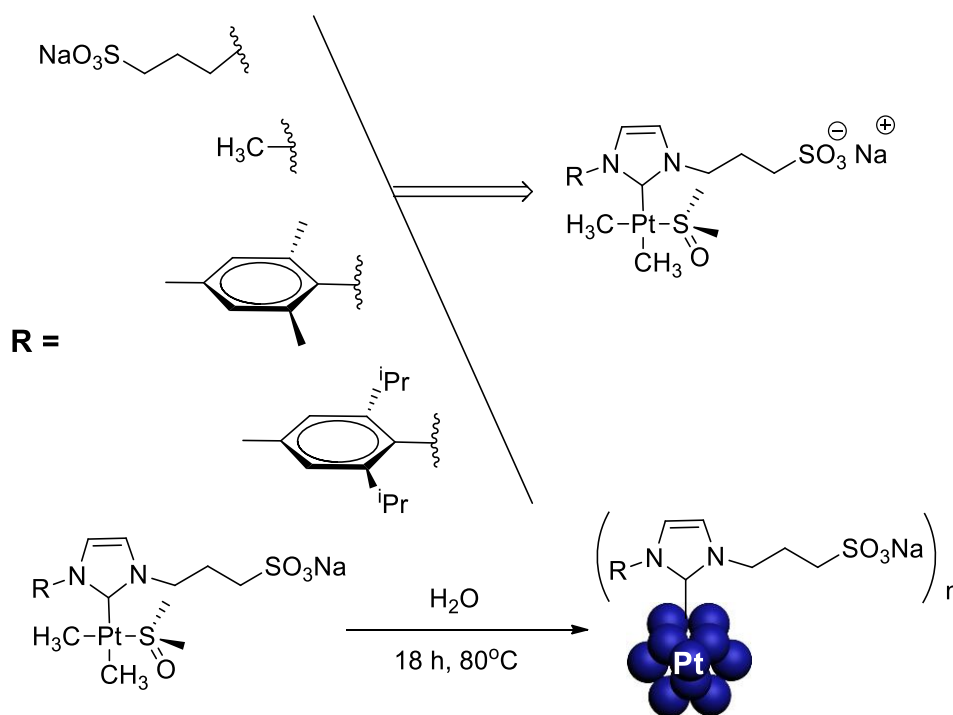


Figure 12. Synthesis of PtNPs from Pt complexes

c) Reduction of metal salts in the presence of NHCs or imidazolium salts

In 2010, F. Glorius et al. report the formation of Pd NPs on magnetite (Fe₃O₄) and subsequent surface modification of the resulting bimetallic NPs by chiral, enantiomerically pure NHCs which are generated from the corresponding NHC salts by deprotonation.¹⁵⁵ Based on the method of using NHCs to synthesize gold NPs, B. Chaudret et al. presented the use of NHC ligands, namely *N,N*-di(*tert*-butyl)imidazole-2-ylidene (ItBu) and 1,3-bis(2,6-diisopropylphenyl)imidazole-2-ylidene (IPr) to stabilize ruthenium nanoparticles. NHC binding was controlled by the substituents on the nitrogen atoms (**Figure 13**).¹⁴⁹ Ruthenium nanoparticles were synthesized by decomposition of (1,5-cyclooctadiene)(1,3,5-cyclooctatriene)ruthenium(0) [(Ru(cod)(cot))] in pentane at room temperature under 3 bar H₂ in the presence of variable amount of the carbene ligands. Furthermore, by the synthesis of the analogous ligands ¹³C-labeled on the carbene carbon,

N-Heterocyclic Carbenes coated nanocrystals and supracrystals

they presented NMR spectroscopic evidence for NHC binding to nanoparticles, which gives us a way to analyze the NPs coated by NHCs. In a recent study, P. D. Beer et al.,¹⁵³ reported the procedure using chloroaurate (III) imidazolium salts as precursors, involving a one-pot deprotonation / reduction sequence (**Figure 14**). In this method, NHC-coated AuNPs and PdNPs are formed after in situ deprotonation of the azolium salt to generate the NHC ligand, followed by reduction of gold or palladium (AuCl_4^- or PdCl_4^-). This method avoids the isolation and characterization of Au-NHC or Pd-NHC complexes which have frequently been used as precursors for metal-NPs (mentioned below), as well as the formation of the free NHC ligand separately, thus reducing the overall number of steps.

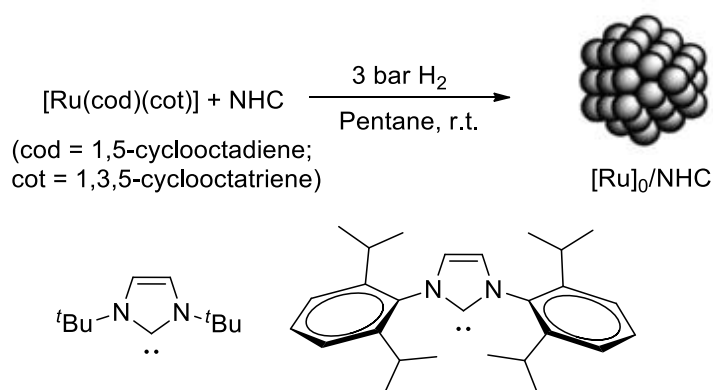


Figure 13. N-heterocyclic carbenes and reaction conditions used for the synthesis of ruthenium nanoparticles

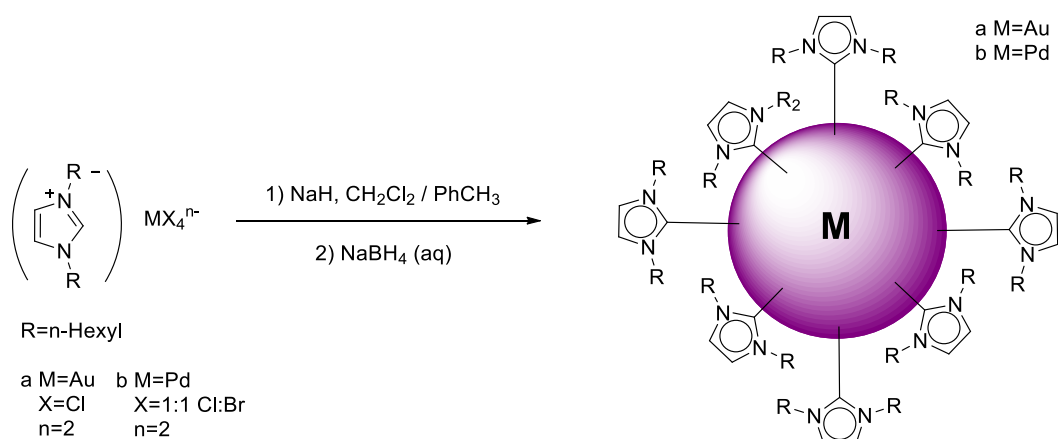


Figure 14. Synthesis of NHC-stabilized NPs from chlorometallate salts

1.4 Stability of gold nanoparticles

Many studies showed that Au^0 nanoparticles do not show detectable cytotoxicity for

relatively short periods of exposure (48–72 h).¹⁵⁶ Thus, it has been generally considered that AuNPs were noncytotoxic, nonimmunogenic, and present biocompatible properties suitable for application in nanoimmunology, nanomedicine, or nanobiotechnology.¹⁵⁷ However, the toxicity and biocompatibility of NPs is highly related to their stability, and in particular to their long-term stability that remains a major concern. So far, there have been a lot of studies reporting the thermal and chemical stability of ligand-stabilized gold nanoparticles. In general, heat-treatment method, cyanide-induced decomposition and oxygen plasma etching were used to examine the stability of gold nanoparticles.

1.4.1 Thermal stability

In 1995, R. W. Murray et al. investigated the gold clusters stabilized by chemisorbed monolayers of octane-, dodecane- and hexadecanethiol by thermogravimetry analysis (TGA).⁴⁴ They found that the mass loss by the gold clusters stabilized by C8SH, C12SH and C16SH beginning at 230, 266 and 310 °C respectively. It was indicated that the thermal stability of alkanethiol-protected gold nanoparticles increased while the chain length increased. Later in 1999, R. W. Murray et al. used TGA to analyze the gold nanoparticles stabilized by monolayers of arenethiols.¹⁵⁸ They found that alkanethiol-protected AuNPs are more thermally stable than arenethiol-coated AuNPs. In the same year, C. Zhong et al. described an investigation of temperature-manipulated size and shape evolution for dodecanethiol-coated AuNPs.¹⁵⁹ They used the two-phase method to prepare the dodecanethiol-stabilized AuNPs which were subjected to heat treatment at 110 °C under reduced pressure. They found that the size of the AuNPs increased. The details of the evolution process were researched in the follow-up study.^{160,161} Based on the experimental data of TEM, FTIR and UV-Vis, it was indicated that the chemical reactivities in the evolution process involve shell desorption, core-coalescence and re-encapsulation. They found that the temperature at which the particles change sizes or shapes was dependent on the chain length of the encapsulating thiols and the compositions of the nanocrystal cores. In 2001, M. Miyake et al. reported a simple method to control the size of alkanethiol-protected Au nanoparticles by heat treatment in the solid state.^{162,163} The size of the Au nanoparticles could be evolved to 3.4–9.7 nm by heating to 150–250 °C in air. It was suggested that the melting of the AuNPs surface induced the particle growth. In 2004, V. Chechik et al. synthesized L-Lysine based dendrimers-coated AuNPs via a one-phase chemical reduction method.¹¹⁶ They found that the size of AuNPs decreased while dendritic generation increased. Furthermore, the thermal

stability of the nanoparticles in solution was controlled by the extent of branching in the protecting dendritic shell. In 2006, Y. S. Shon et al. studied the thermal stability of AuNPs coated with thiols derived from normal and ω -functionalized alkane- and arenethiols.¹⁶⁴ They found that the monolayer-protected AuNPs with longer chains needed higher temperature for complete loss than those with shorter chains. They also found that the linkers used to build nanoparticle multilayer films govern the overall stability of hybrid nanostructures. In 2008, V. M. Rotello et al. explored the effect of subtle structural changes of surface ligands on the cluster stability.¹⁶⁵ They found that the thermodynamic stability of Au cluster was influenced by the surface ligand packing. In 2010, T. R. Lee et al. investigated the thermal stability of gold nanoparticles protected by *n*-octadecanethiol (*n*-C18), 2-hexadecylpropane-1,3-dithiol (C18C2), 2-hexadecyl-2-methylpropane-1,3-dithiol (C18C3), and 1,1,1-tris(mercaptomethyl)heptadecane (*t*-C18).¹⁶⁶ They used UV-visible spectrometry to monitor the thermal stability of AuNPs in decalin at 120 °C. Based on the UV spectra results, they found the following trend in thermal stability of the MPCs: *t*-C18 > C18C2 \approx C18C3 > *n*-C18, which correlates directly with the degree of chelation (tridentate > bidentate > monodentate). Thus, it indicated that the chelation affords enhanced the thermal stability to metal nanoparticles.

1.4.2 Chemical stability

Oxygen plasma etching and cyanide-induced decomposition have been used to examine the chemical stability of AuNPs and other metal nanoparticles. In the case of oxygen plasma etching, in 2009, the SUPRANANO group investigated the stability of silver nanocrystals self-assembled in 2D by oxygen plasma etching.¹⁶⁷ We found that higher ordered self-assemblies remain unchanged, while less ordered organizations coalesce into larger nanocrystals with spheroidal shapes that could be single crystals. In 2014, M. Fialkowski et al. investigated changes in the morphology of AuNPs coated with positively and negatively charged as well as uncharged ligands by deposition onto silicon substrate and subsequent oxygen plasma treatment of the deposit.¹⁶⁸ The plasma treatment affects the morphology of the AuNPs in two ways: (i) making coalescence; (ii) changing the shapes of individual particles. They found that the AuNPs behave like droplets of a non-wetting liquid, exhibiting the ability to move and merge. However, in the case of cyanide-induced decomposition, cyanide degraded the AuNPs by reacting with AuNPs to form Au(CN)²⁻ complexes, dialkylsulfides, and dialkyl cyanides.¹⁶⁹ In 1996, G. M. Whitesides et al. reported the first

investigation of the etching of AuNPs by cyanide.¹⁷⁰ They examined the chemical stability of AuNPs protected by HS(CH₂)_nOH. They found that the rate of KCN-induced decomposition decreased while the length of coating ligand increased. In 1998, R. W. Murray et al. investigated the steric environment of alkanethiol ligand shells of monolayer-protected AuNPs.¹⁶⁹ They found that the rate of NaCN-induced decomposition decreased with increasing alkanethiol chain length and steric bulk. In 2002, V. M. Rotello et al. synthesized a series of gold nanoparticles having amide functionality within the monolayer chains and altering the peripheral end groups of the monolayer to investigate the effect of branched ligands on the chemical stability of AuNPs.¹⁷¹ They found that a correlation exists between the cyanide-induced decomposition rate and the intramonolayer hydrogen bonding and ligand packing density. In 2005, Y. S. Shon et al. reported that the chemical stability of tetraoctylammonium thiolate-coated AuNPs was much higher than tetraoctylammonium bromide-protected AuNPs by cyanide-induced decomposition.¹⁷² In 2009, H. Mattoussi et al. investigated the effects of ligand coordination number and surface curvature on the colloidal stability of AuNPs cap-exchanged with either monothiol- or dithiolane-terminated PEG-OCH₃ ligands.¹⁷³ Through the resistance to NaCN decomposition they found that there was a balance between the coordination number and the density of ligand packing on the nanoparticle surface. For smaller NPs, where a larger surface curvature reduces the ligand packing density, a higher coordination number is clearly beneficial. In comparison, a higher ligand density allowed by the smaller curvature for larger nanocrystals makes monothiol-PEG-capped AuNPs more resistant to cyanide decomposition.

Besides, there have been some studies reporting the kinetic,¹⁶⁵ ultrasonic,¹⁶⁴ pH and solvent stability¹⁴⁴ of AuNPs.

1.5 Self-assembly of nanoparticles

Self-assembly is one of the most promising ways to drive individual particles into highly ordered and functional structures in a controlled way. Because of the self-assembly phenomena of micrometer colloids such as silica spheres and polystyrene beads is known for decades, the attention started to be turned to nanoscale self-assembly of nanoparticles in the early 1990s. Since 1995, semiconducting nanoparticles were self-assembled in compact two dimensions (2D) and three dimensions (3D) with face centered cubic (fcc), hexagonal close packed (hcp), or body centered cubic (bcc) crystalline structures in thermodynamically stable states.¹⁷⁴ This clearly demonstrated that the organization of nanocrystals in supracrystals is

similar to that of carbon atoms in diamonds or to those of Na^+ and Cl^- ions in stable salt. Other types of self-organization of nanocrystals like rings or honeycomb arrangements, linked to the Marangoni instabilities, have also been produced.¹⁷⁵

1.5.1 Self-assembly in two dimensions

Self-assembly of nanoparticles in organized 2D networks is relatively easy to accomplish, compared with 3D assembly. In the past decades, a lot of self-organized nanoparticles in 2D closed-packed superlattices in very large scale with a small number of defects have been synthesized. So far, there have been several methods to fabricate 2D self-assembly of nanoparticles. First, Langmuir-Blodgett (LB) films are effective for depositing thin films of nanocrystals on solid substrates,¹⁷⁶ which are well-known procedures to prepare 2D hexagonal close-packed superlattices. In 2003, R. P. Andres et al. reported a method in which 5 nm AuNPs encapsulated by alkanethiol could be self-assembled into well-ordered monolayers on a water surface, and these nanoparticle films were transferred intact onto various solid substrates. This method included spreading a thin film of a colloidal solution of AuNPs on the water surface. The water surface had a controlled surface curvature. After the solvent evaporated, a close-packed monolayer of AuNPs nucleated at the center of the water surface and grew gradually outward. At last, the monolayers could be transferred from the water surface to a hydrophobic substrate by Langmuir-Schaefer technique. Second, evaporation-induced assembly of colloidal solution of nanoparticles is another convenient way to generate 2D networks. One drop colloidal solution of nanoparticle is deposited on the substrate and then evaporated at the substrate surface. This method is widely used in the SUPRANANO group.^{74,167,177} It is easier and more flexible than the LB film method. However, the superlattices obtained are local ordering with some areas containing multilayers. Third, interfacial self-assembly also is a useful method for creating 2D assemblies. This method is a combination of LB film method and evaporation-induced assembly method. For example, in 2011, C. B. Murray et al. used the liquid-air interfacial assembly approach to grow large-area 2D binary nanocrystal superlattices.¹⁷⁸ Besides, versatile biological templates such as proteins are also frequently used to generate 2D superlattices. For example, in 1997, W. Shenton et al. described the use of bacterial Slayers as templates for the *in situ* nucleation of ordered two-dimensional arrays of cadmium sulphide nanocrystals about 5 nm in size.¹⁷⁹ The bacterial Slayers are self-assembled, two-dimensionally ordered films of proteins that feature in many bacterial cell walls.

1.5.2 Self-assembly in three dimensions

In the past 20 years, self-assemblies of 3D superlattices of inorganic nanoparticles (semiconductors, metals, oxides, etc.) have been produced. These nanocrystal assemblies in three dimensions are called supra- or supercrystals. The structures of 3D supracrystals are similar to the structures of atoms in bulk phase metals and nanocrystals such as bcc, fcc, hcp, or disordered with the formation of so-called amorphous material. Evaporation-induced assembly is a well-known method to generate 3D structures, which allows the nanocrystals to assemble into 3D superlattices by slow and controlled evaporation of the organic solvent, or water on a suitable substrate surface such as silicon wafer. A lot of studies described the use of evaporation method to generate 3D structures. For example, in 2001, the SUPRANANO group succeeded in fabricated 3D superlattices of 8 nm cobalt nanocrystals through evaporation method, and demonstrated that it is possible to obtain 3D superstructures of cobalt nanocrystals.¹⁸⁰ Then in 2003, supracrystals of cobalt nanocrystals with more than 1000 layers of ordered nanocrystals was produced by my group.¹⁸¹ Another way to crystallize nanocrystals into ordered 3D superlattices is diffusing non-solvent into a concentrated solution of nanocrystals.^{182,183} In 2001, A. L. Rogach et al. first reported this approach to crystallization of CdSe nanoparticles into ordered 3D superlattices.¹⁸³ The growth of CdSe crystals was induced by slow diffusion of a non-solvent into concentrated solution of CdSe nanocrystals, either directly or through a buffer layer. The buffer layer is low, but not negligible solubility for nanocrystals. Besides, interfacial self-assembly used to create 2D networks could also be used to prepare supracrystals.¹⁸⁴

Chapter 2

Well-defined Ag and Au-NHC complexes as precursors for one-phase synthesis of nanocrystals

2.1 Abstract

Herein, we report the formation of nanocrystals by one-phase reduction of metal–NHCs (metal = Au, Ag) bearing common NHC ligands, namely 1,3-diethylbenzimidazol-2-ylidene (**L**¹), 1,3-bis(mesityl)imidazol-2-ylidene (**L**²) and 1,3-bis(2,6-*i*-Pr₂C₆H₃)imidazol-2-ylidene (**L**³). We show that both Au and Ag nanocrystals displaying narrow size distribution can be formed by reduction with amine-boranes. The efficiency of the process and the average size and size distribution of the nanocrystals markedly depend on the nature of the metal and NHC ligand, on the sequence in the reactants addition (*i.e.* presence or absence of thiol during the reduction step), and on the presence or absence of oxygen. Dodecanethiol was introduced to produce stable nanocrystals associated with narrow size distributions. A specific reaction is observed with Ag–NHCs in the presence of thiols whereas Au–NHCs remain unchanged. Therefore, different organometallic species are involved in the reduction step to produce the seeds. This can be correlated to the lack of effect of NHCs on Ag nanocrystals size. In contrast, alteration of Au nanocrystals average size can be achieved with a NHC ligand of great steric bulk (**L**³). This demonstrates that a well-defined route for a given metal cannot be extended to another one.

2.2 Nanocrystals: Why Do Silver and Gold N-Heterocyclic Carbene Precursors Behave Differently?

Langmuir **2013**, *29*, 12647

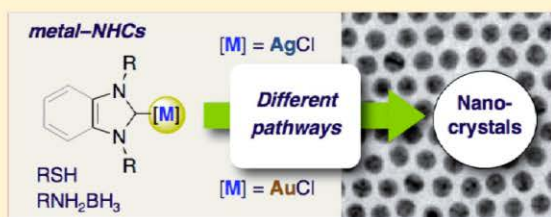
Nanocrystals: Why Do Silver and Gold N-Heterocyclic Carbene Precursors Behave Differently?

Xiang Ling,^{†,‡} Nicolas Schaeffer,[†] Sylvain Roland,^{*,‡} and Marie-Paule Pileni^{*,†}[†]Laboratoire des Matériaux Mésoscopiques et Nanométriques, UMR CNRS 7070, UPMC-Université Paris 6, 4 place Jussieu, 75252 Paris, France[‡]Institut Parisien de Chimie Moléculaire, UMR CNRS 7201, UPMC-Université Paris 6, 4 place Jussieu, 75252 Paris, France

Supporting Information

ABSTRACT: Synthesizing stable Au and Ag nanocrystals of narrow size distribution from metal–N-heterocyclic carbene (NHC) complexes remains a challenge, particularly in the case of Ag and when NHC ligands with no surfactant-like properties are used. The formation of nanocrystals by one-phase reduction of metal–NHCs (metal = Au, Ag) bearing common NHC ligands, namely 1,3-diethylbenzimidazol-2-ylidene (L^1), 1,3-bis(mesityl)imidazol-2-ylidene (L^2), and 1,3-bis(2,6-*Pr*₂C₆H₃)imidazol-2-ylidene (L^3), is presented herein.

We show that both Au and Ag nanocrystals displaying narrow size distribution can be formed by reduction with amine–boranes. The efficiency of the process and the average size and size distribution of the nanocrystals markedly depend on the nature of the metal and NHC ligand, on the sequence in the reactant addition (i.e., presence or absence of thiol during the reduction step), and on the presence or absence of oxygen. Dodecanethiol was introduced to produce stable nanocrystals associated with narrow size distributions. A specific reaction is observed with Ag–NHCs in the presence of thiols whereas Au–NHCs remain unchanged. Therefore, different organometallic species are involved in the reduction step to produce the seeds. This can be correlated to the lack of effect of NHCs on Ag nanocrystal size. In contrast, alteration of Au nanocrystal average size can be achieved with a NHC ligand of great steric bulk (L^3). This demonstrates that a well-defined route for a given metal cannot be extended to another metal.



INTRODUCTION

Over the last decades, Au and Ag nanocrystals have been mainly produced by either thermodecomposition or chemical reduction of noble metal ions.^{1–6} In the latter case, two general approaches have been reported. The first one involves surfactant molecules, and the chemical reduction is performed either in confined media (e.g., reverse micelles)⁷ or under phase transfer conditions.^{8,9} The second general approach is based on single-phase reduction of metal salts or organometallic precursors.^{10–13} Here, the use of organometallic complexes bearing organic ligands makes it possible, by changing the ability of the ligands to give electrons to the metal center and the bulkiness of the ligand or reducing agent, to tune kinetics of metal reduction which in turn enables control of nanocrystal size.

N-Heterocyclic carbenes (NHCs) have emerged as an essential class of ligands in organometallic chemistry.^{14–16} NHCs display particular properties across a wide family of neutral ligands used in catalysis because of their strong σ -donating characteristics,¹⁷ their ability to form stable metal–NHC bonds, and their wide structural diversity.¹⁸ NHCs exhibit a particular geometry associated with a flexible structure, allowing fine-tuning of their steric properties.¹⁹ Metal–NHCs have been extensively explored for application in catalysis²⁰ and

have also showed promising potential as novel therapeutic agents.^{21,22}

Very few reports refer to syntheses and stabilization of metal nanocrystals through metal–NHC complexes.^{23–28} Formation of Au nanocrystals by reduction of the gold complexes 1–3 was reported (Figure 1).^{11a,c} The best control of nanocrystal size and size distribution ($5.75 \text{ nm} \pm 0.49 \text{ nm}$) was achieved by one-phase reduction with 9-BBN of Au–NHC 3 bearing a NHC ligand with long alkyl chains on the nitrogen atoms.²³

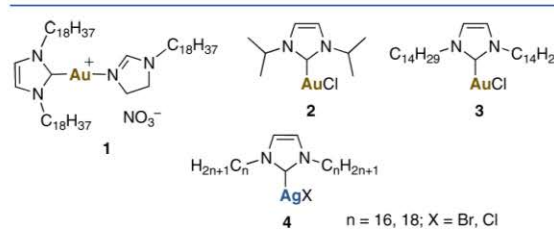


Figure 1. Au and Ag–NHC complexes previously used as precursors for the synthesis of nanocrystals.

Received: June 26, 2013

Revised: September 5, 2013

Published: September 12, 2013

The steric bulk of the NHC and the strength of the reducing agent were found to have a great influence on nanocrystal size, size distribution, and shape. Stabilized NHC-coated Au nanocrystals have also been obtained by exchange of thioether ligands on preformed nanocrystals by 1,3-bis(*tert*-butyl)-imidazol-2-ylidene.²⁴ The formation of Ag nanoparticles was also observed from the reduction of silver complex 4 by NaBH₄ under biphasic conditions (CH₂Cl₂/H₂O).²⁶ SEM images showed rectangular morphologies formed by the assembly of Ag spherical particles presumably capped with imidazolium moieties derived from the NHC.²⁹

We show herein that both Ag and Au-NHCs are suitable precursors for the one-phase synthesis of nanocrystals with narrow size distributions. The use of well-defined metal-NHCs enabled direct comparison of the effect of both the metal and the NHC on nanocrystal formation and size distribution, and the steric effects associated with the ligand have been examined. The reduction of metal-NHCs was investigated in the absence or in the presence of dodecanethiol as an additional coating agent. ¹H NMR experiments have been carried out to gain a better understanding of the species involved in the process. We show that different pathways and intermediates are involved in the production of Ag and Au nanocrystals.

RESULTS AND DISCUSSION

Ag and Au-NHC Complexes. To determine the influence of both the metal and the NHC ligand under strictly identical conditions, a series of six metal-NHC complexes with three different NHCs of various steric demand, and Ag or Au as the metal, have been prepared (Figure 2). Silver(I) chloride

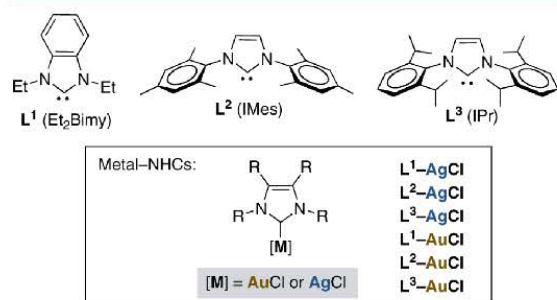


Figure 2. Au and Ag-NHCs used in this study.

complexes L¹-AgCl, L²-AgCl, and L³-AgCl can readily be obtained from the corresponding (benz)imidazolium chlorides by treatment with Ag₂O.^{30,31} According to literature procedures, transfer of the NHC ligand from Ag-NHCs to [AuCl(SMe₂)] affords the corresponding Au-NHCs L¹-AuCl, L²-AuCl, and L³-AuCl in high yields (see Experimental Section). To compare metal complexes bearing exclusively chloride ligands, a protocol was developed to synthesize 1,3-diethylbenzimidazol-2-ylidene silver(I) chloride (L¹-AgCl). NHC ligands L¹-L³ (Et₂Bimy, IMes, and IPr) are commonly used in catalysis.^{14-16,20} They can be classified according to their steric bulk (3 > 2 > 1) that can be evaluated by calculation of the buried volume (%V_{bur}) of the NHC ligands that represents the space occupied by the NHC in the first coordination sphere of the metal center (3: 33.6%; 2: 31.6%; 1: 26.4%).¹⁹

Amine-Borane-Mediated Reduction of Au and Ag-NHCs To Form Nanocrystals. It was previously shown that the sequence in which the reactants (e.g., coating agent and reducing agent) are added could play an important role in controlling the synthesis of nanocrystals.^{32,33} Consequently, we carried out a series of parallel experiments where dodecanethiol (DDT), used as stabilizing agent, was introduced either before or after the reduction step. Reduction of the metallic precursors was investigated with amine-boranes, which are compatible with one-phase conditions.¹⁰ The influence of the strength of the reducing agent that can also play an important role in controlling the size and size distribution of nanocrystals was tuned by using either ammonia-borane (NH₃BH₃) or borane-*tert*-butylamine complex (a weaker reducing agent).

Reduction in the Absence of DDT. In the first instance, we examined the ability of each of the six complexes to form nanocrystals by using NH₃BH₃ as the reducing agent by performing the reduction reaction in the absence of DDT. In a typical experiment, metal-NHCs (0.125 mmol) were mixed in toluene and heated at 100 °C prior addition of NH₃BH₃ (1.25 mmol). The reaction was allowed to proceed for 0.5 h at 100 °C, DDT (1 mmol) was added, and the mixture was stirred for another 0.5 h before workup. Under these conditions, for any complex other than L³-AuCl, a complete precipitation of Au and Ag materials insoluble in toluene was observed within a few minutes after addition of NH₃BH₃ and no nanocrystal formation could be observed by TEM analyses. In contrast, TEM analysis of an aliquot of the toluene solution obtained during reduction of L³-AuCl (before addition of DDT) revealed the presence of Au nanocrystals of about 5.5 nm size. After addition of DDT, stirring for another 30 min, and workup, a dark-purple solid was obtained. Addition of PhCH₃ to the product led to a light-red optically clear colloidal solution. TEM analysis of the solution confirmed the formation of Au nanocrystals with an average size of 5.5 nm and a narrow size distribution of ±7.8% (Figure 3). Replacement of NH₃BH₃ by ^tBuNH₂BH₃ under identical conditions did not produce either Au or Ag nanocrystals. In contrast to NH₃BH₃,

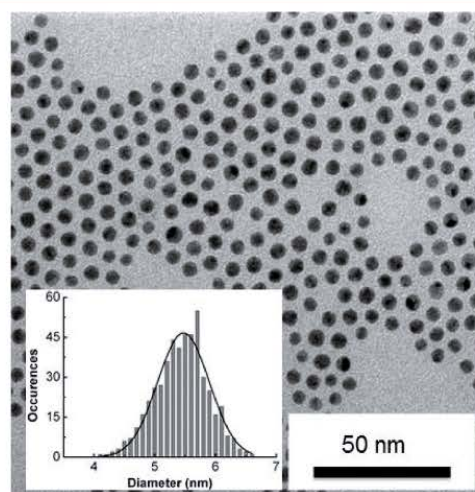


Figure 3. TEM image and size distribution (inset) of Au nanocrystals produced from L³-AuCl by reduction with NH₃BH₃ at 100 °C. Dodecanethiol was added 0.5 h after the addition of NH₃BH₃.

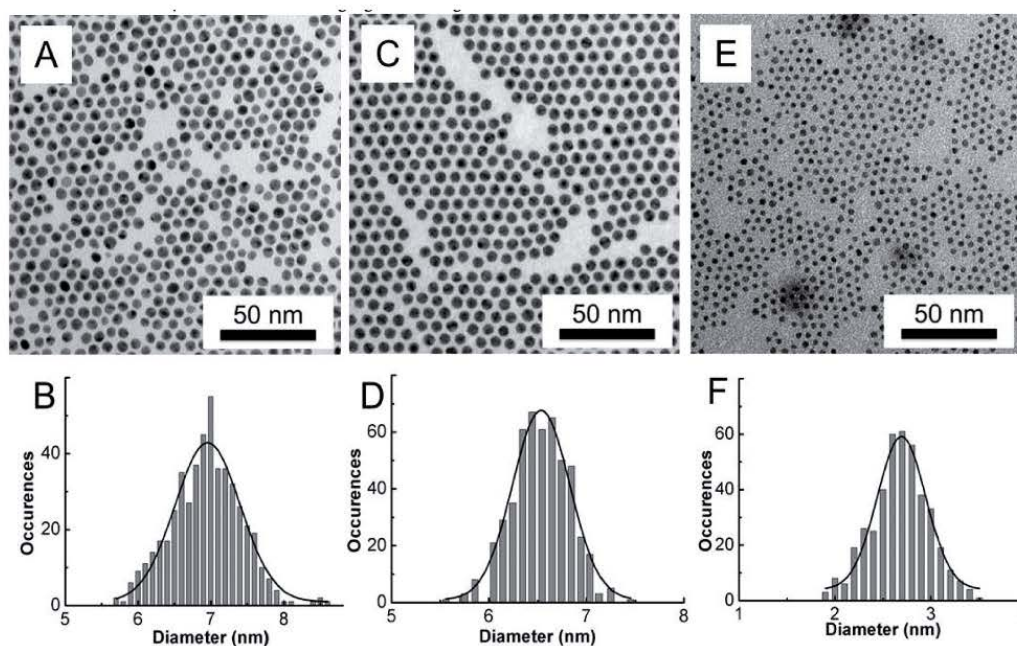


Figure 4. TEM images and size distributions of Au nanocrystals generated by reduction with NH_3BH_3 of $\text{L}^1\text{-AuCl}$ (A,B), $\text{L}^2\text{-AuCl}$ (C,D), and $\text{L}^3\text{-AuCl}$ (E,F) in the presence of dodecanethiol.

$\text{tBuNH}_2\text{BH}_3$ was found not to be appropriate for the reduction of complex $\text{L}^3\text{-AuCl}$, which remains intact in the medium in the presence of this borane as demonstrated by ^1H NMR analysis of the combined washing layers. As previously observed with NH_3BH_3 , the five other complexes led to the fast formation of aggregates.

Comparison of the results obtained from $\text{L}^3\text{-AgCl}$ and $\text{L}^3\text{-AuCl}$ possessing the same bulky NHC ligand demonstrates a dramatic effect of the metal. ^1H NMR analysis of the supernatant (PhCH_3 layer) from the reduction of $\text{L}^3\text{-AgCl}$ showed no trace of the initial complex ($\text{L}^3\text{-AgCl}$), indicating its full transformation in the reaction. Reduction of $\text{L}^3\text{-AgCl}$ might lead to the formation of the corresponding imidazolium salt or imidazoline (aminal). However, no trace of organic compound corresponding to these derivatives or to the free NHC ligand L^3 is detectable. These observations suggest that silver-NHCs are rapidly reduced under the conditions used and that the NHC or the organic moiety from the NHC is incorporated into the aggregates or strongly binds to the surface of the material. In contrast, ^1H NMR analyses of the combined initial supernatants and washing layers from the reduction of $\text{L}^3\text{-AuCl}$, that produces nanocrystals with narrow size distribution, display the signals of the initial gold complex along with those of DDT. As in the silver case, no trace of derivatives of L^3 or of other Au complexes (e.g., a gold hydride complex) could be detected.³⁴ A change in the gold complex/DDT ratio from 1:8 (initial mixture) to 1:10.3 is observed, indicating that $\text{L}^3\text{-AuCl}$ is consumed to generate nanocrystals but also that a significant amount of the complex remains intact in the reaction. This suggests for Au (in contrast to Ag) that the reduction rate is limited by the bulkiness of L^3 . By comparison, the reduction of $\text{L}^1\text{-AuCl}$ and $\text{L}^2\text{-AuCl}$ seems faster, as indicated by the rapid formation of large aggregates likely resulting from the absence of any efficient stabilizing agent

during the reaction. This demonstrates for gold complexes an important effect of the steric bulk of the NHC ligand (compare L^2 and L^3).

Overall, these results suggest that in most cases, NHCs $\text{L}^1\text{-L}^3$ or their derivatives, which are not associated with surfactant-like properties, are not appropriate to efficiently stabilize Ag and Au nanocrystals in solution or to avoid precipitation when the reduction step is performed in the absence of additional coating agent (e.g., DDT). One exception deals with complex $\text{L}^3\text{-AuCl}$ that produces Au nanocrystals with a narrow size distribution. Similarly, it was previously observed that thioether exchange on the Au nanocrystal surface by 1,3-bis(*tert*-butyl)imidazol-2-ylidene progressively led to the formation of aggregates.²⁴ These observations prompted us to investigate amine-borane-mediated reduction of metal-NHCs in the presence of DDT (i.e., the reduction of the complexes takes place in the presence of thiol derivative).

Reduction of Au-NHCs by Amine-Boranes in the Presence of DDT. We first studied the production of Au nanocrystals from gold complexes $\text{L}^1\text{-AuCl}$, $\text{L}^2\text{-AuCl}$, and $\text{L}^3\text{-AuCl}$. In a typical experiment, Au precursors (0.125 mmol) and DDT (1 mmol) were mixed in PhCH_3 and heated at 100 °C for 0.5 h prior addition of NH_3BH_3 (1.25 mmol). The reaction was allowed to proceed for another 0.5 h and toluene was evaporated under a nitrogen flow. The as-formed solids were washed with ethanol, dried, and then dispersed in toluene. A drop of the colloidal solution was deposited on a TEM grid covered by amorphous carbon for TEM analysis. Interestingly, these modified conditions were found to allow formation of nanocrystals from the three Au-NHC complexes regardless of the nature of the NHC ligand (Figure 4). In addition, Au nanocrystals produced from $\text{L}^1\text{-AuCl}$ and $\text{L}^2\text{-AuCl}$ are characterized by narrow size distributions of 6.7% and 4.6%,³⁵ respectively, and similar average sizes of 6.5–6.6 nm (Table 1,

Table 1. Size and Size Distribution of Nanocrystals Formed from the Six Different Metal–NHCs (metal = Ag, Au) by Reduction with Amine–Boranes^a

entry	complex	NH ₃ BH ₃		^t BuNH ₂ BH ₃	
		D (nm)	σ ^b (%)	D (nm)	σ ^b (%)
1	L ¹ –AuCl	6.6	±6.7	6.7	±5.5 ^d
2	L ² –AuCl	6.5	±4.6	6.3	±5.9
3	L ³ –AuCl	2.7	±12.5	n.d. ^c	n.d. ^c
4 ^d	L ¹ –AgCl	6.6	±7.4	6.7	±8.1
5 ^d	L ² –AgCl	6.4	±7.8	6.3	±7.2
6 ^d	L ³ –AgCl	6.4	±8.1	6.5	±9.2

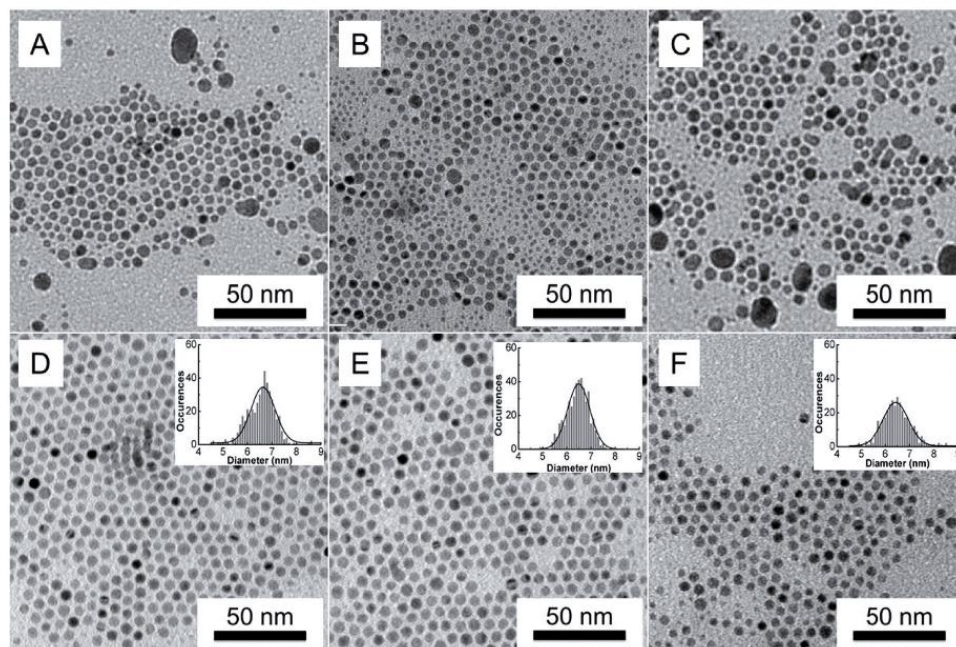
^aDDT is added before the reducing agent. ^bStandard deviation. ^cNot determined. No reduction is observed. ^dSize selection is carried out (see text). Before size selection, smaller seeds (<2 nm) and larger aggregates are also detectable but the average size is identical.

entries 1 and 2). This clearly shows the stabilizing effect of DDT and also indicates that the steric effects associated with L¹ and L² are negligible or very similar although their structures are significantly different. Note that L¹–AuCl and L²–AuCl directly lead after chemical reduction to nanocrystals with an unimodal and narrow size distribution without the need for additional steps of size selection. The best size distribution (4.6%) is obtained with L²–AuCl. Conversely, L³–AuCl exhibits a particular behavior that is demonstrated by the formation of Au nanocrystals of smaller average size (2.7 nm) and larger size distribution (12.5%) (Figure 4E and Table 1, entry 3). These data, confirming that specific steric effects are induced by ligand L³, are in accordance with those described above where precipitation takes place with L¹–AuCl and L²–AuCl when DDT is added after the chemical reduction whereas L³–AuCl produces nanocrystals of narrow size distribution (5.5

nm ± 7.8%). By replacing NH₃BH₃ with ^tBuNH₂BH₃, similar average sizes and size distributions are obtained from L¹–AuCl and L²–AuCl, indicating a negligible influence of the borane (Figure S1), whereas no nanocrystals are produced from L³–AuCl (Table 1, entries 1–3) as already observed with the first protocol (no reduction takes place).

Reduction of Ag–NHCs in the Presence of DDT. The conditions described above for Au precursors were applied to Ag complexes L¹–AgCl, L²–AgCl, and L³–AgCl. Under these conditions, as in the gold case, we clearly observed the formation of Ag nanocrystals, suggesting that the presence of the thiol during the reduction step is also essential to stabilize Ag nanocrystals. However, unlike gold, Ag nanocrystals with rather large size distributions are obtained after the reduction step, as observed by TEM (Figure 5A–C). Hence, size selection was performed on the isolated Ag nanocrystals by precipitation with pyridine followed by washings with ethanol. As shown in Figure 5D–F, the as-formed nanocrystals display virtually identical average sizes (6.4–6.6 nm) and relatively narrow size distributions (7.4–8.1%) (Table 1, entries 4–6). Replacement of NH₃BH₃ by ^tBuNH₂BH₃ also led to stable Ag nanocrystals (Figure S2, Supporting Information). Here, no significant change in the average sizes (6.3–6.7 nm) and size distributions were observed by comparison with NH₃BH₃ (Table 1, entries 4–6). However, the best size distribution (7.2%) is achieved under these conditions by using L²–AgCl as the precursor (Table 1, entry 5).

Comparison of the results obtained from Au and Ag highlight important features. First, no difference in nanocrystal size is observed from the different Ag–NHCs, therefore suggesting a negligible influence of the NHC ligand in the process. In contrast, marked changes are observed with Au by using a bulky NHC ligand such as L³, with a decrease in the


Figure 5. TEM images and size distributions (insets) of Ag nanocrystals produced by chemical reduction with NH₃BH₃ of complexes L¹–AgCl (A, D), L²–AgCl (B, E), and L³–AgCl (C, F) in presence of DDT. (A–C) Before and (D–F) after size selection processes, respectively.

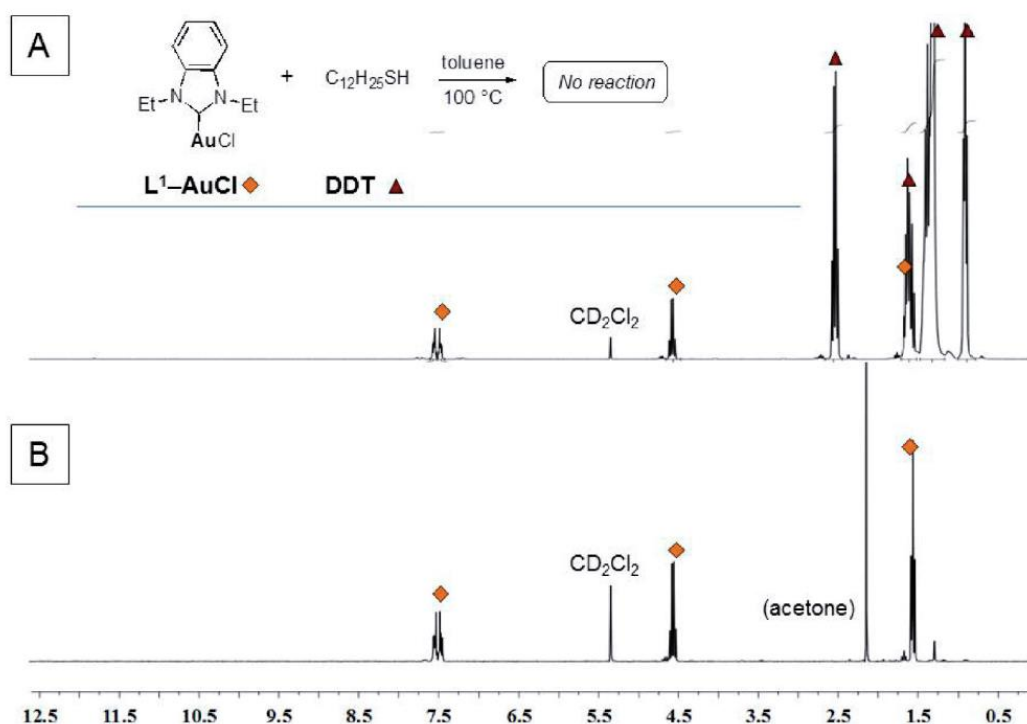


Figure 6. Reaction of L^1 -AuCl with DDT at 100 °C. ^1H NMR spectra of the crude reaction mixture (A) and of the starting complex (B).

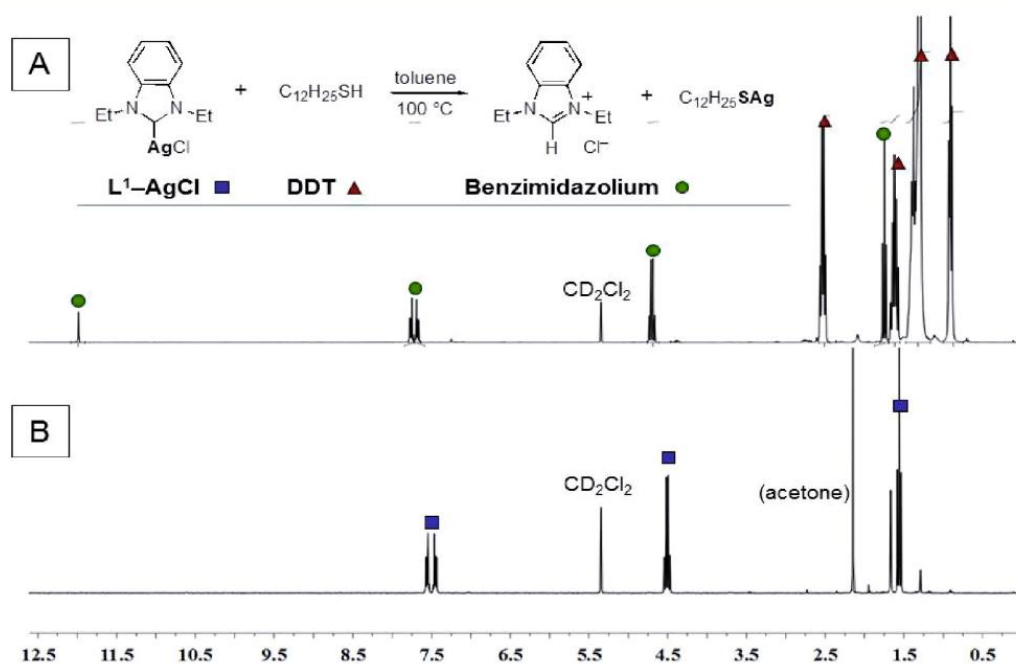


Figure 7. Reaction of L^1 -AgCl with DDT at 100 °C. ^1H NMR spectra of the crude reaction mixture (A) and of the starting complex (B).

nanocrystal size with NH_3BH_3 and no nanocrystal formation with $^t\text{BuNH}_2\text{BH}_3$. Production of smaller nanocrystals is not observed with the corresponding silver complex L^3 -AgCl. This

clearly demonstrates an effect of the metal. Furthermore, to produce narrow size distributions, size selection processes are required with Ag but not with Au. These differences suggest

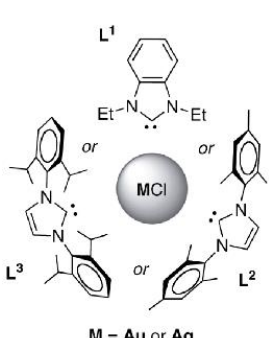
<i>Au and Ag-NHC complexes:</i>	<i>Reaction conditions:</i>	<i>Results :</i>	
 <p>M = Au or Ag</p>	1) NH_3BH_3 2) DDT	Precipitates from $\text{L}^1\text{-AgCl}$, $\text{L}^2\text{-AgCl}$, $\text{L}^3\text{-AgCl}$, $\text{L}^1\text{-AuCl}$, $\text{L}^2\text{-AuCl}$ or Au nanocrystals formation (5.5 nm \pm 7.8%) from $\text{L}^3\text{-AuCl}$	
	1) $^t\text{BuNH}_2\text{BH}_3$ 2) DDT	Precipitates from $\text{L}^1\text{-AgCl}$, $\text{L}^2\text{-AgCl}$, $\text{L}^3\text{-AgCl}$, $\text{L}^1\text{-AuCl}$, $\text{L}^2\text{-AuCl}$ or No reduction ($\text{L}^3\text{-AuCl}$)	
	1) DDT 2) NH_3BH_3	Au nanocrystals : 6.5–6.6 nm ($\text{L}^1\text{-AuCl}$, $\text{L}^2\text{-AuCl}$) or 2.7 nm ($\text{L}^3\text{-AuCl}$) Best size distribution (\pm 4.6%) from $\text{L}^2\text{-AuCl}$	Direct reduction of Au-NHCs No size selection required
	1) DDT 2) NH_3BH_3	Ag nanocrystals: 6.4–6.6 nm (from L-AgCl) Size distribution \pm 7.4–8.1%	Via the silver thiolate Size selection required
	1) DDT 2) $^t\text{BuNH}_2\text{BH}_3$	Au nanocrystals : 6.3–6.7 nm ($\text{L}^1\text{-AuCl}$, $\text{L}^2\text{-AuCl}$) or no reduction ($\text{L}^3\text{-AuCl}$) Best size distribution (\pm 5.5%) from $\text{L}^1\text{-AuCl}$	Direct reduction of Au-NHCs Size selection for $\text{L}^1\text{-AuCl}$ (see Table 1 and ESI)
	1) DDT 2) $^t\text{BuNH}_2\text{BH}_3$	Ag nanocrystals: 6.3–6.7 nm (from L-AgCl) Size distribution \pm 7.2–9.2%	Via the silver thiolate Size selection required

Figure 8. Different conditions tested in this study and influence on Au and Ag nanocrystal formation.

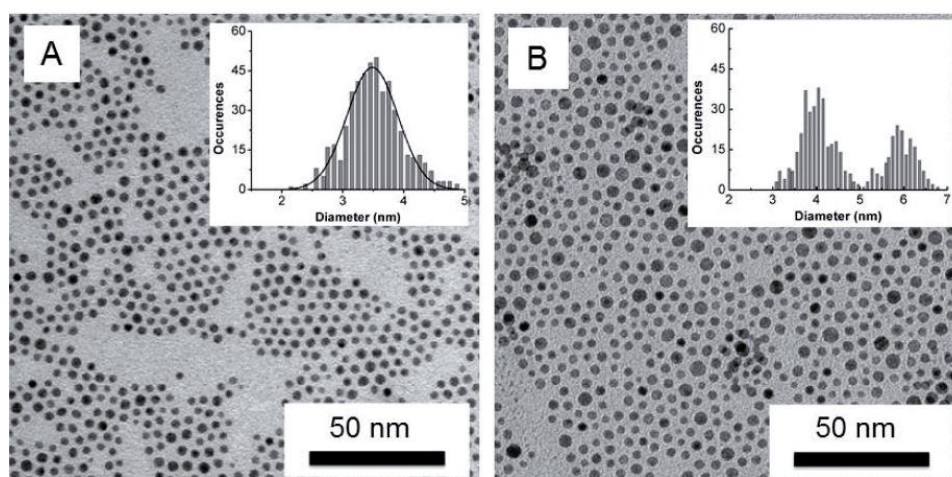


Figure 9. (A) TEM image of Au nanocrystals generated from $\text{L}^3\text{-AuCl}$ by reduction with NH_3BH_3 in the presence of air. DDT is added 30 min after the reducing agent at 100 °C. (B) Au nanocrystals generated by reduction of $\text{L}^2\text{-AuCl}$ with NH_3BH_3 in the presence of air. DDT is added before the reducing agent.

that different routes are involved in the production of nanocrystals from Au or Ag-NHCs.

Nature of Ag and Au Organometallic Species Formed in the Presence of DDT. To determine which organometallic species are directly involved in the reduction step, control experiments have been carried out where metal-NHCs (0.125 mmol) were heated in the presence of DDT (1 mmol) at 100 °C. The crude reaction mixtures were analyzed by ^1H NMR in CD_2Cl_2 . As shown in Figure 6, $\text{L}^1\text{-AuCl}$ remains unchanged upon heating with DDT for 1 h (Figure 6A). The same observation was made with $\text{L}^3\text{-AuCl}$ (data not shown), indicating that DDT does not react with Au-NHC complexes prior to reduction. Therefore, unchanged NHC-AuCl precursors might be reduced by amine-boranes to produce

the nanocrystals. Similarly, it was previously observed that $\text{L}^3\text{-AuCl}$ did not react with a thiosugar derivative in refluxing dichloromethane.³⁶

The same experiments were performed with the corresponding Ag complexes $\text{L}^1\text{-AgCl}$ and $\text{L}^3\text{-AgCl}$. In contrast to gold, the NMR spectra clearly show the complete transformation of silver-NHCs into the corresponding (benz)imidazolium salts as shown in Figure 7 for $\text{L}^1\text{-AgCl}$. The reaction is accompanied by formation of a white precipitate insoluble in organic solvents, confirming the simultaneous production of silver dodecanethiolate which is known to be a highly insoluble oligomer.^{37–39} These data indicate that for any Ag-NHC complexes, the same silver thiolate complex is formed and presumably that the same seeds are involved in Ag nanocrystal

production. This clearly explains the lack of influence of the NHC in the case of Ag as well as the differences between Au and Ag. As a consequence, the size effect observed with Au–NHC complexes can be attributed to steric hindrance due to the NHC ligand. The different conditions tested and a summary of the results are presented in Figure 8.

Localization of NHC Derivatives. As noted above, precipitation of Ag or Au aggregates is not associated with release of the NHC moiety or derivatives in the medium, thus suggesting its incorporation into the material. In the cases where stabilized nanocrystals are formed, derivatives of the NHC might also be released in the supernatant during the process or incorporated at the surface of the nanocrystals along with DDT. The presence of PPh₃ as ligand (with DDT) at the surface of Au nanocrystals was previously proposed with PPh₃AuCl as precursor.¹³ To get more information on the nature and the localization of organic/organometallic compounds generated in the reaction with Au–NHCs, we carried out ¹H NMR analyses of the washing layers and nanocrystals from the reduction of complex L²–AuCl. Analysis of the combined washing layers (PhCH₃ and EtOH) revealed the presence of DDT and of a molecule displaying signals corresponding to a derivative of L² (Figure S3, Supporting Information). The same species is observed in the NMR spectra of the nanocrystals in C₆D₆ (Figure S4, Supporting Information) and in CD₂Cl₂. This demonstrates that a derivative of L² is released in the medium during the process. However, its exact structure and its possible localization at the surface of the nanocrystals could not be determined. The signals observed by NMR do not correspond exactly to the initial complex (L²–AuCl) and could be attributed neither to the imidazolium salt nor to the imidazoline (aminal).⁴⁰ Additional NMR and mass spectroscopy experiments were also inconclusive.

Influence of Oxygen on Nanocrystal Size and Size Distribution. All the experiments described above were carried out under nitrogen. To study the effect of oxygen on the final product, the reduction of L³–AuCl by NH₃BH₃ with DDT added 30 min after the reducing agent was repeated under an atmosphere of air. Under these conditions, a change of the average diameter from 5.5 nm (Figure 3) to 3.5 nm (Figure 9A) was observed along with a marked increase in the size distribution from 7.8% to 12%. Similarly, the reduction under air of L²–AuCl with DDT added before NH₃BH₃ leads to significant changes in the nature of the nanocrystals (Figure 9B). Here, a bimodal distribution is observed with average diameters of 6.0 and 4.0 nm and size distributions of 5.8% and 9.1%, respectively (with exclusion of air, the average diameter is 6.5 nm ± 4.6%, see Figure 4C and Table 1). These data clearly demonstrate that the average sizes of the Au nanocrystals produced under an aerobic atmosphere are smaller with a larger size distribution. Oxygen-induced oxidation of thiols into disulfides might be favored at high temperature and in the presence of metal species.⁴¹ A recent study demonstrated that the thiol-to-disulfide ratio could affect Au nanocrystal size and size dispersity.⁴² Moreover, the gold–thiolate bond in self-assembled monolayers (SAMs) was shown to be easily and rapidly oxidized under ambient conditions, adversely affecting their quality and structure.⁴³

CONCLUSION

In conclusion, by using metal–NHCs as precursors and dodecanethiol as stabilizer, we demonstrate that the sequence

in which the reactants are added markedly affects the pathways of Au and Ag nanocrystal production. A specific reaction is observed between Ag–NHCs and thiols, leading to the formation of silver thiolates whereas the corresponding Au–NHCs remain unchanged. With Au derivatives, highly well-defined nanocrystals of narrow size distribution (4.6–6.7%) are directly produced in a one-step synthesis. The steric hindrance does not play any role in controlling Au nanocrystal size (6.3–6.7 nm) except for a ligand of high steric demand (L³) for which the average diameter of the as-formed nanocrystals is 2.7 nm ± 12.5%. For Ag derivatives, because of silver thiolate formation, no steric effect of the NHC is observed in all cases. The first step of the synthesis induces the formation of Ag nanocrystals with rather large size distributions. After the size selection process, the average Ag nanocrystal size and size distribution reach 6.3–6.7 nm and 7.2–9.2%, respectively. This clearly demonstrates that different routes and species are involved in the synthesis of Au and Ag nanocrystals from metal–NHCs bearing identical ligands on the metal. The formation of silver thiolates through Ag–NHC complexes could also be associated with their biological properties.^{31,32,44} Finally, the presence of air induces a drop in the average size and an increase of size dispersion of Au nanocrystals.

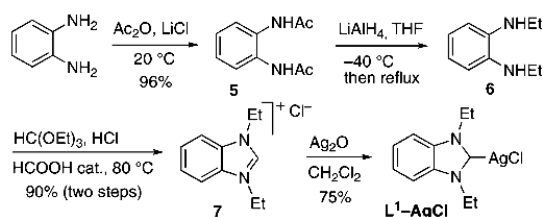
EXPERIMENTAL SECTION

General Considerations. Reagents were purchased from Acros or Sigma-Aldrich and used as received unless stated otherwise. Complexes L³–AgCl and L³–AuCl are commercially available (Strem). THF was distilled from sodium–benzophenone ketyl under N₂. Reactions involving organometallic species or air- or moisture-sensitive compounds were carried out under an atmosphere of argon by using standard Schlenk techniques. Unless otherwise stated, nanocrystal syntheses were carried out in a glovebox under N₂. NMR spectra were recorded on Bruker Nanobay spectrometers at 250, 300, 400, or 600 MHz. In CD₂Cl₂, DMSO-*d*₆, and C₆D₆, proton chemical shifts (δ) are reported relative to the residual protonated solvent (δ = 5.32, 2.50, and 7.16 ppm, respectively). Tetramethylsilane (TMS) was used as internal reference (δ = 0.00 ppm) in CDCl₃. ¹³C chemical shifts (δ) are reported relative to the NMR solvent (CD₂Cl₂: δ = 54.00 ppm; CDCl₃: δ = 77.23 ppm). Coupling constants are reported in hertz (Hz). The following abbreviations are used: s = singlet, d = doublet, t = triplet, q = quadruplet, m = multiplet, br = broad. Melting points are uncorrected and were determined using a Büchi 535 melting point apparatus. Elemental and HRMS analyses were performed at the I.C.S.N. (Service De Microanalyse) and at the I.P.C.M., respectively. Electron micrographs were obtained with a JEOL Model JEM 100CX electron microscope, and high resolution transmission electron microscopy (HRTEM) was performed at 200 kV with a JEOL 2010 microscope. Given their cytotoxicity, gold- and silver–NHCs should be handled with caution.

Ag- and Au–NHC Precursors. Complexes L²–AgCl and L²–AuCl were prepared from *N,N'*-bis(2,4,6-trimethylphenyl)imidazolium chloride according to reported procedures.^{45–47} Complex L¹–AuCl was synthesized from benzimidazole, via the silver bromide complex L¹–AgBr.^{48–51} Silver chloride complex L¹–AgCl was prepared from *o*-phenylenediamine according to Scheme 1.

***N*-(2-Acetamidophenyl)acetamide (5).**^{52,53} To a mixture of acetic anhydride (10.4 g, 102 mmol) and *o*-phenylenediamine (5 g, 46.2 mmol) was added at 0 °C lithium chloride (196 mg, 4.62 mmol). The mixture was stirred at 20 °C for 4 h. The precipitate formed was isolated by filtration, washed with pentane, and dried under vacuum to give the title compound as a white solid (8.5 g, 96%). ¹H NMR (250 MHz, DMSO-*d*₆) δ 9.29 (br s, 2H), 7.54 (dd, 2H, *J* = 5.7 and 3.5 Hz), 7.11 (dd, 2H, *J* = 5.7 and 3.5 Hz), 2.07 (s, 6H).

***N,N'*-Diethyl-1,2-diaminobenzene (6).**⁵³ *N*-(2-Acetamidophenyl)-acetamide (4 g, 20.8 mmol) was slowly added at –40 °C to a solution of LiAlH₄ (powder, 1.8 g, 47.5 mmol) in THF (50 mL). After

Scheme 1. Synthesis of L¹-AgCl

addition, the reaction was refluxed for 16 h and then cooled at 0 °C, and water was added to the reaction flask until the excess LiAlH₄ was hydrolyzed. The solution was filtered through Celite, and dichloromethane (50 mL) was added. Workup was completed by washing with brine (2 × 40 mL), drying over MgSO₄, filtration, and removal of the solvent under reduced pressure to give the title compound as a dark-red oil which was directly used in next step without further purification. A sample of the crude oil was analyzed by NMR spectroscopy. ¹H NMR (250 MHz, CDCl₃) δ 6.79 (dd, 2H, *J* = 5.7 and 3.5 Hz), 6.68 (dd, 2H, *J* = 5.7 and 3.5 Hz), 3.28 (br s, 2H), 3.15 (q, 4H, *J* = 7.2 Hz), 1.31 (t, 6H, *J* = 7.2 Hz).

N,N'-Diethylbenzimidazolium Chloride (7).⁵⁴ The dark-red oil obtained previously was dissolved in HC(OEt)₃ (80 mL). Concentrated aqueous HCl (0.8 mL) and HCO₂H (three drops) were added. The resulting mixture was stirred under argon at 80 °C for 2 h. After cooling to room temperature, ethyl acetate (25 mL) was added to form a precipitate, which was filtered, washed with ethyl acetate (3 × 5 mL), and dried to give 2.9 g of the title compound as a beige powder (90%). Mp 84.4–85.4 °C. ¹H NMR (250 MHz, CDCl₃) δ 11.78 (s, 1H, NCH=N⁺), 7.74–7.63 (m, 4H, ArH), 4.70 (q, 4H, *J* = 7.5 Hz), 1.73 (t, 6H, *J* = 7.5 Hz). ¹³C NMR (75 MHz, CDCl₃) δ 142.5 (NCH=N⁺), 131.2 (Carom), 127.1 (CHarom), 113.1 (CHarom), 42.8 (CH₂N), 14.9 (CH₃CH₂). Anal. Calcd for (C₁₁H₁₅ClN₂)(H₂O)_{0.3}: C, 61.14; H, 7.28; N, 12.96. Found C, 61.40; H, 7.38; N, 12.80. HRMS (ESI) *m/z* calcd for C₁₁H₁₅N₂ 175.12298; found 175.12323 [M - Cl⁻].

1,3-Diethylbenzimidazol-2-ylidene Silver(I) Chloride (L¹-AgCl). To a solution of *N,N'*-diethylbenzimidazolium chloride (0.8 g, 3.8 mmol) in CH₂Cl₂ (45 mL) was added Ag₂O (0.44 g, 1.9 mmol). The mixture was stirred at 20 °C for 16 h and then filtered over Celite. The filtrate was reduced to about 10 mL under reduced pressure. Heptane was added to the residual solution until precipitation of a white solid. The precipitate was isolated by filtration, washed with pentane, and dried under vacuum to give the title compound as an off-white powder (0.9 g, 75%). Mp 156.7–157.6 °C. ¹H NMR (CD₂Cl₂, 250 MHz) δ 7.55–7.52 (m, 2H, ArH), 7.44–7.41 (m, 2H, ArH), 4.47 (q, 4H, *J* = 7.3 Hz), 1.53 (t, 6H, *J* = 7.3 Hz). ¹³C NMR (100 MHz, CD₂Cl₂) δ 186.9 (Ccarbene, small singlet), 133.8 (Carom), 124.3 (CHarom), 111.8 (CHarom), 45.0 (CH₂-N), 16.2 (CH₃-CH₂). The carbenic carbon was clearly visible by HMBC experiment (CDCl₃, 600 MHz). Anal. Calcd for (C₁₁H₁₄AgClN₂)(C₂H₅)₂: C, 42.53; H, 4.72; N, 8.63. Found: C, 42.61; H, 4.62; N, 8.77 (contains residual traces of pentane). HRMS (ESI) *m/z* calcd for C₂₂H₂₆N₄Ag 455.13594; found 455.13573 [2 M - AgCl₂⁻] ([NHC]₂Ag⁺).

Preparation of Ag and Au Nanocrystals. *Typical Conditions Corresponding to Figures 4 and 5 and Table 1.* Silver or gold precursors (0.125 mmol) and dodecanethiol (250 μL, 1 mmol) were dissolved in dry degassed toluene (12.5 mL) and heated at 100 °C (oil bath) under vigorous magnetic stirring. To the mixture was added (at 100 °C) either (a) a solution of NH₃BH₃ (1.25 mmol) in toluene (5 mL) and ethanol (2.5 mL) or (b) a solution of ^tBuNH₂BH₃ (2.5 mmol) in toluene (1 mL). The reaction was allowed to proceed for 30 min (at 100 °C) before cooling to room temperature. Toluene was evaporated under a nitrogen flow. The as-formed nanocrystals were washed with ethanol and dried. The nanocrystals were resuspended in toluene for TEM analyses unless otherwise stated.

Size Selection. Size selection was carried out in the following cases: (i) Reduction of L¹-AuCl by ^tBuNH₂BH₃ (Table 1, entry 1):

The nanocrystals were precipitated once by addition of EtOH to a solution in toluene. (ii) Reduction of Ag-NHCs: Silver nanocrystals were size-segregated twice by precipitation with pyridine and then washed twice with EtOH.⁵⁵

Nanocrystal Size and Size Distribution. The average diameter (*D*) and the size distribution of the nanocrystals were determined by using ImageJ software (dm3 plugin) and by measuring about 500 nanocrystals in arbitrarily chosen areas of the photographs. The size distribution is reported as the standard deviation (σ) which is calculated according to the following formula: $\sigma = \{(D_i - D)^2 / (n - 1)\}^{1/2}$.

Reaction of Ag and Au-NHCs with DDT. Silver or gold precursors (0.125 mmol) and dodecanethiol (250 μL) were dissolved in dry toluene (12.5 mL) and heated at 100 °C under vigorous magnetic stirring for 0.5 h. Toluene was evaporated under nitrogen flow. The residue was then resuspended in CD₂Cl₂ for ¹H NMR analyses.

■ ASSOCIATED CONTENT

● Supporting Information

NMR spectra of new compounds, NMR analyses of Au nanocrystals and washing layers, and additional TEM images of Ag and Au nanocrystals. This material is available free of charge via the Internet at <http://pubs.acs.org>.

■ AUTHOR INFORMATION

Corresponding Authors

*E-mail: marie-paule.pileni@upmc.fr.

*E-mail: sylvain.roland@upmc.fr.

Notes

The authors declare no competing financial interest.

■ ACKNOWLEDGMENTS

This research has been supported from Advanced Grant of the European Research Council under Grant Agreement No. 267129. X.L. is thankful for the financial support from the China Scholarship Council.

■ REFERENCES

- (1) Turkevich, J.; Stevenson, P. L.; Hillier, J. A study of the nucleation and growth processes in the synthesis of colloidal gold. *Discuss. Faraday Soc.* **1951**, *11*, 55.
- (2) Schmid, G. Large clusters and colloids. Metals in the embryonic state. *Chem. Rev.* **1992**, *92*, 1709.
- (3) Cushing, B. L.; Kolesnichenko, V. L.; O'Connor, C. J. Recent advances in the liquid-phase syntheses of inorganic nanoparticles. *Chem. Rev.* **2004**, *104*, 3893.
- (4) Daniel, M.-C.; Astruc, D. Gold nanoparticles: assembly, supramolecular chemistry, quantum-size-related properties, and applications toward biology, catalysis, and nanotechnology. *Chem. Rev.* **2004**, *104*, 293.
- (5) Park, J.; Joo, J.; Soon Gu Kwon, S. G.; Jang, Y.; Hyeon, T. Synthesis of monodisperse spherical nanocrystals. *Angew. Chem., Int. Ed.* **2007**, *46*, 4630.
- (6) Sun, Y. Controlled synthesis of colloidal silver nanoparticles in organic solutions: empirical rules for nucleation engineering. *Chem. Soc. Rev.* **2013**, *42*, 2497.
- (7) Pileni, M.-P. The role of soft colloidal templates in controlling the size and shape of inorganic nanocrystals. *Nat. Mater.* **2003**, *2*, 145–150.
- (8) Brust, M.; Walker, M.; Bethell, D.; Schiffrin, D. J.; Whyman, R. Synthesis of thiol-derivatised gold nanoparticles in a two-phase liquid-liquid system. *J. Chem. Soc., Chem. Commun.* **1994**, 801.
- (9) Brust, M.; Fink, J.; Bethell, D.; Schiffrin, D. J.; Kiely, C. Synthesis and reactions of functionalised gold nanoparticles. *J. Chem. Soc., Chem. Commun.* **1995**, 1655.

- (10) Rowe, M. P.; Plass, K. E.; Kim, K.; Kurdak, Ç.; Zellers, E. T.; Matzger, A. J. Single-phase synthesis of functionalized gold nanoparticles. *Chem. Mater.* **2004**, *16*, 3513.
- (11) Zheng, N.; Fan, J.; Stucky, G. D. One-step one-phase synthesis of monodisperse noble-metallic nanoparticles and their colloidal crystals. *J. Am. Chem. Soc.* **2006**, *128*, 6550 (Au nanocrystals of 6.2 nm \pm 4.8% are formed from PPh₃AuCl by reduction with an amine-borane in the presence of dodecanethiol).
- (12) Tang, Y.; Ouyang, M. Tailoring properties and functionalities of metal nanoparticles through crystallinity engineering. *Nat. Mater.* **2007**, *6*, 754.
- (13) Song, J.; Kim, D.; Lee, D. Size control in the synthesis of 1–6 nm gold nanoparticles via solvent-controlled nucleation. *Langmuir* **2011**, *27*, 13854.
- (14) Bourissou, D.; Guerret, O.; Gabbai, F. P.; Bertrand, G. Stable carbenes. *Chem. Rev.* **2000**, *100*, 39.
- (15) Herrmann, W. A. N-Heterocyclic carbenes: A new concept in organometallic catalysis. *Angew. Chem., Int. Ed.* **2002**, *41*, 1290.
- (16) Hahn, F. E.; Jahnke, M. C. Heterocyclic carbenes: Synthesis and coordination chemistry. *Angew. Chem., Int. Ed.* **2008**, *47*, 3122.
- (17) Jacobsen, H.; Correa, A.; Poater, A.; Costabile, C.; Cavallo, L. Understanding the M–(NHC) (NHC = N-heterocyclic carbene) bond. *Coord. Chem. Rev.* **2009**, *253*, 687.
- (18) Benhamou, L.; Chardon, E.; Lavigne, G.; Bellemin-Laponnaz, S.; César, V. Synthetic routes to N-heterocyclic carbene precursors. *Chem. Rev.* **2011**, *111*, 2705.
- (19) Poater, A.; Cosenza, B.; Correa, A.; Giudice, S.; Ragone, F.; Scarano, V.; Cavallo, L. SambVca: A web application for the calculation of the buried volume of N-heterocyclic carbene ligands. *Eur. J. Inorg. Chem.* **2009**, 1759.
- (20) Diez-Gonzalez, S.; Marion, N.; Nolan, S. P. N-Heterocyclic carbenes in late transition metal catalysis. *Chem. Rev.* **2009**, *109*, 3612.
- (21) Hindi, K. M.; Panzner, M. J.; Tessier, C. A.; Cannon, C. L.; Youngs, W. J. The medicinal applications of imidazolium carbene-metal complexes. *Chem. Rev.* **2009**, *109*, 3859.
- (22) Teyssot, M. L.; Jarrousse, A. S.; Manin, M.; Chevy, A.; Roche, S.; Norre, F.; Beaudoin, C.; Morel, L.; Boyer, D.; Mahiou, R.; Gautier, A. Metal–NHC complexes: A survey of anti-cancer properties. *Dalton Trans.* **2009**, 6894.
- (23) Vignolle, J.; Tilley, T. D. N-Heterocyclic carbene-stabilized gold nanoparticles and their assembly into 3D superlattices. *Chem. Commun.* **2009**, 7230.
- (24) Hurst, E. C.; Wilson, K.; Fairlamb, I. J. S.; Chechik, V. N-Heterocyclic carbene coated metal nanoparticles. *New J. Chem.* **2009**, *33*, 1837.
- (25) Huang, R. T. W.; Wang, W. C.; Yang, R. Y.; Lu, J. T.; Lin, I. J. B. Liquid crystals of gold(I) N-heterocyclic carbene complexes. *Dalton Trans.* **2009**, 7121.
- (26) Lee, C. K.; Vasam, C. S.; Huang, T. W.; Wang, H. M. J.; Yang, R. Y.; Lee, C. S.; Lin, I. J. B. Silver(I) N-heterocyclic carbenes with long N-alkyl chains. *Organometallics* **2006**, *25*, 3768.
- (27) Melaiye, A.; Sun, Z.; Hindi, K.; Milsted, A.; Ely, D.; Reneker, D. H.; Tessier, C. A.; Youngs, W. J. Silver(I)–imidazole cyclophane gem-diol complexes encapsulated by electrospun terephthalic nanofibers: Formation of nanosilver particles and antimicrobial activity. *J. Am. Chem. Soc.* **2005**, *127*, 2285.
- (28) Serpell, C. J.; Cookson, J.; Thompson, A. L.; Brown, C. M.; Beer, P. D. Haloaurate and halopalladate imidazolium salts: structures, properties, and use as precursors for catalytic metal nanoparticles. *Dalton Trans.* **2013**, *42*, 1385.
- (29) No data concerning the size and size distribution of the spherical nanocrystals are reported.
- (30) Garrison, J. C.; Youngs, W. J. Ag(I) N-heterocyclic carbene complexes: Synthesis, structure, and application. *Chem. Rev.* **2005**, *105*, 3978.
- (31) Lin, I. J. B.; Vasam, C. S. Preparation and application of N-heterocyclic carbene complexes of Ag(I). *Coord. Chem. Rev.* **2007**, *251*, 642.
- (32) Goubet, N.; Ding, Y.; Brust, M.; Wang, Z. L.; Pileni, M.-P. A way to control the gold nanocrystals size: Using seeds with different sizes and subjecting them to mild annealing. *ACS Nano* **2009**, *3*, 3622.
- (33) Saunders, A. E.; Sigman, M. B.; Korgel, B. A. Growth kinetics and metastability of monodisperse tetraoctylammonium bromide-capped gold nanocrystals. *J. Phys. Chem. B* **2004**, *108*, 193.
- (34) Treatment of L³–AuCl with LiBEt₃H was previously reported to generate a stable gold hydride complex. Tsui, E. Y.; Muller, P.; Sadighi, J. R. Reactions of a stable monomeric gold(I) hydride complex. *Angew. Chem., Int. Ed.* **2008**, *47*, 8937.
- (35) This result is comparable to that reported in the one-phase reduction of AuPPh₃Cl (see ref 11).
- (36) de Frémont, P.; Stevens, E. D.; Eelman, M. D.; Fogg, D. E.; Nolan, S. P. Synthesis and characterization of gold(I) N-heterocyclic carbene complexes bearing biologically compatible moieties. *Organometallics* **2006**, *25*, 5824.
- (37) Dance, I. G.; Fisher, K. J.; Herath Banda, R. M.; Scudder, M. L. Layered structure of crystalline compounds silver thiolates (AgSR). *Inorg. Chem.* **1991**, *30*, 183.
- (38) Baena, M. J.; Espinet, P.; Lequerica, M. C.; Levelut, A. M. Mesogenic behavior of silver thiolates with layered structure in the solid state: Covalent soaps. *J. Am. Chem. Soc.* **1992**, *114*, 4182.
- (39) Bensebaa, F.; Ellis, T. H.; Kruus, E.; Voicu, R.; Zhou, Y. Characterization of self-assembled bilayers: Silver–alkanethiolates. *Langmuir* **1998**, *14*, 6579.
- (40) Runyon, J. W.; Steinhof, O.; Rasika Dias, H. V.; Calabrese, J. C.; Marshall, W. J.; Arduengo, A. J., III. Carbene-based Lewis pairs for hydrogen activation. *Aust. J. Chem.* **2011**, *64*, 1165.
- (41) Witt, D. Recent developments in disulfide bond formation. *Synthesis* **2008**, 2491.
- (42) Li, Y.; Zaluzhna, O.; Tong, Y. J. Identification of a source of size polydispersity and its solution in Brust–Schiffrin metal nanoparticle synthesis. *Chem. Commun.* **2011**, *47*, 6033.
- (43) Willey, T. M.; Vance, A. L.; van Buuren, T.; Bostedt, C.; Termiello, L. J.; Fadley, C. S. Rapid degradation of alkanethiol-based self-assembled monolayers on gold in ambient laboratory conditions. *Surf. Sci.* **2005**, *576*, 188.
- (44) Eloy, L.; Jarrousse, A.-S.; Teyssot, M.-L.; Gautier, A.; Morel, L.; Jolivald, C.; Cresteil, T.; Roland, S. Anticancer activity of silver–N-heterocyclic carbene complexes: Caspase-independent induction of apoptosis via mitochondrial apoptosis-inducing factor (AIF). *ChemMedChem* **2012**, *7*, 805.
- (45) de Frémont, P.; Scott, N. M.; Stevens, E. D.; Rammial, T.; Lightbody, O. C.; Macdonald, C. L. B.; Clyburne, J. A. C.; Abernethy, C. D.; Nolan, S. P. Synthesis of well-defined N-heterocyclic carbene silver(I) complexes. *Organometallics* **2005**, *24*, 6301.
- (46) Rammial, T.; Abernethy, C. D.; Spicer, M. D.; McKenzie, I. D.; Gay, I. D.; Clyburne, J. A. C. A monomeric imidazol-2-ylidene–silver(I) chloride complex: Synthesis, structure, and solid-state ¹⁰⁹Ag and ¹³C CP/MAS NMR characterization. *Inorg. Chem.* **2003**, *42*, 1391.
- (47) de Frémont, P.; Scott, N. M.; Stevens, E. D.; Nolan, S. P. Synthesis and structural characterization of N-heterocyclic carbene gold(I) complexes. *Organometallics* **2005**, *24*, 2411.
- (48) Rubbiani, R.; Kitanovic, I.; Alborzina, H.; Can, S.; Kitanovic, A.; Onambele, L. A.; Stefanopoulou, M.; Geldmacher, Y.; Sheldrick, W. S.; Wolber, G.; Prokop, A.; Wölfl, S.; Ott, I. Benzimidazol-2-ylidene gold(I) complexes are thioredoxin reductase inhibitors with multiple antitumor properties. *J. Med. Chem.* **2010**, *53*, 8608.
- (49) Er, J. A. V.; Tennyson, A. G.; Kamplain, J. W.; Lynch, V. M.; Bielawski, C. W. Synthesis and study of 5,5'-bibenzimidazolylidenes and their bimetallic complexes. *Eur. J. Inorg. Chem.* **2009**, 1729.
- (50) Hahn, F. E.; Radloff, C.; Pape, T.; Hepp, A. A nickel(II)-cornered molecular rectangle with biscarbene and 4,4'-bipyridine bridging groups. *Organometallics* **2008**, *27*, 6408.
- (51) Wang, H. M. J.; Lin, I. J. B. Facile synthesis of silver(I)–carbene complexes. Useful carbene transfer agents. *Organometallics* **1998**, *17*, 972.

(52) Sabitha, G.; Subba Reddy, B. V.; Srividya, R.; Yadav, J. S. Lithium chloride catalysed acetylation of alcohols, thiols, phenols and amines. *Synth. Commun.* **1999**, *29*, 2311.

(53) Alder, R. W.; Hyland, N. P.; Jeffery, J. C.; Riis-Johannessen, T.; Riley, D. J. Poly(1,1-bis(dialkylamino)propan-1,3-diyl)s; conformationally-controlled oligomers bearing electroactive groups. *Org. Biomol. Chem.* **2009**, *7*, 2704.

(54) Huang, W.; Guo, J.; Xiao, Y.; Zhu, M.; Zou, G.; Tang, J. Palladium–benzimidazolium salt catalyst systems for Suzuki coupling: Development of a practical and highly active palladium catalyst system for coupling of aromatic halides with arylboronic acids. *Tetrahedron* **2005**, *61*, 9783.

(55) Silver-coated particles are highly soluble in hexane and poorly soluble in pyridine. Progressive addition of pyridine to hexane led to agglomeration of the largest particles as a result of their greater van der Waals interactions; see: Taleb, A.; Petit, C.; Pileni, M.-P. Synthesis of highly monodisperse silver nanoparticles from AOT reverse micelles: A way to 2D and 3D self-organization. *Chem. Mater.* **1997**, *9*, 950. The same principle was applied to Au nanocrystals.

Supporting Information

Nanocrystals: Why Do Silver and Gold N-Heterocyclic Carbene Precursors Behave Differently?

Xiang Ling,^{a,b} Nicolas Schaeffer,^a Sylvain Roland*^b and Marie-Paule Pileni*^a

^a *Laboratoire des Matériaux Mésostructurés et Nanométriques, UMR CNRS 7070, UPMC-Université Paris 6, 4 place Jussieu, 75252 Paris, France. Fax: +33 1 44272515; Tel: +33 1 44272516*

E-mail: marie-paule.pileni@upmc.fr

^b *Institut Parisien de Chimie Moléculaire, UMR CNRS 7201, UPMC-Université Paris 6, 4 place Jussieu, 75252 Paris, France. Fax: +33 1 44277360; Tel: +33 1 44275567*

E-mail: sylvain.roland@upmc.fr

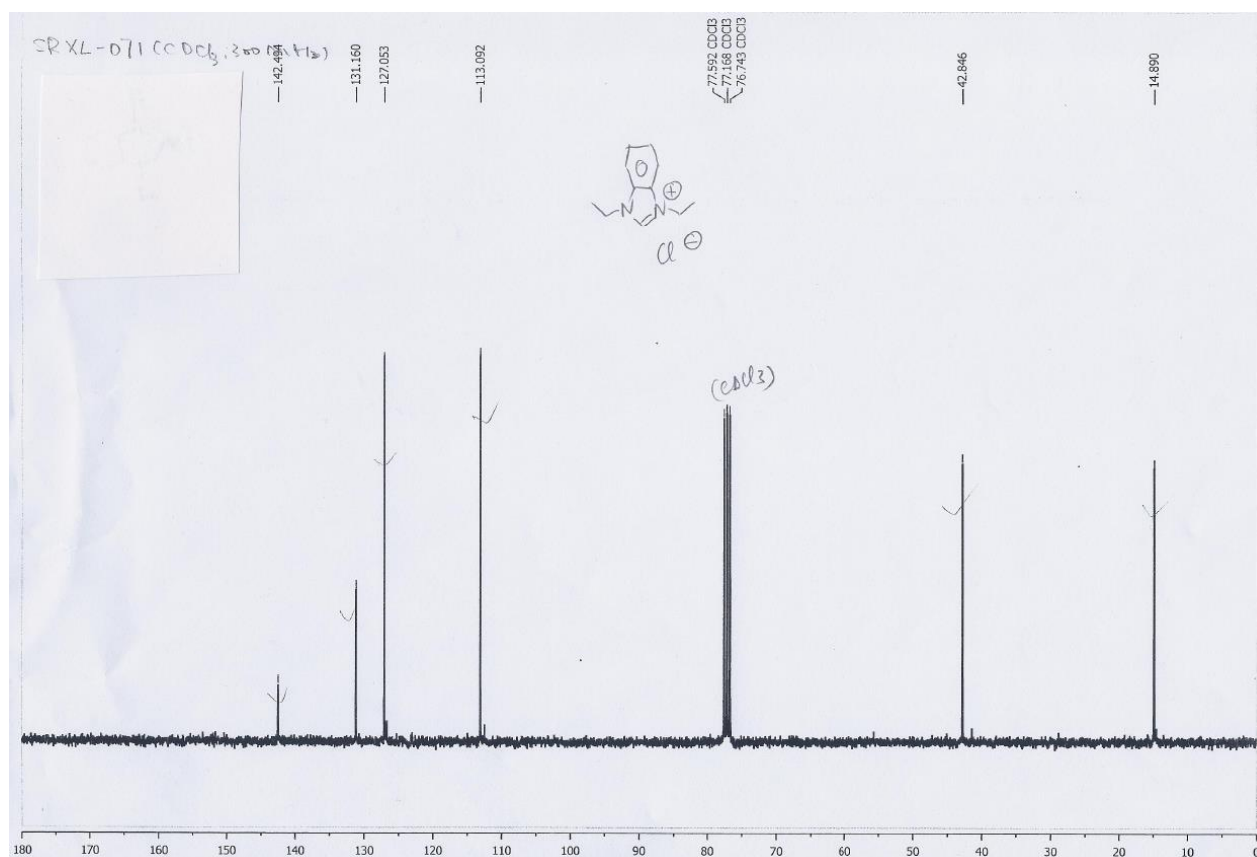
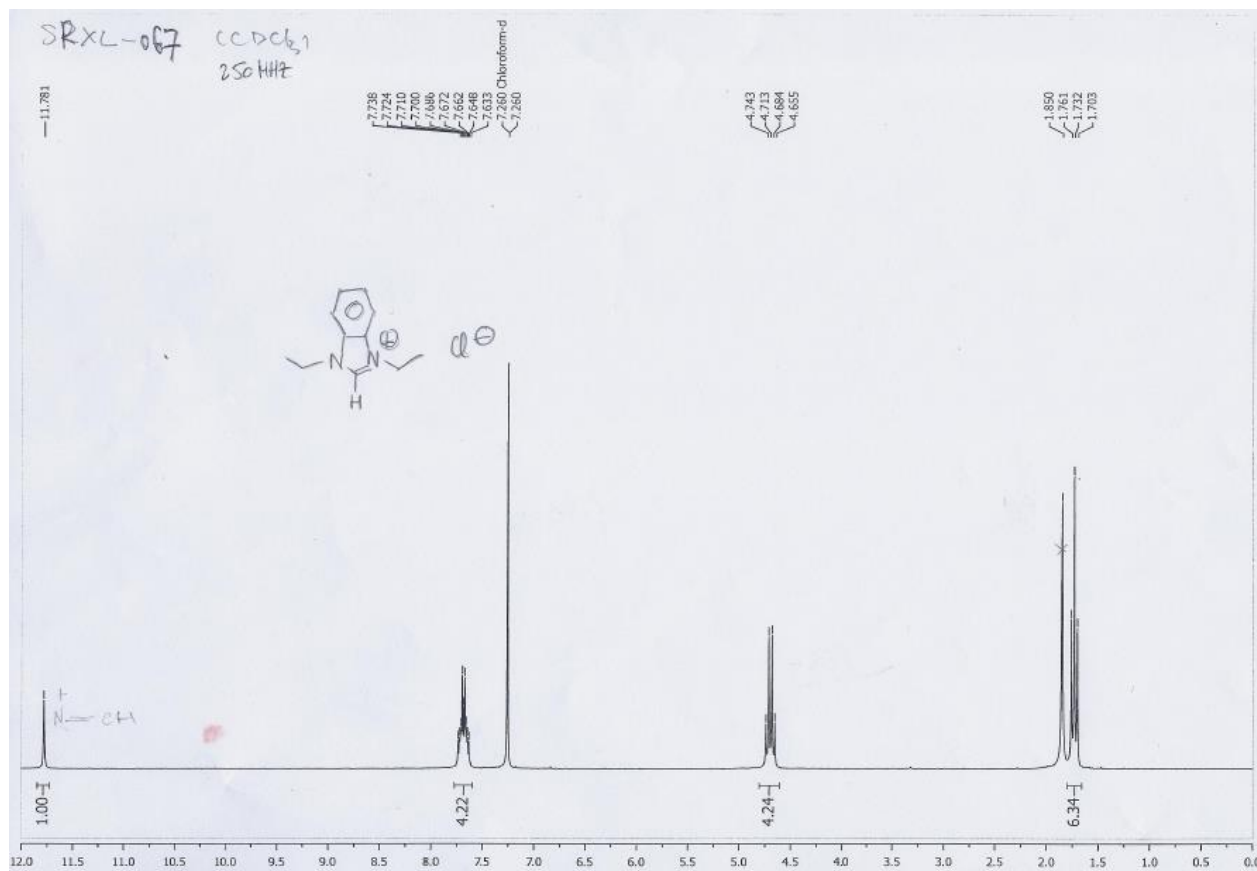
Table of contents

¹ H and ¹³ C NMR spectra of 7 and L¹-AgCl	43
Figure S1	45
Figure S2	46
Figure S3	47
Figure S4	48

Chapter 2 Well-defined Ag and Au-NHC complexes as precursors for one-phase synthesis of nanocrystals

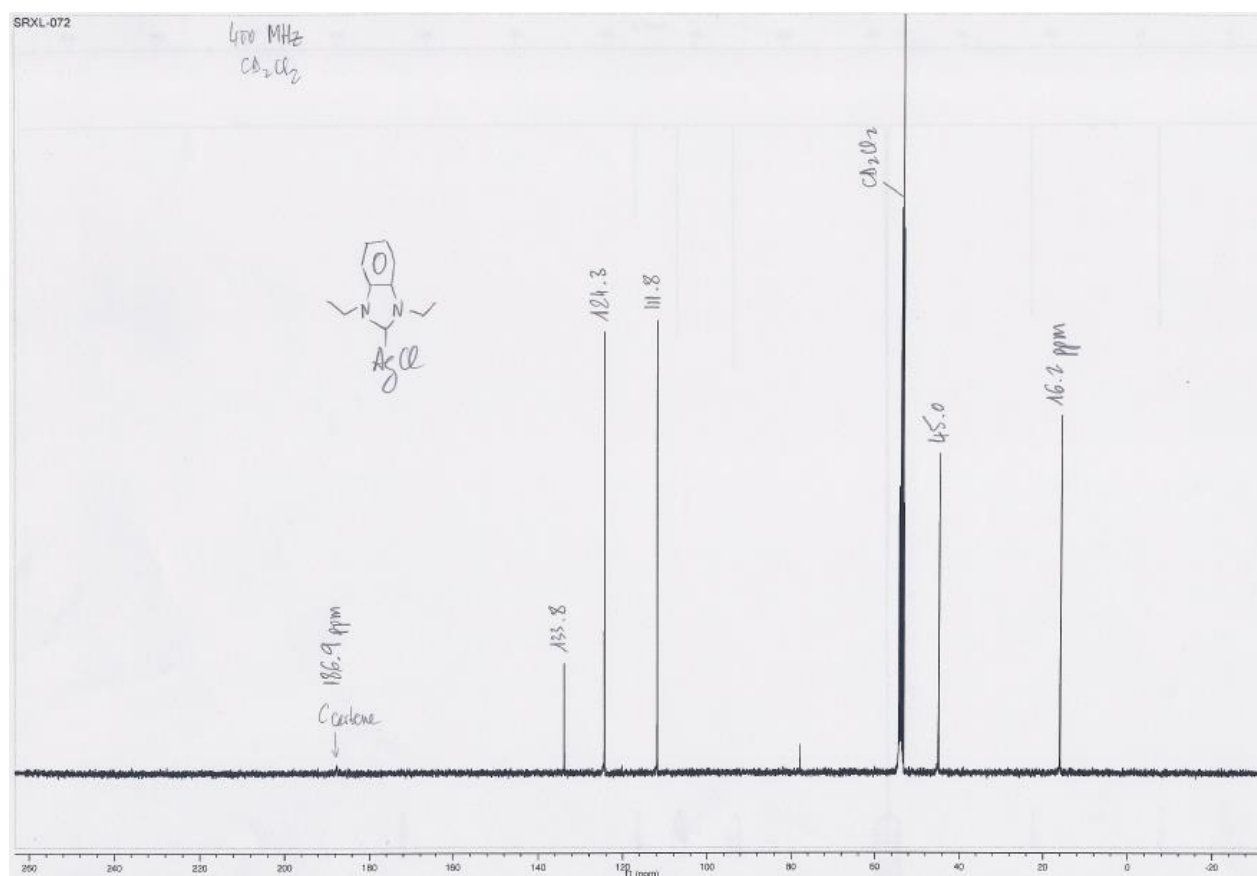
^1H and ^{13}C spectra of new compounds

N,N'-Diethylbenzimidazolium chloride (7)



N-Heterocyclic Carbenes coated Nanocrystals and Supracrystals

1,3-Diethylbenzimidazol-2-ylidene silver(I) chloride (L^1 -AgCl)



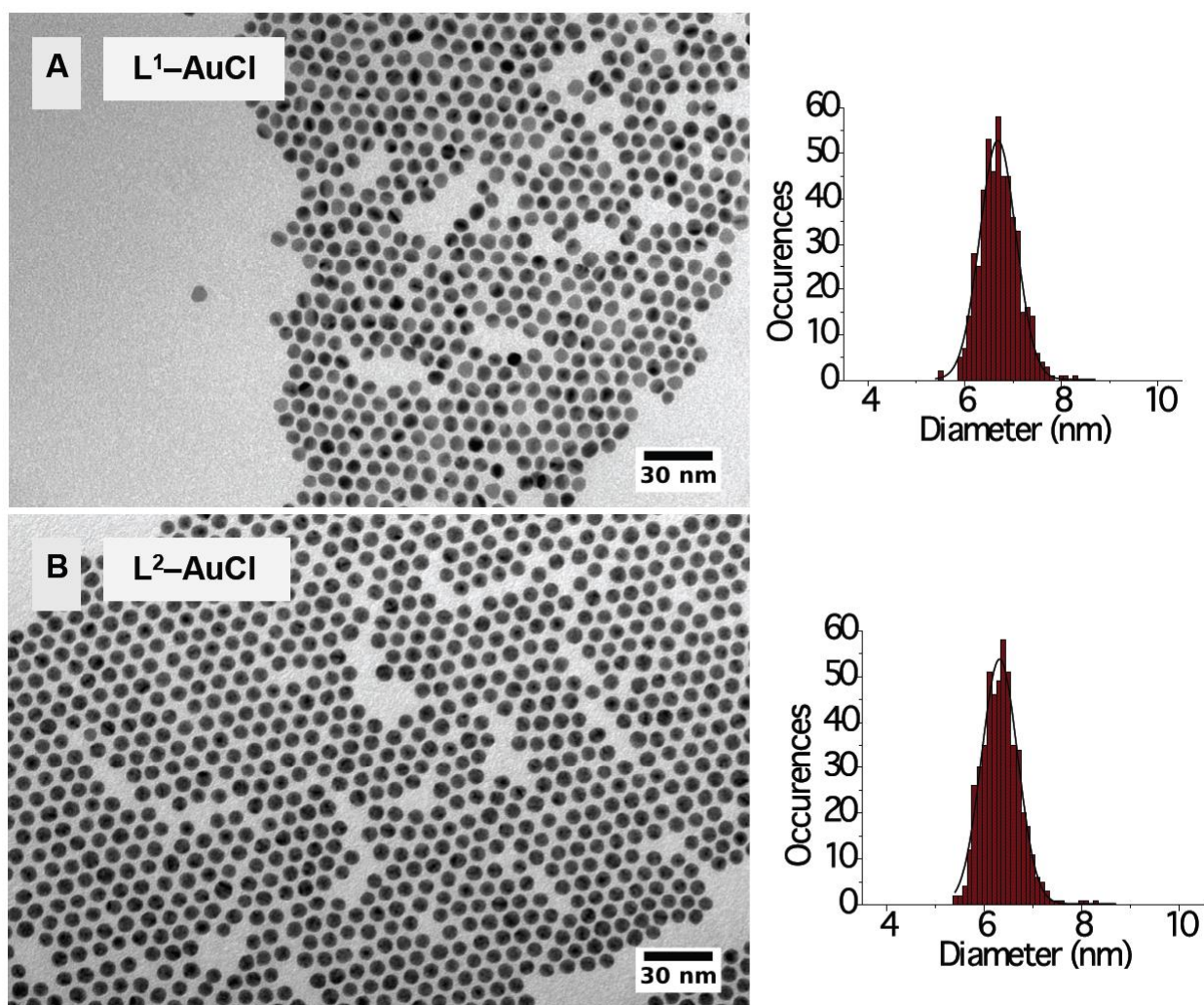


Figure S1. TEM images and size distributions of Au nanocrystals obtained from the reduction of L^1 -AuCl (A) and L^2 -AuCl (B) by t BuNH₂BH₃ in the presence of DDT.

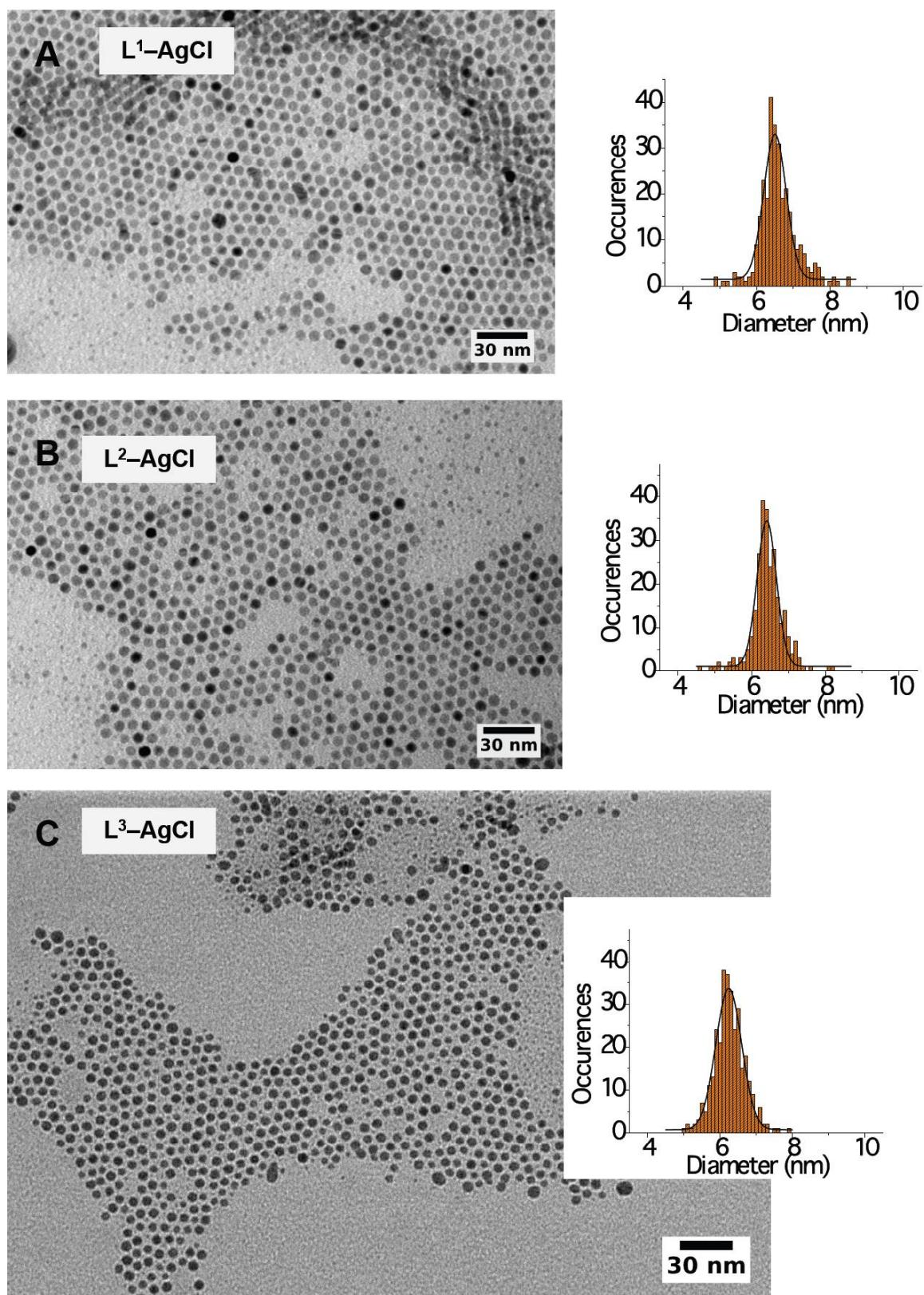


Figure S2. TEM images and size distributions of Ag nanocrystals obtained from the reduction of L¹-AgCl (A), L²-AgCl (B) and L³-AgCl (C) by ^tBuNH₂BH₃ in the presence of DDT.

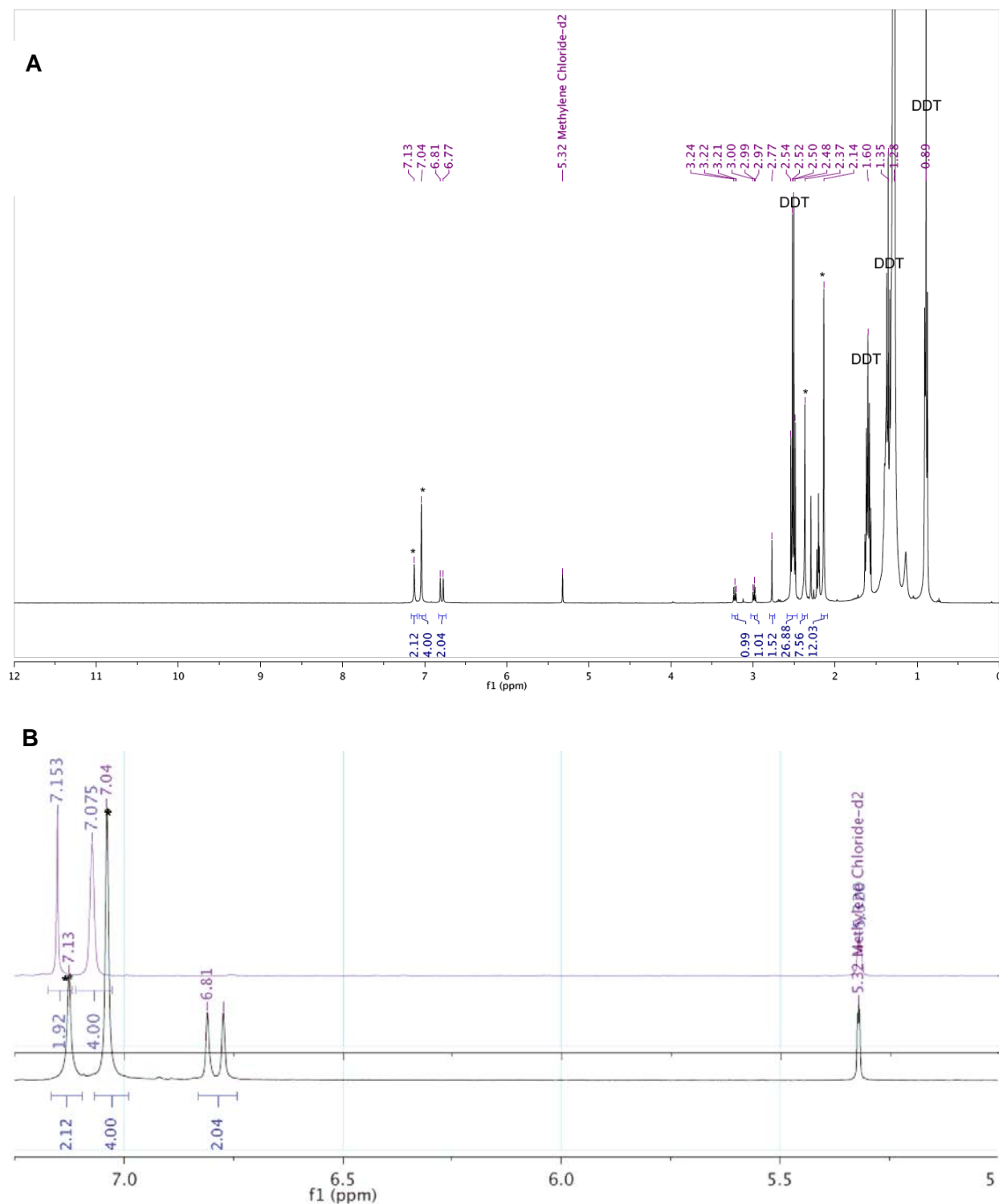


Figure S3. (A) ^1H NMR spectrum in CD_2Cl_2 of the combined washing layers from the preparation of Au nanocrystals by reduction of $\text{L}^2\text{-AuCl}$ with NH_3BH_3 in the presence of DDT. Signals corresponding to a derivative of L^2 are labelled with an asterisk. (B) Zoom of the same spectrum (5.0–7.5 ppm) and stacking with the spectrum of the initial gold complex $\text{L}^2\text{-AuCl}$ (purple spectrum).

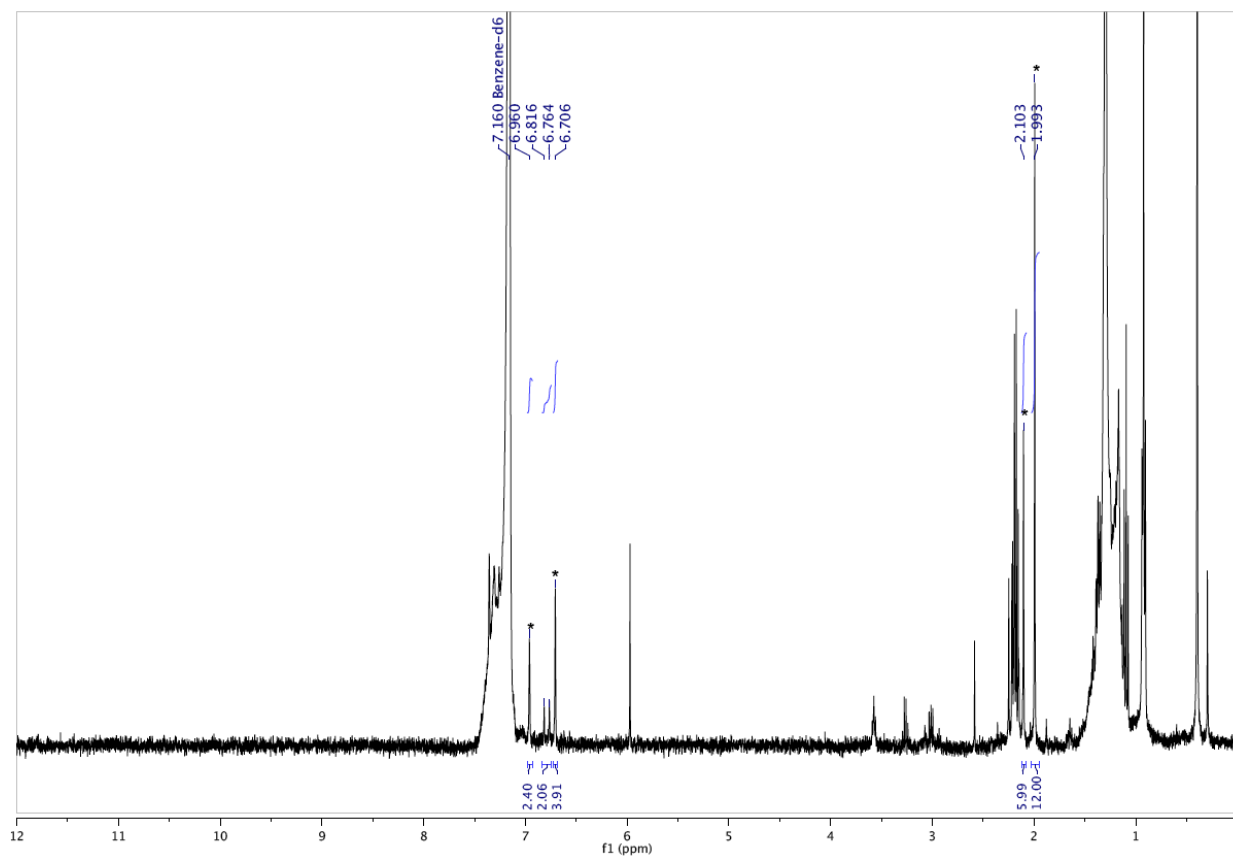


Figure S4. ¹H NMR spectrum in C₆D₆ of Au nanocrystals produced by reduction of L²-AuCl with NH₃BH₃ in the presence of DDT. Signals corresponding to a derivative of L² are labelled with an asterisk.

Chapter 3

Supracrystals of N-heterocyclic carbene-coated Au nanocrystals

3.1 Abstract

Controlling the generation of organized 3D assemblies of individual nanocrystals, called supracrystals, as well as their properties, is an important challenge for the design of new materials, in which the coating agent plays a major role. We present herein a new generation of structured fcc Au supracrystals made of *N*-heterocyclic carbene (NHC)-coated Au nanocrystals. The 3D assemblies were achieved by using benzimidazole-derived NHCs tailored with long alkyl chains at different positions. The average size of the nanocrystal precursors (4, 5 or 6 nm) and their ability to self-assemble were found to be dependent on the length, orientation and number of alkyl chains on the NHC. Thick and large supracrystal domains were obtained from 5 nm Au nanocrystals coated with NHCs substituted by C14 alkyl chains on the nitrogen atoms. Here, the geometry of both the $C_{\text{carbene}}\text{-Au}$ and $\text{N-C}_{\text{alkyl}}$ bonds induces a specific orientation of the alkyl chains, different from that of alkythiols, resulting in Au surface covering by the chains. However, the edge-edge distances in the supracrystals suggest that the supracrystals are stabilized by interdigitation of neighboring nanocrystals alkyl chains, whose terminal part must point outward with the appropriate geometry.

3.2 Supracrystals of N-heterocyclic carbene-coated Au nanocrystals

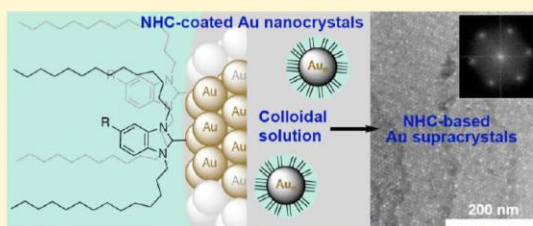
Chem. Mater. **2015**, *27*, 414

Supracrystals of N-Heterocyclic Carbene-Coated Au Nanocrystals

Xiang Ling,^{†,‡} Sylvain Roland,^{*,‡} and Marie-Paule Pileni^{*,†,§}[†]Sorbonne Universités, UPMC-Univ Paris 6, UMR 8233, MONARIS, F-75005, Paris, France[‡]Sorbonne Universités, UPMC-Univ Paris 6, UMR 8232, Institut Parisien de Chimie Moléculaire, F-75005, Paris, France[§]CEA/IRAMIS, CEA Saclay, 91191, Gif-sur-Yvette, France

Supporting Information

ABSTRACT: Controlling the generation of organized 3D assemblies of individual nanocrystals, called supracrystals, as well as their properties, is an important challenge for the design of new materials in which the coating agent plays a major role. We present herein a new generation of structured fcc Au supracrystals made of N-heterocyclic carbene (NHC)-coated Au nanocrystals. The 3D assemblies were achieved by using benzimidazole-derived NHCs tailored with long alkyl chains at different positions. The average size of the nanocrystal precursors (4, 5, or 6 nm) and their ability to self-assemble were found to be dependent on the length, orientation, and number of alkyl chains on the NHC. Thick and large supracrystal domains were obtained from 5 nm Au nanocrystals coated with NHCs substituted by C14 alkyl chains on the nitrogen atoms. Here, the geometry of both the C_{carbene}-Au and N-C_{alkyl} bonds induces a specific orientation of the alkyl chains, different from that of alkylthiols, resulting in Au surface covering by the chains. However, the edge-to-edge distances in the supracrystals suggest that the supracrystals are stabilized by interdigitation of neighboring nanocrystals alkyl chains, whose terminal part must point outward with the appropriate geometry.



INTRODUCTION

New strategies are required to circumvent the current limitations of miniaturization and develop new devices for future technologies. The “bottom-up” strategy, based on the formation of structured assemblies of nanocrystals (NCs), is considered as a promising approach to address this challenge. Owing to their specific properties, AuNCs have attracted particular attention as building blocks for designing such organized superstructures. AuNCs have been widely explored for biomedical applications, nanomaterials and catalysis.¹ Many efforts have been dedicated to the understanding and control of the different parameters involved in their formation.² AuNCs and other metal nanocrystals can self-assemble in various dimensionalities (1D, 2D, and 3D) to form a variety of structures including crystallographic higher order structures such as 3D superlattices called supracrystals. The interest of such colloidal supracrystals lies in their collective properties (electronic, magnetic, or optical properties), which are different from those of discrete nanoparticles and can be exploited for the design of novel materials and devices.³ Despite intense research and progress, challenges remain in the fundamental understanding of the self-assembly process and therefore, in mastering supracrystal formation.⁴

In AuNCs synthesis, it is well-established that the coating agent has a great influence on the average size, size distribution, shape, and stability.² Similarly, the nature/structure of the ligand (coating agent) and its properties (e.g., grafting density, mode of bonding with the nanocrystal surface, and solubility)

have a great influence on the self-assembly properties of the nanocrystals. The structure of the coating agent directly affects some of the competitive forces involved in superlattice formation which are related to the steric interactions (repulsive) and interdigitation phenomena (attractive).⁵ Furthermore, by controlling NCs average size and size distribution, the ligand determines whether supracrystals can form or not. Simulations showed that a polydispersity exceeding 10–12% impedes crystallization.⁶ Therefore, nearly monodisperse AuNCs dispersions with predominantly alkanethiols as well as alkylamines, carboxylic acids (decanoic acid and citrate), and ammoniums as coating agents have been used to grow Au superlattices.⁷ Among these, thiols exhibit the highest bond strength with Au. However, the development of stable and biocompatible materials from Au supracrystals remains a critical issue,⁸ and alternative ligands to sulfur-based ligands are needed to develop new materials.

In the recent decades, N-heterocyclic carbenes (NHCs) have emerged as an essential class of ligands in organometallic chemistry.⁹ Metal–NHCs have been widely investigated for catalytic applications,¹⁰ and their potential as biologically active complexes has been highlighted.¹¹ In both areas, the strength of the Au–C_{carbene} bond has been exploited to get stable Au–NHC complexes.¹² For the same reason, and because of their

Received: July 23, 2014

Revised: December 4, 2014

Published: December 15, 2014

high synthetic flexibility,¹³ NHCs are expected to be highly promising ligands for the development of functionalized materials.^{11c} A few reports described the formation of NHC-based self-assembled monolayers (SAMs) on Au surfaces.¹⁴ It was demonstrated that benzimidazole-derived NHCs provided SAMs with high stability in various conditions.^{14c} In addition, the use of appropriate NHCs has enabled modification of the properties of NHC-coated Au surfaces by chemical post-functionalizations.^{14b,c} Besides, NHCs have been involved as free NHCs or metal–NHC complexes for the preparation/stabilization of metal nanoparticles (metal = Pd, Ru, Ag, Au).¹⁵ However, the access to NHC-coated NCs with a narrow size distribution, a prerequisite for self-assembly into organized superstructures, remains a critical issue. Only one report described the obtention of 3D organized AuNCs superstructures with three NCs layers, obtained by slow evaporation of a concentrated solution of relatively monodisperse AuNCs on a transmission electron microscopy (TEM) grid.^{15d} Long-distance organized structures are required to observe changes in the physical properties (i.e., collective properties). To the best of our knowledge, no thick film made of 3D superlattice involving long-range 3D ordered organization of NHC-coated metal NCs has been reported to date. In addition, no information is available in the literature on the influence of the NHC shape on the self-assembly properties of NHC-coated NCs. This prompted us to design different benzimidazole-based NHC ligands (L^1 – L^5) as coating agents to study the influence of the NHC structure on the average size, size distribution, and the self-assembly properties of NHC-coated AuNCs (Figure 1). We sought to introduce long alkyl chains at different positions (R^1 or R^2) of the NHC ligands, pointing in different directions of the space, so as to explore the effect of the long alkyl chains with different spatial arrangements (I–III).

Herein, we report a new generation of NHC-based metal supracrystals, with large and thick domains, made of ordered 3D assemblies of NHC-coated AuNCs. The preparation of NHC-coated AuNCs (NHC = L^1 – L^5) stabilized by three different families of NHC ligands I–III, tailored with long alkyl chains at different positions, is described. The effect of the structure and shape of the NHC on nanocrystal size and on the self-assembly properties of NHC-coated AuNCs is discussed.

EXPERIMENTAL SECTION

Synthesis of NHC-Coated Au Nanocrystals. Reagents were purchased from commercial sources and used as received unless stated otherwise. Dichloromethane was distilled from CaH_2 . Dry and degassed (argon bubbling) toluene was used. Unless otherwise stated, nanocrystals syntheses were carried out in a glovebox under N_2 . The AuNC synthetic route is depicted in Scheme 1. The NHC ligands L^1 – L^5 were not isolated. They were generated in situ, as previously reported,^{15l} by deprotonation of the precursor benzimidazolium chloraurate salts 1–5 whose syntheses are detailed in the Supporting Information.

General Procedure. To a suspension of sodium hydride (60% dispersion in mineral oil, 7.4 mg, 0.188 mmol) in a 1:1 mixture of CH_2Cl_2 /toluene (7.2 mL) was added dropwise at 0.6 °C (ice bath) a solution of chloraurate benzimidazolium salt (1–5, Scheme 1) (0.12 mmol) in CH_2Cl_2 (1.8 mL). The mixture was stirred for 30 min at the same temperature. A solution of NaBH_4 (24 mg, 0.62 mmol) in water (0.9 mL) was added dropwise while maintaining the temperature at 0.6 °C (ice bath). After addition, the mixture was allowed to stir at

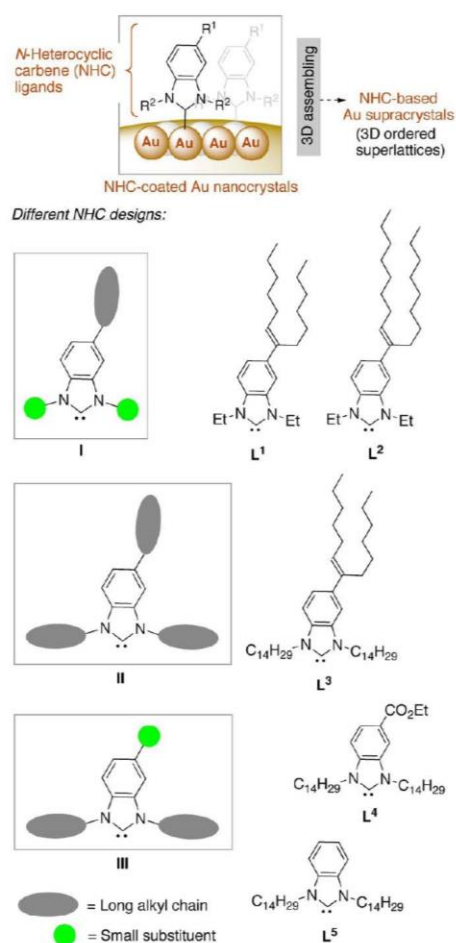
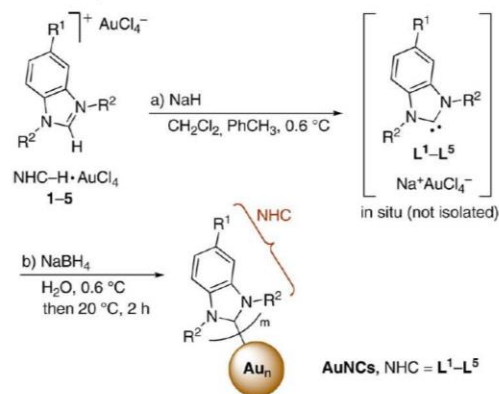


Figure 1. N-Heterocyclic carbene (NHC) ligands used in this study to investigate the preparation of NHC-coated Au nanocrystals and their 3D assembly into ordered superstructures.

Scheme 1. Synthesis of NHC-Stabilized AuNCs



room temperature for 2 h. The solvents were removed under a nitrogen flow to give a dark powder. The powder was washed with ethanol and the suspension was centrifuged. The

supernatant (EtOH) was removed. The residue was dried under a nitrogen stream to give Au nanocrystals as a dark powder. The as-formed nanocrystals were used for nuclear magnetic resonance (NMR) and X-ray photoelectron spectroscopy (XPS) analyses. The nanocrystals were resuspended in toluene to give a clear purple-red colloidal solution which was used for TEM analyses.

Size Selection. About 4 mL of the clear colloidal solution in toluene were centrifuged at 15 000 rpm for 30 min after which the supernatant was removed. The residual precipitate was dissolved in toluene (2 mL) and centrifuged at 13 000 rpm for 30 min. In the supernatant, NHC-coated Au nanocrystals with improved size distribution were obtained. The clear colloidal solution in toluene (supernatant) was used for TEM analyses and for the preparation of Au supracrystals.

Preparation of the 3D Superlattices (Supracrystals). A colloidal solution of Au nanocrystals ($[Au] = 5 \text{ mM}$) in toluene ($200 \mu\text{L}$) was introduced into a beaker with a silicon wafer ($5 \times 5 \text{ mm}^2$) at the bottom. The solvent was slowly evaporated (evaporation time = 4–5 h) under a nitrogen atmosphere at 50°C . The films formed on the silicon wafer and their structures were analyzed by scanning electron microscopy (SEM), high-resolution scanning electron microscopy (HRSEM), and small-angle X-ray diffraction (SAXRD).

Instrumentation. TEM, SEM, and HRSEM images were obtained with a JEOL JEM-1001 (100 kV), JEOL JSM-5510 LV, or Hitachi su-70 instruments, respectively. SAXRD measurements were performed with a homemade system with a rotating copper anode generator operating with a small-size focus ($0.1 \times 0.1 \text{ mm}^2$ in cross section) at 40 kV and 20 mA.

RESULTS AND DISCUSSION

Preparation of NHC-Coated Au Nanocrystals.

To prepare NHC-coated AuNCs with a series of NHC ligands, we were particularly attracted by the procedure described by Beer using chloroaurate(III) imidazolium salts as precursors,^{15f} involving a one-pot deprotonation/reduction sequence. In this method, NHC-coated AuNCs are formed after in situ deprotonation of the azolium salt to generate the NHC ligand, followed by reduction of gold. This avoids the isolation and characterization of Au–NHC complexes which have been frequently used as precursors for AuNCs synthesis,^{15a–g} as well as the formation of the free NHC ligand separately,^{15h–k} thus reducing the overall number of steps. Therefore, a series of new chloroaurate benzimidazolium salts 1–5 (NHC–H·AuCl₄) was synthesized to investigate the formation of NHC-coated AuNCs through this sequence (Figure 2). Both benzimidazole and imidazole-based NHCs have previously been used to investigate the stabilization of metal NCs.¹⁵ Herein, benzimidazole was preferentially chosen as the framework owing to the possibility to introduce appropriate substituents on the aromatic ring from easily accessible precursors. The salts 1–5 were readily obtained in two to five steps from commercially available 5-benzimidazole carboxylic acid or benzimidazole (see Scheme S1 in the Supporting Information). The long alkyl chains at position 5 on the benzene ring (1–3) were introduced by double addition of alkyl Grignard reagents on 5-ethoxycarbonyl benzimidazole whereas those on the nitrogen atoms (3–5) were introduced by simple N-alkylation of the benzimidazole unit.

These different combinations of long alkyl chains correspond to three different NHC ligand shapes as illustrated in Figure 1. In the first family (I: L¹, L²), long aliphatic chains of different

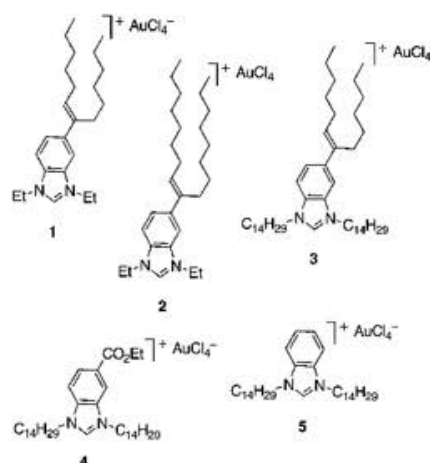


Figure 2. Structure of benzimidazolium chloroaurate precursors 1–5.

lengths (C7–C9) are positioned at position 5 (R¹) of the aromatic ring whereas the nitrogen atoms bear small ethyl substituents. In the second NHC family (II: L³), the long aliphatic chains are placed both on the nitrogen atoms (C14) and at position 5 of the aromatic ring to form a starlike ligand. In the last series (III: L⁴, L⁵), the long alkyl chains are only present on the nitrogen atoms. Here, an ester group was introduced at position 5 (R¹) to modulate the electronic properties of the NHC (L⁴). We also sought to determine the compatibility of this function, which is suitable for further postfunctionalization, with the preparation of NCs and supracrystals.

The synthesis of NHC-stabilized AuNCs was investigated with the chloroaurate benzimidazolium salt 5. The salt was deprotonated with NaH in CH₂Cl₂/PhCH₃ to form the NHC L⁵. To optimize the synthesis, various conditions (solvents and reducing agents) were tested for the second step of in situ reduction. TEM analyses revealed that the best AuNC quality in terms of size and shape homogeneity was achieved with NaBH₄ (aq) as the reducing agent, in biphasic conditions (Figure S1 in the Supporting Information).^{15f} Thus, the typical procedure presented in Scheme 1 was applied to 1–5. After deprotonation of the chloroaurate benzimidazolium salts by NaH, an aqueous solution of NaBH₄ was added dropwise by carefully controlling the temperature at 0.6°C and the reaction was allowed to proceed for 2 h at room temperature. Evaporation of the solvents and washing with ethanol gave L¹–L⁵-stabilized AuNCs as dark powders. The as-formed NCs were dispersed in toluene to give a clear purple-red colloidal solution. A drop of the solution was deposited on a TEM grid covered by amorphous carbon for TEM analysis. TEM analyses confirmed the formation of NCs regardless of the NHC ligand used (L¹–L⁵) (Figure S2 in the Supporting Information). To check the reproducibility of the procedure, each experiment was repeated three times. For a given NHC, similar results were obtained regardless of the batch.

¹H NMR and XPS were used to confirm the presence of the NHC ligands as stabilizing coating agents at the surface of the NCs. The ¹H NMR spectrum of L⁵-coated AuNCs in CD₂Cl₂ revealed the presence of NHC-based species with no detectable trace of the initial benzimidazolium precursor 5 nor of the corresponding chloride salt (Figure S3 in the Supporting

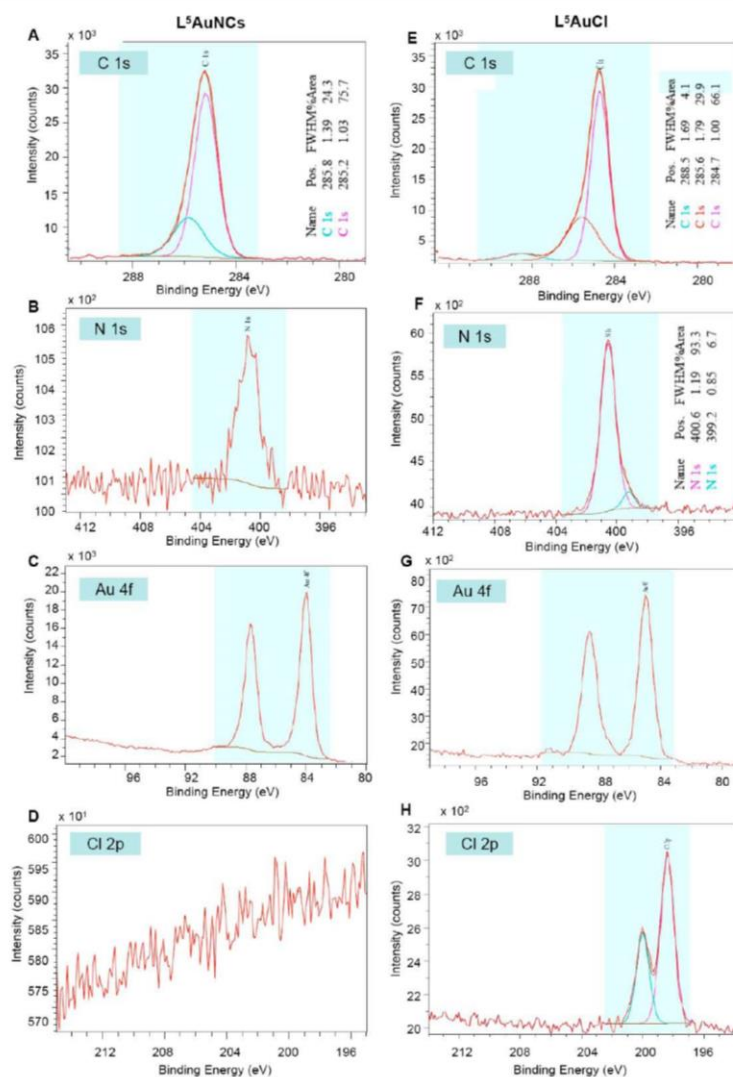


Figure 3. XPS analyses of L⁵-based Au nanocrystals (L⁵AuNCs) (A–D) and of the well-defined Au^I complex L⁵AuCl (E–H).

Information), which are respectively characterized by signals at 9.55 (5 in CD₂Cl₂) or around 11.6 ppm (chloride salt), corresponding to the C2 proton of the benzimidazolium moiety. This demonstrates that the formation of Au nanocrystals is not the result of a stabilization by an azolium salt. In addition, both the NMR signals patterns and the chemical shifts observed for the aromatic protons and the methylene groups on the nitrogen atoms (N–CH₂) are very similar (but not identical) to those of the well-defined L⁵AuCl complex used as a reference (Figure S3). This suggests that in situ-generated NHCs are transferred to the surface of the NC Au core and keep their structural integrity to generate NHC–[Au] moieties which are involved in the nanocrystal structure stabilization. This was confirmed by an important broadening of some peaks in the ¹H NMR spectrum of L⁵AuNCs. This broadening, which is due to the surrounding environment, is particularly significant here for the signals of the long alkyl chains, and is characteristic of ligands bound at the surface of NCs.

XPS was used to further demonstrate the presence of the NHC ligands at the surface of L⁵-based AuNCs. The well-defined L⁵AuCl gold(I) complex was used as a reference. XPS data of L⁵-based nanocrystals and L⁵AuCl are presented in Figure 3. Comparison of the C 1s spectra of L⁵AuNCs and L⁵AuCl shows that both structures have the same profile (Figure 3A,E). This indicates that the structural integrity of L⁵ is maintained in L⁵-coated AuNCs. This was confirmed by the C 1s binding energies observed for L⁵AuNCs (285.2 and 285.8 eV) which are consistent with those previously reported for NHC-coated AuNCs and Au surfaces.^{14ac} The XPS data also show the presence of nitrogen, with a N 1s signal having a binding energy of 401 eV, similar to that of the well-defined L⁵AuCl gold(I) complex, further supporting the presence of the NHC ligand (possessing two nitrogen atoms) at the surface of the NCs (Figure 3B,F). The Au 4f signal of L⁵AuNCs shows the presence of a predominant Au species, with two typical binding energies corresponding to Au 4f_{5/2} and Au 4f_{7/2} of 88.0

and 84.0 eV, respectively, which are consistent with binding energies of bulk metallic Au⁰ (Figure 3C).¹⁶ The Au 4f_{7/2} binding energy in L⁵AuCl, which is a gold(I) complex, is slightly higher than that of L⁵AuNCs, with a value of 85.0 eV consistent with an electron-rich Au^I complex (Figure 3G). These data show that the surface of the L⁵AuNCs has an overall oxidation state close to zero. This is consistent with a NC surface predominantly made of Au⁰ atoms combined with a lower number of NHC–[Au^I] species, the latter having a binding energy relatively close to that of zerovalent Au ($\Delta E \sim 1$ eV). No Cl 2p signal is visible in the XPS spectrum of L⁵AuNCs, corroborating NMR observations demonstrating that no azolium chloride salts are present to stabilize the NCs (Figure 3D). These data also show that no chloride-based Au^I or Au^{III} complexes (L⁵AuCl or L⁵AuCl₃), Au^{III} salts, nor Au–oxygen-containing species are present (or detectable) at the surface of the NCs. The XPS data also show a N/Au ratio of 1:4.4 corresponding to a NHC/Au ratio of 1 for 8.8. For Au(111) coated with linear alkanethiols, the maximum S/Au ratio was shown to be 1:3.¹⁷ Considering that each NHC ligand L⁵ bears two long alkyl chains, separated by the benzimidazole core, the N/Au ratio observed here suggests a relatively high packing of the NHC ligands L⁵ at the surface of the nanocrystals.

The different average sizes, ranging from 3.5 to 5.9 nm, observed by TEM with the different ligands (Table 1, and

Table 1. Summary of Au Nano- and Supracrystal Properties: Average Diameter (*d*), Size Distribution (Standard Deviation, σ), and Edge-to-Edge Distance in the Supracrystal (δ)^a

entry	NHC ligand	before size selection		after size selection		δ (nm)
		<i>d</i> (nm)	σ (%)	<i>d</i> (nm)	σ (%)	
1	L ¹	5.9	13.3	6.0	9.2	
2	L ²	5.7	20.4	5.7	11.2	1.89
3	L ³	3.5	19.9	4.0	11.9	
4	L ⁴	5.4	16.4	5.2	10.2	1.84
5	L ⁵	4.7	15.5	5.0	10.1	2.04

^aThe experiments were repeated three times. The results for one batch of NCs are presented here. Similar results were obtained with two other batches (see Table S1 in the Supporting Information).

Table S1 in the Supporting Information), suggest that the size of the NCs is controlled by the NHC ligand. This control, which is similarly observed in the different batches, seems to be dependent on the NHC family used and thus on the NHC shape. The following classification of the NHC ligands can be made based on the size of the NCs formed: L¹/L² > L⁴/L⁵ > L³. These three groups clearly correspond to the three different families (I–III) of NHCs presented in Figure 1.

TEM analyses revealed the presence of relatively nonuniform AuNCs displaying size distributions ranging from 13.3 to 20.4% (Table 1 and Figure S2). To study the self-assembly properties of AuNCs, size selection was required to reduce the size distribution. We found that NCs with narrower size distributions of 9–12% could readily be obtained by centrifuging at different speeds (Tables 1 and S1). After this procedure, the average size remains similar to that observed before the selection. This confirms the influence of the NHC ligand on NC size. As shown in Figure 4, L¹- and L²-coated AuNCs, in which both NHCs are substituted with long alkyl

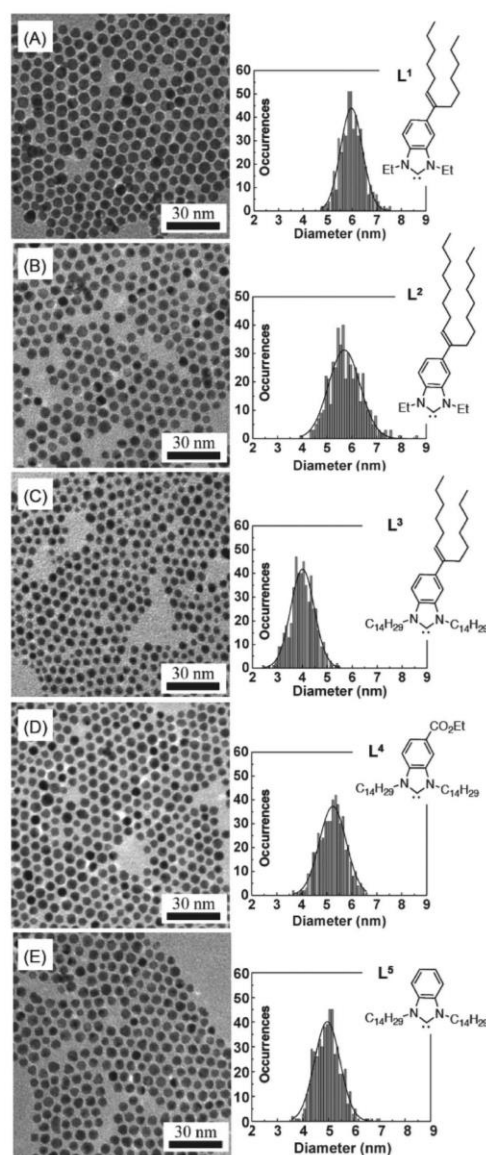


Figure 4. TEM images and size distributions of NHC-coated Au nanocrystals with ligand L¹ (A), L² (B), L³ (C), L⁴ (D), or L⁵ (E).

chains at position 5, display similar average size of 5.7 and 6.0 nm, respectively (Table 1, entries 1 and 2, and Figure 4A,B). By comparison, AuNCs stabilized by L⁴ and L⁵, which contain the long alkyl chains on the nitrogen atoms, are characterized by an average size of 5.0–5.2 nm (Table 1, entries 4 and 5, and Figure 4D,E). Finally, L³-derived AuNPs, in which the ligand is characterized by long aliphatic chains both on the nitrogen atoms and at position 5 of the aromatic ring, display the smallest size of 4.0 nm (Table 1, entry 3, and Figure 4C). This shows that the size of AuNCs can be tuned from ca. 4 to 6 nm by changing the combination and position of the alkyl chains on the NHC ligand. This effect was consistently observed in repeated experiments (Table 1, and Table S1 in the Supporting Information).

These results show that the NHC ligands L^1 and L^2 , possessing the smallest substituents (Et) on the nitrogen atoms, give the largest AuNCs (ca. 6 nm), whereas L^3 – L^5 , with long alkyl chains on the nitrogen atoms, lead to smaller NCs (4 or 5 nm). It has been previously shown that the use of bulky ligands (thiols) in AuNCs results in smaller core sizes by comparison with nonbulky ligands.¹⁸ Due to greater steric hindrance, bulky ligands induce greater steric overlap than nonbulky ligands as the size of the NC, and thus its radius of curvature increases. Consequently, the transport of metal atoms to the NC core, which is required for NC growth, is more rapidly stopped, producing NCs with smaller sizes. In the case of NHC ligands, due to the specific orientation of the N–C_{alkyl} bond, the nitrogen atom substituents play a major role in the steric interactions both with the metallic core and the neighboring ligand and the C14 alkyl chains in L^3 – L^5 likely occupy a larger volume near the surface of the NC than the ethyl groups of L^1 and L^2 , resulting in the formation of L^3 – L^5 -coated AuNCs of reduced sizes by comparison with L^1 – L^2 . 3D representations of L^1 , L^3 , and L^5 are presented in Figure 5.¹⁹ In the case of L^1 , the

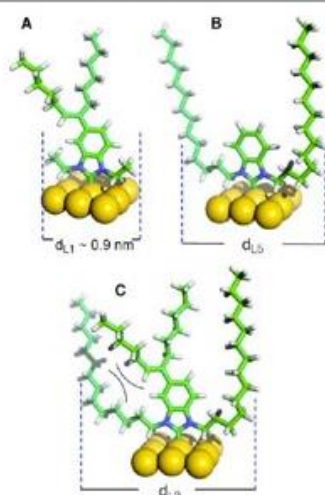


Figure 5. 3D representations of L^1 (A), L^5 (B), and L^3 (C), corresponding to the three different designs of NHC ligands (I–III in Figure 1).

distance between the ends of the ethyl groups on the nitrogen atoms was estimated at 0.9 nm (d_{L1} , Figure 5A). This value is in agreement with the distance previously measured on a Au(111) surface coated with a similar benzimidazole-based NHC (0.84 nm).^{14c} This distance is directly related to the volume occupied by L^1 at the surface of the NC. In L^5 , long alkyl chains are placed on the nitrogen atoms and point on both sides of the NHC ligand. Due to the geometry, these long chains are more distant to each other than in L^1 . Moreover, gauche defects are likely to occur at a distance from the nitrogen atom exceeding two carbons. Therefore, the maximum distance between the alkyl chains in L^5 as well as its volume might be higher than in L^1 ($d_{L5} > d_{L1}$, Figure 5B). This suggests that long alkyl chains on the nitrogen atoms induce greater covering of Au surface as well as greater steric overlap with neighboring ligands, therefore resulting in smaller NCs. In the case of L^3 (Figure 5C), the steric repulsion between the alkyl chains on the benzimidazole backbone and the C14 chains on the nitrogen atoms may push

the *N*-alkyl chains outwardly, leading to an increase of the NHC volume by comparison with L^5 as well as an increase of steric overlap ($d_{L3} > d_{L5} > d_{L1}$).

Preparation of NHC-Based Au Supracrystals. Several methods, involving self-assembly or assisted assembly processes, have been used to generate organized 3D superstructures from inorganic nanocrystals.³ Among these, the evaporation-mediated methods have given straightforward access to highly ordered and large-domain NC-based superstructures on solid surfaces. This approach, which has been previously used for the preparation of thiol-based AuNC superstructures, was investigated for the preparation of NHC-based Au supracrystals. In a typical procedure, a colloidal dispersion in toluene of L^1 – L^5 -stabilized AuNCs was poured into a beaker with a silicon wafer at the bottom, and the solvent was evaporated under an atmosphere of nitrogen at 50 °C (Figure S4 in the Supporting Information). At the end of the evaporation process, the as-formed materials were analyzed by SEM. The SEM images confirmed the formation of films. However, significant differences in the film morphology were observed depending on the NHC ligand (L^1 – L^5) involved in AuNC coating (Figures 6–8). To check the reproducibility of the results, each experiment was repeated several times from different batches of AuNCs. In addition, for one given batch of nanocrystals, two evaporation experiments were carried out in parallel. For the same ligand, the same film morphology was consistently observed. For Au supracrystals derived from L^1 (Figure 6A), a film consisting of a discontinuous top layer with small domains (e.g., zone a) and an underlying film (zone b) was observed. The maximum size of the top layer domains is 2–3 μm . HRSEM of zone a showed very small ordered domains having various heights and dislocations as confirmed by fast Fourier transform (FFT) of different parts of the domains (Figure 6B, FFT patterns of zone a¹ and a²). In contrast, the underlying film (zone b in Figure 6A) was found to be disordered (Figure 6C, FFT patterns of zone b¹). With NHC ligand L^2 , for which the aliphatic chain length is increased by two carbon atoms, the SEM images (Figures 6D) also showed in a discontinuous top layer (e.g., zone a) along with an underlying film (zone b). However, domains up to ca. 6 μm , larger than those obtained with L^1 -coated NCs, were observed in the top layer. In addition, these domains, analyzed by HRSEM (Figure 6E), were found to be highly ordered in a hexagonal pattern as confirmed by FFT (Figure 6E, pattern of zone a¹), the underlying film still being disordered (Figure 6F, FFT pattern of zone b¹).

With L^3 -based AuNCs, characterized by a ligand with long chains both on the nitrogen atoms and at position 5 of the aromatic ring, an amorphous colloidal film with a homogeneous distribution of very small scale supracrystals was obtained (Figure 7A). HRSEM images of zone a (bright zone) show very small organized domains (Figure 7B, FFT pattern of zones a¹ and a²), whereas the dark areas (zone b in Figure 7A) are disordered (Figure 7C, and FFT pattern of zones b¹). In contrast, the evaporation of colloidal solutions of L^4 - and L^5 -based AuNCs led in both cases to thick homogeneous films (ca. 0.5–1 μm) which are characterized by domains up to 8–10 μm with small surface defects and separated by cracks (Figure 8A,B). These domains, larger than those obtained from L^1 – L^3 , were found to be highly ordered in a hexagonal pattern as clearly demonstrated by the HRSEM images and confirmed by FFT (Figure 8C and S5).

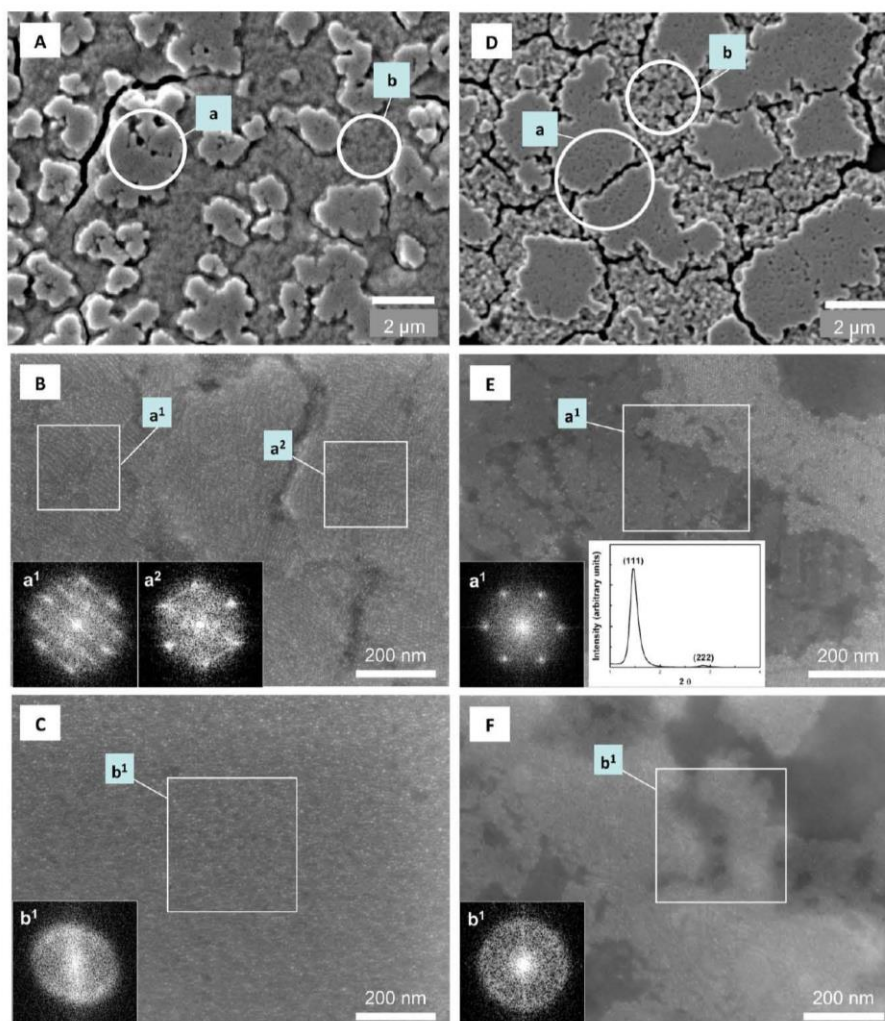


Figure 6. SEM images, HRSEM images, and SAXRD patterns of Au supracrystals coated by L^1 (A–C) and L^2 (D–F).

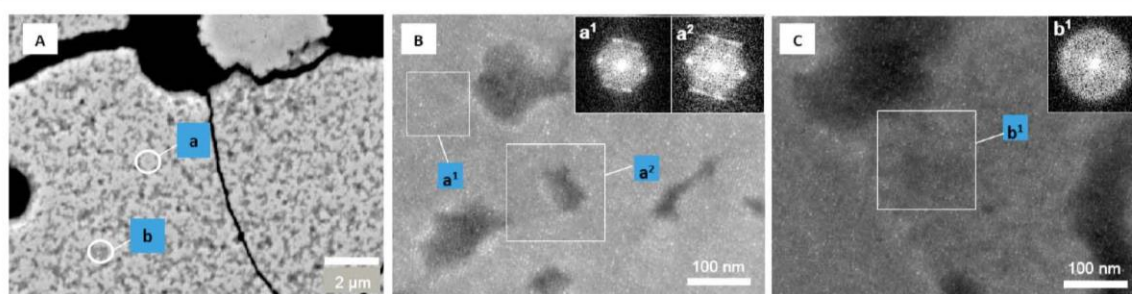


Figure 7. SEM image (A) and HRSEM images of zone a (B) and zone b (C) of Au supracrystals coated by L^3 .

To better understand the structure of the NHC-based Au supracrystals, SAXRD was used. The main peak of the SAXRD patterns (Figures 6E, 8C, and S5 for L^2 , L^5 , and L^4 , respectively) confirmed the formation of fcc (face-centered cubic) supracrystals with NHC ligands L^2 , L^4 , and L^5 .

These results show that the ability of the NHC-coated AuNCs presented here to self-assemble in organized structures is highly dependent on the position and length of the long alkyl chains on the NHC ligand. The ability of the NCs to self-assemble or not is independent of the size distribution (9.2–11.9%), which is similar for the different NCs, and independent

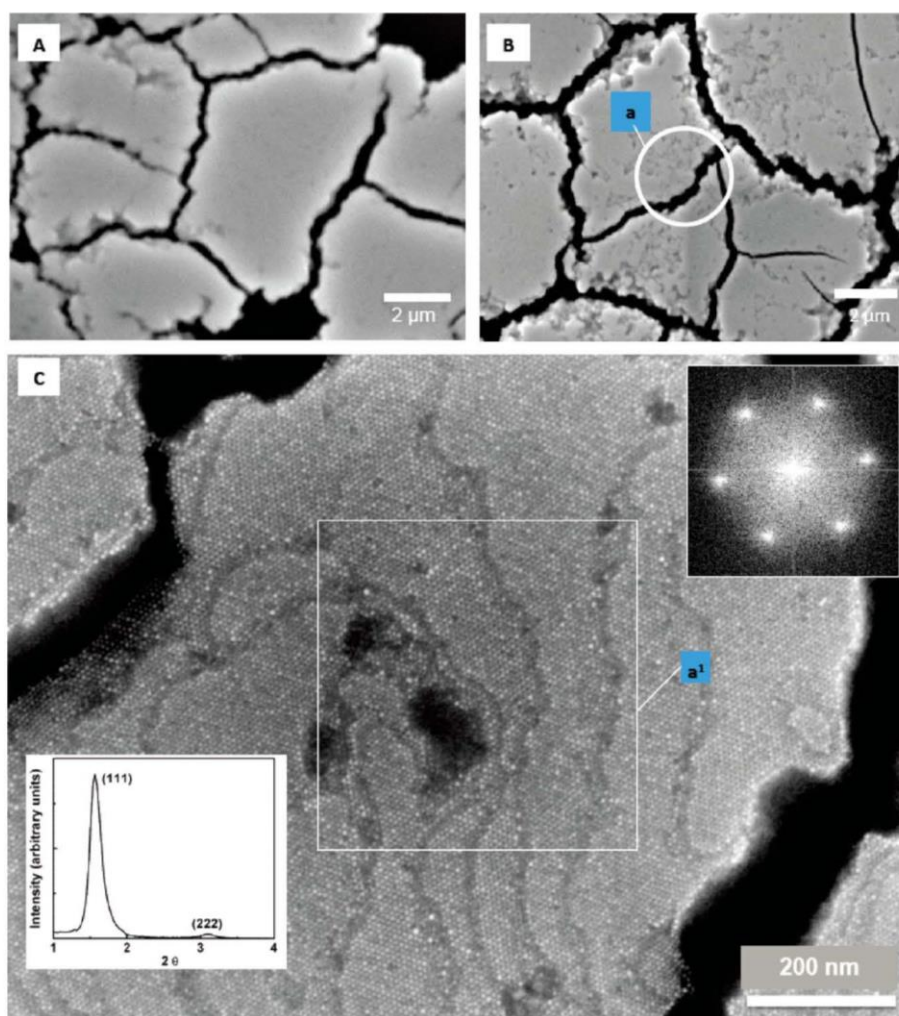


Figure 8. SEM images of Au supracrystals coated by L^4 (A) and L^5 (B). HRSEM image and SAXRD pattern for L^5 -based supracrystals (C).

of the average size of the NCs (4–6 nm). Although the smallest NCs derived from L^3 lead to a virtually amorphous colloidal film, a comparison of the different families of NHC used in the study strongly suggests that the structural properties and the shape of the NHC play a major role. With the first family of NHCs (L^1 – L^2), possessing outward-oriented long alkyl chains at position 5 of the benzimidazole core, films with similar morphologies are formed. However, comparison of L^1 and L^2 shows that the chain length plays an important role in obtaining organized superstructures. Organized domains up to 6 μm are generated with L^2 possessing the longest C9 chains at position 5, whereas L^1 leads to small-organized domains. This suggests that the chains in L^1 are too short to provide efficient stabilization of an organized assembly by interdigitation. With ligand L^3 that represents another NHC design where the chains are placed both on the nitrogen atoms and on the aromatic ring and point in at least three different directions, an amorphous film is generated. By comparison with L^1 and L^4 – L^5 , this lack of organization can be attributed to too short chains at position 5 and to an important steric overlap, associated with the

presence of four long alkyl chains on each ligand, which prevents interdigitation. It could also be attributed to a low covering of the metallic NC core by the ligand due to its volume, which is larger than that of L^1 – L^2 and L^4 – L^5 . In the third family of NHCs (L^4 – L^5), the long alkyl chains are oriented on both sides of the ligand and point initially, not outward the NC core, but rather in the direction of the metallic surface. Surprisingly, this design leads to highly organized large-domain films.

The edge-to-edge distances in the supracrystal were determined from the main peak of the SAXRD patterns by using the Bragg's law for L^2 , L^4 , and L^5 -based supracrystals (Table 1). For L^5 the distance is 2.04 nm. An estimation of the distance between the Au atom and the extremity of the aromatic part of the NHC gave a value of about 0.75 nm. This implies a remaining distance of 0.5 nm between the aromatic cores of two NHC ligands belonging to two neighboring AuNCs. To stabilize organized 3D NC superstructures, the long C14 alkyl chains on the nitrogen atoms must be involved in stabilizing interdigitations. For interdigitation to take place,

the long alkyl chains cannot adopt all-trans zigzag configuration but likely contain near-surface gauche defects so that the chains point outward with the appropriate geometry. This possible mode of action is presented in Figure 9. The estimated distance of 0.5 nm between the aromatic NHC cores (blue area) corresponds in the supracrystal to the interdigitation of at least five carbons of the alkyl chains.

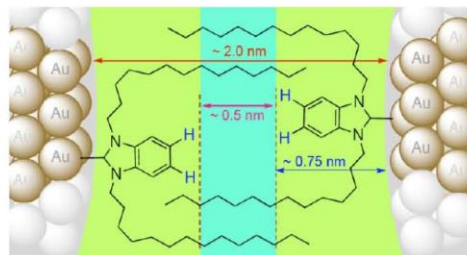


Figure 9. Proposed model for the self-assembly of 5 nm Au nanocrystals capped with L^5 .

CONCLUSION

We have shown here that thick and large supracrystal domains can be obtained from the 3D assembly of AuNCs coated with appropriate NHCs. The position, combination, and length of the long alkyl chains on the NHC ligand has a great influence on the AuNCs self-assembly properties. The best ligand design is unexpected, and corresponds to long alkyl chains pointing initially in the direction of the metallic Au core. A model is proposed in which gauche defects enable the alkyl chains to point outward with the appropriate geometry, resulting in stabilizing interdigitations in the supracrystals. NHCs form stronger bonds than thiols with Au and present high synthetic flexibility. Therefore, this new generation of NHC-coated Au supracrystals open new perspectives for the development of alternative stable and biocompatible Au-based materials, for their functionalization, and for the exploration of their properties.

ASSOCIATED CONTENT

Supporting Information

Detailed syntheses of compounds 1–5 and L^5AuCl , NMR spectras, and additional data (size distributions and TEM and SEM images) for AuNCs. This material is available free of charge via the Internet at <http://pubs.acs.org>.

AUTHOR INFORMATION

Corresponding Authors

*E-mail: sylvain.roland@upmc.fr.

*E-mail: mp.pileni@orange.fr.

Author Contributions

The manuscript was written through contributions of all authors. All authors have given approval to the final version of the manuscript.

Notes

The authors declare no competing financial interest.

ACKNOWLEDGMENTS

This research has been supported from an Advanced Grant of the European Research Council under Grant Agreement No.

267129. X.L. is thankful for the financial support of the China Scholarship Council. The authors thank the reviewers for their helpful comments for improvement and C. Calers for his invaluable assistance in XPS analyses.

REFERENCES

- (1) (a) Daniel, M.-C.; Astruc, D. *Chem. Rev.* **2004**, *104*, 293. (b) Sardar, R.; Funston, A. M.; Mulvaney, P.; Murray, R. W. *Langmuir* **2009**, *25*, 13840. (c) Boisselier, E.; Astruc, D. *Chem. Soc. Rev.* **2009**, *38*, 1759. (d) Guo, S.; Wang, E. *Anal. Chim. Acta* **2007**, *598*, 181. (e) Burda, C.; Chen, X.; Narayanan, R.; El-Sayed, M. A. *Chem. Rev.* **2005**, *105*, 1025. (f) Roucoux, A.; Schulz, J.; Patin, H. *Chem. Rev.* **2002**, *102*, 3757. (g) Astruc, D.; Lu, F.; Aranzas, J. R. *Angew. Chem., Int. Ed.* **2005**, *44*, 7852. (h) *Nanoparticles and catalysis*; Astruc, D., Ed.; Wiley-VCH: Weinheim, Germany, 2008.
- (2) (a) Alexandridis, P. *Chem. Eng. Technol.* **2011**, *34*, 15. (b) Zhao, P.; Li, N.; Astruc, D. *Coord. Chem. Rev.* **2013**, *257*, 638. (c) Cushing, B. L.; Kolesnichenko, V. L.; O'Connor, C. J. *Chem. Rev.* **2004**, *104*, 3893.
- (3) (a) Nie, Z.; Petukhova, A.; Kumacheva, E. *Nat. Nanotechnol.* **2010**, *5*, 15. (b) Pileni, M. P. *Acc. Chem. Res.* **2007**, *40*, 685. (c) Pileni, M. P. *Acc. Chem. Res.* **2008**, *41*, 1799. (d) Pileni, M. P. *J. Phys.: Condens. Matter* **2011**, *23*, 503102. (e) Pileni, M. P. *Acc. Chem. Res.* **2012**, *45*, 1965. (f) Talapin, D. V.; Lee, J.-S.; Kovalenko, M. V.; Shevchenko, E. V. *Chem. Rev.* **2010**, *110*, 389. (g) Prasad, B. L. V.; Sorensen, C. M.; Klabunde, K. J. *Chem. Soc. Rev.* **2008**, *37*, 1871. (h) Xu, L.; Ma, W.; Wang, L.; Xu, C.; Kuang, H.; Kotov, N. A. *Chem. Soc. Rev.* **2013**, *42*, 3114. (i) Podsiadlo, P.; Krylova, G.; Demortière, A.; Shevchenko, E. *J. Nanopart. Res.* **2011**, *13*, 15.
- (4) (a) Motte, L.; Billoudet, F.; Pileni, M.-P. *J. Phys. Chem.* **1995**, *99*, 16425. (b) Stoeva, S. L.; Prasad, B. L. V.; Uma, S.; Stoimenov, P. K.; Zaikovski, V.; Sorensen, C. M.; Klabunde, K. J. *J. Phys. Chem. B* **2003**, *107*, 7441. (c) Whetten, R. L.; Shafiqullin, M. N.; Khoury, J. T.; Schaff, T. G.; Vezmar, I.; Alvarez, M. M.; Wilkinson, A. *Acc. Chem. Res.* **1999**, *32*, 397. (d) Sigman, M. B.; Saunders, A. E.; Korgel, B. A. *Langmuir* **2003**, *20*, 978. (e) Yan, H.; Cingarapu, S.; Klabunde, K. J.; Chakrabarti, A.; Sorensen, C. M. *Phys. Rev. Lett.* **2009**, *102*, 095501. (f) Compton, O. C.; Osterloh, F. E. *J. Am. Chem. Soc.* **2007**, *129*, 7793.
- (5) Bishop, K. J. M.; Wilmer, C. E.; Soh, S.; Grzybowski, B. A. *Small* **2009**, *5*, 1600.
- (6) Auer, S.; Frenkel, D. *Nature* **2001**, *413*, 711.
- (7) (a) Weitz, D. A.; Oliveria, M. *Phys. Rev. Lett.* **1984**, *52*, 1433. (b) Prasad, B. L. V.; Stoeva, S. L.; Sorensen, C. M.; Klabunde, K. J. *Langmuir* **2002**, *18*, 7515. (c) Whetten, R. L.; Khoury, J. T.; Alvarez, M. M.; Murthy, S.; Vezmar, I.; Wang, Z. L.; Stephens, P. W.; Cleveland, C. L.; Luedtke, W. D.; Landman, U. *Adv. Mater.* **1996**, *8*, 428. (d) Goubet, N.; Portalès, H.; Yan, C.; Arfaoui, I.; Albouy, P.-A.; Mermat, A.; Pileni, M.-P. *J. Am. Chem. Soc.* **2012**, *134*, 3714. (e) Prasad, B. L. V.; Stoeva, S. L.; Sorensen, C. M.; Klabunde, K. J. *Chem. Mater.* **2003**, *15*, 935. (f) Abecassis, B.; Testard, F.; Spalla, O. *Phys. Rev. Lett.* **2008**, *100*, 115504. (g) Brown, L. O.; Hutchinson, J. E. *J. Phys. Chem. B* **2001**, *105*, 8911.
- (8) For a recent example, see: Gao, J.; Huang, X.; Liu, H.; Zan, F.; Ren, J. *Langmuir* **2012**, *28*, 4464.
- (9) (a) Bourissou, D.; Guerret, O.; Gabbai, F. P.; Bertrand, G. *Chem. Rev.* **2000**, *100*, 39. (b) Herrmann, W. A. *Angew. Chem., Int. Ed.* **2002**, *41*, 1290. (c) Hahn, F. E.; Jahnke, M. C. *Angew. Chem., Int. Ed.* **2008**, *47*, 3122. (d) Lin, J. C. Y.; Huang, R. T. W.; Lee, C. S.; Bhattacharyya, A.; Hwang, W. S.; Lin, I. J. B. *Chem. Rev.* **2009**, *109*, 3561. (e) Schuster, O.; Yang, L.; Raubenheimer, H. G.; Albrecht, M. *Chem. Rev.* **2009**, *109*, 3445.
- (10) Diez-Gonzalez, S.; Marion, N.; Nolan, S. P. *Chem. Rev.* **2009**, *109*, 3612.
- (11) (a) Hindi, K. M.; Panzner, M. J.; Tessier, C. A.; Cannon, C. L.; Youngs, W. J. *Chem. Rev.* **2009**, *109*, 3859. (b) Teyssot, M. L.; Jarrousse, A. S.; Manin, M.; Chevry, A.; Roche, S.; Norre, F.; Beaudoin, C.; Morel, L.; Boyer, D.; Mahiou, R.; Gautier, A. *Dalton Trans* **2009**, 6894. (c) Merces, L.; Albrecht, M. *Chem. Soc. Rev.* **2010**, *39*, 1903. (d) Gautier, A.; Cisnetti, F. *Metallomics* **2012**, *4*, 23.

- (e) Oehninger, L.; Rubbiani, R.; Ott, I. *Dalton Trans.* **2013**, *42*, 3269.
 (f) Liu, W.; Gust, R. *Chem. Soc. Rev.* **2013**, *42*, 755.
 (12) Pyykkö, P.; Runeberg, N. *Chem.—Asian J.* **2006**, *1*, 623.
 (13) Benhamou, L.; Chardon, E.; Lavigne, G.; Bellemin-Laponnaz, S.; César, V. *Chem. Rev.* **2011**, *111*, 2705.
 (14) (a) Weidner, T.; Baio, J. E.; Mundstock, A.; Große, C.; Karthäuser, S.; Bruhn, C.; Siemeling, U. *Aust. J. Chem.* **2011**, *64*, 1177.
 (b) Zhukhovitskiy, A. V.; Mavros, M. G.; Van Voorhis, T.; Johnson, J. A. *J. Am. Chem. Soc.* **2013**, *135*, 7418. (c) Crudden, C. M.; Horton, J. H.; Ebralidze, I. I.; Zenkina, McLean, A. B.; Drevniok, B.; She, Z.; Kraatz, H.-B.; Mosey, N. J.; Seki, T.; Keske, E. C.; Leake, J. D.; Rousina-Webb, A.; Wu, G. *Nat. Chem.* **2014**, *6*, 409.
 (15) (a) Melaiye, A.; Sun, Z.; Hindi, K.; Milsted, A.; Ely, D.; Reneker, D. H.; Tessier, C. A.; Youngs, W. J. *J. Am. Chem. Soc.* **2005**, *127*, 2285.
 (b) Lee, C. K.; Vasam, C. S.; Huang, T. W.; Wang, H. M. J.; Yang, R. Y.; Lee, C. S.; Lin, I. J. B. *Organometallics* **2006**, *25*, 3768. (c) Huang, R. T. W.; Wang, W. C.; Yang, R. Y.; Lu, J. T.; Lin, I. J. B. *Dalton Trans.* **2009**, 7121. (d) Vignolle, J.; Tilley, T. D. *Chem. Commun.* **2009**, 7230.
 (e) Ranganath, K. V. S.; Kloesges, J.; Schäfer, A. H.; Glorius, F. *Angew. Chem., Int. Ed.* **2010**, *49*, 7786. (f) Lara, P.; Rivada-Wheelaghan, O.; Conejero, S.; Poteau, R.; Philippot, K.; Chaudret, B. *Angew. Chem., Int. Ed.* **2011**, *50*, 12080. (g) Gonzales-Galves, D.; Lara, P.; Rivada-Wheelaghan, O.; Conejero, S.; Chaudret, B.; Philippot, K.; van Leeuwen, P. W. N. M. *Catal. Sci. Technol.* **2013**, *3*, 99. (h) Ling, X.; Schaeffer, N.; Roland, S.; Pileni, M.-P. *Langmuir* **2013**, *29*, 12647.
 (i) Hurst, E. C.; Wilson, K.; Fairlamb, L. J. S.; Chechik, V. *New J. Chem.* **2009**, *33*, 1837. (j) Richter, C.; Schaepe, K.; Glorius, F.; Ravoo, B. *J. Chem. Commun.* **2014**, *50*, 3204. (Pd/Au). (k) Rodriguez-Castillo, M.; Laurencin, D.; Tielens, F.; van der Lee, A.; Clement, S.; Guari, Y.; Richeter, S. *Dalton Trans.* **2014**, *43*, 5978. (l) Serpell, C. J.; Cookson, J.; Thompson, A. L.; Brown, C. M.; Beer, P. D. *Dalton Trans.* **2013**, *42*, 1385.
 (16) (a) Park, E. D.; Lee, J. S. *J. Catal.* **1999**, *186*, 1. (b) Venezia, A. M.; Pantaleo, G.; Longo, A.; Di Carlo, G.; Casaletto, M. P.; Liotta, F. L.; Deganello, G. *J. Phys. Chem. B* **2005**, *109*, 2821. (c) Casaletto, M. P.; Longo, A.; Martorana, A.; Prestianni, A.; Venezia, A. M. *Surf. Interface Anal.* **2006**, *38*, 215.
 (17) (a) Cossaro, A.; Mazzarello, R.; Rousseau, R.; Casalis, L.; Verdini, A.; Kohlmeyer, A.; Floreano, L.; Scandolo, S.; Morgante, A.; Klein, M. L.; Scoles, G. *Science* **2008**, *321*, 943. (b) Häkkinen, H. *Nat. Chem.* **2012**, *4*, 443. (c) Djebaili, T.; Richardi, J.; Abel, S.; Marchi, M. *J. Phys. Chem. C* **2013**, *117*, 17791.
 (18) Krommenhoek, P. J.; Wang, J.; Hentz, N.; Johnston-Peck, A. C.; Kozek, K. A.; Kalyuzhny, G.; Tracy, J. B. *ACS Nano* **2012**, *6*, 4903.
 (19) NHC 3D models were built with Avogadro and minimized with UFF.

Supporting Information

Supracrystals of *N*-Heterocyclic Carbene-Coated Au Nanocrystals

Xiang Ling,^{a,b} Sylvain Roland*^b and Marie-Paule Pileni*^{a,c}

^a Sorbonne Universités, UPMC-Univ Paris 6, UMR 8233, MONARIS, F-75005, Paris, France

^b Sorbonne Universités, UPMC-Univ Paris 6, UMR 8232, Institut Parisien de Chimie Moléculaire, F-75005, Paris, France

^c CEA/IRAMIS, CEA Saclay, 91191, Gif-sur-Yvette, France

Table of contents

General information	61
Scheme S1: General synthetic scheme	62
Synthesis of chloroaurate(III) benzimidazolium salts	63
Synthesis of L⁵AuCl	68
Figure S1: Reduction conditions tested with L⁵ and TEM images	70
Figure S2: TEM images of AuNCs before size selection	71
Table S1: Reproducibility: Average sizes and size distributions of different AuNCs batches	71
Figure S3: HRSEM image and SAXRD pattern of supracrystals made of L⁴ -coated AuNCs	72
Figure S4. Evaporation device for Au supracrystals preparation	73
Figure S5. HRSEM image and SAXRD pattern of L⁴ -coated Au supracrystals	73

General Information

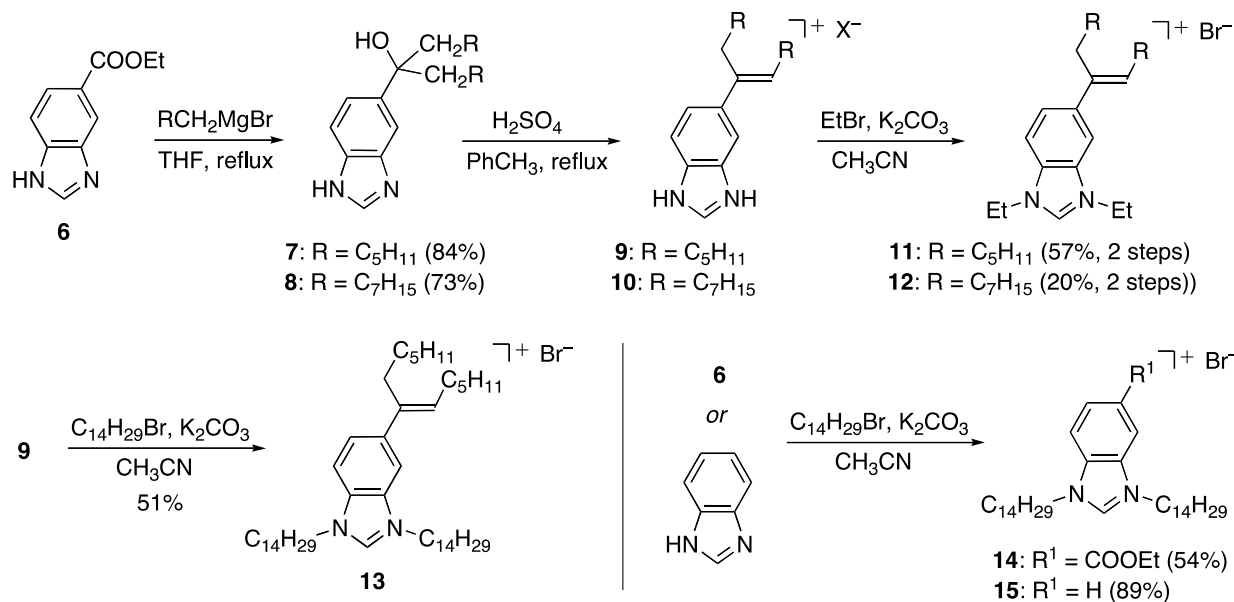
Reagents were purchased from commercial sources and used as received unless stated otherwise. 5-Ethoxycarbonyl benzimidazole (**6**) was prepared from benzimidazole-5-carboxylic acid according to a literature procedure.¹ THF was distilled from sodium-benzophenone ketyl under nitrogen atmosphere. Dichloromethane was distilled from CaH₂. Reactions involving organometallic species or air- or moisture-sensitive compounds were carried out under an atmosphere of argon by using standard Schlenk techniques. Purification by column chromatography were performed on silica gel (Kieselgel 60 Merck, granulometry 40–60 or 15–40 μm) or on Alumina (aluminium oxide 90 active neutral Merck, 63–200 μm). NMR spectra were recorded on Bruker Nanobay spectrometers 300 or 400 MHz. In CDCl₃ and CD₂Cl₂, proton chemical shifts (δ) are reported relative to the residual protonated solvent ($\delta = 7.26$ and 5.32 ppm, respectively). ¹³C chemical shifts (δ) are reported relative to the NMR solvent (CD₂Cl₂: $\delta = 54.00$ ppm; CDCl₃: $\delta = 77.16$ ppm). Coupling constants are reported in Hertz (Hz). The following abbreviations are used : s = singlet, d = doublet, t = triplet, q = quadruplet, m = multiplet, br = broad). Elemental analyses were performed at the "Institut de Chimie des Substances Naturelles" (service de microanalyse). HRMS were performed at the "Institut Parisien de Chimie Moléculaire" (UPMC-Univ Paris 6). XPS analyses were carried out at the "Laboratoire de Réactivité de Surface" (UPMC-Univ Paris 6).

¹ Barrow, J. C.; Coburn, C.; Selnick, H. G.; Ngo, P. L. "Preparation of 2-(pyridin-4-yl)acetamides as thrombin inhibitors" U. S. Patent 20020193398, December 19, 2002.

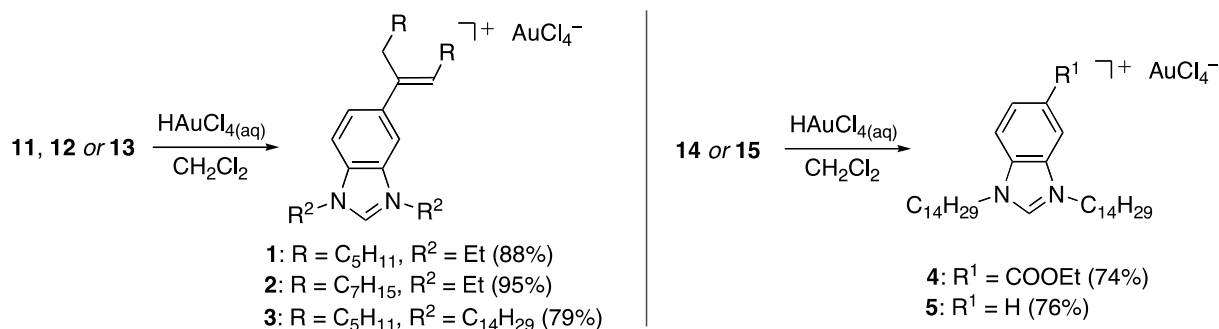
Synthesis of Chloroaurate(III) Benzimidazolium Salts (1–5) [NHC–H·AuCl₄]

Scheme S1: General synthetic scheme.

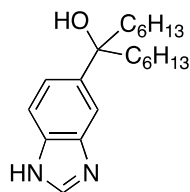
Benzimidazolium bromide salts :



Benzimidazolium chloroaurate salts :

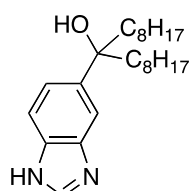


5-[1,1-Dihexyl-1-(hydroxy)methyl]benzimidazole (**7**).² To a solution of 5-ethoxycarbonyl benzimidazole (**6**) (2 g, 10.6 mmol) in THF (30 mL) was added dropwise at 0 °C a



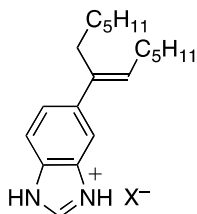
solution of hexylmagnesium bromide 2 M in Et₂O (18.6 mL, 37.2 mmol). The mixture was allowed to reflux for 5 h, after which it was cooled to 0 °C and quenched with NH₄Cl_(aq) 10% (5 mL) and water (10 mL). The organic and aqueous layers were separated and the aqueous layer was extracted with Et₂O. The combined organic phases were dried over MgSO₄ and concentrated *in vacuo*. The residue was purified by silica gel chromatography (EtOAc:CH₂Cl₂ = 3:1) to give the title compound as a light brown oil (2.8 g, 84%). ¹H NMR (300 MHz, CDCl₃) δ 8.32 (s, 1H), 7.82 (s, 1H), 7.64 (d, *J* = 8.5 Hz, 1H), 7.29 (d, *J* = 8.5 Hz, 1H), 6.05 (br s, 2H), 1.94–1.77 (m, 4H), 1.35–1.08 (m, 16H), 0.78 (t, *J* = 6.6 Hz, 6H). ¹³C NMR (75 MHz, CDCl₃) δ 142.17, 141.03, 137.22, 136.67, 120.75, 115.27, 112.10, 77.63, 43.40, 31.85, 29.82, 23.70, 22.69, 14.11.

5-[1,1-Dioctyl-1-(hydroxy)methyl]benzimidazole (**8**). To a solution of ester **6** (2 g, 10.6 mmol) in THF



(30 mL) was added dropwise at 0 °C a solution of octylmagnesium bromide 2 M in Et₂O (18.6 mL, 37.2 mmol). The mixture was allowed to reflux for 5 h, after which it was cooled to 0 °C and quenched with NH₄Cl_(aq) 10% (5 mL) and water (10 mL). The organic and aqueous layers were separated and the aqueous layer was extracted with Et₂O. The combined organic phases were dried over MgSO₄ and concentrated *in vacuo*. The residue was purified by silica gel chromatography (EtOAc:CH₂Cl₂ = 3:1) to give the title compound as a light brown oil (2.9 g, 73%). ¹H NMR (300 MHz, CD₂Cl₂) δ 8.07 (s, 1H), 7.80 (s, 1H), 7.60 (d, *J* = 8.5 Hz, 1H), 7.27 (dd, *J* = 8.5 and 1.5 Hz, 1H), 1.95–1.75 (m, 4H), 1.45–0.90 (m, 24H), 0.84 (t, *J* = 6.8 Hz, 6H). ¹³C NMR (75 MHz, CDCl₃) δ 142.04, 140.87, 137.20, 136.54, 120.70, 115.46, 112.09, 77.60, 43.47, 31.96, 30.20, 29.64, 29.40, 23.72, 22.75, 14.20.

(*E*)-5-[1-(Hexyl)-hept-1-en-1-yl]benzimidazole (**9**) (protonated form). To a solution of alcohol **7** (0.95



g, 3 mmol) in toluene (20 mL) was added conc. H₂SO₄ (0.08 mL). The solution was allowed to reflux for 16 h, after which it was cooled to 20 °C and sat. NaHCO_{3(aq)} (20 mL) was added. The organic phase was separated and the aqueous phase was extracted with EtOAc. The combined organic phases were dried over MgSO₄ and concentrated *in vacuo*. The residue was purified by silica gel chromatography (EtOAc:CH₂Cl₂ = 1:1) to give 0.8 g of the title compound as a light brown oil. (*E*)/(*Z*) ratio = 94:6. The nature of the counterion (X⁻) could not be determined. ¹H NMR (300 MHz, CDCl₃) δ 12.02 (br s, 2H), 9.94 (s, 1H), 7.88 (d, *J* = 8.7 Hz, 1H), 7.83 (s, 1H), 7.47 (dd, *J* = 8.7 and 1.3 Hz, 1H), 5.64 (t, *J* = 7.3 Hz, 1H), 2.28–2.20 (m, 2H), 2.16 (q, *J* = 7.3 Hz, 2H), 1.25–1.02 (m, 14H),

² The procedure was adapted from: (a) Cho, S. Y.; Grimsdale, A. C.; Jones, D. J.; Watkins, S. E.; Holmes, A. B. *J. Am. Chem. Soc.* **2007**, *129*, 11910–11911. (b) de Arriba, Á. L. F.; Simón, L.; Alcázar, V.; Cuellar, J.; Lozano-Martínez, P.; Morán, J. R. *Adv. Synth. Catal.* **2011**, *353*, 2681.

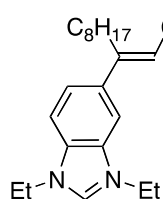
N-heterocyclic carbene coated Nanocrystals and Supracrystals

0.89 (t, $J = 6.9$ Hz, 3H), 0.80 (t, $J = 6.9$ Hz, 3H). ^{13}C NMR (75 MHz, CDCl_3) 143.64, 139.23, 139.02, 131.97, 130.29, 128.61, 126.32, 114.21, 111.71, 31.77, 31.69, 30.07, 29.51, 29.20, 28.84, 28.62, 22.65, 14.15, 14.12.

(E)-5-[1-(Octyl)-non-1-en-1-yl]benzimidazole (**10**) (protonated form). To a solution of alcohol **8** (1.12 g, 3 mmol) in toluene (20 mL) was added conc. H_2SO_4 (0.08 mL). The solution was allowed to reflux for 16 h, after which it was cooled to 20 °C and sat. $\text{NaHCO}_{3(\text{aq})}$ (20 mL) was added. The organic phase was separated and the aqueous phase was extracted with EtOAc. The combined organic phases were dried over MgSO_4 and concentrated *in vacuo*. The residue was purified by silica gel chromatography (EtOAc: $\text{CH}_2\text{Cl}_2 = 1:1$) to give 0.9 g of the title compound as a light brown oil. (*E*)/(*Z*) ratio = 94:6. The nature of the counterion (X^-) could not be determined. ^1H NMR (400 MHz, CDCl_3) δ 11.75 (br s, 2H), 9.55 (s, 1H), 7.85 (d, $J = 8.7$ Hz, 1H), 7.82 (s, 1H), 7.47 (d, $J = 8.7$ Hz, 1H), 5.65 (t, $J = 7.2$ Hz, 1H), 2.50–2.30 (m, 2H), 2.16 (q, $J = 7.5$ Hz, 2H), 1.50–1.06 (m, 22H), 0.90 (t, $J = 6.8$ Hz, 3H), 0.83 (t, $J = 6.9$ Hz, 3H). ^{13}C NMR (75 MHz, CDCl_3) 140.93, 140.51, 139.33, 137.57, 137.13, 129.26, 122.28, 115.31, 112.76, 32.02, 31.99, 30.41, 30.13, 29.75, 29.58, 29.42, 28.89, 28.82, 22.81, 22.78, 14.24, 14.21.

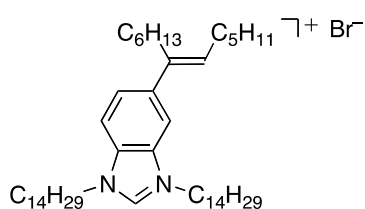
(E)-1,3-Diethyl-5-[1-(hexyl)-hept-1-en-1-yl]benzimidazolium bromide (**11**). To a solution of alkene **9** (0.75 g, 2.5 mmol) in CH_3CN (10 mL) was added K_2CO_3 (0.35 g, 2.5 mmol) and EtBr (0.56 mL, 7.5 mmol). The mixture was stirred at 80 °C for 24 h. The solvent was removed under reduced pressure. The residue was taken off in CH_2Cl_2 and filtered through a short pad of Celite to remove the precipitate (KBr). The filtrate was concentrated under reduced pressure. The residue was washed with Et_2O and pentane and dried under vacuum to give the title compound as a light yellow solid (0.7 g, 52% from **7**). ^1H NMR (400 MHz, CDCl_3) δ 11.10 (s, 1H), 7.62 (s, 2H), 7.53 (s, 1H), 5.70 (t, $J = 7.2$ Hz, 1H), 4.69–4.63 (m, 4H), 2.60–2.50 (m, 2H), 2.22 (q, $J = 7.3$ Hz, 2H), 1.78–1.73 (m, 6H), 1.25–1.07 (m, 14H), 0.90 (t, $J = 6.4$ Hz, 3H), 0.84 (t, $J = 6.4$ Hz, 3H). ^{13}C NMR (100 MHz, CDCl_3) δ 144.22, 141.37, 138.97, 132.82, 131.65, 129.93, 126.59, 112.57, 110.04, 43.14, 42.92, 31.78, 31.71, 30.22, 29.50, 29.23, 28.91, 28.61, 22.69, 15.10, 15.08, 14.18, 14.14. HRMS (ESI) m/z calcd for $\text{C}_{24}\text{H}_{39}\text{N}_2$ [$\text{M}-\text{Br}^-$] $^+$ 355.3113, found 355.3109. The (*E*) configuration of the major isomer was determined by NOESY experiments (see page S16).

(E)-1,3-Diethyl-5-[1-(octyl)-non-1-en-1-yl]benzimidazolium bromide (**12**). To a solution of alkene **10** (0.97 g, 2.7 mmol) in CH₃CN (10 mL) was added K₂CO₃ (0.37 g, 2.7 mmol) and EtBr (0.62 mL, 8.1



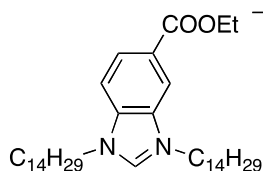
mmol). The mixture was stirred at 80 °C for 24 h. The solvent was removed under reduced pressure. The residue was taken off in CH₂Cl₂ and filtered through a short pad of Celite to remove the precipitate (KBr). The filtrate was concentrated under reduced pressure. The residue was washed with pentane and dried under vacuum to give the title compound as a white solid (0.3 g, 20% from **8**). ¹H NMR (400 MHz, CDCl₃) δ 11.45 (s, 1H), 7.61 (d, *J* = 8.8 Hz, 1H), 7.59 (d, *J* = 8.8 Hz, 1H), 7.51 (s, 1H), 5.69 (t, *J* = 7.2 Hz, 1H), 4.69–4.63 (m, 4H), 2.55–2.52 (m, 2H), 2.21 (q, *J* = 7.2 Hz, 2H), 1.75–1.70 (m, 6H), 1.25–1.12 (m, 22H), 0.92–0.79 (m, 6H). ¹³C NMR (100 MHz, CDCl₃) δ 144.07, 142.29, 138.96, 132.76, 131.63, 129.93, 126.44, 112.54, 110.01, 43.02, 42.81, 31.94, 30.19, 29.81, 29.55, 29.54, 29.47, 29.32, 28.93, 28.64, 22.77, 22.73, 15.10, 15.07, 14.21, 14.18. HRMS (ESI) *m/z* calcd for C₂₈H₄₇N₂ [M–Br]⁺ 411.3739, found 411.3739.

(E)-1,3-Ditetradecyl-5-[1-(hexyl)-hept-1-en-1-yl]benzimidazolium bromide (**13**). A mixture of **9** (1.8 g,



6.1 mmol), K₂CO₃ (1.01 g, 7.32 mmol) and *n*-tetradecyl bromide (5.5 mL, 18.3 mmol) in CH₃CN (10 mL) was stirred at reflux for 24 h. The solvent was removed under reduced pressure. The residue was taken off in CH₂Cl₂ and filtered through a short pad of Celite to remove the precipitate (KBr). The filtrate was concentrated under reduced pressure. The residue was purified by chromatography on alumina (neutral, eluent : CH₂Cl₂) to give the title compound as a light yellow oil (2.4 g, 51%). ¹H NMR (300 MHz, CDCl₃) δ 11.29 (s, 1H), 7.58 (d, *J* = 8.8 Hz, 1H), 7.53 (d, *J* = 8.8 Hz, 1H), 5.63 (t, *J* = 6.9 Hz, 1H), 4.70–4.40 (m, 4H), 2.55–2.40 (m, 2H), 2.15 (q, *J* = 7.5 Hz, 2H), 2.10–1.80 (m, 4H), 1.50–1.01 (m, 58H), 0.90–0.70 (m, 12H). ¹³C NMR (100 MHz, CDCl₃) δ 143.47, 142.13, 138.59, 132.23, 131.38, 129.75, 126.05, 112.61, 109.60, 47.53, 47.21, 31.64, 31.39, 31.33, 29.80, 29.41, 29.37, 29.34, 29.27, 29.15, 29.12, 29.08, 28.83, 28.51, 28.24, 26.32, 26.30, 22.40, 22.30, 13.82, 13.78, 13.74. HRMS (ESI) *m/z* calcd for C₄₈H₈₇N₂ [M–Br]⁺ 691.6869, found 691.6871.

5-Ethoxycarbonyl-1,3-(ditetradecyl)benzimidazolium bromide (**14**). A mixture of ester **6** (1.9 g, 10

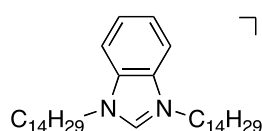


mmol), K₂CO₃ (1.38 g, 10 mmol) and *n*-tetradecyl bromide (9 mL, 30 mmol) in CH₃CN (10 mL) was stirred at reflux for 24 h. The solvent was removed under reduced pressure. The residue was taken off in CH₂Cl₂ and filtered through a short pad of Celite to remove the precipitate (KBr). The filtrate was concentrated under reduced pressure. The residue was recrystallized from CH₂Cl₂/pentane and dried under vacuum to give the title compound as white solid (3.6 g, 54%). ¹H NMR (400 MHz, CDCl₃) δ 11.82 (s, 1H), 8.38 (s, 1H), 8.33 (dd, *J* = 8.7 and 1.3 Hz, 1H), 7.75 (d, *J*

N-heterocyclic carbene coated Nanocrystals and Supracrystals

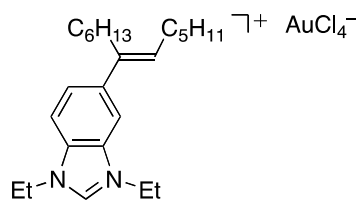
= 8.7 Hz, 1H), 4.69–4.64 (m, 4H), 4.48 (q, $J = 7.1$ Hz, 2H), 2.13–2.02 (m, 4H), 1.47 (t, $J = 7.1$ Hz, 3H), 1.50–1.12 (m, 44H), 0.86 (t, $J = 6.8$ Hz, 6H). ^{13}C NMR (100 MHz, CDCl_3) δ 164.78, 145.20, 134.09, 131.34, 129.91, 128.21, 115.10, 113.11, 62.35, 48.17, 48.13, 32.04, 29.79, 29.76, 29.70, 29.62, 29.52, 29.50, 29.47, 29.16, 29.14, 26.69, 22.80, 14.45, 14.23. Anal. calcd for $(\text{C}_{38}\text{H}_{67}\text{BrN}_2\text{O}_2) \cdot (\text{H}_2\text{O})_{0.5}$: C 67.83, H 10.19, N 4.16; found C 67.63, H 10.25, N 4.20. HRMS (ESI) m/z calcd for $\text{C}_{38}\text{H}_{67}\text{N}_2\text{O}_2$ $[\text{M}-\text{Br}^-]^+$ 583.5197, found 583.5193.

1,3-(Ditetradecyl)benzimidazolium bromide (15). A mixture of benzimidazole (1.18 g, 10 mmol), K_2CO_3 (1.38 g, 10 mmol) and *n*-tetradecyl bromide (9.0 mL, 30 mmol) in CH_3CN (10 mL) was stirred at reflux for 24 h. The solvent was removed under reduced pressure. The residue was taken off in CH_2Cl_2 and filtered through a short pad of Celite to remove the precipitate (KBr). The filtrate was concentrated under reduced pressure. The residue was recrystallized from CH_2Cl_2 /pentane and dried under vacuum to give the title compound as a white solid (5.3 g, 89%).



^1H NMR (400 MHz, CDCl_3) δ 11.61 (s, 1H), 7.75–7.60 (m, 4H), 4.62 (t, $J = 7.4$ Hz, 4H), 2.14–1.98 (m, 4H), 1.48–1.13 (m, 44H), 0.87 (t, $J = 6.7$ Hz, 6H). ^{13}C NMR (400 MHz, CDCl_3) δ 143.18, 131.50, 127.19, 113.18, 47.84, 32.06, 29.81, 29.78, 29.72, 29.71, 29.64, 29.52, 29.49, 29.19, 26.72, 22.83, 14.25. Anal. calcd for $(\text{C}_{35}\text{H}_{63}\text{BrN}_2) \cdot (\text{H}_2\text{O})_{0.5}$: C 69.97, H 10.74, N 4.66; found C 69.90, H 10.84, N 4.69. HRMS (ESI) m/z calcd for $\text{C}_{35}\text{H}_{63}\text{N}_2$ $[\text{M}-\text{Br}^-]^+$ 511.4986, found 511.4983.

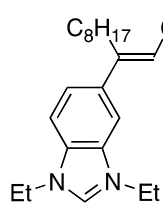
(E)-1,3-Diethyl-5-[1-(hexyl)-hept-1-en-1-yl]benzimidazolium tetrachloroaurate(III) (1).³ To a solution of **11** (0.18 g, 0.42 mmol) in CH_2Cl_2 (12 mL) was added under stirring a solution of $\text{HAuCl}_4 \cdot 3\text{H}_2\text{O}$ (0.15 g, 0.42 mmol) in water (12 mL). The mixture was stirred vigorously for 2 h at 20 °C. During the course of the reaction, the yellow color of the aqueous layer disappeared, while the organic phase became deep red. The organic layer was separated, concentrated and dried under vacuum to give the title compound as a blood red oil (0.256 g, 88%).



^1H NMR (400 MHz, CDCl_3) δ 9.45 (s, 1H), 7.68 (d, $J = 8.8$ Hz, 1H), 7.63 (dd, $J = 8.8$ and 1.2 Hz, 1H), 7.56 (s, 1H), 5.72 (t, $J = 7.3$ Hz, 1H), 4.58 (q, $J = 7.4$ Hz, 4H), 2.53 (t, $J = 7.0$ Hz, 2H), 2.20 (q, $J = 7.4$ Hz, 2H), 1.76–1.69 (m, 6H), 1.39–1.10 (m, 14H), 0.88 (t, $J = 6.5$, 3H), 0.82 (t, $J = 6.5$ Hz, 3H). ^{13}C NMR (100 MHz, CDCl_3) δ 144.35, 139.17, 138.81, 132.83, 131.69, 130.00, 126.90, 112.90, 110.14, 43.40, 43.15, 31.69, 31.61, 30.09, 29.37, 29.14, 28.82, 28.53, 22.59, 14.88, 14.83, 14.10, 14.08. HRMS (ESI) m/z calcd for $\text{C}_{24}\text{H}_{39}\text{N}_2$ $[\text{M}-\text{AuCl}_4^-]^+$ 355.3113, found 355.3108.

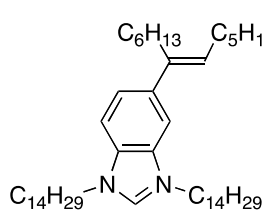
³ The procedure was adapted from: Serpell, C. J.; Cookson, J.; Thompson, A. L.; Brown, C. M.; Beer, P. D., *Dalton Trans.* **2013**, 42, 1385.

(*E*)-1,3-Diethyl-5-[1-(octyl)-non-1-en-1-yl]benzimidazolium tetrachloroaurate(III) (**2**). To a solution of **12** (0.206 g, 0.42 mmol) in CH₂Cl₂ (12 mL) was added under stirring a solution of HAuCl₄·3H₂O



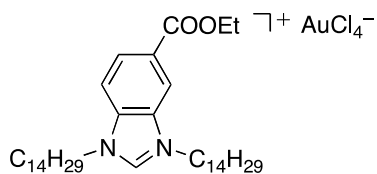
(0.15 g, 0.42 mmol) in water (12 mL). The mixture was stirred vigorously for 2 h at 20 °C. During the course of the reaction, the yellow color of the aqueous layer disappeared, while the organic phase became deep red. The organic layer was separated, concentrated and dried under vacuum to give the title compound as a blood red oil (0.3 g, 95%). ¹H NMR (400 MHz, CDCl₃) δ 9.31 (s, 1H), 7.69 (d, *J* = 8.8 Hz, 1H), 7.61 (dd, *J* = 8.8 and 1.3 Hz, 1H), 7.55 (s, 1H), 5.71 (t, *J* = 7.3 Hz, 1H), 4.55 (q, *J* = 7.3 Hz, 4H), 2.52 (t, *J* = 7.0 Hz, 2H), 2.19 (q, *J* = 7.6 Hz, 2H), 1.71 (t, *J* = 7.6 Hz, 3H), 1.70 (t, *J* = 7.6 Hz, 3H), 1.50–1.10 (m, 22H), 0.84 (t, *J* = 6.4 Hz, 3H), 0.80 (t, *J* = 6.4 Hz, 3H). ¹³C NMR (100 MHz, CDCl₃) δ 144.13, 138.93, 138.66, 132.61, 131.54, 129.87, 126.75, 112.85, 110.00, 43.29, 43.03, 31.70, 29.92, 29.56, 29.34, 29.31, 29.23, 29.10, 29.06, 28.72, 28.43, 22.54, 22.50, 14.73, 14.67, 14.01, 14.00. HRMS (ESI) *m/z* calcd for C₂₈H₄₇N₂ [M–AuCl₄]⁺ 411.3739, found 411.3736.

(*E*)-1,3-Ditetradecyl-5-[1-(hexyl)-hept-1-en-1-yl]benzimidazolium tetrachloroaurate(III) (**3**). To a



solution of **13** (0.94 g, 1.35 mmol) in CH₂Cl₂ (36 mL) was added under stirring a solution of HAuCl₄·3H₂O (0.53 g, 1.35 mmol) in water (36 mL). The mixture was stirred vigorously for 2 h at 20 °C. During the course of the reaction, the yellow color of the aqueous layer disappeared, while the organic phase became deep red. The organic layer was separated, concentrated and dried under vacuum to give the title compound as an orange oil (1.1 g, 79%). ¹H NMR (400 MHz, CDCl₃) δ 9.41 (s, 1H), 7.67 (d, *J* = 8.8 Hz, 1H), 7.63 (d, *J* = 8.8 Hz, 1H), 7.53 (s, 1H), 5.73 (t, *J* = 7.3 Hz, 1H), 4.61–4.44 (m, 4H), 2.54 (t, *J* = 6.7 Hz, 2H), 2.21 (q, *J* = 7.3 Hz, 2H), 2.10–1.95 (m, 4H), 1.52–1.13 (m, 58H), 0.95–0.75 (m, 12H). ¹³C NMR (100 MHz, CDCl₃) δ 144.28, 139.79, 138.73, 132.83, 131.74, 130.04, 126.88, 112.94, 110.09, 48.21, 47.92, 31.92, 31.68, 31.60, 30.96, 30.08, 29.69, 29.68, 29.65, 29.64, 29.56, 29.43, 29.36, 29.15, 29.06, 28.82, 28.54, 26.69, 26.67, 22.68, 22.58, 22.57, 14.10, 14.06, 14.04. HRMS (ESI) *m/z* calcd for C₄₈H₈₇N₂ [M–AuCl₄]⁺ 691.6869, found 691.6863.

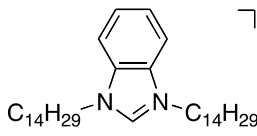
5-Ethoxycarbonyl-1,3-(ditetradecyl)benzimidazolium tetrachloroaurate(III) (**4**). To a solution of **14** (0.37 g, 0.56 mmol) in CH₂Cl₂ (16 mL) was added under stirring a



solution of HAuCl₄·3H₂O (0.2 g, 0.56 mmol) in water (16 mL). The mixture was stirred vigorously for 2 h at 20 °C. During the course of the reaction, the yellow color of the aqueous layer disappeared, while the organic phase became deep red. The organic layer was separated, concentrated and dried under vacuum to give the title compound as a red oil (0.38 g, 74%). ¹H NMR (400 MHz, CDCl₃) δ 9.77 (s, 1H), 8.39 (d, *J* = 1.6 Hz, 1H), 8.33 (dd, *J* = 8.8 and 1.6 Hz, 1H),

N-heterocyclic carbene coated Nanocrystals and Supracrystals

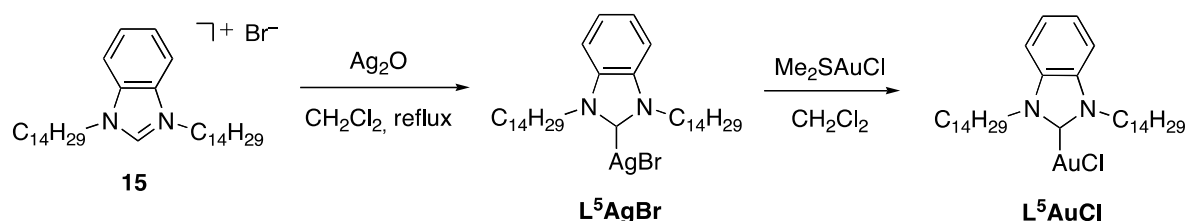
7.82 (d, $J = 8.8$ Hz, 1H), 4.57 (t, $J = 7.5$ Hz, 4H), 4.44 (q, $J = 7.1$ Hz, 2H), 2.11–2.02 (m, 4H), 1.40 (t, $J = 7.1$ Hz, 3H), 1.48–1.14 (m, 44H), 0.84 (t, $J = 6.8$ Hz, 6H). ^{13}C NMR (100 MHz, CDCl_3) δ 164.67, 142.38, 134.10, 131.37, 130.12, 128.54, 115.30, 113.64, 62.17, 48.50, 48.45, 31.92, 29.70, 29.68, 29.66, 29.64, 29.56, 29.45, 29.43, 29.36, 29.08, 29.05, 26.76, 22.68, 14.37, 14.12. HRMS (ESI) m/z calcd for $\text{C}_{38}\text{H}_{67}\text{N}_2\text{O}_2$ $[\text{M}-\text{AuCl}_4]^-$ 583.5197, found 583.5191.

1,3-(Ditetradecyl)benzimidazolium tetrachloroaurate(III) (**5**). To a solution of **15** (0.25 g, 0.42 mmol)  AuCl_4^- in CH_2Cl_2 (12 mL) was added under stirring a solution of $\text{HAuCl}_4 \cdot 3\text{H}_2\text{O}$ (0.15 g, 0.42 mmol) in water (12 mL). The mixture was stirred vigorously for 2 h at 20 °C. During the course of the reaction, the yellow color of the aqueous layer disappeared, while the organic phase became deep red.

The organic layer was separated, concentrated and dried under vacuum to give the title compound as an orange solid (0.27g, 76%). ^1H NMR (400 MHz, CDCl_3) δ 9.63 (s, 1H), 7.81–7.65 (m, 4H), 4.55 (t, $J = 6.4$ Hz, 4H), 2.20–2.00 (m, 4H), 1.51–1.15 (m, 44H), 0.87 (t, $J = 6.2$ Hz, 6H). ^{13}C NMR (100 MHz, CDCl_3) δ 140.53, 131.58, 127.82, 113.51, 48.36, 32.06, 29.83, 29.80, 29.75, 29.66, 29.61, 29.55, 29.50, 29.18, 26.82, 22.83, 14.25. Anal. calcd for $(\text{C}_{35}\text{H}_{63}\text{AuCl}_4\text{N}_2) \cdot (\text{H}_2\text{O})$: C 48.39, H 7.54, N 3.22; found C 48.46, H 7.49, N 3.06. HRMS (ESI) m/z calcd for $\text{C}_{35}\text{H}_{63}\text{N}_2$ $[\text{M}-\text{AuCl}_4]^-$ 511.4986, found 511.4980.

Gold(I) complex L⁵AuCl.

General scheme:



L^5AgBr :⁴ Ag_2O (0.278 g, 1.2 mmol) was added to a solution of **15** (0.592 g, 1.0 mmol) in CH_2Cl_2 (20 mL). The mixture was refluxed for 20 h, and filtered over celite. The filtrate was reduced to ca. 10 mL under reduced pressure. Pentane was added to the residual solution until precipitation of a white solid. The precipitate was isolated by filtration, washed with pentane and dried under vacuum to give the title compound as a white powder (0.546 g, 82%). ^1H NMR (400 MHz, CD_2Cl_2) δ 7.52 (dd, $J = 6.2$ and 3.1 Hz, 1H), 7.41 (dd, $J = 6.2$ and 3.1 Hz, 1H), 4.41 (t, $J = 7.3$ Hz, 2H), 1.98–1.78 (m, 2H), 1.42–1.12 (m, 22H), 0.88 (t, $J = 6.9$ Hz, 3H). ^{13}C NMR (400 MHz, CD_2Cl_2) δ 134.31, 124.44, 112.17, 50.16, 32.52, 30.84, 30.27, 30.24, 30.21, 30.14, 30.05, 29.94, 29.83, 27.42, 23.27, 14.45.

L^5AuCl : To a solution of L^5AgBr (0.51 g, 0.74 mmol) in CH_2Cl_2 (45 mL) was added $[\text{AuCl}(\text{SMe}_2)]$ (0.215 g, 0.74 mmol). The resulting solution was stirred at 20 °C for 4 h. The grey precipitate formed

⁴ The procedure was adapted from : Wang, H. M. J.; Lin, I. J. B. *Organometallics*, **1998**, *17*, 972.

(AgBr) was filtered off and the remaining clear solution was reduced to ca. 5 mL under reduced pressure. Hexane was added to the residual solution until precipitation of a white solid. The precipitate was isolated by filtration, washed with hexane and dried under vacuum to give the title compound as a white powder (0.515 g, 90%). ^1H NMR (400 MHz, CD_2Cl_2) δ 7.50 (dd, $J = 6.3$ and 3.0 Hz, 1H), 7.42 (dd, $J = 6.2$ and 3.1 Hz, 1H), 4.47 (dd, $J = 10.0$ and 4.7 Hz, 2H), 2.16–1.83 (m, 2H), 1.44–1.13 (m, 22H), 0.88 (t, $J = 6.9$ Hz, 3H). ^{13}C NMR (101 MHz, CD_2Cl_2) δ 178.45, 133.54, 133.49, 124.60, 124.56, 111.91, 49.30, 49.17, 32.31, 30.29, 30.06, 30.03, 30.00, 29.93, 29.83, 29.74, 29.61, 27.13, 23.07, 14.25.

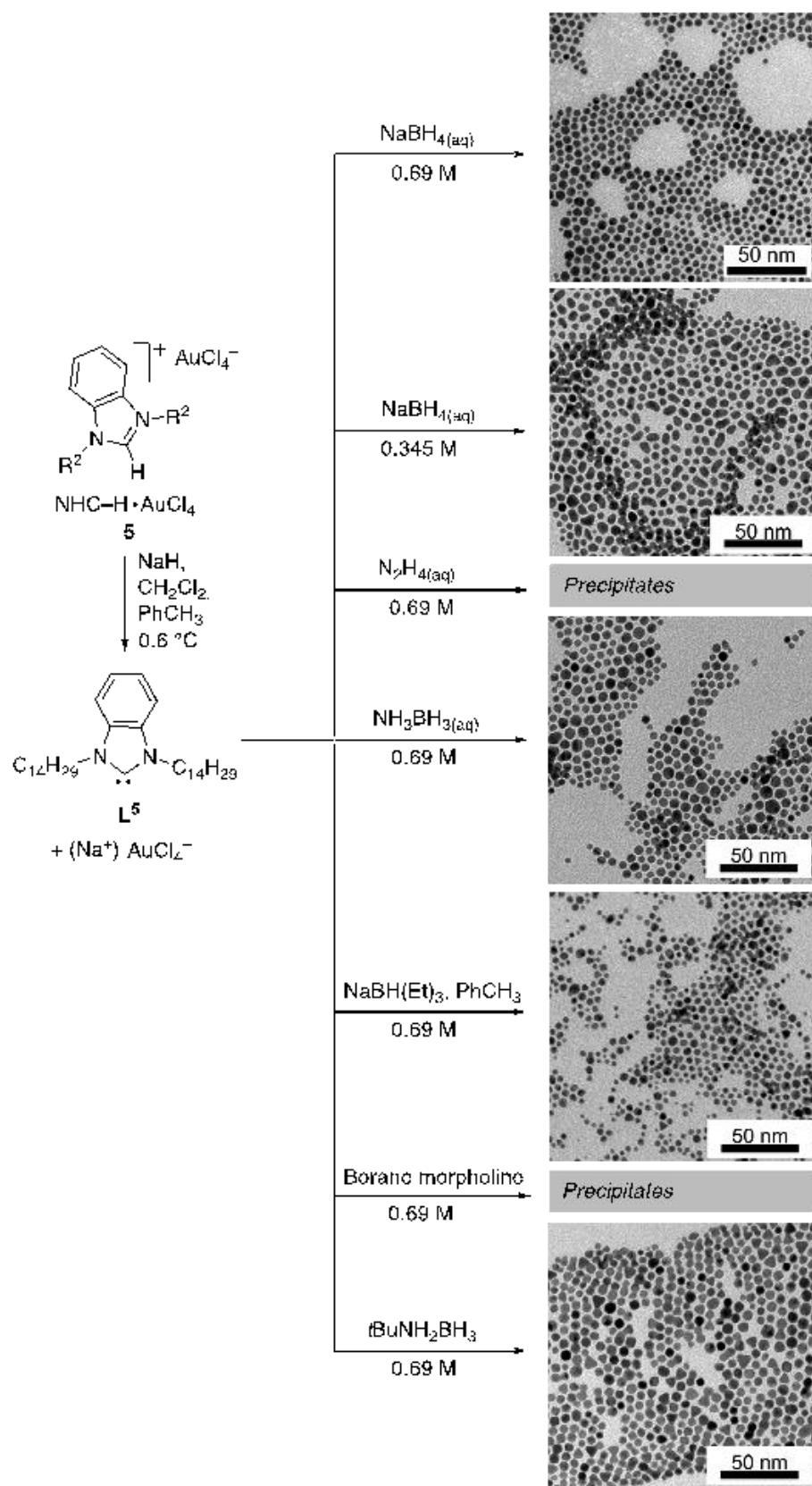


Figure S1. Different conditions tested (reduction step) with L^5 and TEM images for the preparation L^5 -coated Au NCs. The reduction was performed at 0.6 °C.

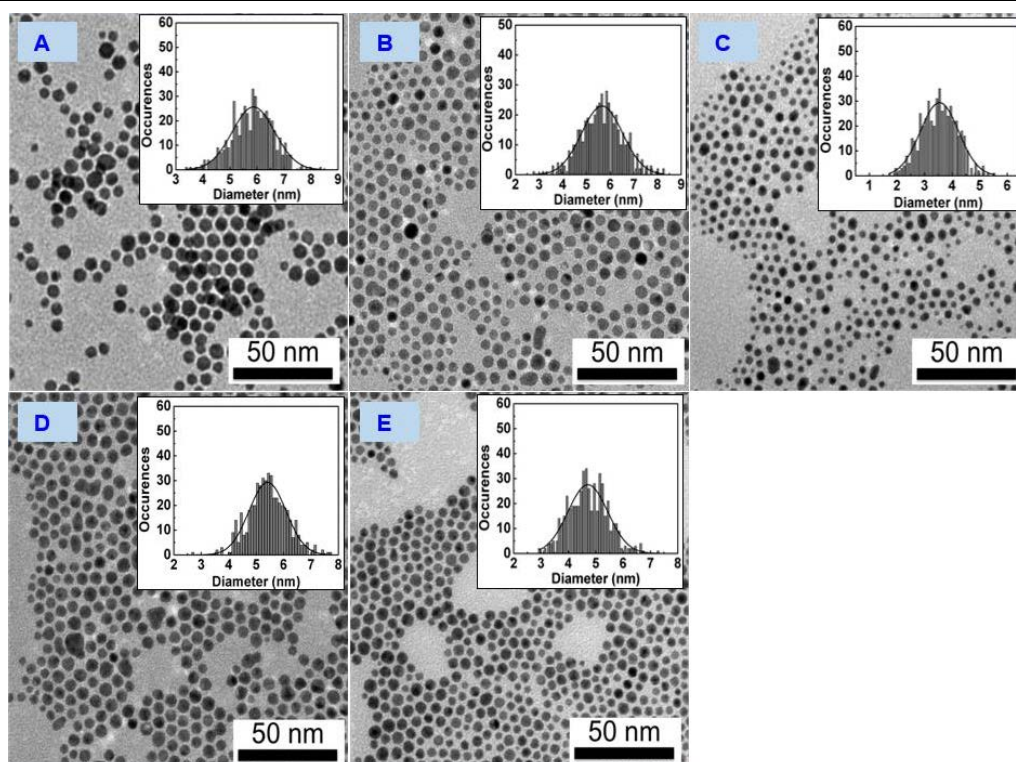


Figure S2. TEM images and size distributions (insets) of Au nanocrystals stabilized by L^1 (A), L^2 (B), L^3 (C), L^4 (D) and L^5 (E), before size selection.

Table S1: Reproducibility: Average sizes and size distributions of different AuNCs batches.

NCs Batch 2					
Entry	NHC Ligand	Before size selection		After size selection	
		d (nm)	σ (%)	d (nm)	σ (%)
1	L^1	5.9	15.8	6.1	9.0
2	L^2	5.6	19.2	5.8	10.9
3	L^3	3.7	20.5	3.9	11.6
4	L^4	5.3	17.2	5.2	10.9
5	L^5	4.9	16.4	5.1	9.6

NCs Batch 3					
Entry	NHC Ligand	Before size selection		After size selection	
		d (nm)	σ (%)	d (nm)	σ (%)
1	L^1	5.7	13.9	5.9	9.8
2	L^2	5.5	21.4	5.7	11.6
3	L^3	3.9	23.2	4.1	12.3
4	L^4	5.4	16.8	5.3	11.2
5	L^5	4.8	17.5	4.9	10.1

N-heterocyclic carbene coated Nanocrystals and Supracrystals

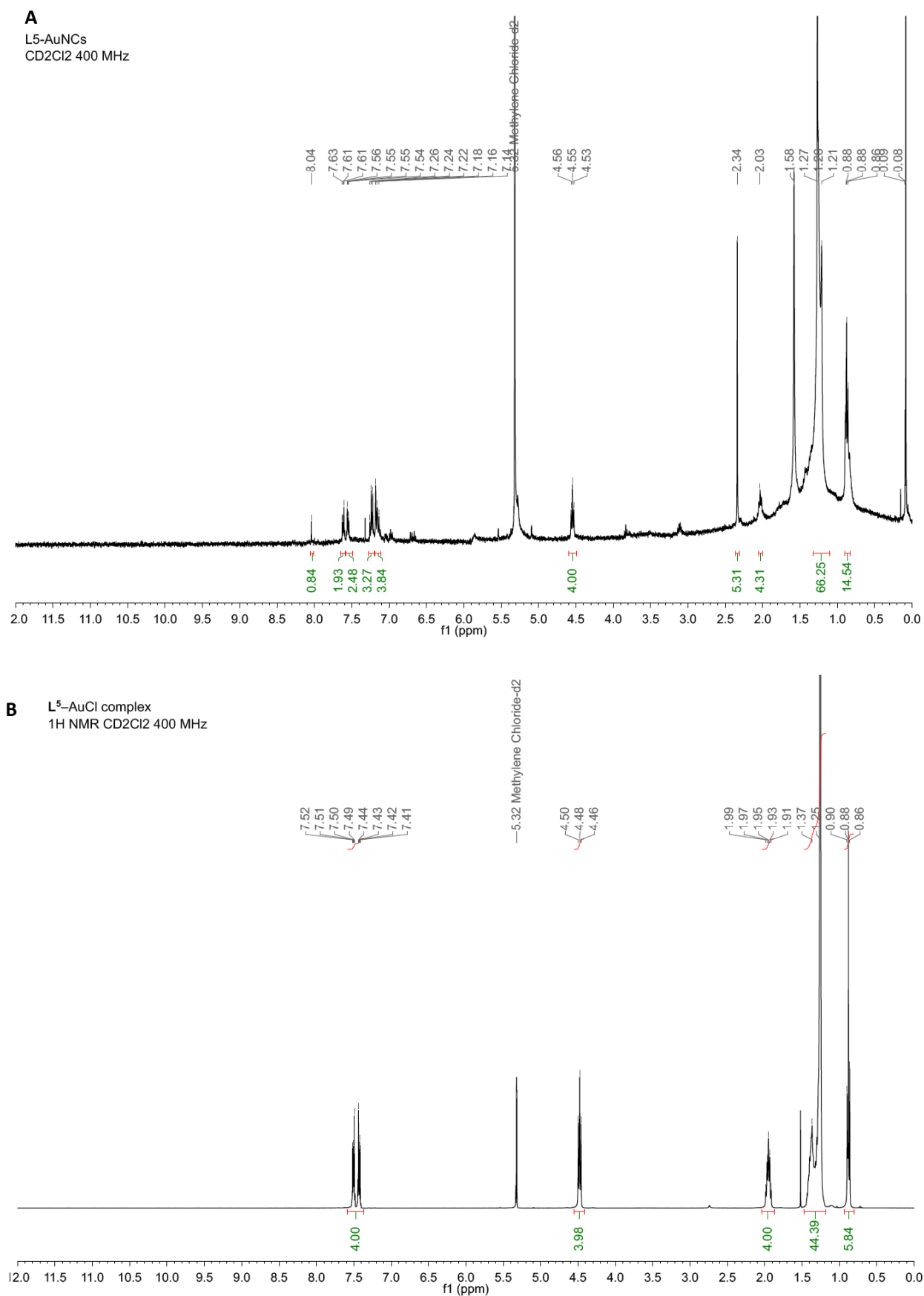


Figure S3. ¹H NMR spectra of L⁵-coated AuNCs in CD₂Cl₂ (A) and L⁵-AuCl (B).

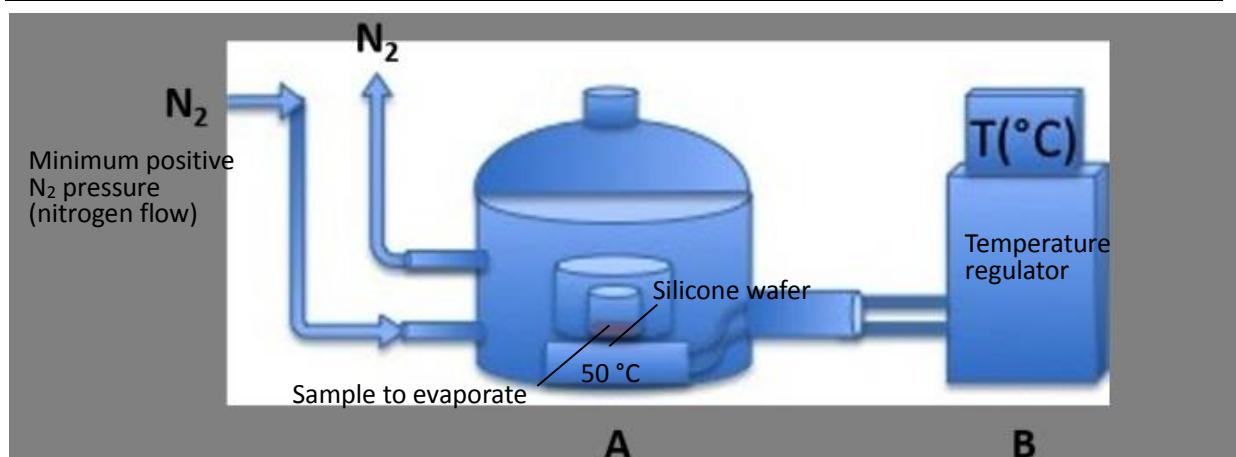


Figure S4. Evaporation device for Au supracrystals preparation.

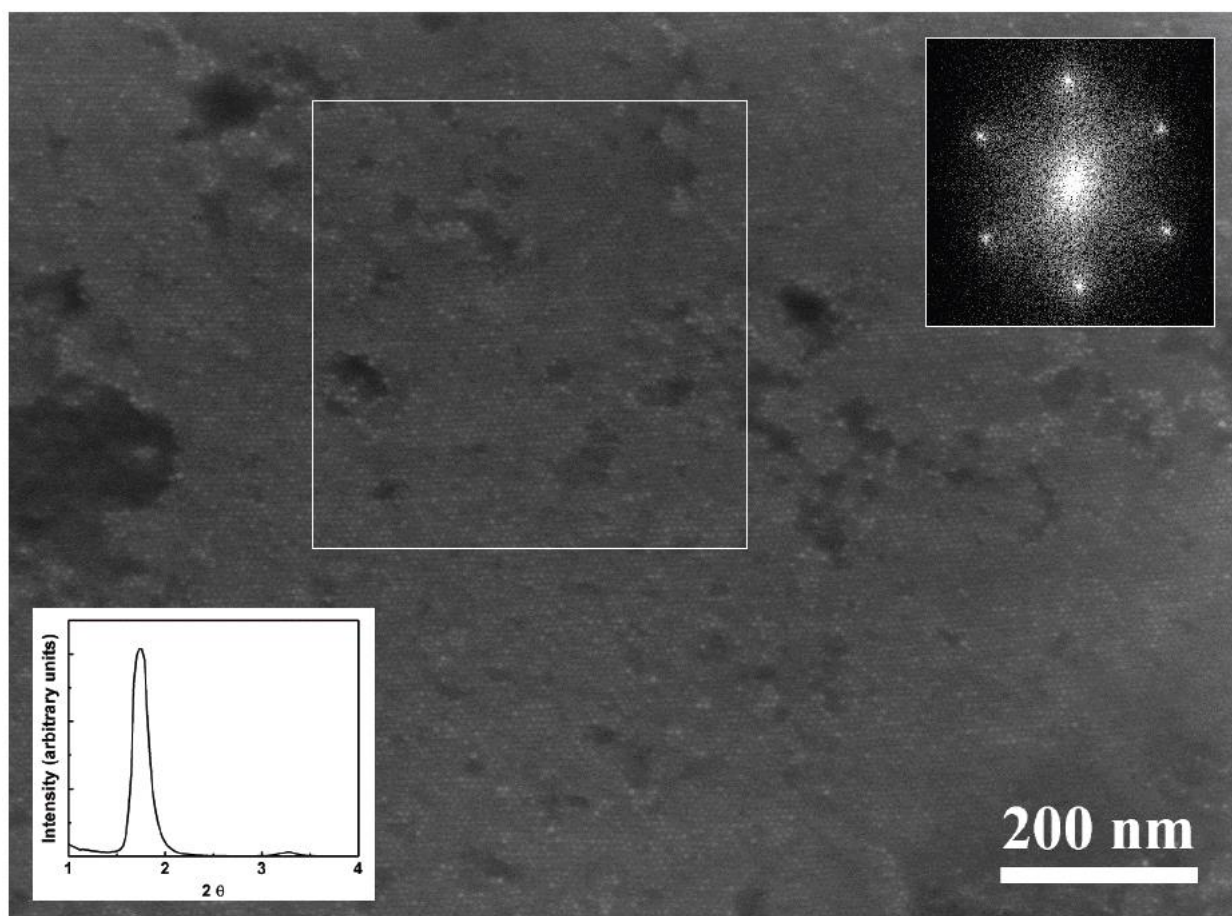


Figure S5. HRSEM image and SAXRD pattern of supracrystals made of L⁴-coated Au nanocrystals.

Chapter 4

Superior Oxygen Stability of N-Heterocyclic Carbene-coated Au Nanocrystals – Comparison with Thiol-coated Analogues

4.1 Abstract

The oxygen stability of Au nanocrystals (NCs) coated with different *N*-heterocyclic carbenes (NHCs) or dodecanethiol (DDT) was investigated. A dominant effect of the ligand type was observed with a significantly greater oxygen resistance of NHC-coated Au NCs compared to the thiol-based analogues. NHC-coated Au NCs are stable to 10 W oxygen plasma etching for up to 180 s whereas the integrity of DDT-coated Au NCs is strongly affected by the same treatment from 60–80 s. In the latter case, the average size of the NCs (from 2.6 to 6.3 nm) and the synthetic method have no effect on the stability. The increased stability of NHC-coated Au NCs is related to a lower release of ligand-derived species under oxygen treatment.

4.2 Articles: Superior Oxygen Stability of N-Heterocyclic Carbene-coated Au Nanocrystals – Comparison with Thiol-coated Analogues

Superior Oxygen Stability of N-Heterocyclic Carbene-coated Au Nanocrystals – Comparison with Thiol-coated Analogues

Xiang Ling,^{a,b,c} Nicolas, Schaeffer,^{a,b} Sylvain Roland,^{*c} and Marie-Paule Pileni^{*a,b,d}

^a Sorbonne Universités, UPMC-Univ Paris 6, UMR 8233, MONARIS, F-75005, Paris, France

^b CNRS, UMR 8233, MONARIS, F-75005, Paris, France

^c Sorbonne Universités, UPMC-Univ Paris 6, UMR 8232, Institut Parisien de Chimie Moléculaire, F-75005, Paris, France

^d CEA/IRAMIS, CEA Saclay, 91191, Gif-Sur-Yvette, France

INTRODUCTION

Au nanocrystals have attracted increasing interest for their particular optical and electronic properties,¹⁻³ and their potential applications in biology,⁴⁻⁷ and catalysis.⁸⁻¹⁰ Furthermore, many studies demonstrated that Au NCs do not show detectable cytotoxicity for relatively short periods of exposure (48–72 h).^{11,12} Thus, it has been generally accepted that Au nanocrystals are non-cytotoxic and present biocompatible properties suitable for applications in nanomedicine or nanobiotechnology.^{13,14} However, the toxicity and biocompatibility of nanocrystals is highly related to their stability,^{15,16} and more particularly to their long-term stability. The long-term stability of Au nanocrystals is still a major concern for the development of reliable and safe applications.¹⁷ So far, functionalized thiol-coated Au NCs have been the most widely studied for biomedical applications. However, recent studies showed that the thiol–Au covalent bond, which is generally considered as a strong bond, is subject to cleavage when exposed to air, high salt concentration, elevated temperatures or high pH, resulting in compromised long-term stability.¹⁸⁻²¹

N-Heterocyclic Carbenes (NHCs) have emerged as a major class of ligands in organometallic chemistry.²²⁻²⁵ Owing to their strong σ -donating properties, NHC ligands can form strong bonds with metal centers to give stable metal-NHC complexes. Furthermore, NHCs exhibit a particular geometry and high synthetic flexibility allowing fine-tuning of their steric and electronic properties.²⁶ Thus, metal-NHC complexes have been extensively investigated for catalytic applications,²⁷ and have shown promising potential in the

biomedical field.^{28–31} For the same reasons, NHCs are expected to be highly promising ligands for the development of stable and functionalized materials. In recent years, an increasing number of studies described the use of NHC ligands to stabilize nanocrystals.^{32–51} A few reports also focussed on the formation of NHC-based self-assembled monolayers (SAMs) on Au surfaces.^{52–54} Benzimidazole-derived NHCs were shown to provide SAMs with high stability in various conditions, including oxidative treatment with 1% hydrogen peroxide.⁵⁴ However, to the best of our knowledge, the stability of NHC-coated NCs under oxygen exposure, which is a major cause of degradation, was virtually not explored.

We present herein an investigation of the stability of various NHC- and DDT-coated Au NCs upon exposure to either oxygen plasma treatment or pure oxygen flow (Figure 1).⁵⁵ For this comparative study, we prepared a series of DDT-coated Au NCs (**DDT Au^{1–5}**) of different sizes, from H AuCl₄ (**1**), [Au(PPh₃)Cl] (**2**) or [Au(NHC)Cl] complexes (**3–5**) as precursors (Table 1 and Figure 2) through three different methods, involving either a reverse micelle system (see experimental, method A),⁵⁶ or procedures derived from the Stucky's method (methods B and C).^{57,58} We also prepared a series of NHC-coated Au NCs (Figure 1, **NHC Au^{6–10}**) with different NHC ligand structures (Figure 3, **NHC^{A–E}**) from the corresponding azolium chloroaurate salts (**6–10**) (method D).⁵¹ We demonstrate here that NHC-coated Au nanocrystals exhibit greater resistance to oxygen plasma etching and pure oxygen treatment than DDT-coated Au nanocrystals.

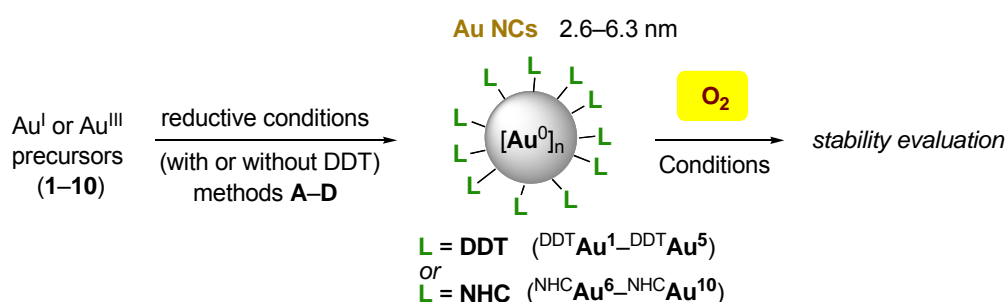


Figure 1. DDT-coated and NHC-coated Au NCs submitted to oxygen treatments.

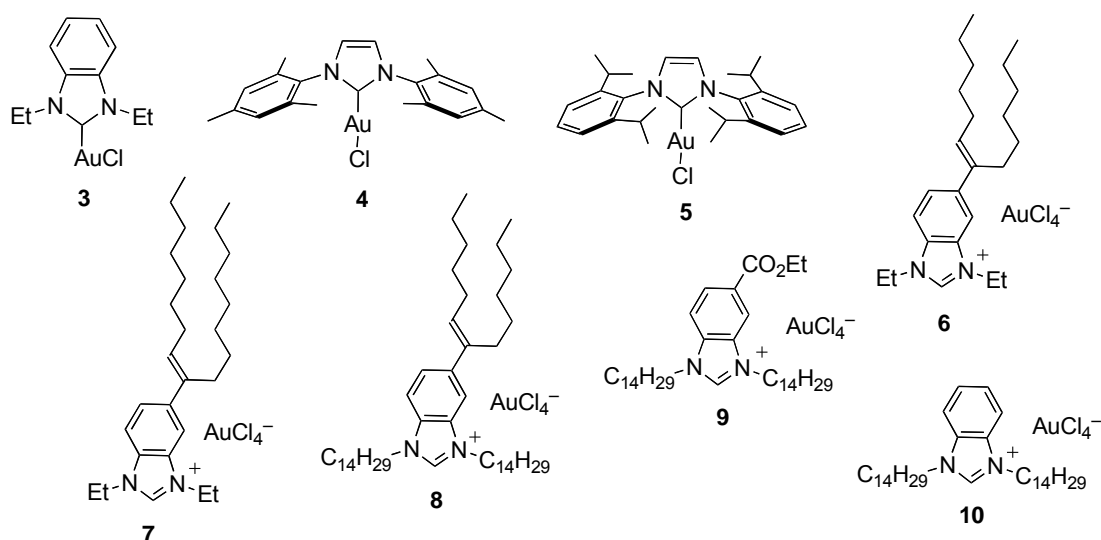


Figure 2. Au^I and Au^{III} precursors used in this study for the preparation of Au NCs.

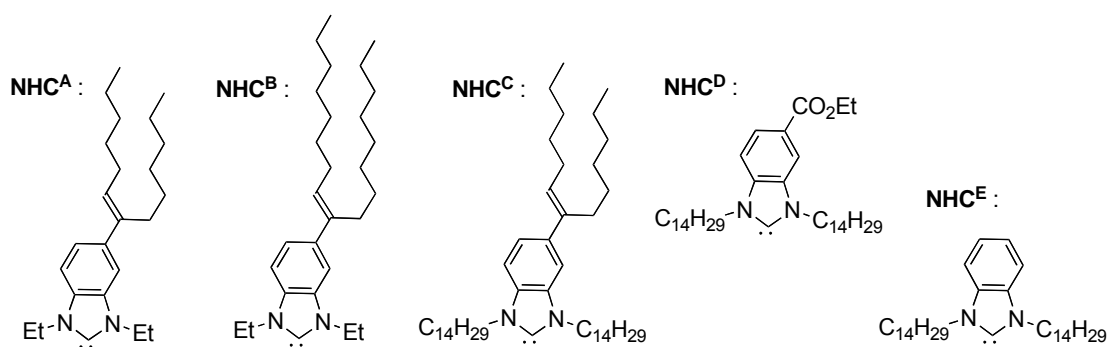


Figure 3. NHC ligands used in this study for NHC-coated Au NCs.

EXPERIMENTAL SECTION

Chemicals and Materials. Common reagents were purchased from commercial sources and used as received unless stated otherwise. Au complexes [HAuCl₄] (1), [(PPh₃)AuCl] (2), and [(IPr)AuCl] (5) were purchased from commercial sources (Strem and Sigma-Aldrich) and used as received. Complexes [(Et₂Bimy)AuCl] (3) and [(IMes)AuCl] (4) were prepared according to the procedure previously reported.⁴³ Benzimidazolium chloraurate salts (6–10) were synthesized as previously described.⁵¹ Dichloromethane was distilled from CaH₂. Dry and degassed (argon bubbling) toluene was used. Au NCs preparations were carried out in a glove-box according to methods B–D (Table 1). The nanocrystals were re-suspended in toluene for TEM analyses unless otherwise stated.

Table 1. Preparation of Au NCs: precursors, methods and NC sizes.

Au ^I or Au ^{III} precursor	method	Au NCs	D (nm) ^[a]	σ (%) ^[b]
[HAuCl ₄] (1)	A	^{DDT} Au ¹	6.1	7.4
[(PPh ₃)AuCl] (2)	B	^{DDT} Au ²	6.0	4.8
[(Et ₂ Bimy)AuCl] (3)	C	^{DDT} Au ³	6.3	6.7
[(IMes)AuCl] (4)	C	^{DDT} Au ⁴	6.2	6.4
[(IPr)AuCl] (5)	C	^{DDT} Au ⁵	2.6	11.5
[(NHC ^A H ⁺)•(AuCl ₄ ⁻)] (6)	D	^{NHC} Au ⁶	5.9	9.2
[(NHC ^B H ⁺)•(AuCl ₄ ⁻)] (7)	D	^{NHC} Au ⁷	5.7	10.1
[(NHC ^C H ⁺)•(AuCl ₄ ⁻)] (8)	D	^{NHC} Au ⁸	4.0	11.5
[(NHC ^D H ⁺)•(AuCl ₄ ⁻)] (9)	D	^{NHC} Au ⁹	5.1	8.6
[(NHC ^E H ⁺)•(AuCl ₄ ⁻)] (10)	D	^{NHC} Au ¹⁰	4.9	9.8

[a] Average size of Au NCs. [b] Standard deviation for the size distribution.

Preparation of Au nanocrystals.

Method A: This method gave DDT-coated Au NCs ^{DDT}Au¹ via reverse micelles.⁵⁵ An aqueous solution of [HAuCl₄] (**1**) (0.2 M, 15 μL) was added to a solution of NaAOT in isooctane (0.2 M, 3 mL) and aqueous hydrazine (0.75 M, 12 μL) was added under stirring. Immediately after addition, the color of the medium turned from yellow to dark red, indicating the formation of Au NCs. After 20 min, dodecanethiol (DDT, 20 μL) was added to the reaction mixture. After 2 h, EtOH was added to the solution followed by centrifugation at 4500 rpm for 5 min to remove AOT (surfactant). The black precipitate was recovered and dried under a nitrogen flow to give ^{DDT}Au¹ NCs.

Method B: This method gave DDT-coated Au NCs ^{DDT}Au² by one-phase reduction according to Stucky's method.^{56,57} The synthesis was carried out by using two solutions. For the first one, [(PPh₃)AuCl] (**2**) (0.25 mmol) was dissolved in toluene (25 mL) and DDT (2 mmol) was added under stirring. The second solution was obtained by dissolving borane *tert*-butylamine complex (2.5 mmol) in toluene (15 mL). Both solutions were stirred at 100 °C until complete dissolution of all products and mixed together. After mixing, a rapid color change was observed from colorless to dark red. The colloidal solution was dried with a nitrogen flow to give a dark powder. EtOH was added and the mixture was stirred and centrifuged to give a black precipitate which was recovered after removal of the supernatant and dried under a nitrogen flow. Dispersion of the precipitate in toluene and centrifugation

gave Au NCs ^{DDT}Au² after removal of the supernatant and drying.

Method C: This method gave DDT-coated Au NCs ^{DDT}Au³, ^{DDT}Au⁴ and ^{DDT}Au⁵ by one-phase reduction of [Au(NHC)Cl] complexes (**3–5**) (Figure 2).⁴³ A solution of **3–5** (0.125 mmol) and DDT (250 μ L, 1 mmol) in toluene (12.5 mL) was heated at 100 °C (oil bath) under vigorous magnetic stirring. To the mixture was added (at 100 °C) a solution of NH₃BH₃ (1.25 mmol) in toluene (5 mL) and ethanol (2.5 mL). The reaction was allowed to proceed for 30 min (at 100 °C) before cooling down to room temperature. Toluene was evaporated under a nitrogen flow. The as-formed precipitate was washed with ethanol and dried to give Au NCs ^{DDT}Au^{3–5}.

Method D: This method gave NHC-coated Au NCs ^{NHC}Au^{6–10} by reduction of azolium chloroaurate salts (**6–10**) (Figure 2).^{51,44} In this procedure, the NHC ligands (**NHC^{A–E}**, Figure 3) are generated in situ (not isolated). To a suspension of sodium hydride (60% dispersion in mineral oil, 7.4 mg, 0.188 mmol) in a 1:1 mixture of CH₂Cl₂/toluene (7.2 mL) was added dropwise at 0.6 °C (ice bath) a solution of chloroaurate benzimidazolium salt (**6–10**) (0.12 mmol) in CH₂Cl₂ (1.8 mL). The mixture was stirred for 30 min. A solution of NaBH₄ (24 mg, 0.62 mmol) in water (0.9 mL) was added dropwise while maintaining the temperature at 0.6 °C (ice bath). After addition, the mixture was allowed to stir at room temperature for 2 h. The solvents were removed under a nitrogen flow to give a dark powder. The powder was washed with ethanol and the suspension was centrifuged. The supernatant (EtOH) was removed. The residue was dried under a nitrogen stream to give Au NCs ^{NHC}Au^{6–10} as dark powders. Subsequently, size selection was performed to obtain NHC-coated Au nanocrystals with improved size distribution.⁵¹

Instruments. Transmission Electron Microscopy (TEM) was performed with a JEOL model JEM-1001 (100 kV). NMR spectra were recorded on a Bruker Nanobay spectrometer 400 MHz. In CD₂Cl₂, proton chemical shifts (δ) are reported relative to the residual protonated solvent ($\delta = 5.32$ ppm).

Reactive Ion Etching (RIE). *Experimental Conditions:* After deposit of the nanocrystals solution on the TEM grids covered by amorphous carbon, the samples were loaded into the RIE apparatus (reactive ion system Plassys MG 200). The plasma treatment was carried out using oxygen as the etching gas, with a plasma power of 10 W, a working pressure maintained at 6.4 μ bar, and an oxygen flow rate of 10 sccm.

Results and Discussion

Etching of dodecanethiol-coated Au NCs with oxygen plasma.

The stability to oxygen plasma exposure of dodecanethiol-coated Au NCs $^{DDT}\text{Au}^{1-5}$, obtained by various methods (A–C) and from different precursors was examined. Au NCs $^{DDT}\text{Au}^1$, prepared through reverse micelles, were suspended in toluene and deposited on a carbon-covered copper TEM grid. The TEM image showed a hexagonal-arranged 2D network of $^{DDT}\text{Au}^1$ with well-separated NCs having an average size of 6.1 nm (Figure 4A). Following the deposit, the sample was loaded into the RIE apparatus and submitted to oxygen plasma for 60 s. After this exposure time, the TEM image showed that the NCs started to be affected by the oxidative treatment as attested by the presence of a few pairs of associated NCs (see Figure S1 in the Supplementary Information). By extending the exposure time to 80 s, the formation of a large proportion of coalesced objects was observed. This demonstrated that $^{DDT}\text{Au}^1$ start to decompose from 60 s of exposure and are clearly affected by the oxidative treatment at 80 s (Figure 4C).

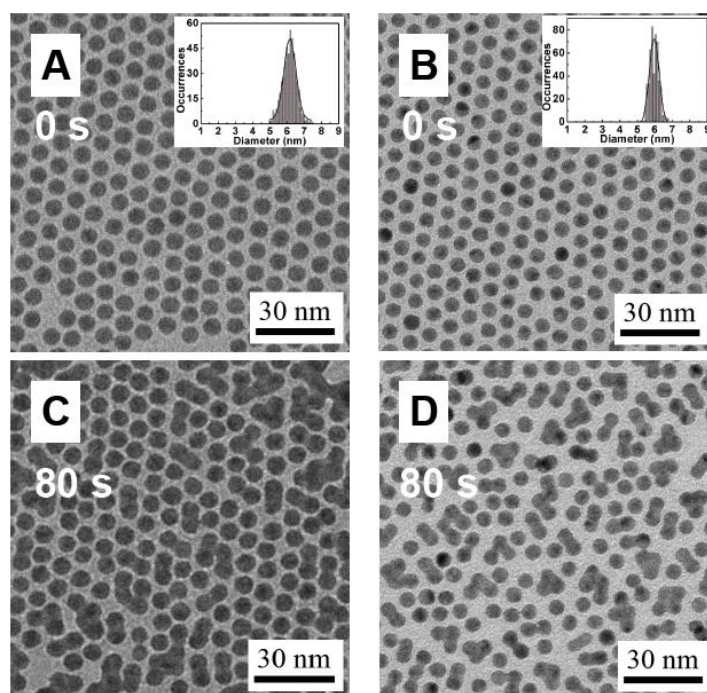


Figure 4. TEM images of $^{DDT}\text{Au}^1$ (A) and $^{DDT}\text{Au}^2$ (B) deposited on an amorphous carbon-covered TEM grid before oxygen plasma exposure ($t = 0$ s). Same areas after exposure to oxygen plasma for 80 s at 10 W of $^{DDT}\text{Au}^1$ (C) and $^{DDT}\text{Au}^2$ (D).

A similar treatment was applied to DDT-coated Au NCs $^{DDT}\text{Au}^2$, synthesized from $[\text{Au}(\text{PPh}_3)\text{Cl}]$ as precursor through one-phase reduction (see Experimental section). One drop of the $^{DDT}\text{Au}^2$ dispersion in toluene was deposited on a copper TEM grid covered by

amorphous carbon and analyzed before oxygen exposure. As for $^{DDT}Au^1$, the initial TEM image showed a well-ordered hexagonal-packed monolayer of $^{DDT}Au^2$ with an average NC size of 6.0 nm associated with a narrow size distribution (Figure 4B and Table 1). All the NCs are well-separated on the surface. Following the deposit, the sample was treated for 60 s with oxygen plasma. After this treatment, no changes in either the $^{DDT}Au^2$ nanocrystals integrity or their 2D assembly was detectable from the TEM images (see Figure S1 in the Supplementary Information). However, when the exposure to oxygen plasma was increased to 80 s, a dramatic alteration of the monolayer was observed. The TEM images show that many adjacent Au nanocrystals have bound together and formed ill-defined objects resulting from coalescence (Figure 4B).

Similar experiments were carried out with Au NCs $^{DDT}Au^3$, $^{DDT}Au^4$ and $^{DDT}Au^5$, prepared by one-phase reduction of Au–NHC complexes in the presence of DDT. This Au NCs series was considered as DDT-coated. DDT was shown to be essential for the formation of stable Au NCs from Au–NHC complexes **3–5**, for which the NHC ligand is likely ill-suited for efficient Au NCs stabilization.⁴³ Dispersions of $^{DDT}Au^3$, $^{DDT}Au^4$ and $^{DDT}Au^5$ in toluene were deposited on copper TEM grids covered by amorphous carbon. The TEM images of these samples, used as references, showed that $^{DDT}Au^3$ and $^{DDT}Au^4$ are arranged in 2D hexagonal networks with well-separated NCs. $^{DDT}Au^{3-4}$ NCs are characterized by narrow size distributions and similar average sizes of 6.3 and 6.2 nm, respectively (Figures 5A and 5B). As previously observed,⁴³ $^{DDT}Au^5$ nanocrystals exhibit a smaller average size of 2.6 nm with a slightly broader size distribution and a less orderly 2D arrangement (Figure 5C and Table 1). After deposit and TEM control, the samples of $^{DDT}Au^{3-5}$ were exposed for 60 s to oxygen plasma into the RIE apparatus. The TEM images showed that this treatment induces no changes in either the nanocrystals integrity or their ordering regardless of the sample concerned ($^{DDT}Au^3$, $^{DDT}Au^4$ or $^{DDT}Au^5$) (Figure S2 in the Supplementary Information). The time of etching with oxygen plasma was then increased from 60 s to 80 s. Under these conditions, the presence of a lot of coalesced objects was observed on the TEM grid for all NCs samples $^{DDT}Au^3$, $^{DDT}Au^4$ and $^{DDT}Au^5$ (Figure 5D, 5E and 5F), thus demonstrating a dramatic impact of the oxidative treatment on their integrity.

This first series of experiments demonstrated that all dodecanethiol-coated Au NCs $^{DDT}Au^{1-5}$ are similarly affected by oxygen plasma treatment. Their resistance against aggregation when arranged as 2D networks is independent of the NCs sizes as shown by the similar resistance of $^{DDT}Au^4$ (6.2 nm) and $^{DDT}Au^5$ (2.6 nm). In addition, the method to prepare

the NCs (methods A–C), also seems to have no effect on the stability. All DDT-coated Au NCs ${}^{\text{DDT}}\text{Au}^{1-5}$ coalesce at 80 s of exposure, suggesting that DDT ligands on the surface have partially been desorbed, and inducing agglomeration of the nanocrystals.

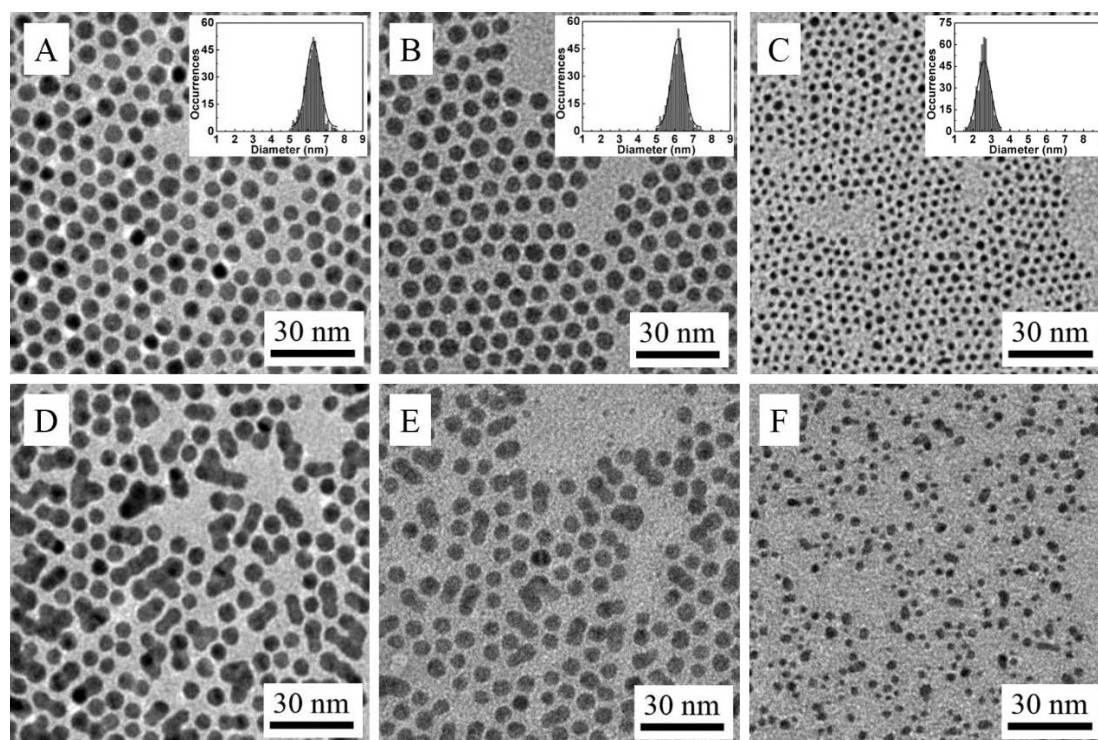


Figure 5. TEM images of ${}^{\text{DDT}}\text{Au}^3$ (A), ${}^{\text{DDT}}\text{Au}^4$ (B) and ${}^{\text{DDT}}\text{Au}^5$ (C) deposited on an amorphous carbon covered TEM grid before oxygen plasma exposure. Same areas after exposure to oxygen plasma for 80 s at 10 W of ${}^{\text{NHC}}\text{Au}^3$ (D), ${}^{\text{NHC}}\text{Au}^4$ (E) and ${}^{\text{NHC}}\text{Au}^5$ (F).

Etching of NHC-coated Au NCs with oxygen plasma.

NHC-coated Au NCs ${}^{\text{NHC}}\text{Au}^{6-10}$ are stabilized by three different families of NHC ligands ($\text{NHC}^{\text{A-E}}$) bearing long alkyl chains at different positions (Figure 3).⁵¹ The structure of the NHC was previously shown to have an effect on the NCs size, likely related to the volume of the NHC. NHC-stabilized Au nanocrystals ${}^{\text{NHC}}\text{Au}^{6-10}$ were dispersed in toluene and deposited on copper TEM grids covered by amorphous carbon. As previously observed, the TEM images, used as references, showed that ${}^{\text{NHC}}\text{Au}^6$ and ${}^{\text{NHC}}\text{Au}^7$ have similar average sizes of 5.7–5.9 nm whereas ${}^{\text{NHC}}\text{Au}^9$ and ${}^{\text{NHC}}\text{Au}^{10}$ exhibit slightly smaller average sizes of 5.1–4.9 nm (Table 1, Figures 6A, 6C and Figures S3A, S3B). ${}^{\text{NHC}}\text{Au}^8$, stabilized by the most bulky NHC^{C} ligand is characterized by a smaller average size of 4.0 nm (Table 1, Figure 6B). After TEM control, the samples were loaded into the RIE apparatus and submitted to oxygen plasma for 80 s. At this exposure time, in contrast to DTT-coated Au NCs, no changes in either the NCs integrity or their 2D assembly was detectable by TEM for all NHC-based Au NCs. The

Chapter 4 Superior Oxygen Stability of N-Heterocyclic Carbene-coated Au Nanocrystals – Comparison with Thiol-coated Analogues

exposure time was then increased to 120 s. Here again, the TEM images revealed that NHC Au^{9-10} remained structurally not affected by the oxidative treatment (Figures 6D–F and S3). This demonstrated that all the NHC-coated Au NCs used in this study are resistant to oxygen plasma treatment for at least 120 s, regardless of the NCs size and the NHC ligand structure. Subsequently, NHC Au^{10} was used as a sample to test an extended exposure time of 180 s. The TEM image demonstrated that the integrity and the 2D arrangement of the NCs remained unchanged under these conditions (Figure S4). This experiment could not be reproduced with the same quality on other samples as the carbon film on copper grids is strongly affected at this exposure time and totally broken down at an exposure time exceeding 180 s. For the same reason, no further tests could be implemented at longer times.

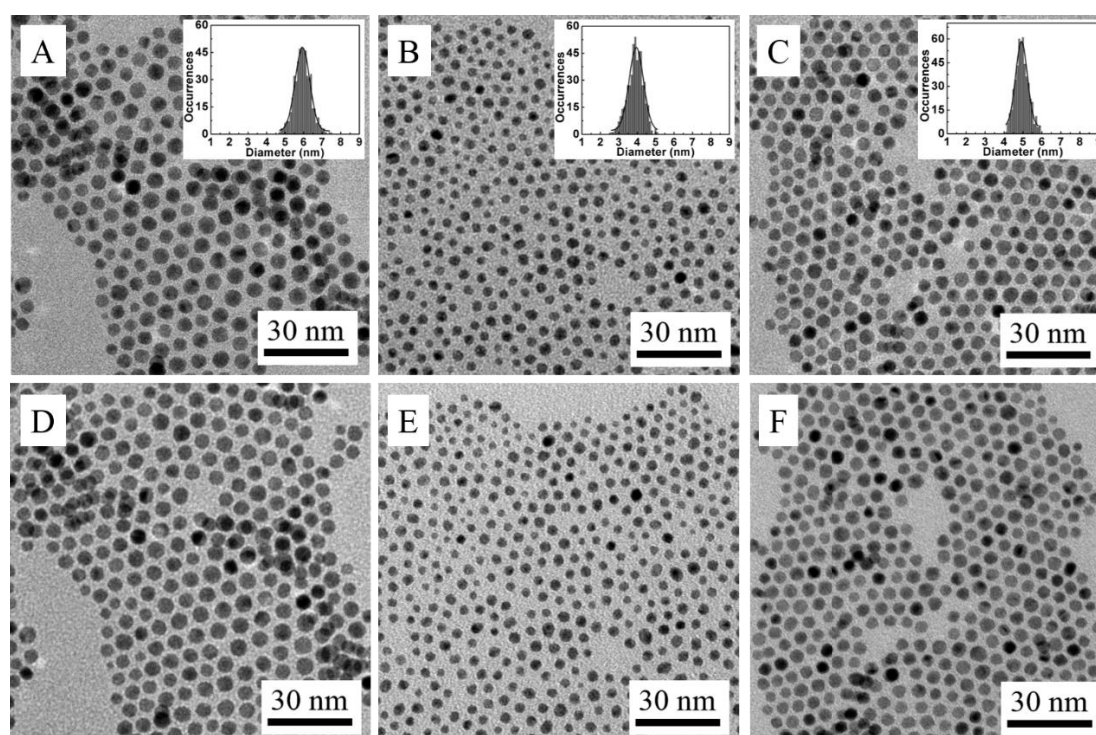


Figure 6. TEM images of NHC Au^6 (A), NHC Au^8 (B) and NHC Au^{10} (C) deposited on an amorphous carbon covered TEM grid before oxygen plasma exposure. Same areas after exposure to oxygen plasma for 120 s at 10 W of NHC Au^6 (D), NHC Au^8 (E) and NHC Au^{10} (F).

The results for DDT-coated Au nanocrystals showed that their stability was similar, regardless of the sizes of Au nanocrystals and the synthetic method. Compared with DDT-coated Au nanocrystals, NHC-coated Au NCs show a remarkable higher resistance to oxygen plasma which similarly, seems to be independent of NCs size and NHC structure. This indicates that NHC ligands provide much more stability to Au nanocrystals than dodecanethiol. This is consistent with literature reports highlighting the use of strong headgroup-substrate binding as a particularly effective strategy for generating films that

provide long-term stability to the underlying metal substrates and NCs.¹⁶ In the case of thiol-coated Au surfaces, typical thiols are expected to bind to gold with a S–Au binding energy of approximately 125 kJ mol⁻¹.^{59,60} For NHC-coated Au(111) surfaces, a calculated C_{carbene}–Au bond strength of 150 kJ mol⁻¹ was reported, approximately 25 kJ mol⁻¹ higher than that of thiols.⁵⁴

Influence of pure oxygen on ^{NHC}Au and ^{DDT}Au nanocrystals. NMR analyses.

To further evaluate the stability of NHC-protected Au nanocrystals and compare with thiol-based NCs, control experiments have been implemented where the dry solid samples of **NHC^E**-stabilized Au nanocrystals (^{NHC}**Au¹⁰**) and DDT-coated NCs ^{DDT}**Au¹** were exposed to a pure oxygen flow for one week (see device in Figure S5 in the Supplementary Information). ¹H NMR spectroscopy was used to analyze the colloidal solutions of the samples before and after exposure to oxygen. The initial ¹H NMR spectrum of Au NCs ^{NHC}**Au¹⁰** in CD₂Cl₂ before treatment (Figure 7A) shows a significant broadening of some peaks, which is characteristic of ligands bound at the surface of nanocrystals. After oxygen treatment, the dry sample was dissolved in CD₂Cl₂ and directly analyzed. By comparison with the initial sample, no visible changes were detected in the solution. In both experiments, the dissolution of ^{NHC}**Au¹⁰** in CD₂Cl₂ gave a deep colored mixture with no visible precipitate. The ¹H NMR spectrum (Figure 7B) of the sample after treatment was found to be very similar to that of the initial sample. It shows a major species corresponding to the bound NHC ligand as observed before oxygen exposure (Figure 7A). However, a new set of peaks (*), corresponding to a single minor species, is also visible. This new set of signals has the same profile than the bound NHC ligand although it presents slightly different chemical shifts. For this reason, it could be attributed to a **NHC^E**-derived molecule. On the basis of the NMR integration of the signals around 4.5 ppm, less than 17% of the bound **NHC^E** ligands have been converted to this new compound.

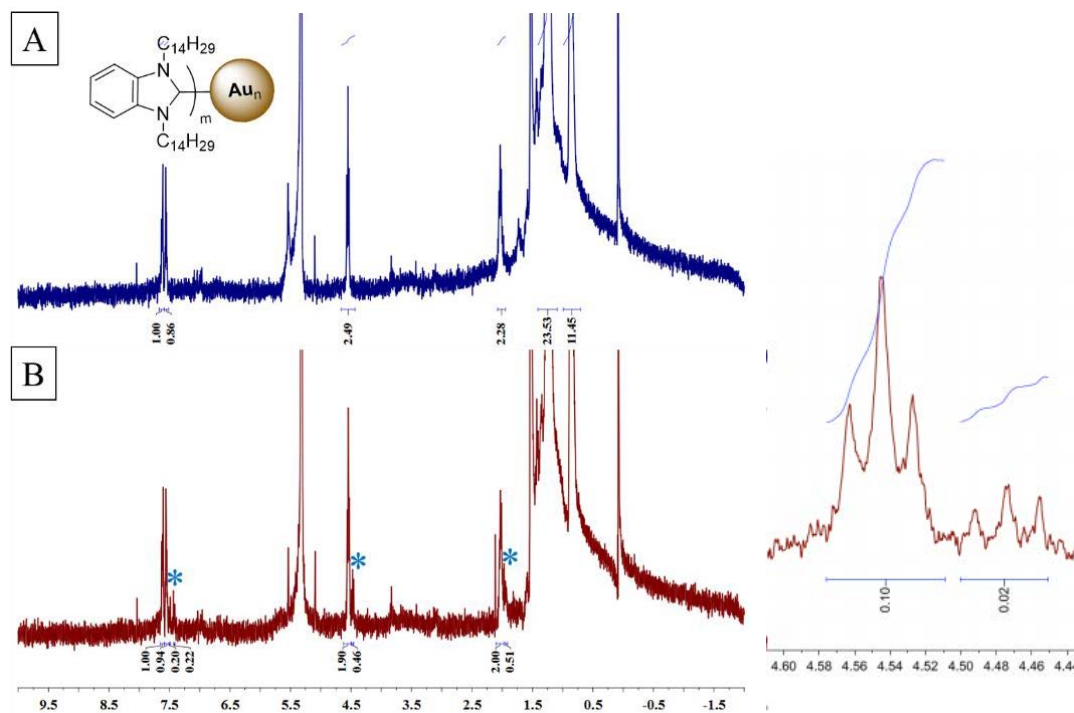


Figure 7. ¹H NMR spectra of ^{NHC}Au¹⁰ before exposure (A) and after exposure (B) to a pure oxygen flow for one week.

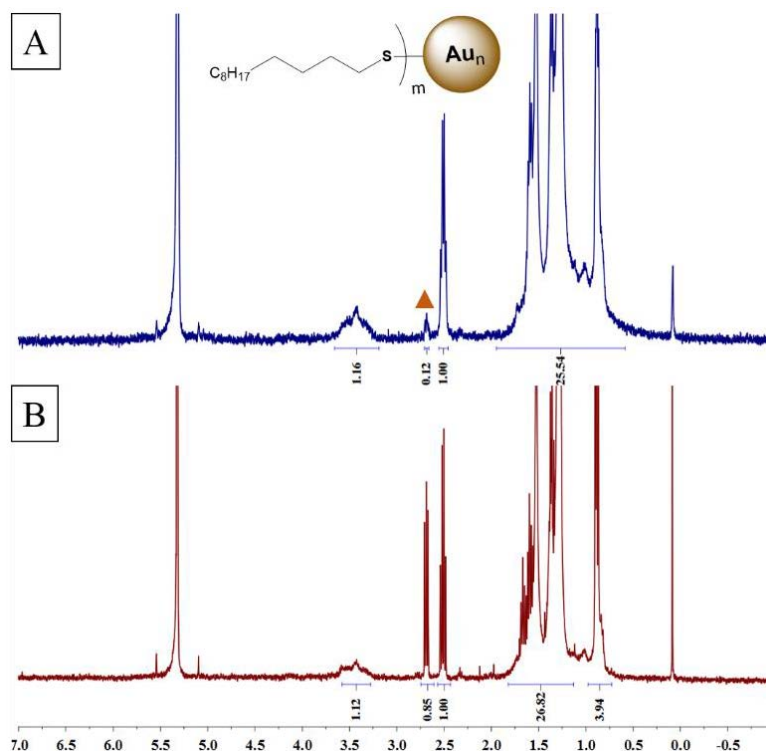


Figure 8. ¹H NMR spectra of ^{DDT}Au¹ before exposure (A) and after exposure (B) to a pure oxygen flow for one week.

The same experiments were performed with DDT-stabilized Au nanocrystals ^{DDT}Au¹. The initial ¹H NMR spectra of ^{DDT}Au¹ before exposure to oxygen presents typical broad signals

corresponding to DDT bound at the Au surface [ref NMR spectrum]. In contrast to NHC-coated NCs, the colloidal solution of $^{DDT}Au^1$ contains a significant amount of free ligands. From the NMR spectrum, the ratio of bound DDT to free ligands was estimated at 1:1 (Figure 8A). The thin signals observed at 2.50 and 2.69 ppm (small triplet) originate from the α -methylene protons of free DDT and of traces of the free disulfide ($C_{24}H_{50}S_2$, ~5% of free DDT), respectively.[ref NMR] After oxygen treatment, the dry sample was dissolved in CD_2Cl_2 . By comparison with the initial sample, the solution presents a lighter color and a precipitate is clearly visible, indicating a possible degradation of the NCs. This was confirmed by the 1H NMR spectrum showing that the amount of free disulfide and DDT significantly increased (Figure 8B). Based on the integrations, the proportion of bound DDT was estimated at 35% of all DDT-based species present in the solution. Free DDT is still largely present with a percentage of 35%. The main difference resides in the increased amount of disulfide (~15%) that indicates that about 30% of the dodecanethiol have been oxidized into disulfide.

These data clearly show that the exposure to oxygen induces the oxidation of a significant amount of DDT into its corresponding disulfide. By comparison, the oxygen treatment of NHC-coated Au NCs induces the formation of lower amounts of ligand-derived species that might be related to the increased stability of the NHC–Au moieties. Thus, although NHC ligands bound to the surface of nanocrystals are not completely insensitive to the effect of oxygen, they show more resistance to oxygen than the thiol.

CONCLUSION

We showed herein that NHC-stabilized Au nanocrystals exhibited considerably greater resistance to oxygen plasma than DDT-protected Au nanocrystals. The stability of the DDT-stabilized Au nanocrystals is independent of the sizes of Au nanocrystals and the methods to generate the nanocrystals. In addition, we demonstrated that NHC ligands bound to the surface of Au NCs are significantly more resistant to O_2 -induced transformations than dodecanethiol.

ASSOCIATED CONTENT

Supporting Information. Additional TEM images of Au NCs exposure to oxygen plasma and set-up for exposure to pure oxygen flow. This material is available free of charge via the Internet at <http://pubs.acs.org>.

AUTHOR INFORMATION

Corresponding Author

* mp.pileni@orange.fr

* sylvain.roland@upmc.fr

Author Contributions

The manuscript was written through contributions of all authors. All authors have given approval to the final version of the manuscript.

Notes

The authors declare no competing financial interest.

ACKNOWLEDGMENT

This research has been supported from Advanced Grant of the European Research Council under Grant Agreement No. 267129. X.L. thanks for the financial support of the China Scholarship Council.

REFERENCES

- (1) Schatz, G. C. Using theory and computation to model nanoscale properties. *PNAS* **2007**, *104*, 6885.
- (2) El-Sayed, M. A. Small is different: Shape-, size-, and composition-dependent properties of some colloidal semiconductor nanocrystals. *Acc. Chem. Res.* **2004**, *37*, 326.
- (3) Elghanian, R.; Storhoff, J. J.; Mucic, R. C.; Letsinger, R. L.; Mirkin, C. A. Selective colorimetric detection of polynucleotides based on the distance-dependent optical properties of gold nanoparticles. *Science* **1997**, *277*, 1078.
- (4) Jain, P. K.; El-Sayed, I. H.; El-Sayed, M. A. Au nanoparticles target cancer. *Nano Today* **2007**, *2*, 18.
- (5) Sperling, R. A.; Rivera gil, P.; Zhang, F.; Zanella, M.; Parak, W. J. Biological applications of gold nanoparticles. *Chem. Soc. Rev.* **2008**, *37*, 1896.
- (6) Bardhan, R.; Lal, S.; Joshi, A.; Halas, N. J. Theranostic Nanoshells: From Probe Design to Imaging and Treatment of Cancer. *Acc. Chem. Res.* **2011**, *44*, 936.
- (7) Saha, K.; Agasti, S. S.; Kim, C.; Li, X. N.; Rotello, V. M. Gold Nanoparticles in Chemical and Biological Sensing. *Chem. Rev.* **2012**, *112*, 2739.
- (8) Chen, M. S.; Goodman, D. W. Catalytically active gold: From nanoparticles to ultrathin films. *Acc. Chem. Res.* **2006**, *39*, 739.
- (9) Corma, A.; Serna, P. Chemoselective hydrogenation of nitro compounds with supported

gold catalysts. *Science* **2006**, *313*, 332.

(10) Hashmi, A. S. K.; Hutchings, G. J. Gold catalysis. *Angew. Chem. Int. Ed.* **2006**, *45*, 7896.

(11) Feng, L.; Tianjun, L.; Li, W. In *7th Asian-Pacific Conference on Medical and Biological Engineering*; Peng, Y., Weng, X., Eds.; Springer Berlin Heidelberg: 2008; 19, 186.

(12) Jain, S.; Hirst, D. G.; O'Sullivan, J. M. Gold nanoparticles as novel agents for cancer therapy. *Br. J. Radiol.* **2012**, *85*, 101.

(13) De Jong, W. H.; Borm, P. J. A. Drug delivery and nanoparticles: Applications and hazards. *Int. J. Nanomed.* **2008**, *3*, 133.

(14) Baptista, P.; Pereira, E.; Eaton, P.; Doria, G.; Miranda, A.; Gomes, I.; Quaresma, P.; Franco, R. Gold nanoparticles for the development of clinical diagnosis methods. *Anal. Bioanal. Chem.* **2008**, *391*, 943.

(15) Wu, L.; Zhang, J.; Watanabe, W. Physical and chemical stability of drug nanoparticles. *Adv. Drug Deliv. Rev.* 2011, *63*, 456.

(16) Srisombat, L.; Jamison, A. C.; Randall Lee, T. Stability: A key issue for self-assembled monolayers on gold as thin-film coatings and nanoparticle protectants. *Colloids and Surfaces A: Physicochem. Eng. Aspects* **2011**, *390*, 1.

(17) Gates, B. Determining the Stability of Nanoparticles in Solution and Implications for Using these Materials. *WorkSafeBC Publications*, Final Report Date: April 2012, RS2009-DG04.

(18) Li, F.; Zhang, H.; Dever, B.; Li, X.-F.; Le, X. C. Thermal Stability of DNA Functionalized Gold Nanoparticles. *Bioconjugate Chem.* **2013**, *24*, 1790.

(19) Herdt, A. R.; Drawz, S. M.; Kang, Y. J.; Taton, T. A. DNA dissociation and degradation at gold nanoparticle surfaces. *Colloid Surf. B-Biointerfaces* **2006**, *51*, 130.

(20) Bhatt, N.; Huang, P.-J. J.; Dave, N.; Liu, J. Dissociation and Degradation of Thiol-Modified DNA on Gold Nanoparticles in Aqueous and Organic Solvents. *Langmuir*, **2011**, *27*, 6132.

(21) Alkilany, A. M.; Abulateefeh, S. R.; Mills, K. K.; Yaseen, A. I. B.; Hamaly, M. A.; Alkhatib, H. S.; Aiedeh, K. M.; Stone, J. W. Colloidal Stability of Citrate and Mercaptoacetic Acid Capped Gold Nanoparticles upon Lyophilization: Effect of Capping Ligand Attachment and Type of Cryoprotectants. *Langmuir*, **2014**, *30*, 13799.

(22) Bourissou, D.; Guerret, O.; Gabbai, F. P.; Bertrand, G. Stable carbenes. *Chem. Rev.* **2000**, *100*, 39.

(23) Herrmann, W. A. N-heterocyclic carbenes: A new concept in organometallic catalysis.

Angew. Chem. Int. Ed. **2002**, *41*, 1290.

(24) Hahn, F. E.; Jahnke, M. C. Heterocyclic carbenes: Synthesis and coordination chemistry. *Angew. Chem. Int. Ed.* **2008**, *47*, 3122.

(25) Hopkinson, M. N.; Richter, C.; Schedler, M.; Glorius, F. An overview of *N*-heterocyclic carbenes. *Nature* **2014**, *510*, 485.

(26) Nelson, D. J.; Nolan, S. P. Quantifying and understanding the electronic properties of *N*-heterocyclic carbenes. *Chem. Soc. Rev.* **2013**, *42*, 6723.

(27) Diez-Gonzalez, S.; Marion, N.; Nolan, S. P. *N*-Heterocyclic Carbenes in Late Transition Metal Catalysis. *Chem. Rev.* **2009**, *109*, 3612.

(28) Hindi, K. M.; Panzner, M. J.; Tessier, C. A.; Cannon, C. L.; Youngs, W. J. The Medicinal Applications of Imidazolium Carbene-Metal Complexes. *Chem. Rev.* **2009**, *109*, 3859.

(29) Teyssot, M. L.; Jarrousse, A. S.; Manin, M.; Chevry, A.; Roche, S.; Norre, F.; Beaudoin, C.; Morel, L.; Boyer, D.; Mahiou, R.; Gautier, A. Metal-NHC complexes : a survey of anti-cancer properties. *Dalton Trans.* **2009**, 6894.

(30) Merces, L.; Albrecht, M. Beyond catalysis : *N*-heterocyclic carbene complexes as components for medical, luminescent, and functional materials applications. *Chem. Soc. Rev.* **2010**, *39*, 1903.

(31) Visbal, R.; Conception Gimeno, M. *N*-heterocyclic carbene metal complexes : photoluminescence and applications. *Chem. Soc. Rev.* **2014**, *43*, 3551.

(32) Melaiye, A.; Sun, Z.; Hindi, K.; Milsted, A.; Ely, D.; Reneker, D. H.; Tessier, C. A.; Youngs, W. J. *J. Am. Chem. Soc.* **2005**, *127*, 2285.

(33) Lee, C. K.; Vasam, C. S.; Huang, T. W.; Wang, H. M. J.; Yang, R. Y.; Lee, C. S.; Lin, I. J. B. *Organometallics* **2006**, *25*, 3768.

(34) Scholten, J. D.; Ebeling, G.; Dupont, J. On the involvement of NHC carbenes in catalytic reactions by iridium complexes, nanoparticle and bulk metal dispersed in imidazolium ionic liquids. *Dalton Trans.* **2007**, 5554.

(35) Huang, R. T. W.; Wang, W. C.; Yang, R. Y.; Lu J. T.; Lin, I. J. B. Liquid crystals of gold(I) *N*-heterocyclic carbene complexes. *Dalton Trans.* **2009**, 7121.

(36) Hurst, E. C.; Wilson, K.; Fairlamb, I. J. S.; Chechik, V. *N*-Heterocyclic carbene coated metal nanoparticles. *New J. Chem.* **2009**, *33*, 1837.

(37) Vignolle, J.; Tilley, T. D. *N*-Heterocyclic carbene-stabilized gold nanoparticles and their assembly into 3D superlattices. *Chem. Commun.* **2009**, 7230.

(38) Aslanov, L. A.; Zakharov, V. N.; Kakharov, M. A.; Kamyshny, A. L.; Magdassi, Sh.,

Yatsenko, A. V. Stabilization of Silicon Nanoparticles by Carbenes. *Russian J. Coord. Chem.* **2010**, *36*, 330.

(39) Choi, J.; Kang, N.; Yang, H. Y.; Kim, H. J.; Son, S. U. Colloidal Synthesis of Cubic-Phase Copper Selenide Nanodiscs and Their Optoelectronic Properties. *Chem. Mater.* **2010**, *22*, 3586.

(40) Ranganath, K. V. S.; Kloesges, J.; Schäfer, A. H.; Glorius, F. Asymmetric Nanocatalysis : *N*-Heterocyclic Carbenes as Chiral Modifiers of Fe₃O₄/Pd nanoparticles. *Angew. Chem. Int. Ed.* **2010**, *49*, 7786.

(41) Lara, P.; Rivada-Wheelaghan, O.; Conejero, S.; Poteau, R.; Philippot, K.; Chaudret, B. Ruthenium Nanoparticles Stabilized by *N*-Heterocyclic Carbenes: Ligand Location and Influence on Reactivity. *Angew. Chem. Int. Ed.* **2011**, *50*, 12080. (42) Gonzales-Galves, D.; Lara, P.; Rivada-Wheelaghan, O.; Conejero, S.; Chaudret, B.; Philippot, K.; van Leeuwen, P. W. N. M. NHC-stabilized ruthenium nanoparticles as new catalysts for the hydrogenation of aromatics. *Catal. Sci. Technol.* **2013**, *3*, 99.

(43) Ling, X.; Schaeffer, N.; Roland, S.; Pileni, M.-P. Nanocrystals: Why Do Silver and Gold *N*-Heterocyclic Carbene Precursors Behave Differently? *Langmuir* **2013**, *29*, 12647.

(44) Serpell, C. J.; Cookson, J.; Thompson, A. L.; Brown, C. M.; Beer, P. D. Haloaurate and halopalladate imidazolium salts : structures, properties, and use as precursors for catalytic metal nanoparticles. *Dalton Trans.* **2013**, *42*, 1385.

(45) Song, S. G.; Satheeshkumar, C.; Park, J.; Ahn, J.; Premkumar, T.; Lee, Y.; Song, C. *N*-Heterocyclic Carbene-Based Conducting Polymer–Gold Nanoparticle Hybrids and Their Catalytic Application. *Macromolecules* **2014**, *47*, 6566.

(46) Baquero, E. A.; Tricard, S.; Flores, J. C.; de Jesús, E.; Chaudret, B. Highly Stable Water-Soluble Platinum Nanoparticles Stabilized by Hydrophilic *N*-Heterocyclic Carbenes. *Angew. Chem. Int. Ed.* **2014**, *53*, 13220.

(47) Liu, H.-X.; He, X.; Zhao, L. Metallamacrocycle-modified gold nanoparticles : a new pathway for surface functionalization. *Chem Commun.* **2014**, *50*, 971.

(48) Richter, C.; Schaepe, K.; Glorius, F.; Ravoo, B. J. Tailor-made *N*-heterocyclic carbenes for nanoparticle stabilization. *Chem. Commun.* **2014**, *50*, 3204.

(49) Rodriguez-Castillo, M.; Laurencin, D.; Tielens, F.; van der Lee, A.; Clement, S.; Guari, Y.; Richeter, S. Reactivity of gold nanoparticles towards *N*-heterocyclic carbenes. *Dalton Trans.* **2014**, *43*, 5978

(50) Crespo, J.; Guari, Y.; Ibarra, A.; Larionova, J.; Lasanta, T.; Laurencin, D.;

Chapter 4 Superior Oxygen Stability of N-Heterocyclic Carbene-coated Au Nanocrystals – Comparison with Thiol-coated Analogues

Lopez-de-Luzuriaga, J. M.; Monge, M.; Olmos, M. E.; Richeter, S. Ultrasmall NHC-coated gold nanoparticles obtained through solvent free thermolysis of organometallic Au(I) complexes. *Dalton Trans.* **2014**, *43*, 15713.

(51) Ling, X.; Roland, S.; Pileni, M.-P. Supracrystals of N-Heterocyclic Carbene-Coated Au Nanocrystals. *Chem. Mater.* **2015**, *27*, 414.

(52) Weidner, T.; Baio, J. E.; Mundstock, A.; Große, C.; Karthäuser, S.; Bruhn, C.; Siemeling, U. NHC-Based Self-Assembled Monolayers on Solid Gold Substrates. *Aust. J. Chem.* **2011**, *64*, 1177.

(53) Zhukhovitskiy, A. V.; Mavros, M. G.; Van Voorhis, T.; Johnson, J. A. Addressable carbene anchors for gold surfaces. *J. Am. Chem. Soc.* **2013**, *135*, 7418.

(54) Crudden, C. M.; Horton, J. H.; Ebralidze, I. I.; Zenkina, McLean, A. B.; Drevniok, B.; She, Z.; Kraatz, H.-B.; Mosey, N. J.; Seki, T.; O. V.; Keske, E. C.; Leake, J. D.; Rousina-Webb, A.; Wu, G. Ultra stable self-assembled monolayers of N-heterocyclic carbenes on gold. *Nat. Chem.* **2014**, *6*, 409.

(55) Klecha, E.; Ingert, D.; Walls, M.; Pileni, M. P. Immunity of Coated Self-Ordered Silver Nanocrystals: A New Intrinsic Property Due to the Nanocrystal Ordering. *Langmuir* **2009**, *25*, 2824.

(56) Salzemann, C.; Zhai, W.; Goubet, N.; Pileni, M.-P. How to Tune the Au Internanocrystal Distance in Two-Dimensional Self-Ordered Superlattices. *J. Phys. Chem. Lett.* **2010**, *1*, 149.

(57) Zheng, N.; Fan, J.; Stucky, G. D. One-Step One-Phase Synthesis of Monodisperse Noble-Metallic Nanoparticles and Their Colloidal Crystals. *J. Am. Chem. Soc.* **2006**, *128*, 6550.

(58) Goubet, N.; Richardi, J.; Albouy, P.-A.; Pileni, M.-P. Which Forces Control Supracrystal Nucleation in Organic Media ? *Adv. Funct. Mater.* **2011**, *21*, 2693.

(59) Lavrich, D. J.; Wetterer, S. M.; Bernasek, S. L.; Scoles, G. Physisorption and Chemisorption of Alkanethiols and Alkyl Sulfides on Au(111). *J. of Phys. Chem. B* **1998**, *102*, 3456.

(60) Nuzzo, R. G.; Dubois, L. H.; Allara, D. L. Fundamental studies of microscopic wetting on organic surfaces. 1. Formation and structural characterization of a self-consistent series of polyfunctional organic monolayers. *J. Am. Chem. Soc.* **1990**, *112*, 558.

Supporting Information

Superior Oxygen Stability of N-Heterocyclic Carbene-coated Au Nanocrystals – Comparison with Thiol-coated Analogues

Xiang Ling,^{a,b,c} Nicolas, Schaeffer,^{a,b} Sylvain Roland,^{*c} and Marie-Paule Pileni^{*a,b,d}

^a Sorbonne Universités, UPMC-Univ Paris 6, UMR 8233, MONARIS, F-75005, Paris, France

^b CNRS, UMR 8233, MONARIS, F-75005, Paris, France

^c Sorbonne Universités, UPMC-Univ Paris 6, UMR 8232, Institut Parisien de Chimie Moléculaire, F-75005, Paris, France

^d CEA/IRAMIS, CEA Saclay, 91191, Gif-Sur-Yvette, France

Table of contents

Figure S1	93
Figure S2	93
Figure S3	94
Figure S4	95
Figure S5	95

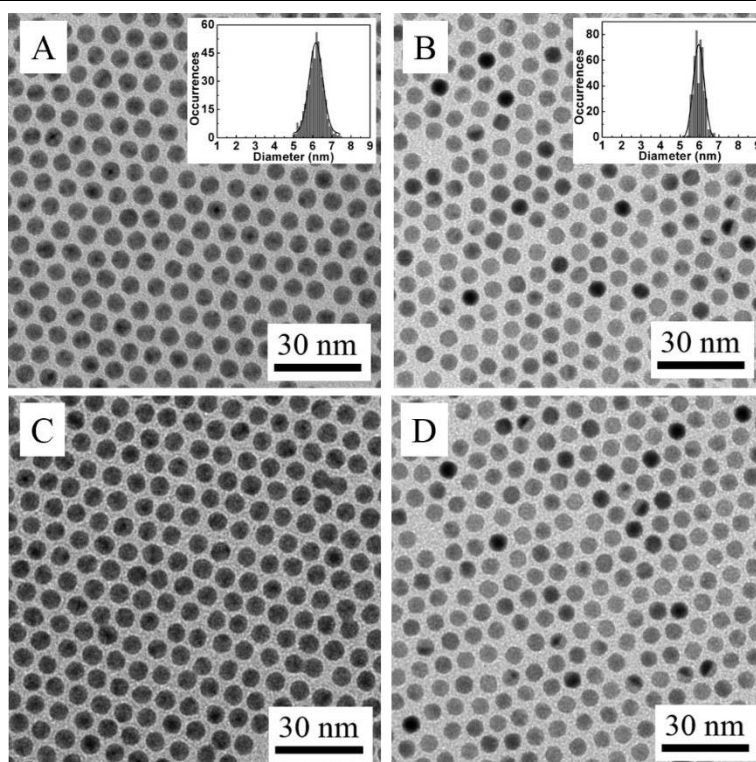


Figure S1. TEM images of $^{DDT}Au^1$ (A) and $^{DDT}Au^2$ (B) deposited on an amorphous carbon covered TEM grid before oxygen plasma exposure. Same areas after exposure to oxygen plasma for 60 s at 10 W of $^{DDT}Au^1$ (C) and $^{DDT}Au^2$ (D).

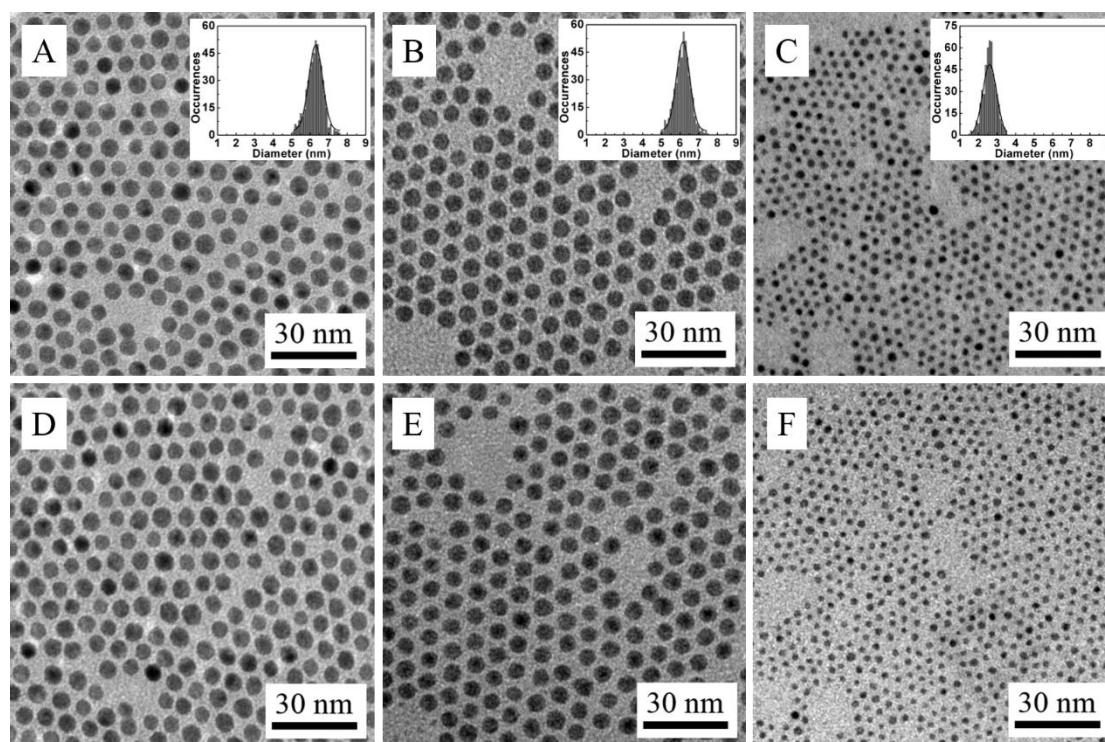


Figure S2. TEM images of $^{DDT}Au^3$ (A), $^{DDT}Au^4$ (B) and $^{DDT}Au^5$ (C) deposited on an amorphous carbon covered TEM grid before oxygen plasma exposure. Same areas after exposure to oxygen plasma for 60 s at 10 W of $^{DDT}Au^3$ (D), $^{DDT}Au^4$ (E) and $^{DDT}Au^5$ (F).

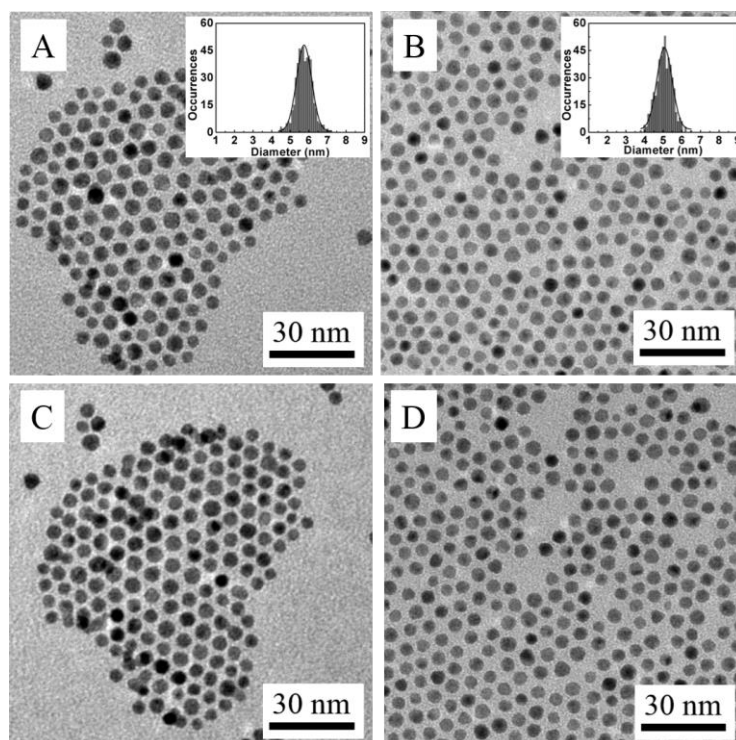


Figure S3. TEM images of $^{\text{NHC}}\text{Au}^7$ (A) and $^{\text{NHC}}\text{Au}^9$ (B) deposited on an amorphous carbon covered TEM grid before oxygen plasma exposure. Same areas after exposure to oxygen plasma for 120 s at 10 W of $^{\text{NHC}}\text{Au}^7$ (C) and $^{\text{NHC}}\text{Au}^9$ (D).

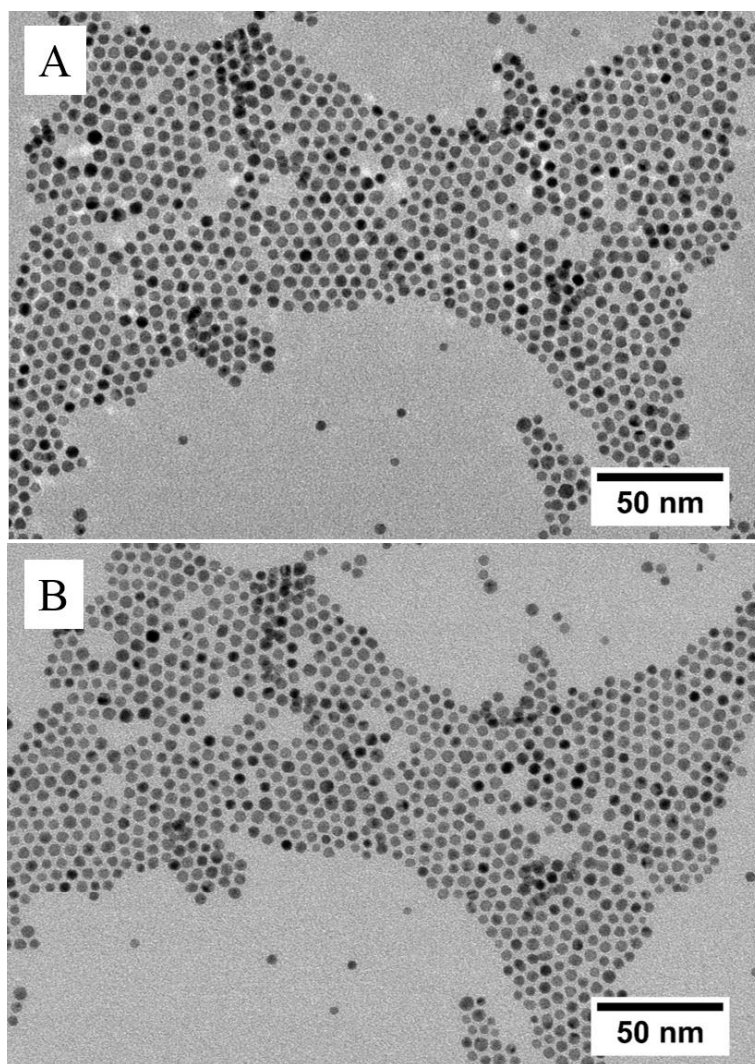


Figure S4. TEM images of $^{\text{NHC}}\text{Au}^{10}$ (A) deposited on an amorphous carbon covered TEM grid before oxygen plasma exposure. Same areas after exposure to oxygen plasma for 180 s at 10 W of $^{\text{NHC}}\text{Au}^{10}$ (B).

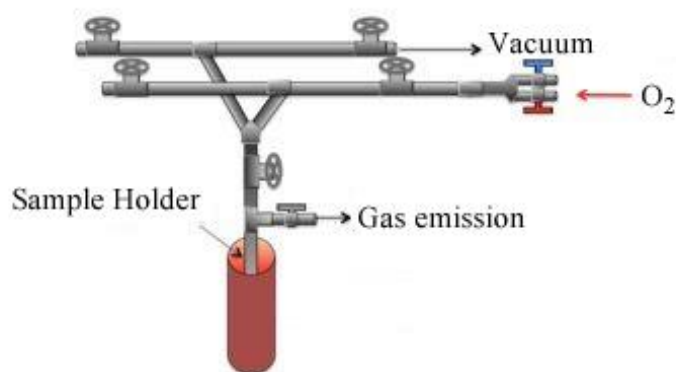


Figure S5. Device for the experiments with exposure to pure oxygen experiment.

Conclusions and Perspectives

Nanomaterials are nanostructured materials, characterized by a well-defined grain size or a dimension from several nanometers to several dozen nanometers (<50nm). Nanomaterials have received remarkable attention due to their unique properties. Particularly, noble metal (Au, Ag) nanoparticles exhibit special mechanical, electronic, optical and magnetic properties and present a high potential for developing applications in many domains with important societal impacts. Au nanoparticles are the most outstanding members of the metal nanoparticles groups due to their higher stability by comparison with other metal nanoparticles. In the last decades, N-Heterocyclic carbenes have emerged as an essential class of neutral ligands in organometallic chemistry because of their high synthetic flexibility, specific geometry and strong metal–C_{carbene} bond in metal complexes. Although all these properties have been widely studied and exploited for applications in homogeneous catalysis and for the development of biologically active complexes, the use of NHCs in nanomaterials remains largely unexplored. In this thesis, we focus on exploring the potential of NHC ligands in the field of nanomaterials, as coating agents for gold (and silver) nanocrystals synthesis, stabilization and self-assembly into supracrystals.

The first part deals with the use of Au-NHCs and Ag-NHCs as precursors to generate the corresponding metal nanocrystals. We describe the formation of nanocrystals by one-phase reduction of metal–NHCs (metal = Au, Ag) bearing common NHC ligands, namely 1,3-diethylbenzimidazol-2-ylidene, 1,3-bis(mesityl)imidazol-2-ylidene and 1,3-bis(2,6-*i*Pr₂C₆H₃)imidazol-2-ylidene. We demonstrate that the efficiency of the process and the average size and size distribution of the nanocrystals markedly depends on the structure of the NHC ligand, on the sequence in the reactants addition (i.e. presence or absence of thiol during the reduction step), and on the presence or absence of oxygen. We also demonstrate that in this part that different pathways are involved to generate nanocrystals from Au or Ag precursors. We observe by ¹H NMR experiments a specific reaction between Ag-NHCs and thiols leading to the formation of silver thiolates whereas the corresponding Au-NHCs remain unchanged under the same conditions.

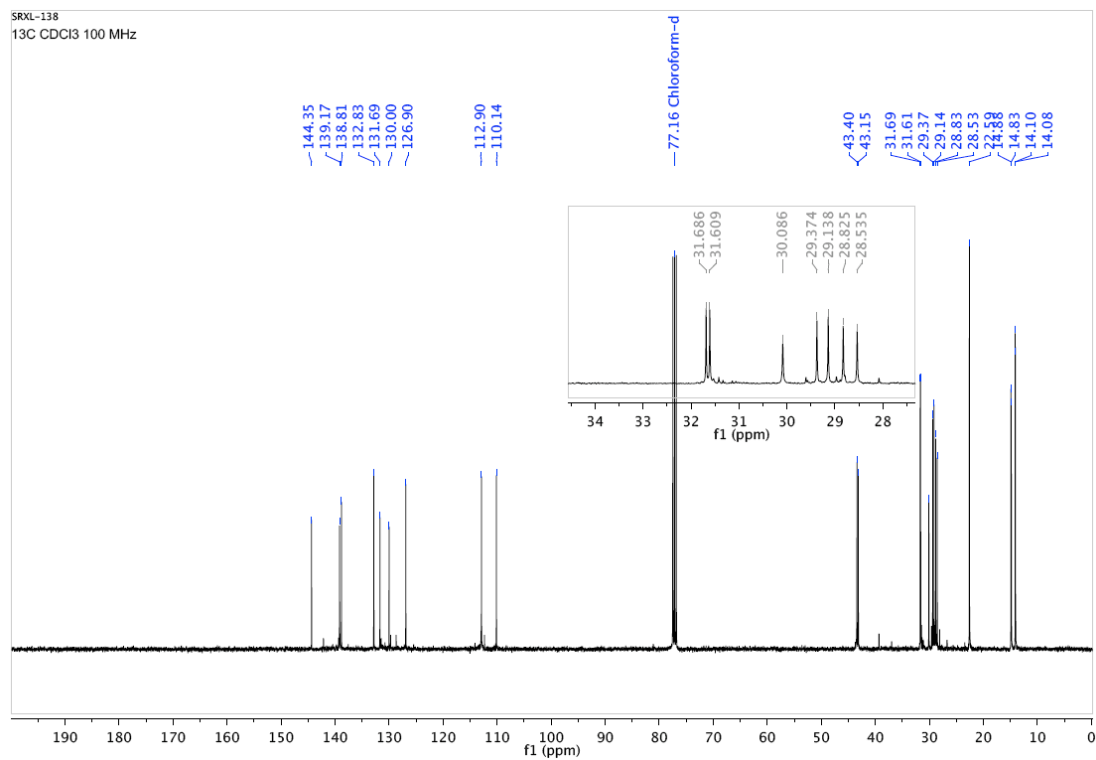
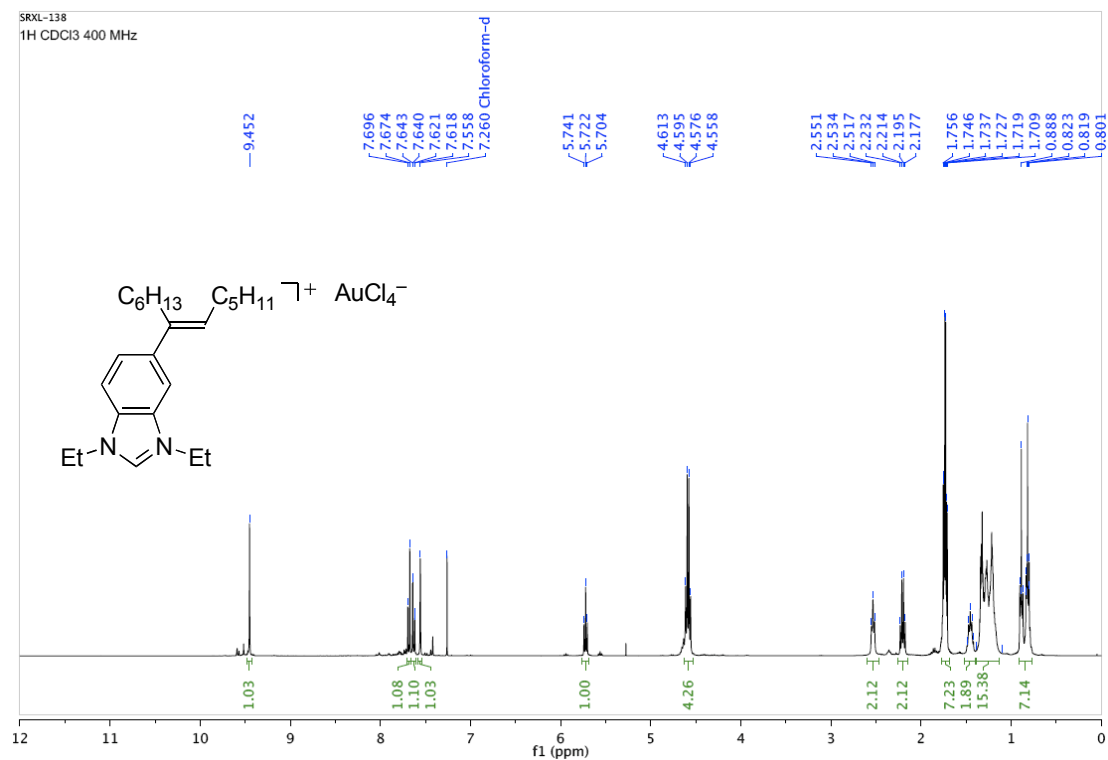
The second part is related to the obtainment of Au supracrystals from the 3D self-assembly of NHC-coated AuNCs, by using NHC ligands as the sole stabilizing and coating agent of nanocrystals. We describe different NHC-stabilized Au nanocrystals with average sizes ranging from 4.0 to 6.0 nm. We demonstrate here that NHCs with appropriate design can

N-heterocyclic carbene coated Nanocrystals and Supracrystals

stabilize Au nanocrystals without additives. We also describe a new generation of structured fcc Au supracrystals made of NHC-coated Au nanocrystals. We demonstrate in this study that large and thick supracrystal films can be obtained from the 3D assembly of Au nanocrystals coated with appropriate NHCs. The average size of the NHC-coated Au nanocrystal and their ability to self-assemble are found to be highly dependent on the position, combination and length of the alkyl chains on the NHCs. We also demonstrate by the edge-edge distances in the supracrystals that the supracrystals are stabilized by interdigitation of neighboring nanocrystals alkyl chains, whose terminal part must point outward with the appropriate geometry.

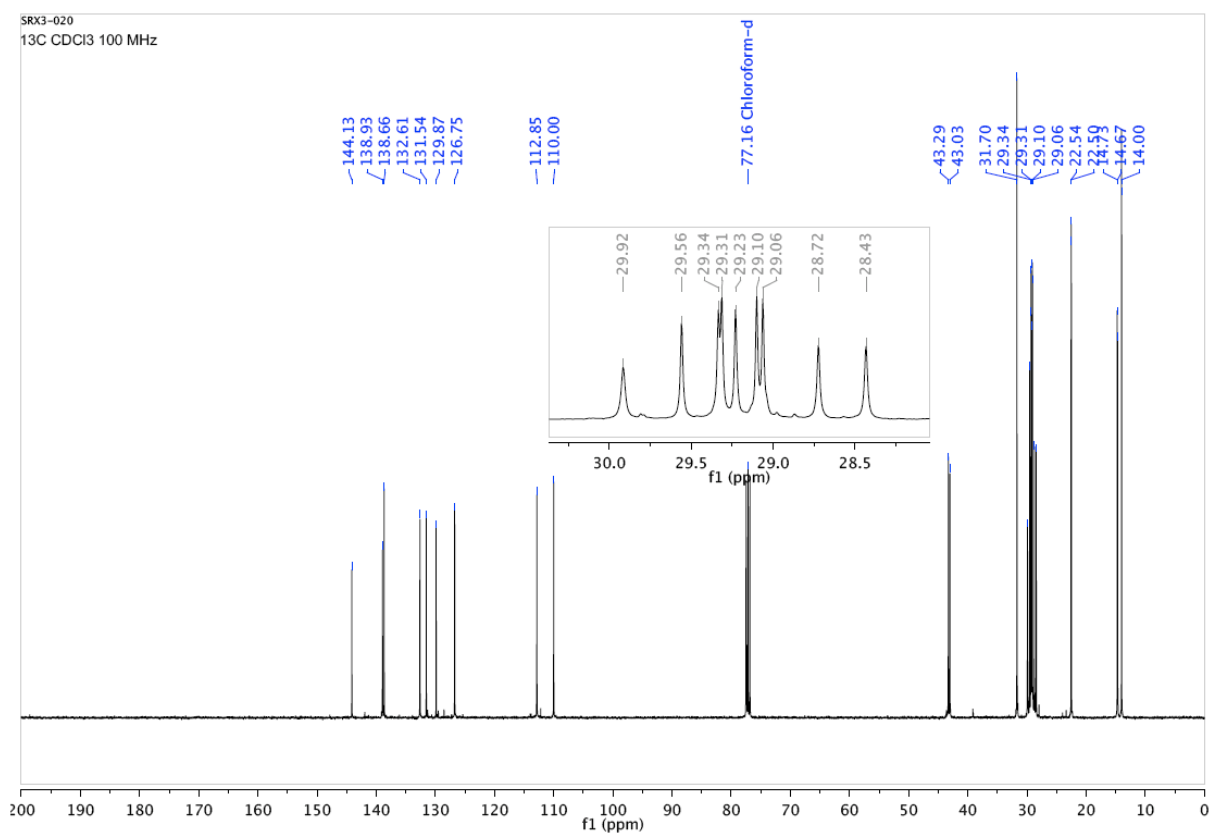
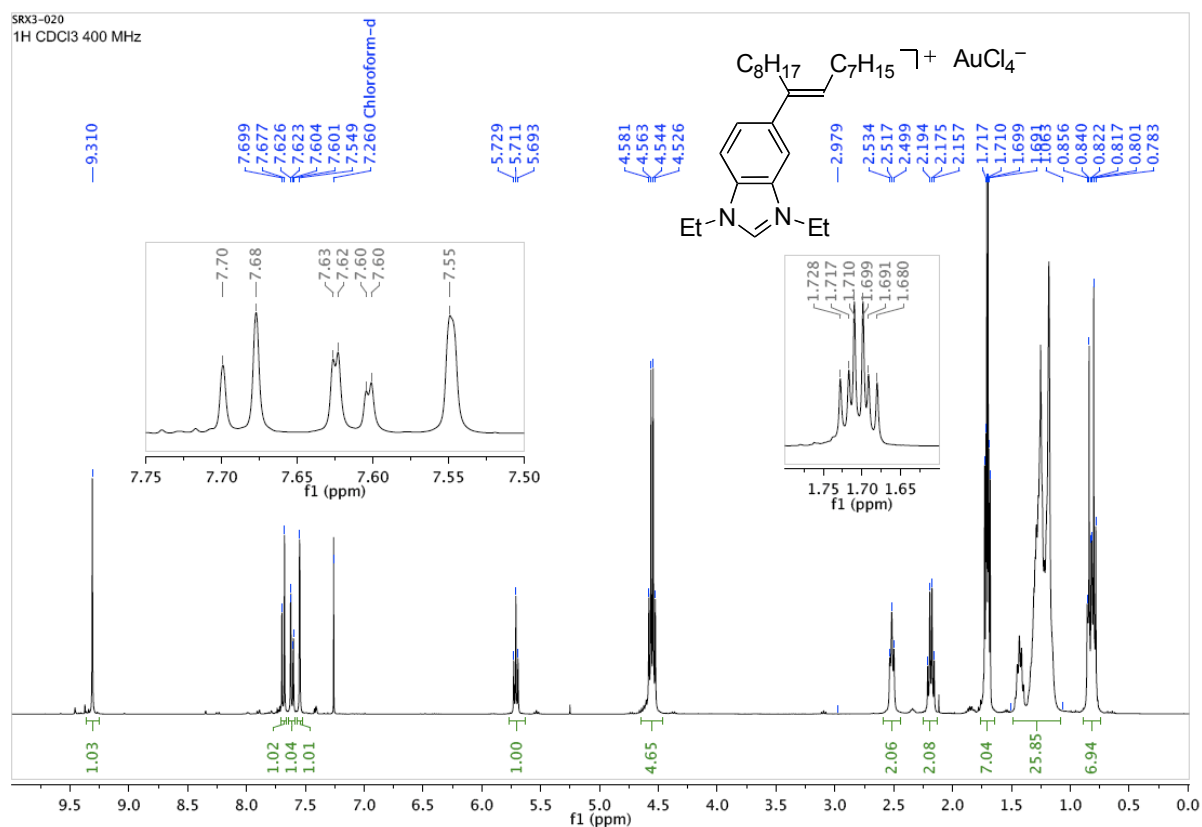
The third part focus on the study and comparison of the stability to oxygen of Au nanocrystals coated with typical thiols or NHC ligands. We demonstrate that NHC-coated Au nanocrystals exhibit greater resistant to oxygen plasma than dodecanethiol-coated Au nanocrystals. The stability of the dodecanethiol-stabilized Au nanocrystals is independent of the sizes of Au nanocrystals and the methods to generate the nanocrystals. We also demonstrate that NHC ligands bound to the surface of Au nanocrystals are significant more resistant to oxygen-induced transformations than dodecanethiol.

Appendices

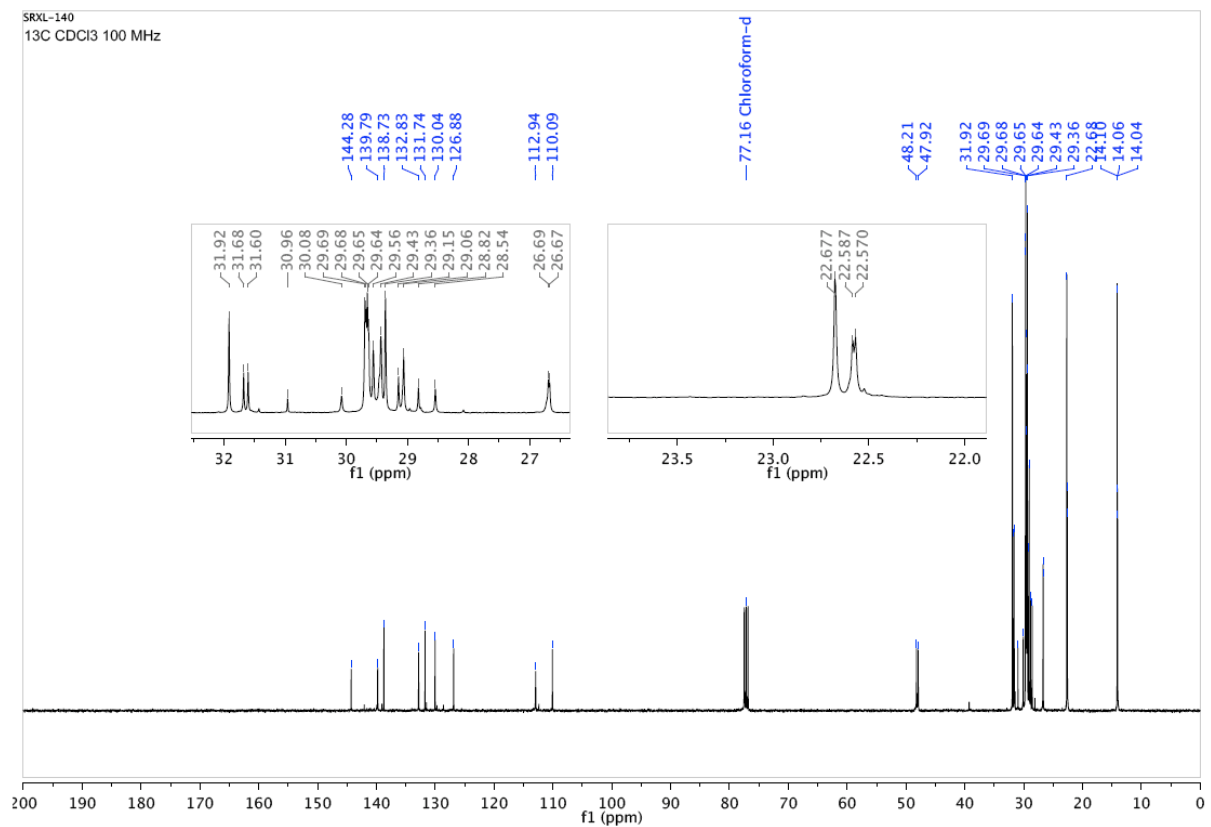
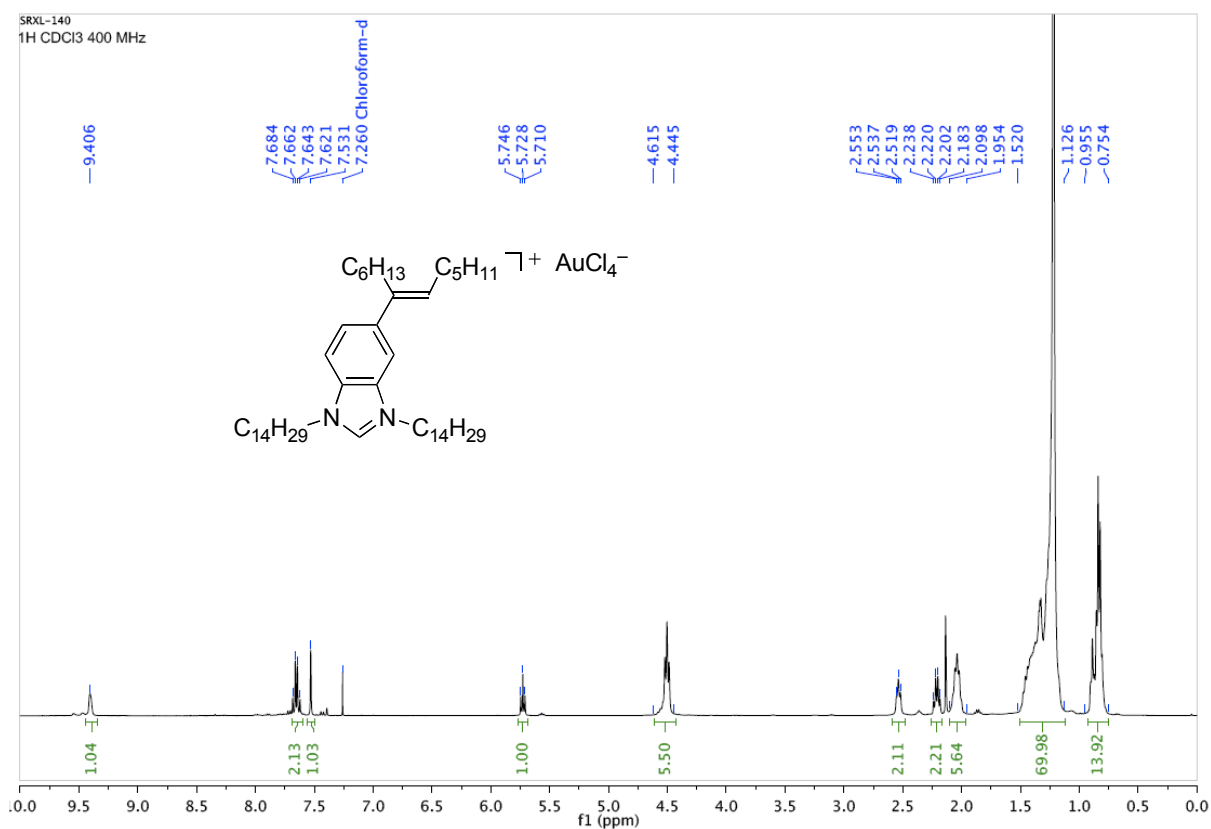
¹H and ¹³C NMR spectra (Chapter 3 supporting information)*(E)*-1,3-Diethyl-5-[1-(hexyl)-hept-1-en-1-yl]benzimidazolium tetrachloroaurate(III) (**1**)

N-heterocyclic carbene coated Nanocrystals and Supracrystals

(E)-1,3-Diethyl-5-[1-(octyl)-non-1-en-1-yl]benzimidazolium tetrachloroaurate(III) (2)

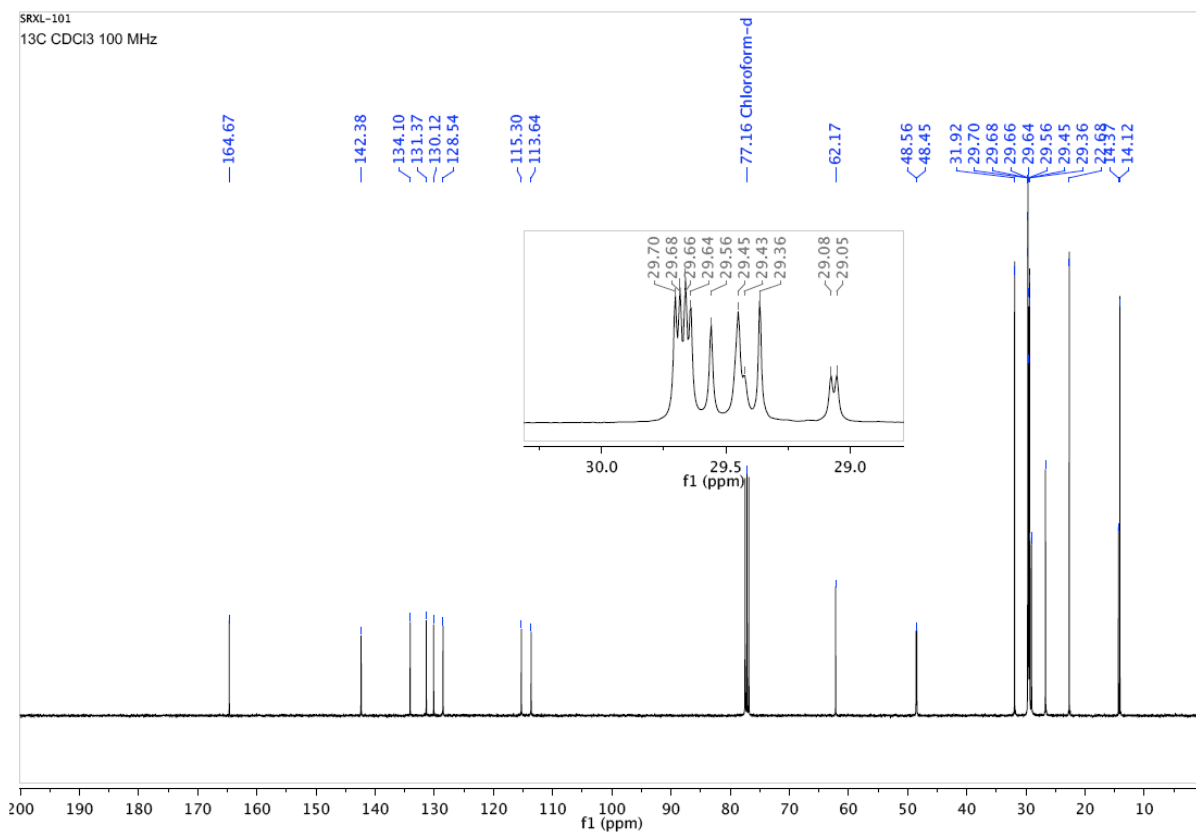
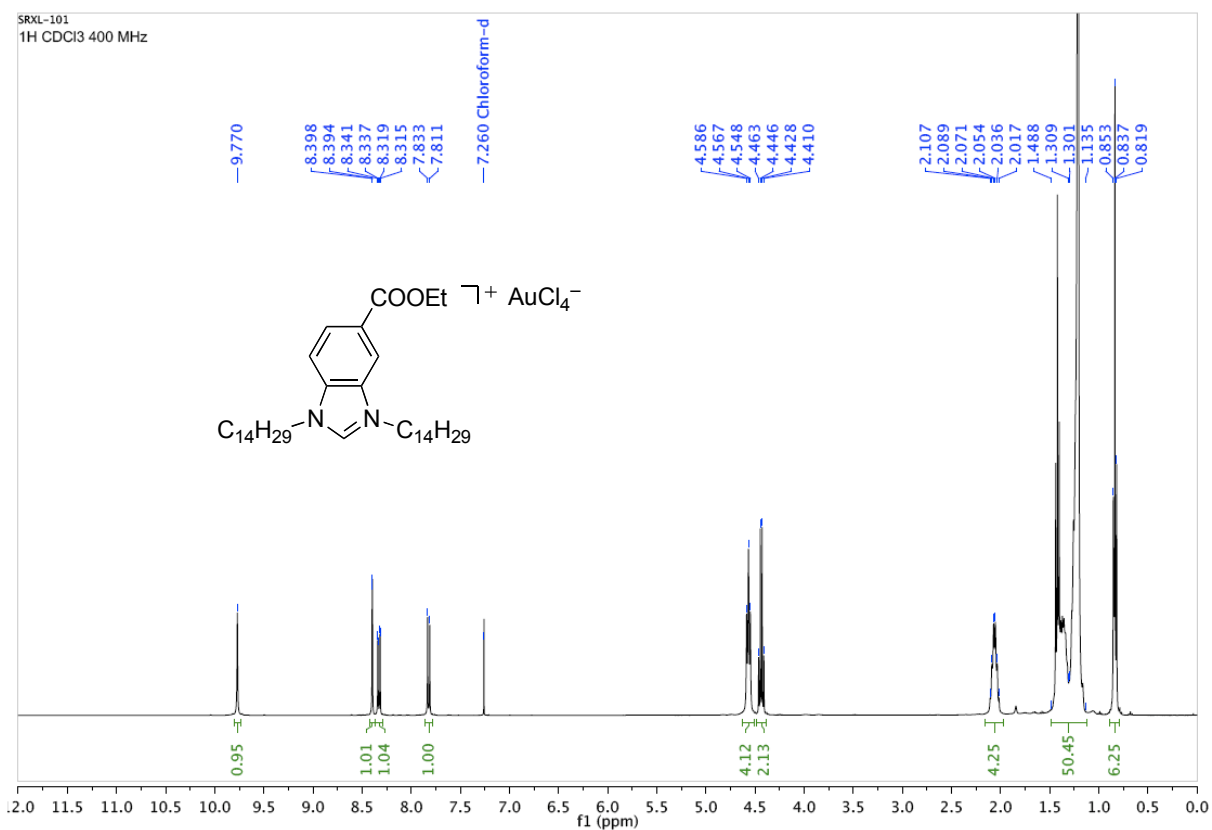


(E)-1,3-Ditetradecyl-5-[1-(hexyl)-hept-1-en-1-yl]benzimidazolium tetrachloroaurate(III) (3)

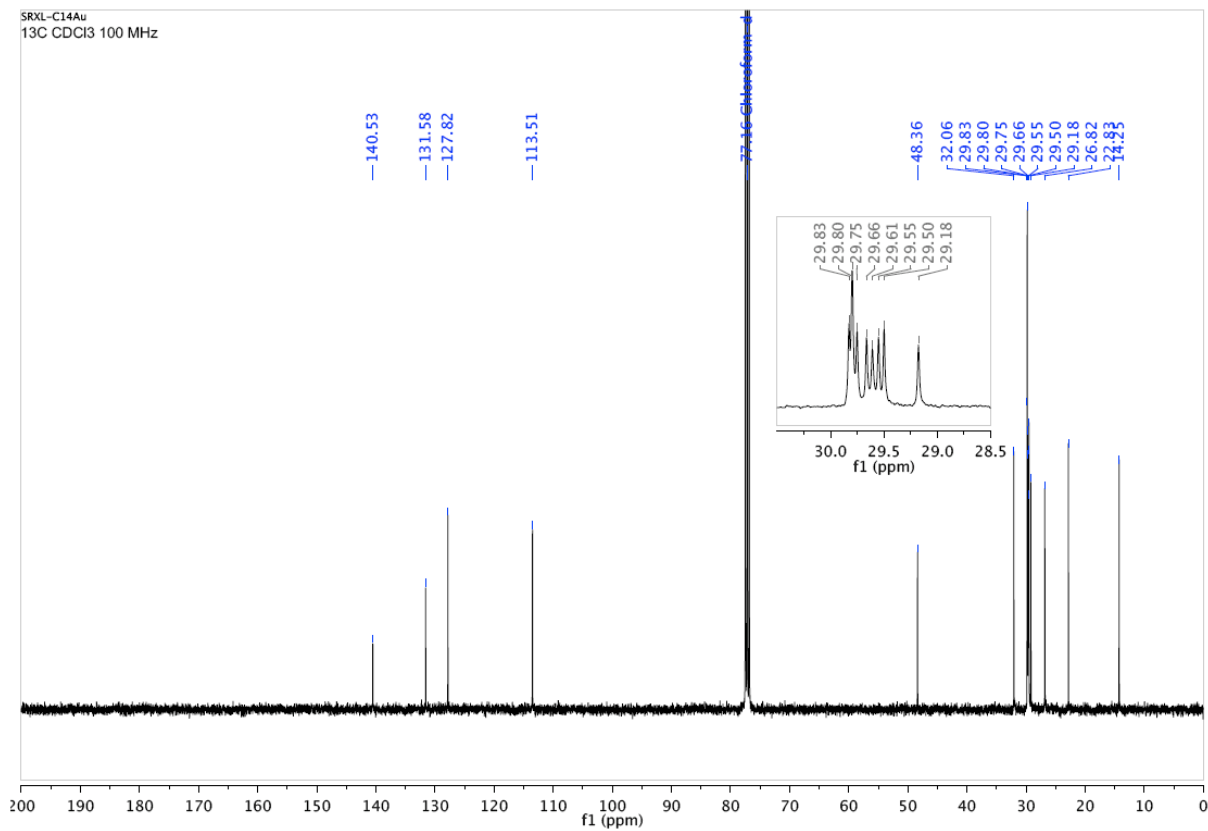
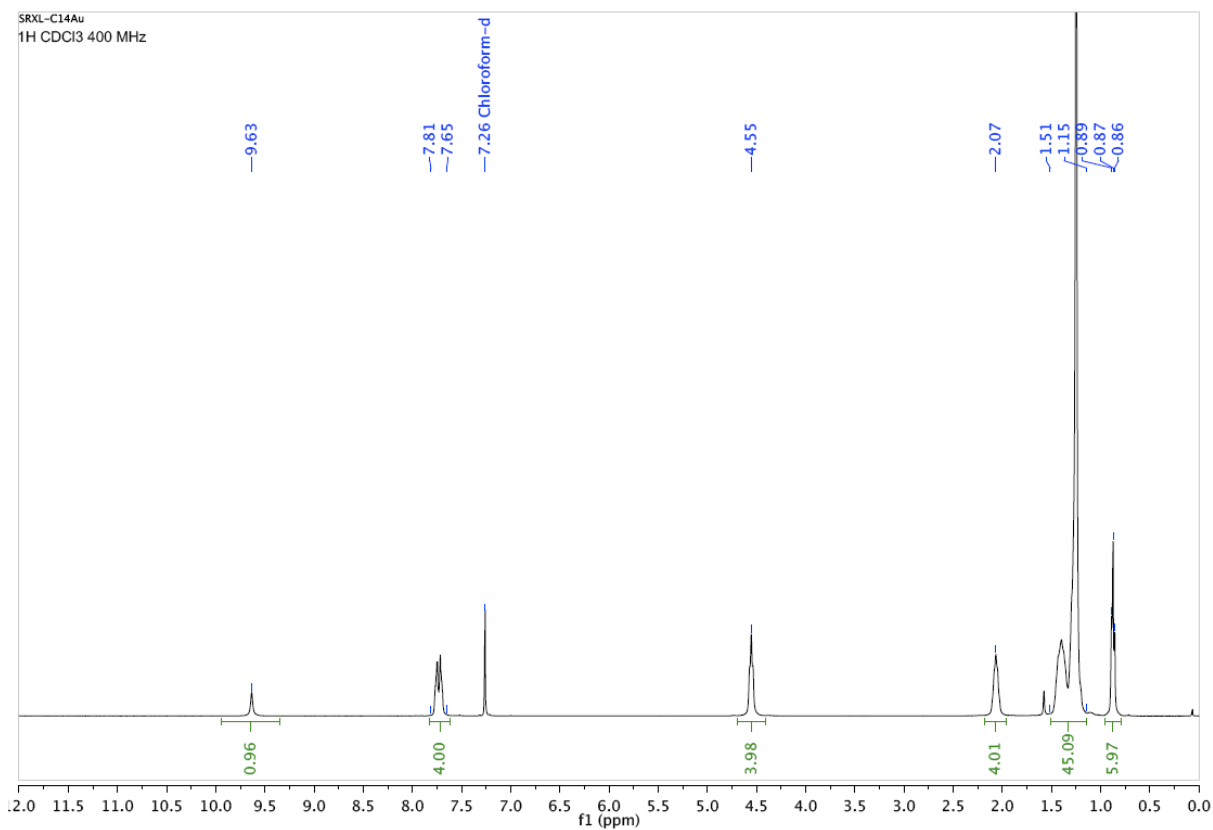


N-heterocyclic carbene coated Nanocrystals and Supracrystals

5-Ethoxycarbonyl-1,3-(ditetradecyl)benzimidazolium tetrachloroaurate(III) (4)

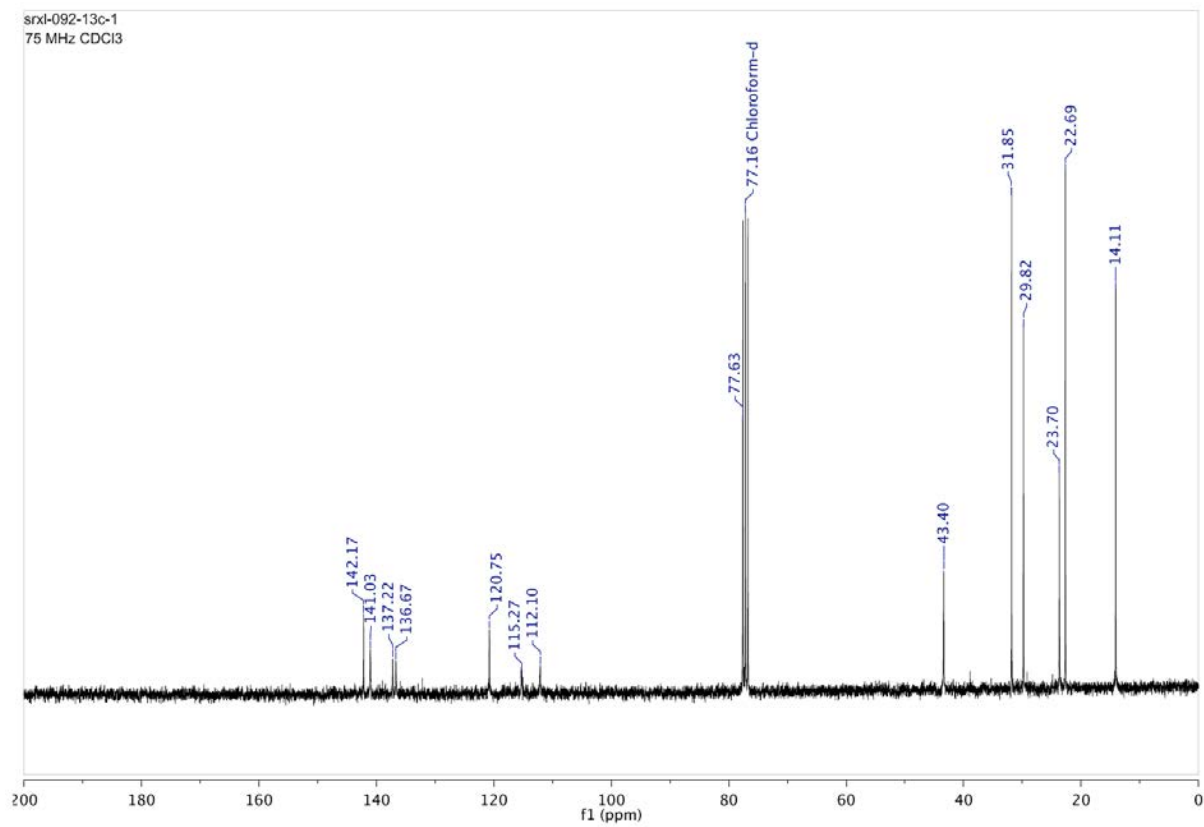
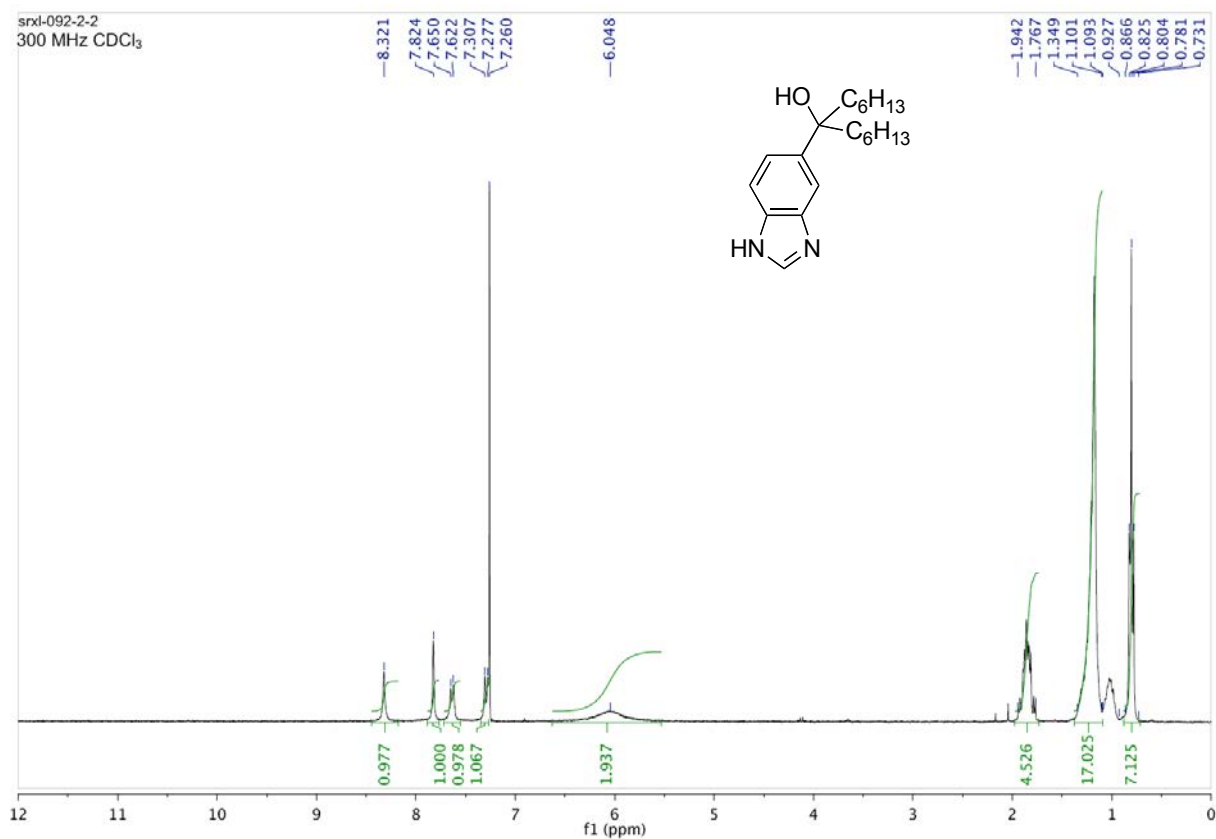


1,3-(Ditetradecyl)benzimidazolium tetrachloroaurate(III) (5)

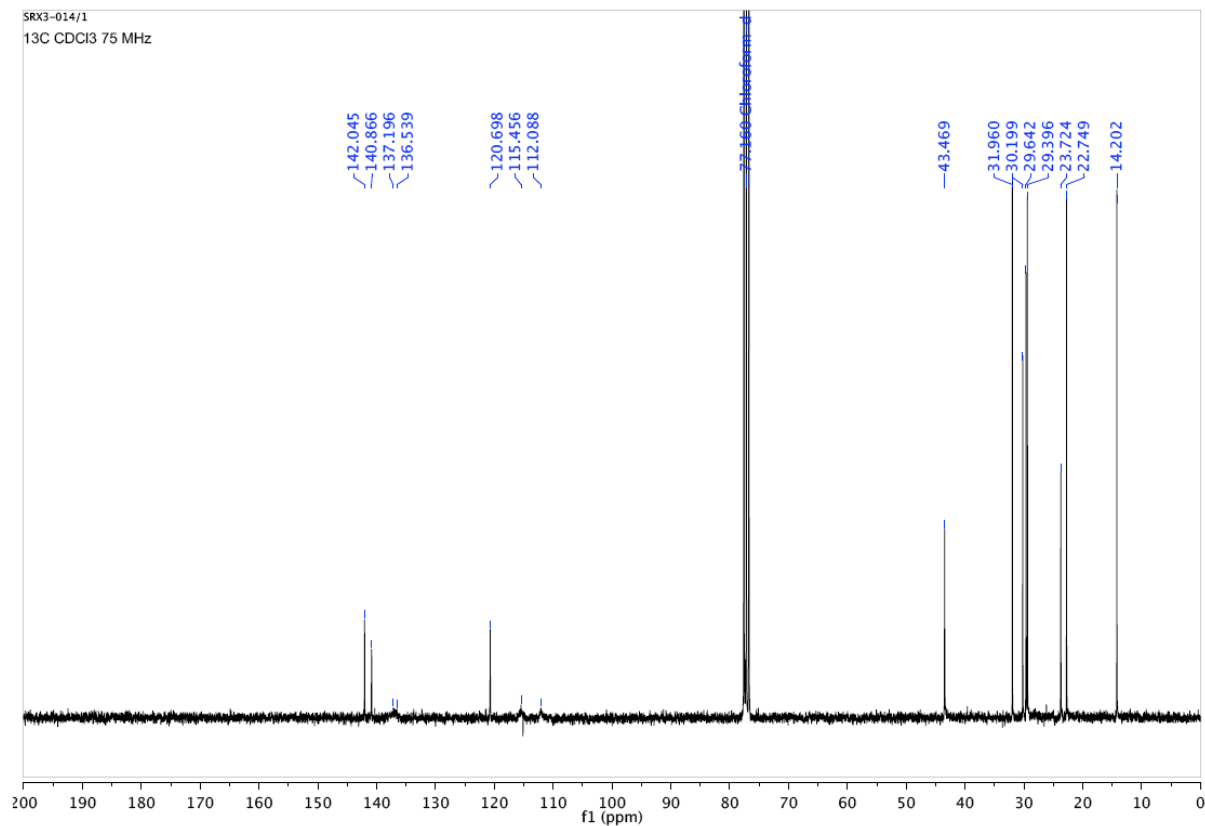
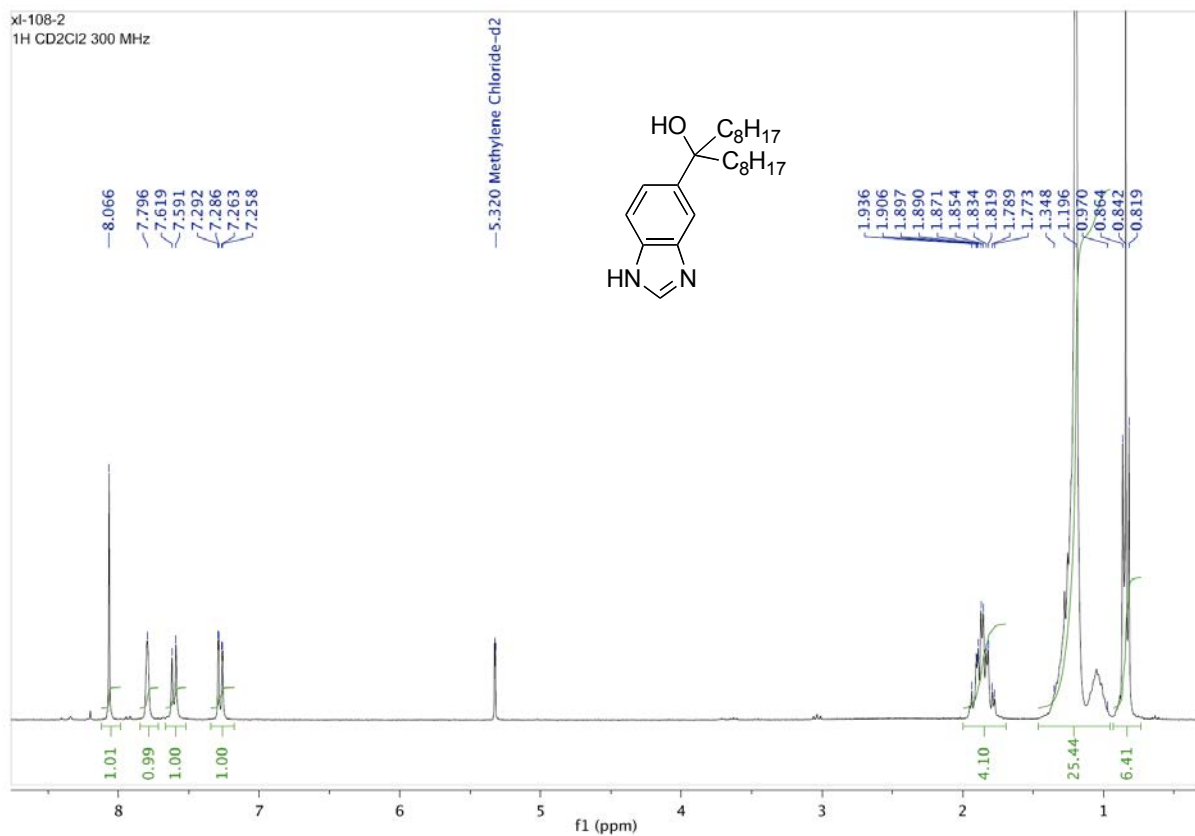


N-heterocyclic carbene coated Nanocrystals and Supracrystals

5-[1,1-Dihexyl-1-(hydroxy)methyl]benzimidazole (7)

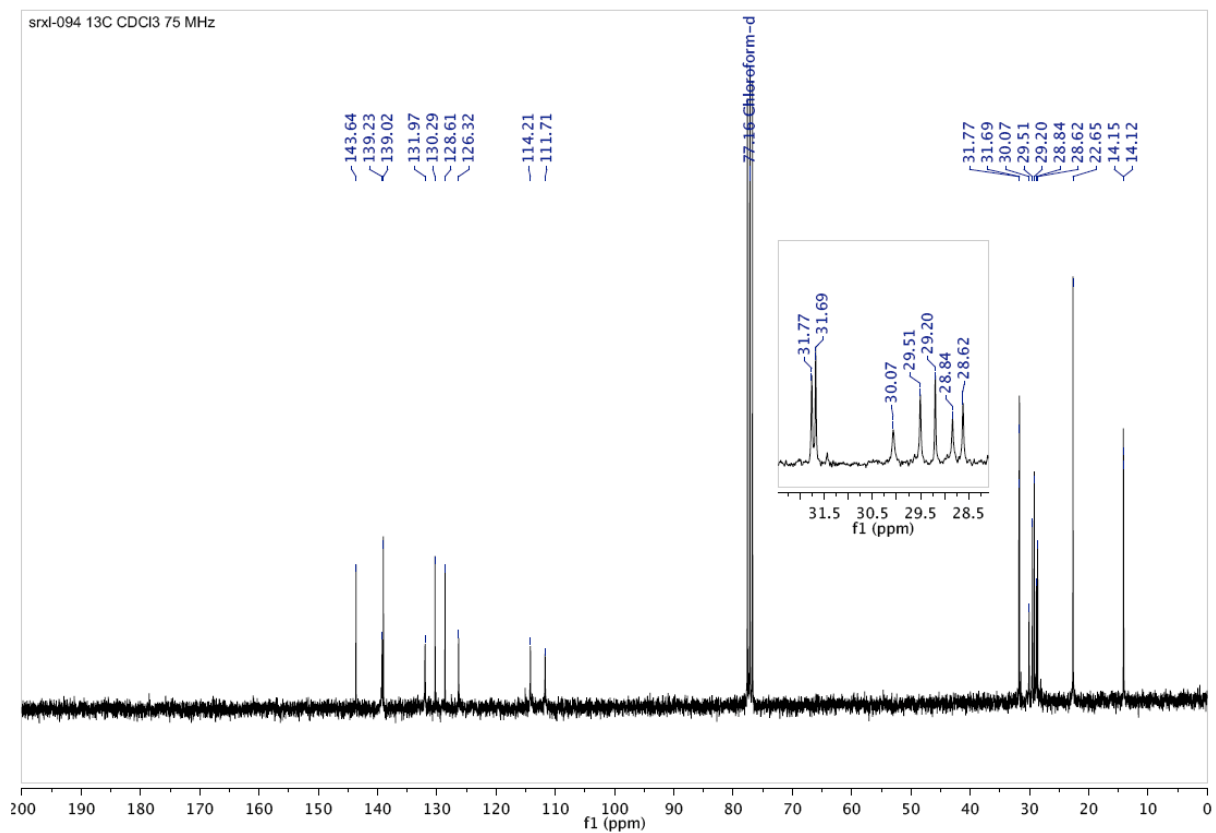
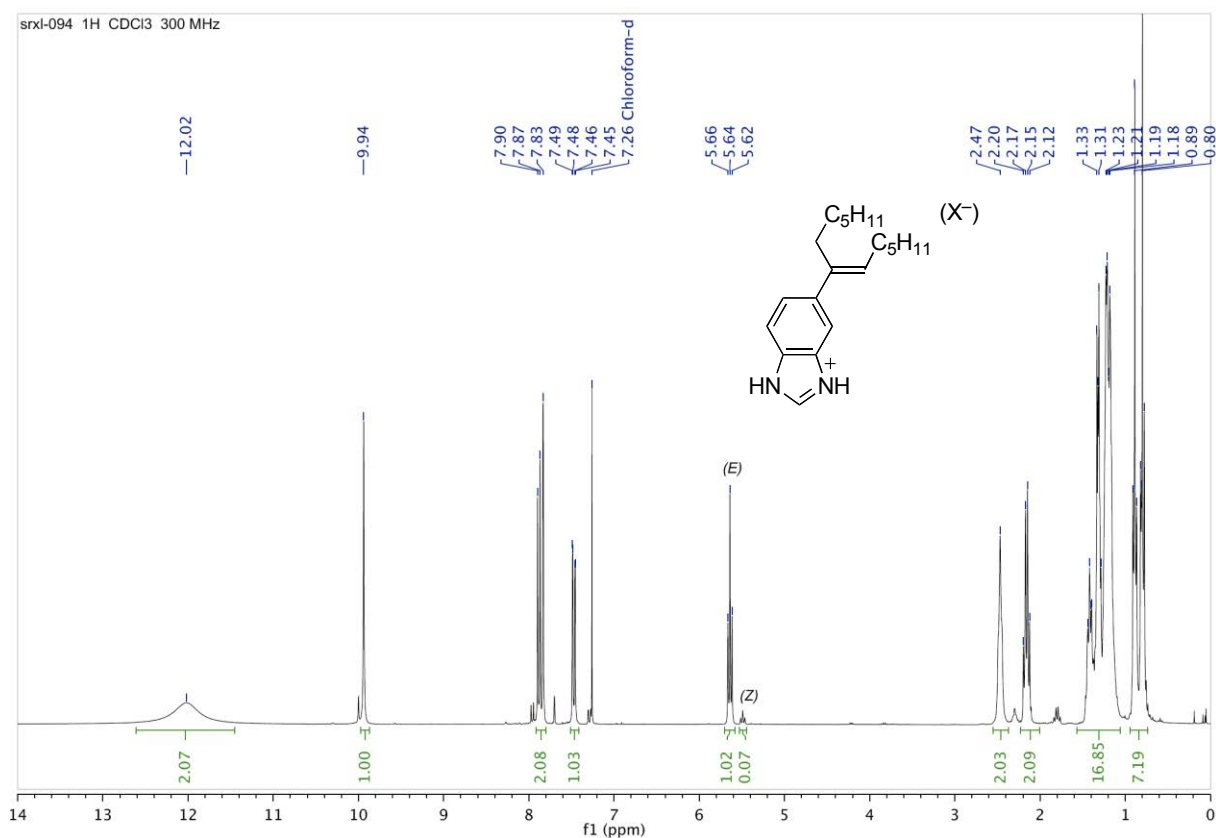


5-[1,1-Dioctyl-1-(hydroxy)methyl]benzimidazole (8)

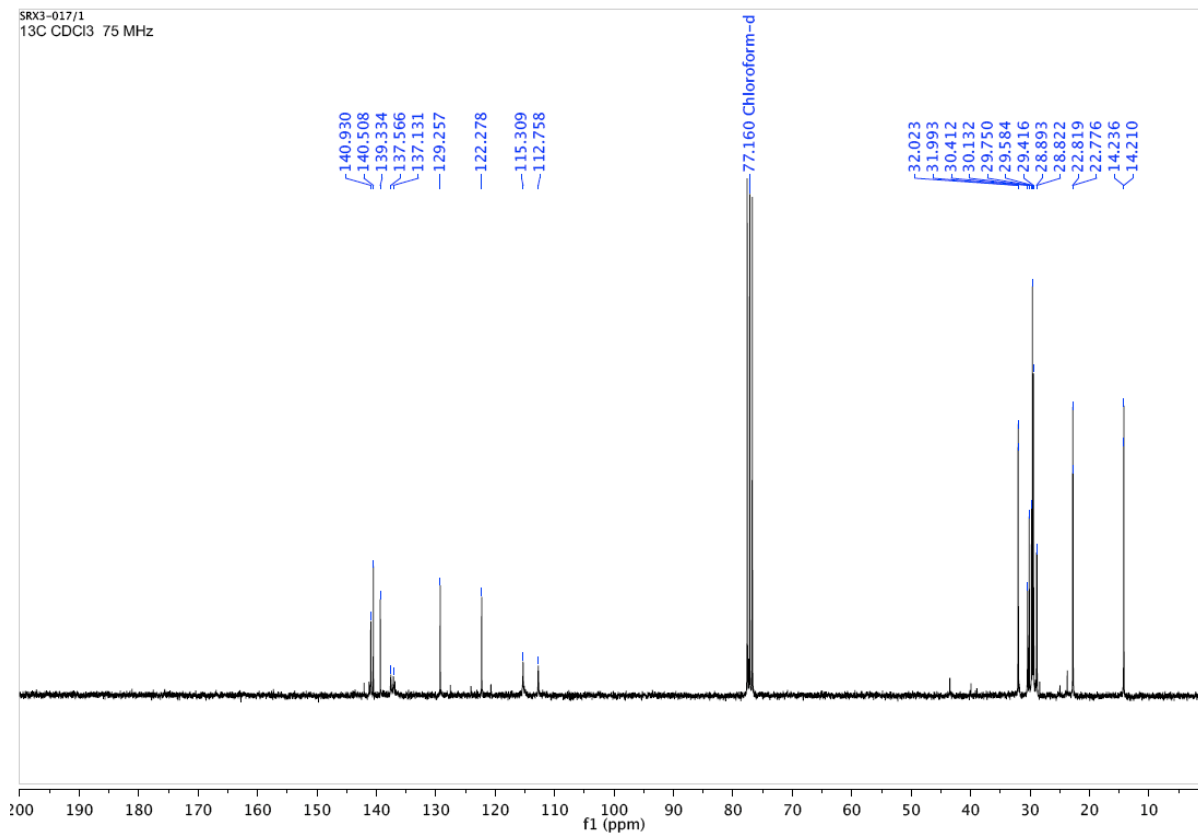
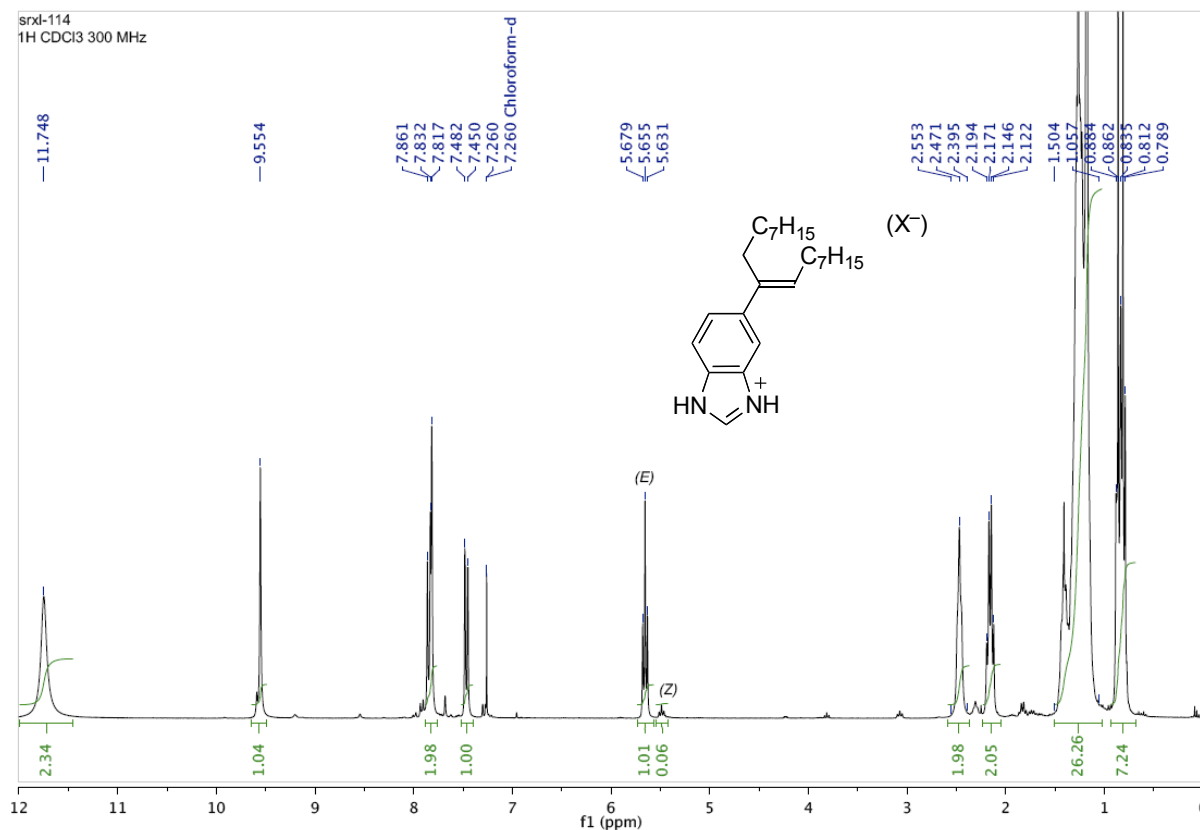


N-heterocyclic carbene coated Nanocrystals and Supracrystals

(E)-5-[1-(Hexyl)-hept-1-en-1-yl]benzimidazole (9)

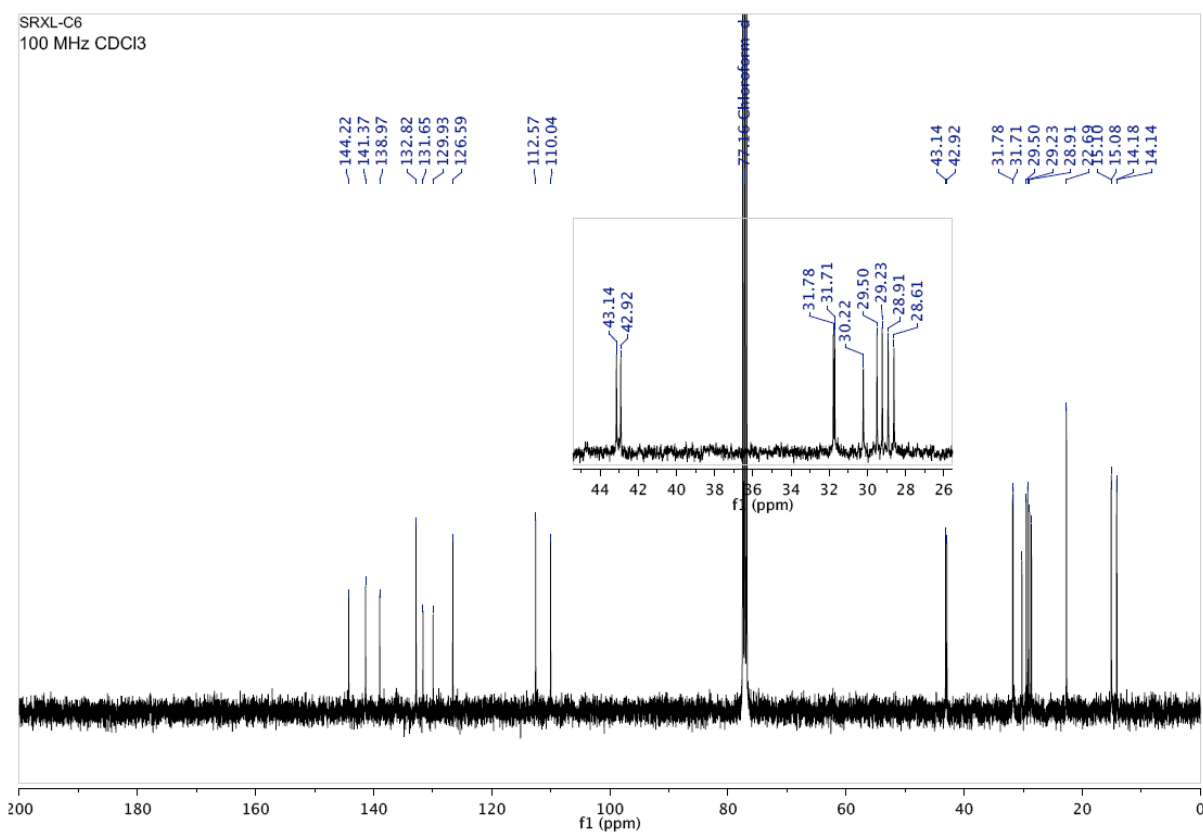
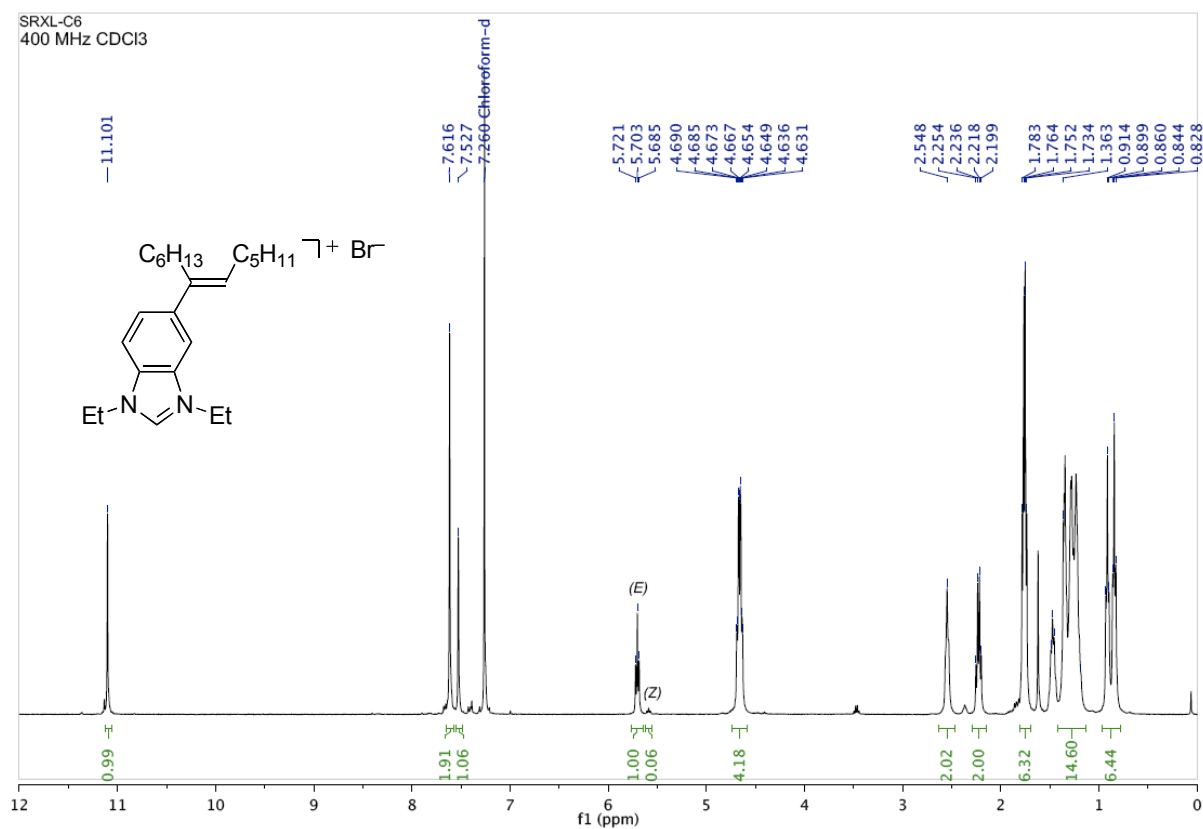


(E)-5-[1-(Hexyl)-hept-1-en-1-yl]benzimidazole (10)

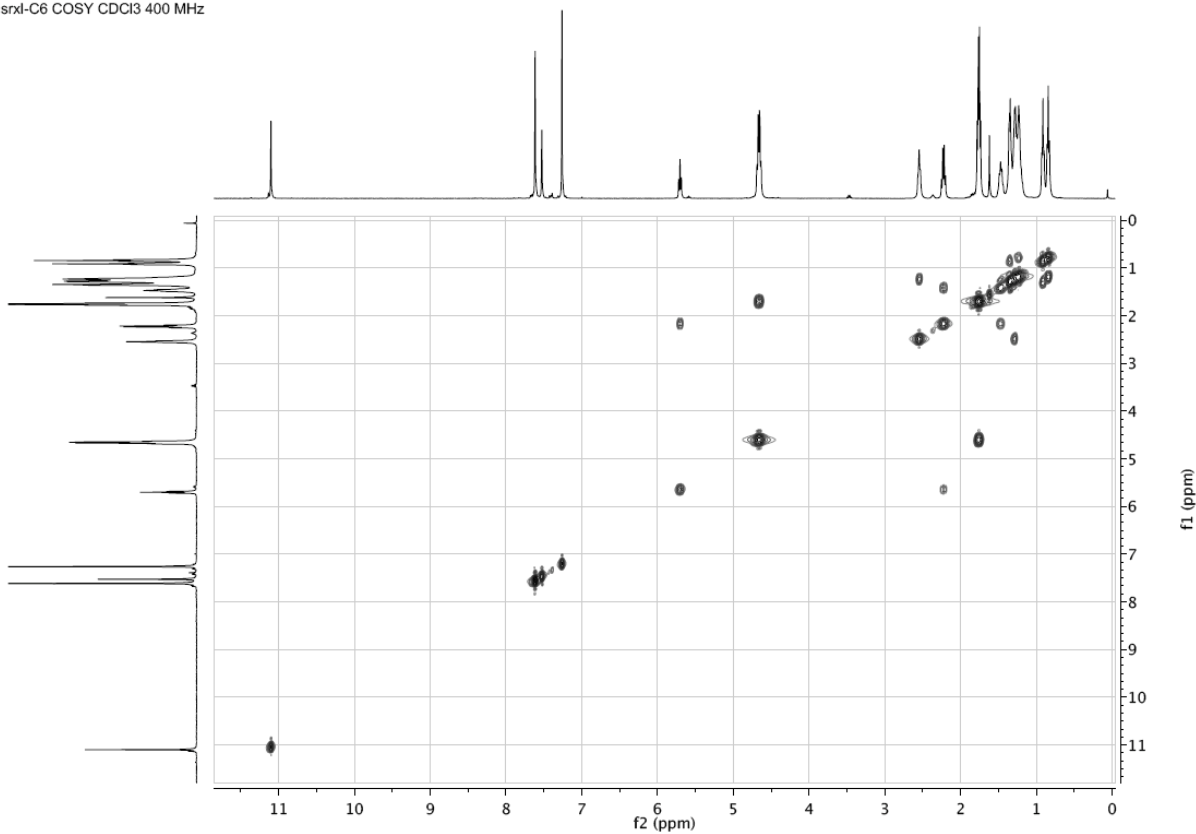


N-heterocyclic carbene coated Nanocrystals and Supracrystals

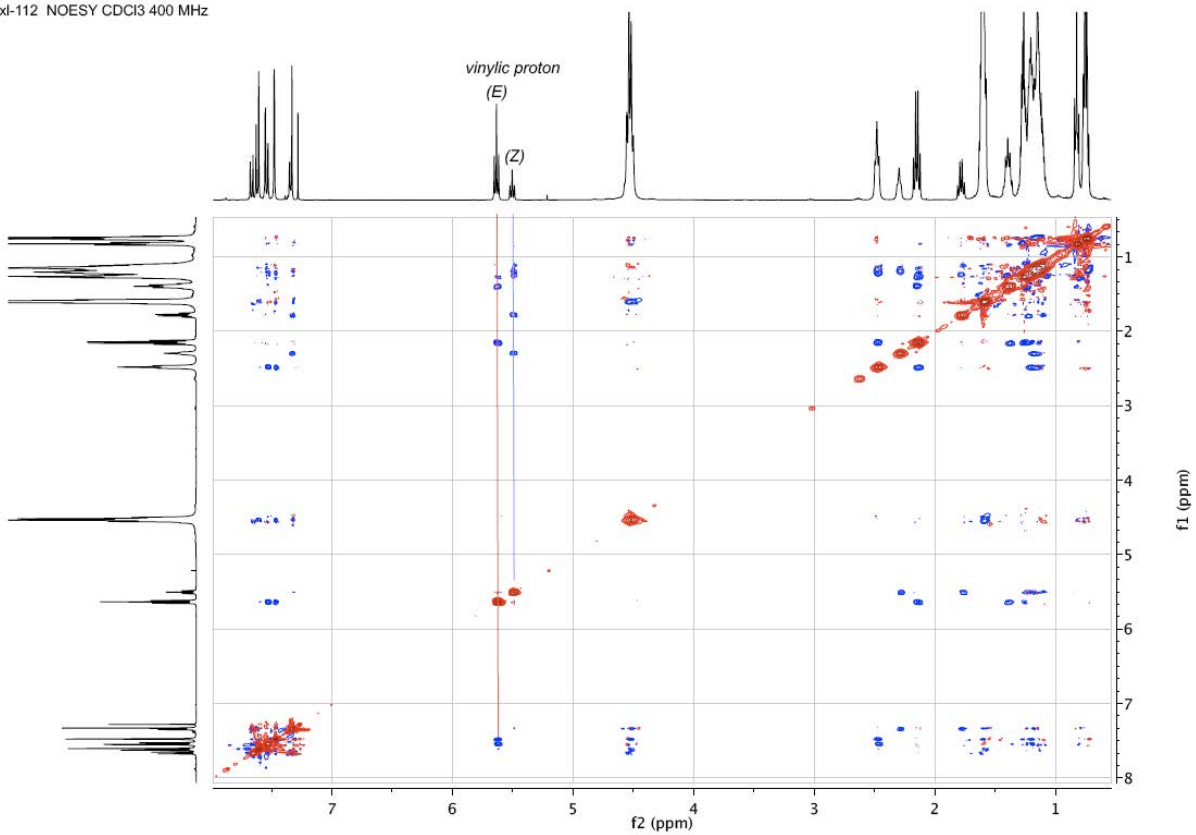
(E)-1,3-Diethyl-5-[1-(hexyl)-hept-1-en-1-yl]benzimidazolium bromide (11)



srxl-C6 COSY CDCl3 400 MHz

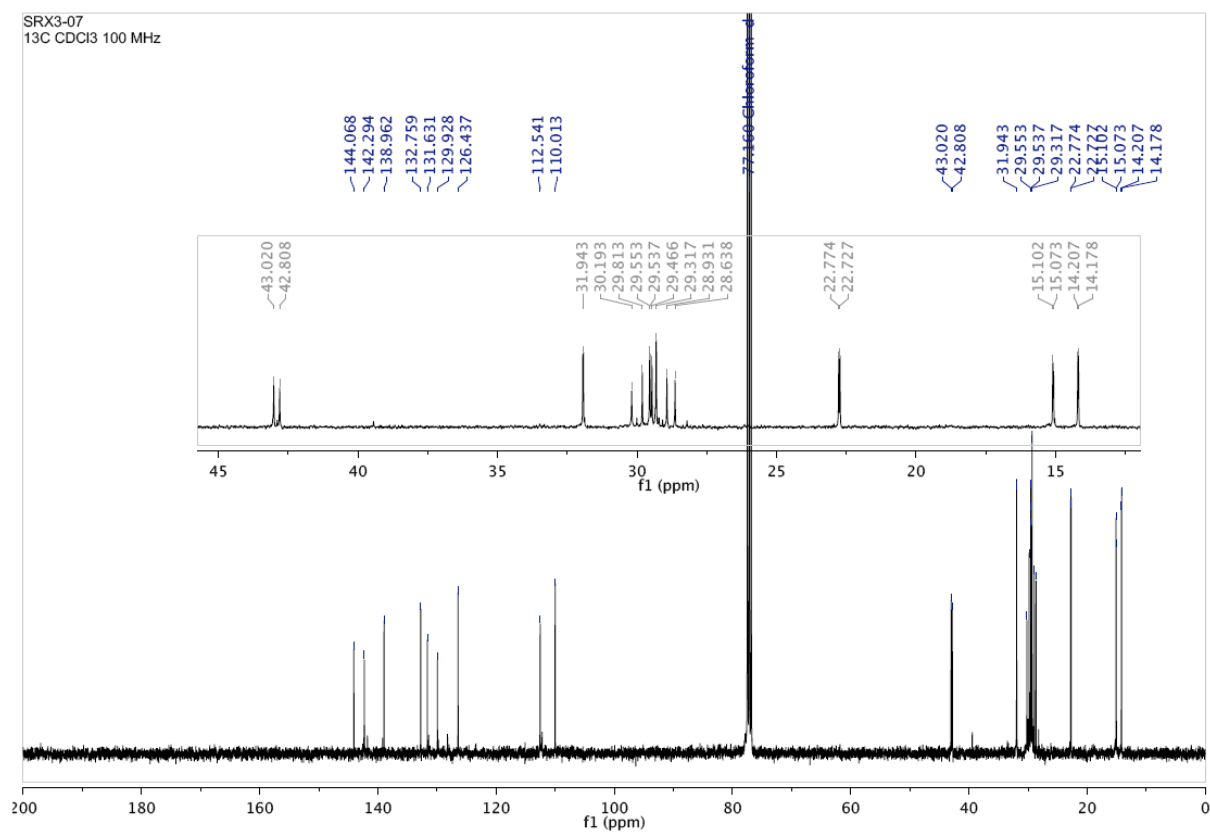
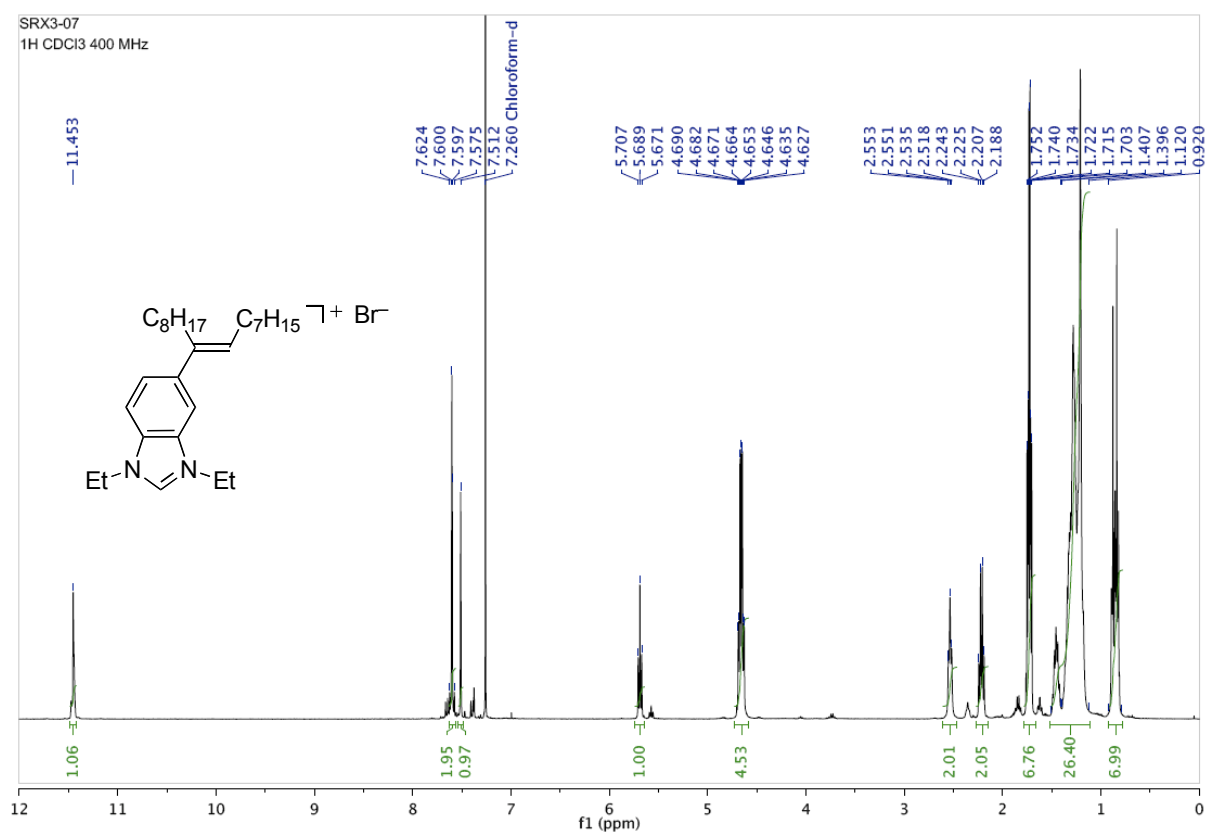


xl-112 NOESY CDCl3 400 MHz

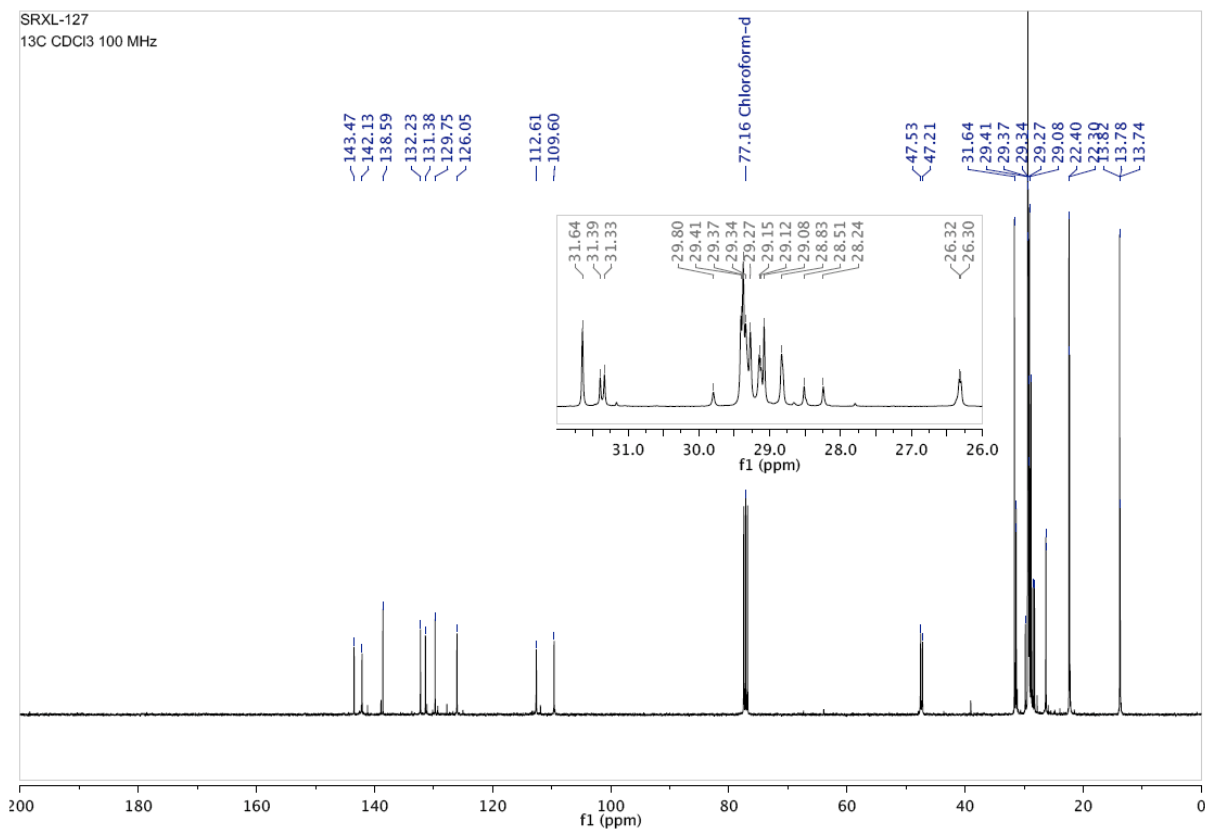
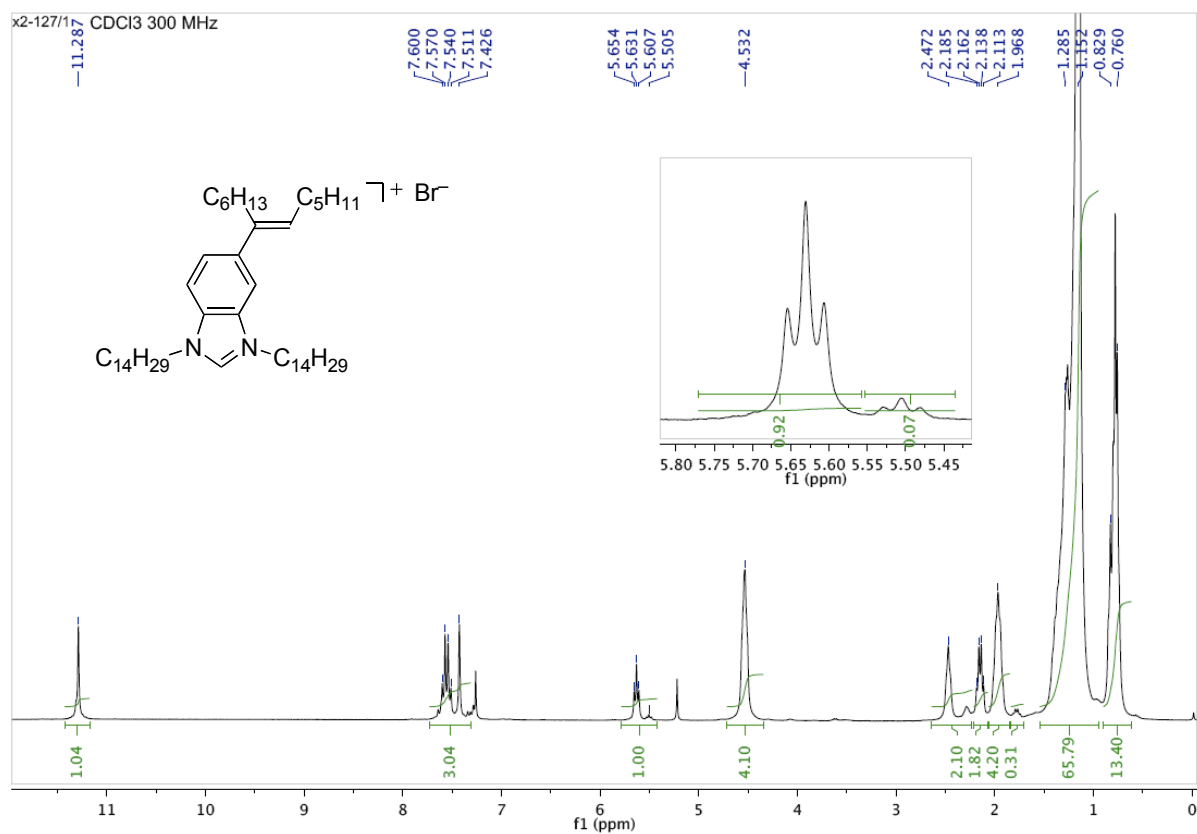


N-heterocyclic carbene coated Nanocrystals and Supracrystals

(E)-1,3-Diethyl-5-[1-(octyl)-non-1-en-1-yl]benzimidazolium bromide (**12**)

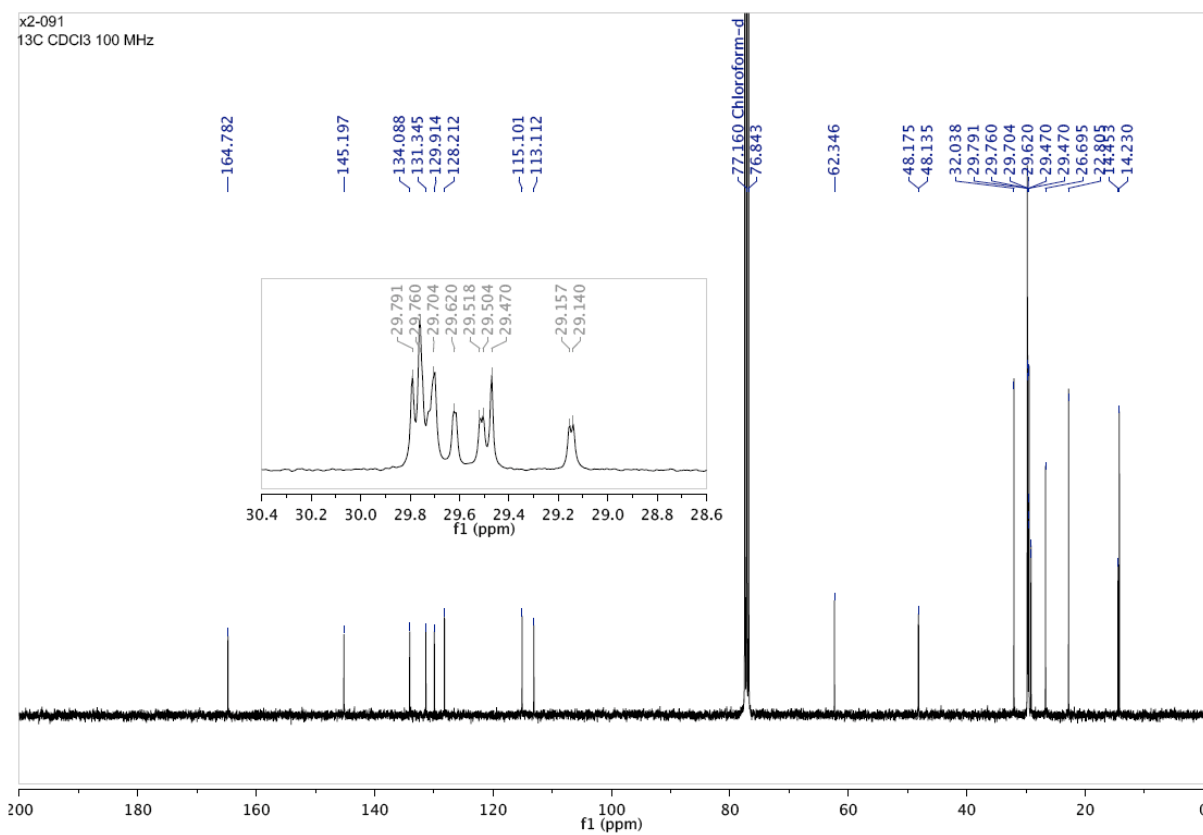
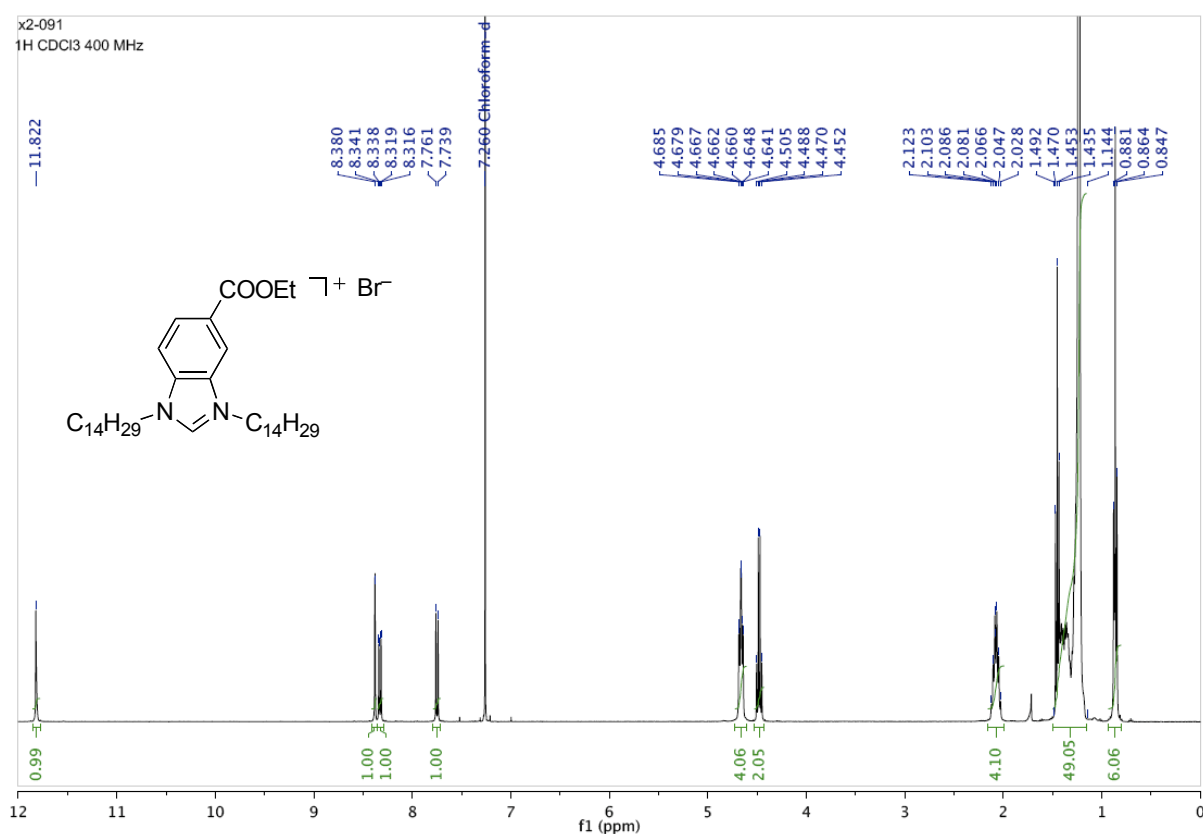


(E)-1,3-Ditetradecyl-5-[1-(hexyl)-hept-1-en-1-yl]benzimidazolium bromide (13)

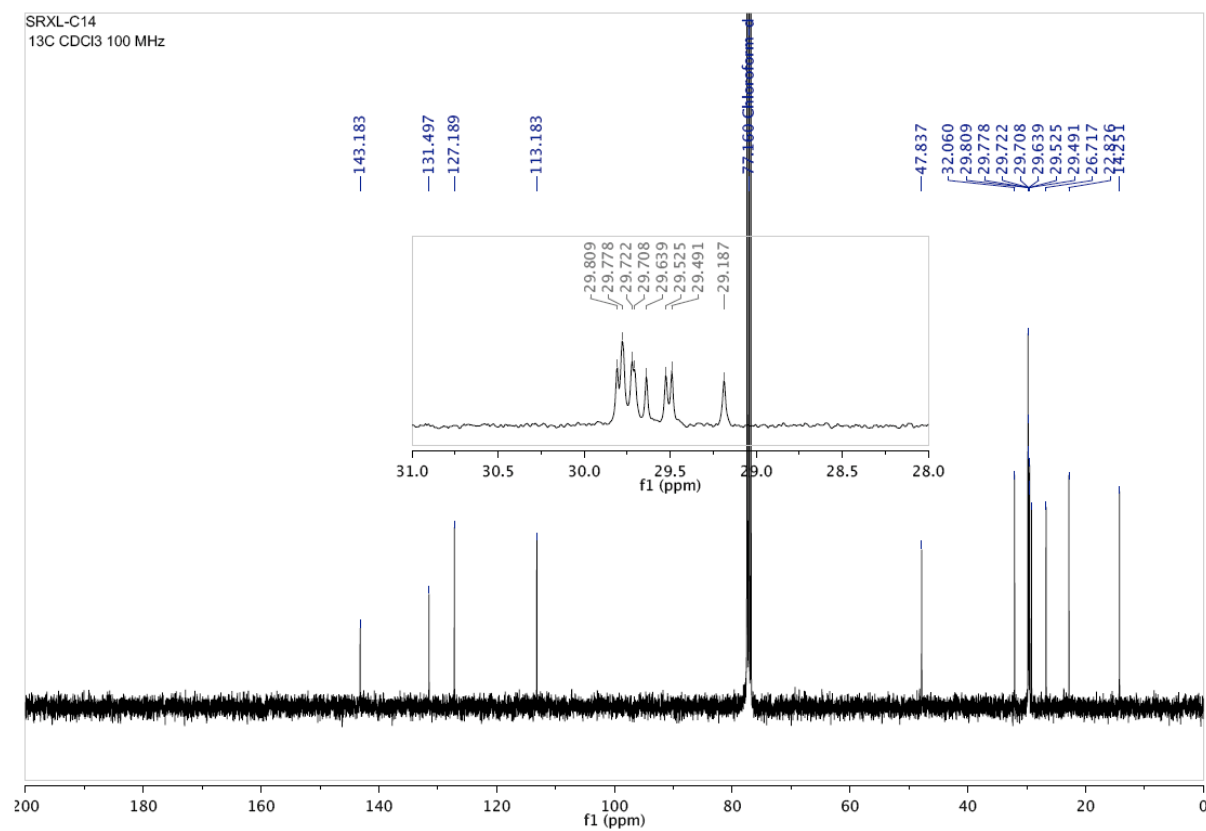
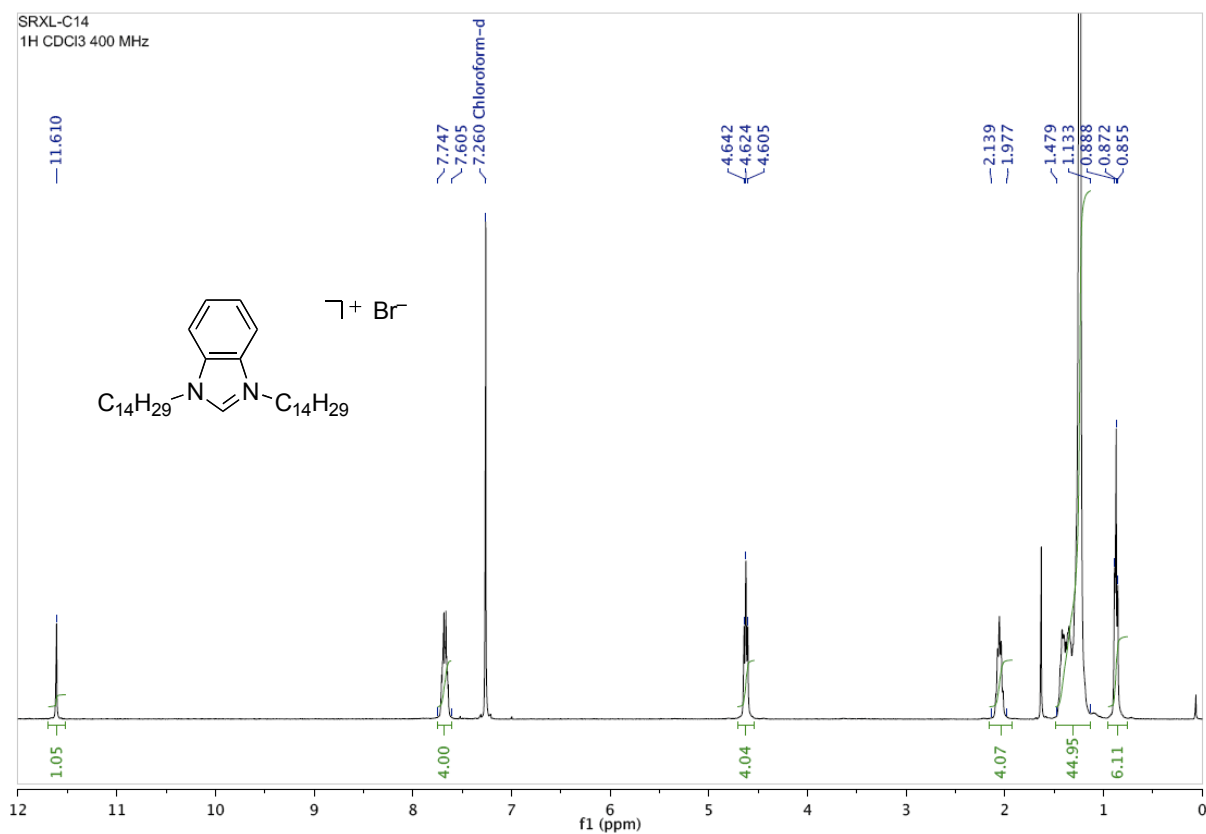


N-heterocyclic carbene coated Nanocrystals and Supracrystals

5-Ethoxycarbonyl-1,3-(ditetradecyl)benzimidazolium bromide (14)



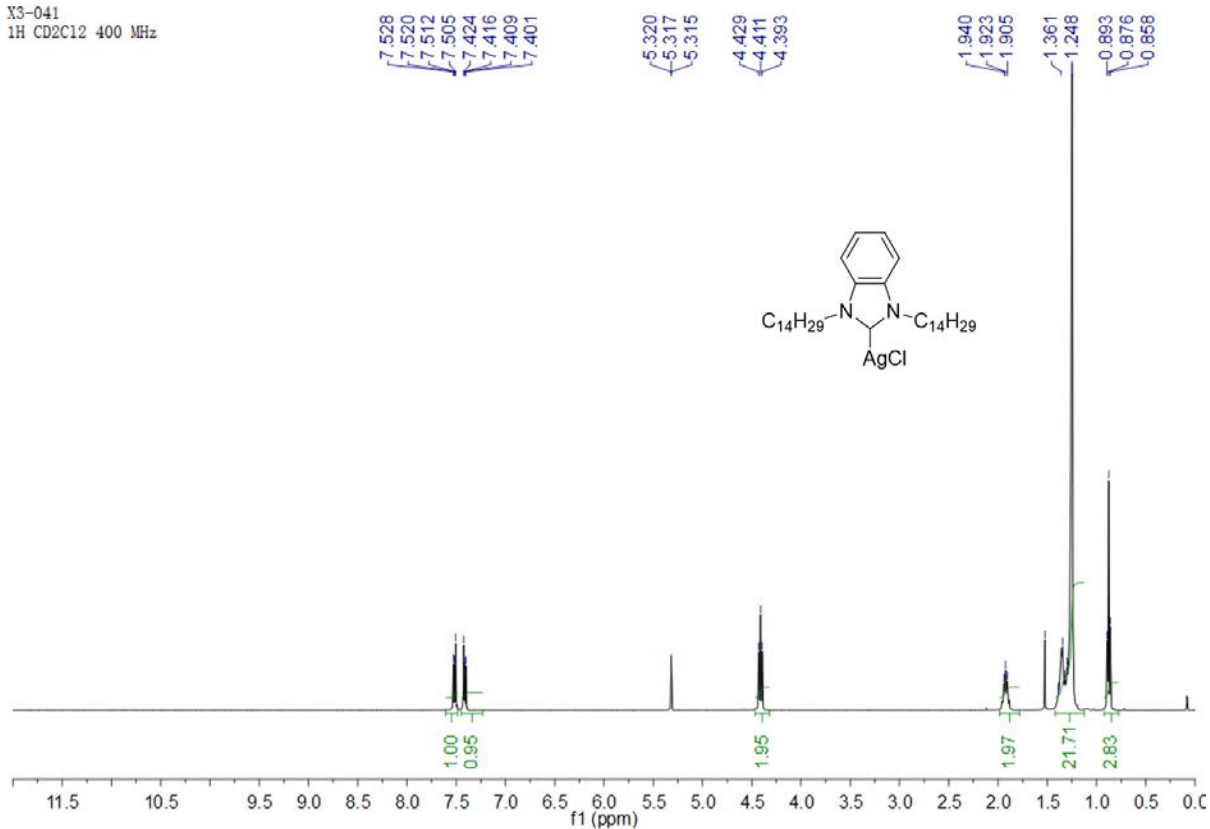
1,3-(Ditetradecyl)benzimidazolium bromide (15)



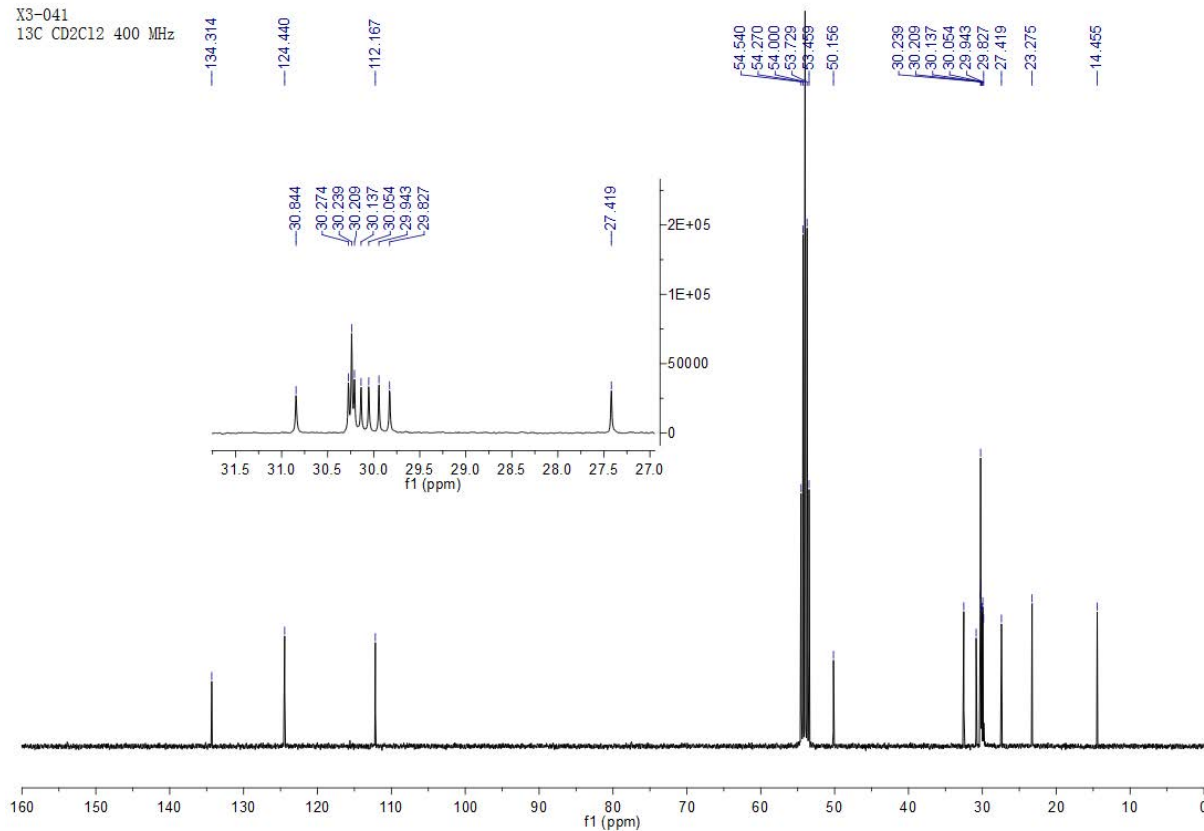
N-heterocyclic carbene coated Nanocrystals and Supracrystals

Silver(I) complex L^5AgBr

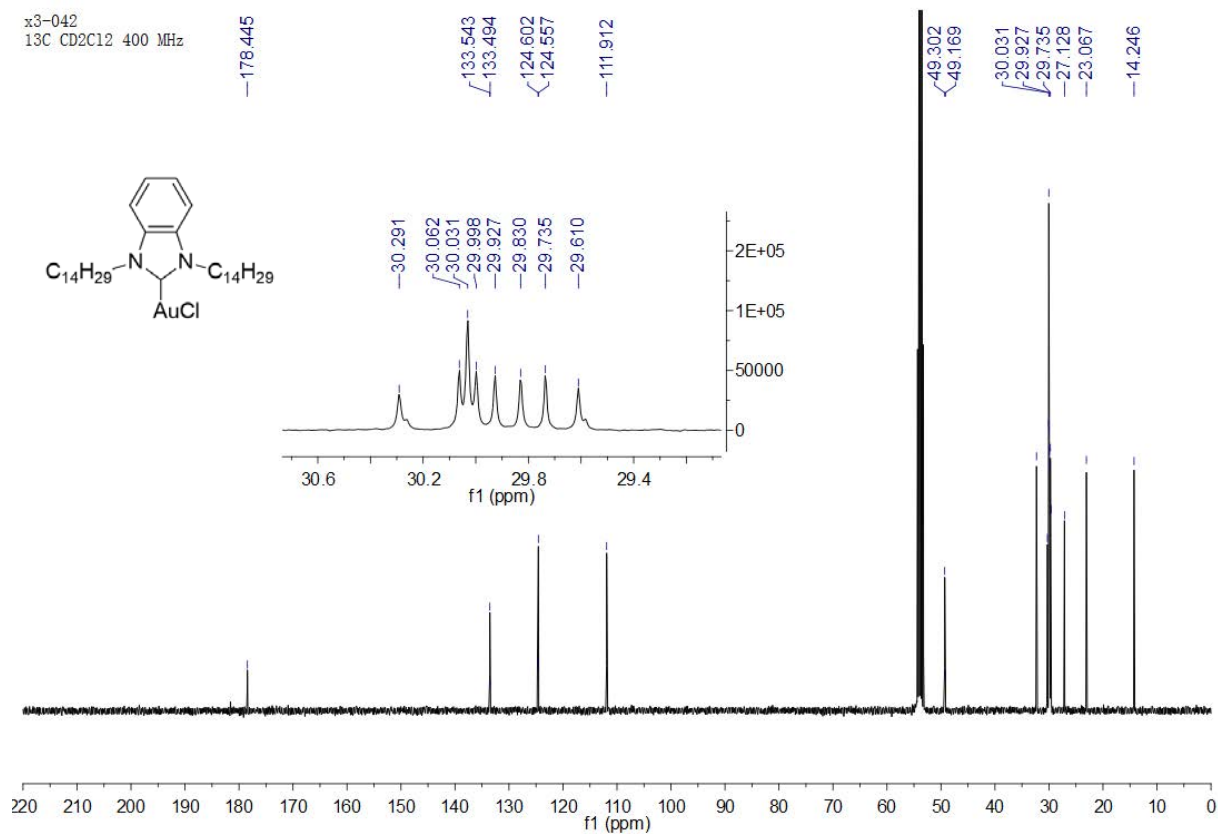
X3-041
1H CD2C12 400 MHz



X3-041
13C CD2C12 400 MHz



Gold(I) complex L^5AuCl



Bibliography

- (1) Burda, C.; Chen, X.; Narayanan, R.; El-Sayed, M. A. Chemistry and Properties of Nanocrystals of Different Shapes. *Chem. Rev.* **2005**, *105*, 1025.
- (2) Chen, X.; Mao, S. S. Titanium Dioxide Nanomaterials: Synthesis, Properties, Modifications, and Applications. *Chem. Rev.* **2007**, *107*, 2891.
- (3) Xia, Y.; Xiong, Y.; Lim, B.; Skrabalak, S. E. Shape-Controlled Synthesis of Metal Nanocrystals: Simple Chemistry Meets Complex Physics? *Angew. Chem. Int. Ed.* **2009**, *48*, 60.
- (4) Daniel, M.-C.; Astruc, D. Gold Nanoparticles: Assembly, Supramolecular Chemistry, Quantum-Size-Related Properties, and Applications toward Biology, Catalysis, and Nanotechnology. *Chem. Rev.* **2003**, *104*, 293.
- (5) Hakkinen, H. The gold-sulfur interface at the nanoscale. *Nat. Chem.* **2012**, *4*, 443.
- (6) Bardhan, R.; Lal, S.; Joshi, A.; Halas, N. J. Theranostic Nanoshells: From Probe Design to Imaging and Treatment of Cancer. *Acc. Chem. Res.* **2011**, *44*, 936.
- (7) Schatz, G. C. Using theory and computation to model nanoscale properties. *PNAS* **2007**, *104*, 6885.
- (8) Elghanian, R.; Storhoff, J. J.; Mucic, R. C.; Letsinger, R. L.; Mirkin, C. A. Selective Colorimetric Detection of Polynucleotides Based on the Distance-Dependent Optical Properties of Gold Nanoparticles. *Science* **1997**, *277*, 1078.
- (9) Haruta, M.; Daté, M. Advances in the catalysis of Au nanoparticles. *Appl. Catal., A* **2001**, *222*, 427.
- (10) Costello, C. K.; Yang, J. H.; Law, H. Y.; Wang, Y.; Lin, J. N.; Marks, L. D.; Kung, M. C.; Kung, H. H. On the potential role of hydroxyl groups in CO oxidation over Au/Al₂O₃. *Appl. Catal., A* **2003**, *243*, 15.
- (11) Chen, M.; Goodman, D. W. Catalytically Active Gold: From Nanoparticles to Ultrathin Films. *Acc. Chem. Res.* **2006**, *39*, 739.
- (12) Corma, A.; Serna, P. Chemoselective Hydrogenation of Nitro Compounds with Supported Gold Catalysts. *Science* **2006**, *313*, 332.
- (13) Hashmi, A. S. K.; Hutchings, G. J. Gold Catalysis. *Angew. Chem. Int. Ed.* **2006**, *45*, 7896.
- (14) Min, B. K.; Friend, C. M. Heterogeneous Gold-Based Catalysis for Green Chemistry: Low-Temperature CO Oxidation and Propene Oxidation. *Chem. Rev.* **2007**, *107*, 2709.

- (15) Jain, P. K.; El-Sayed, I. H.; El-Sayed, M. A. Au nanoparticles target cancer. *Nano Today* **2007**, *2*, 18.
- (16) Sperling, R. A.; Rivera Gil, P.; Zhang, F.; Zanella, M.; Parak, W. J. Biological applications of gold nanoparticles. *Chem. Soc. Rev.* **2008**, *37*, 1896.
- (17) El-Sayed, M. A. Small Is Different: Shape-, Size-, and Composition-Dependent Properties of Some Colloidal Semiconductor Nanocrystals. *Acc. Chem. Res.* **2004**, *37*, 326.
- (18) Saha, K.; Agasti, S. S.; Kim, C.; Li, X.; Rotello, V. M. Gold Nanoparticles in Chemical and Biological Sensing. *Chem. Rev.* **2012**, *112*, 2739.
- (19) Faraday, M. The Bakerian Lecture: Experimental Relations of Gold (and Other Metals) to Light. *Phil. Trans. R. Soc. Lond.* **1857**, *147*, 145.
- (20) Turkevich, J.; Stevenson, P. C.; Hillier, J. A study of the nucleation and growth processes in the synthesis of colloidal gold. *Discuss. Faraday Soc.* **1951**, *11*, 55.
- (21) FRENS, G. Controlled Nucleation for the Regulation of the Particle Size in Monodisperse Gold Suspensions. *Nature-Phys Sci.* **1973**, *241*, 20.
- (22) Wang, Y.; Xia, Y. Bottom-Up and Top-Down Approaches to the Synthesis of Monodispersed Spherical Colloids of Low Melting-Point Metals. *Nano Lett.* **2004**, *4*, 2047.
- (23) Parab, H.; Jung, C.; Woo, M.-A.; Park, H. An anisotropic snowflake-like structural assembly of polymer-capped gold nanoparticles. *J. Nanopart. Res.* **2011**, *13*, 2173.
- (24) Kimling, J.; Maier, M.; Okenve, B.; Kotaidis, V.; Ballot, H.; Plech, A. Turkevich Method for Gold Nanoparticle Synthesis Revisited. *J. Phy. Chem. B* **2006**, *110*, 15700.
- (25) Pong, B.-K.; Elim, H. I.; Chong, J.-X.; Ji, W.; Trout, B. L.; Lee, J.-Y. New Insights on the Nanoparticle Growth Mechanism in the Citrate Reduction of Gold(III) Salt: Formation of the Au Nanowire Intermediate and Its Nonlinear Optical Properties. *J. Phys. Chem. C* **2007**, *111*, 6281.
- (26) Polte, J.; Ahner, T. T.; Delissen, F.; Sokolov, S.; Emmerling, F.; Thünemann, A. F.; Kraehnert, R. Mechanism of Gold Nanoparticle Formation in the Classical Citrate Synthesis Method Derived from Coupled In Situ XANES and SAXS Evaluation. *J. Am. Chem. Soc.* **2010**, *132*, 1296.
- (27) Ji, X.; Song, X.; Li, J.; Bai, Y.; Yang, W.; Peng, X. Size Control of Gold Nanocrystals in Citrate Reduction: The Third Role of Citrate. *J. Am. Chem. Soc.* **2007**, *129*, 13939.
- (28) Shankar, S. S.; Bhargava, S.; Sastry, M. Synthesis of gold nanospheres and nanotriangles by the Turkevich approach. *J. Nanosci. Nanotechnol.* **2005**, *5*, 1721.
- (29) Kumar, S.; Gandhi, K. S.; Kumar, R. Modeling of Formation of Gold Nanoparticles by

- Citrate Method. *Ind. Eng. Chem. Res.* **2006**, *46*, 3128.
- (30) Li, C.; Li, D.; Wan, G.; Xu, J.; Hou, W. Facile synthesis of concentrated gold nanoparticles with low size-distribution in water: temperature and pH controls. *Nanoscale Res. Lett.* **2011**, *6*, 440.
- (31) Rahman, M. R.; Saleh, F. S.; Okajima, T.; Ohsaka, T. pH Dependence of the Size and Crystallographic Orientation of the Gold Nanoparticles Prepared by Seed-Mediated Growth. *Langmuir* **2011**, *27*, 5126.
- (32) Xia, H.; Bai, S.; Hartmann, J. r.; Wang, D. Synthesis of Monodisperse Quasi-Spherical Gold Nanoparticles in Water via Silver(I)-Assisted Citrate Reduction. *Langmuir* **2009**, *26*, 3585.
- (33) Patungwasa, W.; Hodak, J. H. pH tunable morphology of the gold nanoparticles produced by citrate reduction. *Mater. Chem. Phys.* **2008**, *108*, 45.
- (34) Rohiman, A.; Anshori, I.; Surawijaya, A.; Idris, I. Study of Colloidal Gold Synthesis Using Turkevich Method. *AIP Conf. Proc.* **2011**, *1415*, 39.
- (35) Jun-Hyun, K.; Brian, W. L.; Roarke, D. B.; Brett, W. B. Controlled synthesis of gold nanoparticles by fluorescent light irradiation. *Nanotechnology* **2011**, *22*, 285602.
- (36) Su, C.-H.; Wu, P.-L.; Yeh, C.-S. Sonochemical Synthesis of Well-Dispersed Gold Nanoparticles at the Ice Temperature. *J. Phy. Chem. B* **2003**, *107*, 14240.
- (37) Ojea-Jiménez, I.; Romero, F. M.; Bastús, N. G.; Puentes, V. Small Gold Nanoparticles Synthesized with Sodium Citrate and Heavy Water: Insights into the Reaction Mechanism. *J. Phys. Chem. C* **2010**, *114*, 1800.
- (38) Brown, K. R.; Fox, A. P.; Natan, M. J. Morphology-Dependent Electrochemistry of Cytochrome c at Au Colloid-Modified SnO₂ Electrodes. *J. Am. Chem. Soc.* **1996**, *118*, 1154.
- (39) Troughton, E. B.; Bain, C. D.; Whitesides, G. M.; Nuzzo, R. G.; Allara, D. L.; Porter, M. D. Monolayer films prepared by the spontaneous self-assembly of symmetrical and unsymmetrical dialkyl sulfides from solution onto gold substrates: structure, properties, and reactivity of constituent functional groups. *Langmuir* **1988**, *4*, 365.
- (40) Giersig, M.; Mulvaney, P. Preparation of ordered colloid monolayers by electrophoretic deposition. *Langmuir* **1993**, *9*, 3408.
- (41) Brust, M.; Walker, M.; Bethell, D.; Schiffrin, D. J.; Whyman, R. Synthesis of thiol-derivatised gold nanoparticles in a two-phase Liquid-Liquid system. *J. Chem. Soc., Chem. Commun.* **1994**, 801.
- (42) Hostetler, M. J.; Wingate, J. E.; Zhong, C.-J.; Harris, J. E.; Vachet, R. W.; Clark, M. R.;

- Londono, J. D.; Green, S. J.; Stokes, J. J.; Wignall, G. D.; Glish, G. L.; Porter, M. D.; Evans, N. D.; Murray, R. W. Alkanethiolate Gold Cluster Molecules with Core Diameters from 1.5 to 5.2 nm: Core and Monolayer Properties as a Function of Core Size. *Langmuir* **1998**, *14*, 17.
- (43) Schaaff, T. G.; Shafiqullin, M. N.; Khoury, J. T.; Vezmar, I.; Whetten, R. L.; Cullen, W. G.; First, P. N.; Gutiérrez-Wing, C.; Ascensio, J.; Jose-Yacamán, M. J. Isolation of Smaller Nanocrystal Au Molecules: Robust Quantum Effects in Optical Spectra. *J. Phy. Chem. B* **1997**, *101*, 7885.
- (44) Terrill, R. H.; Postlethwaite, T. A.; Chen, C.-h.; Poon, C.-D.; Terzis, A.; Chen, A.; Hutchison, J. E.; Clark, M. R.; Wignall, G. Monolayers in Three Dimensions: NMR, SAXS, Thermal, and Electron Hopping Studies of Alkanethiol Stabilized Gold Clusters. *J. Am. Chem. Soc.* **1995**, *117*, 12537.
- (45) Johnson, S. R.; Evans, S. D.; Brydson, R. Influence of a Terminal Functionality on the Physical Properties of Surfactant-Stabilized Gold Nanoparticles. *Langmuir* **1998**, *14*, 6639.
- (46) Porter, L. A.; Ji, D.; Westcott, S. L.; Graupe, M.; Czernuszewicz, R. S.; Halas, N. J.; Lee, T. R. Gold and Silver Nanoparticles Functionalized by the Adsorption of Dialkyl Disulfides. *Langmuir* **1998**, *14*, 7378.
- (47) Vitale, F.; Fratoddi, I.; Battocchio, C.; Piscopiello, E.; Tapfer, L.; Russo, M.; Polzonetti, G.; Giannini, C. Mono- and bi-functional arenethiols as surfactants for gold nanoparticles: synthesis and characterization. *Nanoscale Res. Lett.* **2011**, *6*, 103.
- (48) Akola, J.; Walter, M.; Whetten, R. L.; Häkkinen, H.; Grönbeck, H. On the Structure of Thiolate-Protected Au₂₅. *J. Am. Chem. Soc.* **2008**, *130*, 3756.
- (49) Toikkanen, O.; Ruiz, V.; Rönnholm, G.; Kalkkinen, N.; Liljeroth, P.; Quinn, B. M. Synthesis and Stability of Monolayer-Protected Au₃₈ Clusters. *J. Am. Chem. Soc.* **2008**, *130*, 11049.
- (50) Goulet, P. J. G.; Lennox, R. B. New Insights into Brust–Schiffrin Metal Nanoparticle Synthesis. *J. Am. Chem. Soc.* **2010**, *132*, 9582.
- (51) Kanaras, A. G.; Kamounah, F. S.; Schaumburg, K.; Kiely, C. J.; Brust, M. Thioalkylated tetraethylene glycol: a new ligand for water soluble monolayer protected gold clusters. *Chem. Commun.* **2002**, 2294.
- (52) Zheng, M.; Li, Z.; Huang, X. Ethylene Glycol Monolayer Protected Nanoparticles: Synthesis, Characterization, and Interactions with Biological Molecules. *Langmuir* **2004**, *20*, 4226.
- (53) Sardar, R.; Shumaker-Parry, J. S. 9-BBN Induced Synthesis of Nearly Monodisperse

- ω -Functionalized Alkylthiol Stabilized Gold Nanoparticles. *Chem. Mater.* **2009**, *21*, 1167.
- (54) Di Pasqua, A. J.; Mishler Li, R. E.; Ship, Y.-L.; Dabrowiak, J. C.; Asefa, T. Preparation of antibody-conjugated gold nanoparticles. *Mater. Lett.* **2009**, *63*, 1876.
- (55) Leontowich, A. F. G.; Calver, C. F.; Dasog, M.; Scott, R. W. J. Surface Properties of Water-Soluble Glycine-Cysteamine-Protected Gold Clusters. *Langmuir* **2009**, *26*, 1285.
- (56) Busby, M.; Chiorboli, C.; Scandola, F. Relaxation Dynamics and Transient Behavior of Small Arenethiol Passivated Gold Nanoparticles. *J. . Phy. Chem. B* **2006**, *110*, 6020.
- (57) Gupta, R. K.; Srinivasan, M. P.; Dharmarajan, R. Synthesis of short chain thiol capped gold nanoparticles, their stabilization and immobilization on silicon surface. *Colloids Surf., A* **2011**, *390*, 149.
- (58) Zubarev, E. R.; Xu, J.; Sayyad, A.; Gibson, J. D. Amphiphilic Gold Nanoparticles with V-Shaped Arms. *J. Am. Chem. Soc.* **2006**, *128*, 4958.
- (59) Müller, C. I.; Lambert, C. Electrochemical and Optical Characterization of Triarylamine Functionalized Gold Nanoparticles. *Langmuir* **2011**, *27*, 5029.
- (60) Zhang, D.; Neumann, O.; Wang, H.; Yuwono, V. M.; Barhoumi, A.; Perham, M.; Hartgerink, J. D.; Wittung-Stafshede, P.; Halas, N. J. Gold Nanoparticles Can Induce the Formation of Protein-based Aggregates at Physiological pH. *Nano Lett.* **2009**, *9*, 666.
- (61) Oh, E.; Susumu, K.; Goswami, R.; Mattoussi, H. One-Phase Synthesis of Water-Soluble Gold Nanoparticles with Control over Size and Surface Functionalities. *Langmuir* **2010**, *26*, 7604.
- (62) Manna, A.; Chen, P.-L.; Akiyama, H.; Wei, T.-X.; Tamada, K.; Knoll, W. Optimized Photoisomerization on Gold Nanoparticles Capped by Unsymmetrical Azobenzene Disulfides. *Chem. Mater.* **2002**, *15*, 20.
- (63) Li, Y.; Zaluzhna, O.; Tong, Y. J. Identification of a source of size polydispersity and its solution in Brust-Schiffrin metal nanoparticle synthesis. *Chem. Commun.* **2011**, *47*, 6033.
- (64) Tang, Z.; Xu, B.; Wu, B.; Germann, M. W.; Wang, G. Synthesis and Structural Determination of Multidentate 2,3-Dithiol-Stabilized Au Clusters. *J. Am. Chem. Soc.* **2010**, *132*, 3367.
- (65) Sistach, S.; Beija, M.; Rahal, V.; Brûlet, A.; Marty, J.-D.; Destarac, M.; Mingotaud, C. Thermoresponsive Amphiphilic Diblock Copolymers Synthesized by MADIX/RAFT: Properties in Aqueous Solutions and Use for the Preparation and Stabilization of Gold Nanoparticles. *Chem. Mater.* **2010**, *22*, 3712.
- (66) Zhang, S.; Leem, G.; Lee, T. R. Monolayer-Protected Gold Nanoparticles Prepared Using

Long-Chain Alkanethioacetates. *Langmuir* **2009**, *25*, 13855.

(67) Vickers, M. S.; Cookson, J.; Beer, P. D.; Bishop, P. T.; Thiebaut, B. Dithiocarbamate ligand stabilised gold nanoparticles. *J. Mater. Chem.* **2006**, *16*, 209.

(68) Wojczykowski, K.; Mei, Jutzi, P.; Ennen, I.; Hutten, A.; Fricke, M.; Volkmer, D. Reliable stabilization and functionalization of nanoparticles through tridentate thiolate ligands. *Chem. Commun.* **2006**, 3693.

(69) Wang, S.; Qian, K.; Bi, X.; Huang, W. Influence of Speciation of Aqueous HAuCl₄ on the Synthesis, Structure, and Property of Au Colloids. *J. Phys. Chem. C* **2009**, *113*, 6505.

(70) Volkert, A. A.; Subramaniam, V.; Ivanov, M. R.; Goodman, A. M.; Haes, A. J. Salt-Mediated Self-Assembly of Thiocetic Acid on Gold Nanoparticles. *ACS Nano* **2011**, *5*, 4570.

(71) Béthencourt, M. I.; Srisombat, L.-o.; Chinwangso, P.; Lee, T. R. SAMs on Gold Derived from the Direct Adsorption of Alkanethioacetates Are Inferior to Those Derived from the Direct Adsorption of Alkanethiols. *Langmuir* **2009**, *25*, 1265.

(72) Biradar, S. C.; Shinde, D. B.; Pillai, V. K.; Kulkarni, M. G. Polydentate disulfides for enhanced stability of AuNPs and facile nanocavity formation. *J. Mater. Chem.* **2012**, *22*, 10000.

(73) Zheng, N.; Fan, J.; Stucky, G. D. One-Step One-Phase Synthesis of Monodisperse Noble-Metallic Nanoparticles and Their Colloidal Crystals. *J. Am. Chem. Soc.* **2006**, *128*, 6550.

(74) Goubet, N.; Richardi, J.; Albouy, P.-A.; Pileni, M.-P. Which Forces Control Supracrystal Nucleation in Organic Media? *Adv. Funct. Mater.* **2011**, *21*, 2693.

(75) Walter, M.; Akola, J.; Lopez-Acevedo, O.; Jadzinsky, P. D.; Calero, G.; Ackerson, C. J.; Whetten, R. L.; Grönbeck, H.; Häkkinen, H. A unified view of ligand-protected gold clusters as superatom complexes. *PNAS* **2008**, *105*, 9157.

(76) Shem, P. M.; Sardar, R.; Shumaker-Parry, J. S. One-Step Synthesis of Phosphine-Stabilized Gold Nanoparticles Using the Mild Reducing Agent 9-BBN. *Langmuir* **2009**, *25*, 13279.

(77) Moores, A.; Goettmann, F.; Sanchez, C.; Le Floch, P. Phosphinine stabilised gold nanoparticles; synthesis and immobilisation on mesoporous materials. *Chem. Commun.* **2004**, 2842.

(78) Yang, Y.; Chen, S. Surface Manipulation of the Electronic Energy of Subnanometer-Sized Gold Clusters: An Electrochemical and Spectroscopic Investigation.

Nano Lett. **2002**, *3*, 75.

(79) Carageorghopol, A.; Chechik, V. Mechanistic aspects of ligand exchange in Au nanoparticles. *Phys. Chem. Chem. Phys.* **2008**, *10*, 5029.

(80) Schmid, G.; Pfeil, R.; Boese, R.; Bandermann, F.; Meyer, S.; Calis, G. H. M.; van der Velden, J. W. A. Au₅₅[P(C₆H₅)₃]₁₂Cl₆ - ein Goldcluster ungewöhnlicher Größe. *Chem. Ber.* **1981**, *114*, 3634.

(81) Pettibone, J. M.; Hudgens, J. W. Gold Cluster Formation with Phosphine Ligands: Etching as a Size-Selective Synthetic Pathway for Small Clusters? *ACS Nano* **2011**, *5*, 2989.

(82) de Silva, N.; Ha, J.-M.; Solovyov, A.; Nigra, M. M.; Ogino, I.; Yeh, S. W.; Durkin, K. A.; Katz, A. A bioinspired approach for controlling accessibility in calix[4]arene-bound metal cluster catalysts. *Nat. Chem.* **2010**, *2*, 1062.

(83) Jena, B. K.; Raj, C. R. Synthesis of Flower-like Gold Nanoparticles and Their Electrocatalytic Activity Towards the Oxidation of Methanol and the Reduction of Oxygen. *Langmuir* **2007**, *23*, 4064.

(84) Li, G.; Li, D.; Zhang, L.; Zhai, J.; Wang, E. One-Step Synthesis of Folic Acid Protected Gold Nanoparticles and Their Receptor-Mediated Intracellular Uptake. *Chem. Eur. J.* **2009**, *15*, 9868.

(85) Yavuz, M. S.; Li, W.; Xia, Y. Facile Synthesis of Gold Icosahedra in an Aqueous Solution by Reacting HAuCl₄ with N-Vinyl Pyrrolidone. *Chem. Eur. J.* **2009**, *15*, 13181.

(86) Gittins, D. I.; Caruso, F. Spontaneous Phase Transfer of Nanoparticulate Metals from Organic to Aqueous Media. *Angew. Chem. Int. Ed.* **2001**, *40*, 3001.

(87) Gandubert, V. J.; Lennox, R. B. Assessment of 4-(Dimethylamino)pyridine as a Capping Agent for Gold Nanoparticles. *Langmuir* **2005**, *21*, 6532.

(88) Lange, H.; Maultzsch, J.; Meng, W.; Mollenhauer, D.; Paulus, B.; Peica, N.; Schlecht, S.; Thomsen, C. Adsorption Behavior of 4-Methoxypyridine on Gold Nanoparticles. *Langmuir* **2011**, *27*, 7258.

(89) Sastry, M.; Kumar, A.; Mukherjee, P. Phase transfer of aqueous colloidal gold particles into organic solutions containing fatty amine molecules. *Colloids Surf., A* **2001**, *181*, 255.

(90) Kumar, A.; Mandal, S.; Pasricha, R.; Mandale, A. B.; Sastry, M. Investigation into the Interaction between Surface-Bound Alkylamines and Gold Nanoparticles. *Langmuir* **2003**, *19*, 6277.

(91) Wangoo, N.; Bhasin, K. K.; Mehta, S. K.; Suri, C. R. Synthesis and capping of water-dispersed gold nanoparticles by an amino acid: Bioconjugation and binding studies. *J.*

Colloid Interface Sci. **2008**, *323*, 247.

(92) Nikoobakht, B.; El-Sayed, M. A. Evidence for Bilayer Assembly of Cationic Surfactants on the Surface of Gold Nanorods. *Langmuir* **2001**, *17*, 6368.

(93) Cheng, W.; Dong, S.; Wang, E. Synthesis and Self-Assembly of Cetyltrimethylammonium Bromide-Capped Gold Nanoparticles. *Langmuir* **2003**, *19*, 9434.

(94) Mirkhalaf, F.; Paprotny, J.; Schiffrin, D. J. Synthesis of Metal Nanoparticles Stabilized by Metal–Carbon Bonds. *J. Am. Chem. Soc.* **2006**, *128*, 7400.

(95) Zhang, S.; Chandra, K. L.; Gorman, C. B. Self-Assembled Monolayers of Terminal Alkynes on Gold. *J. Am. Chem. Soc.* **2007**, *129*, 4876.

(96) Maity, P.; Tsunoyama, H.; Yamauchi, M.; Xie, S.; Tsukuda, T. Organogold Clusters Protected by Phenylacetylene. *J. Am. Chem. Soc.* **2011**, *133*, 20123.

(97) Maity, P.; Wakabayashi, T.; Ichikuni, N.; Tsunoyama, H.; Xie, S.; Yamauchi, M.; Tsukuda, T. Selective synthesis of organogold magic clusters Au₅₄(C[triple bond, length as m-dash]CPh)₂₆. *Chem. Commun.* **2012**, *48*, 6085.

(98) Maity, P.; Takano, S.; Yamazoe, S.; Wakabayashi, T.; Tsukuda, T. Binding Motif of Terminal Alkynes on Gold Clusters. *J. Am. Chem. Soc.* **2013**, *135*, 9450.

(99) Wan, X.-K.; Tang, Q.; Yuan, S.-F.; Jiang, D.-e.; Wang, Q.-M. Au₁₉ Nanocluster Featuring a V-Shaped Alkynyl–Gold Motif. *J. Am. Chem. Soc.* **2015**, *137*, 652.

(100) Wan, X.-K.; Yuan, S.-F.; Tang, Q.; Jiang, D.-e.; Wang, Q.-M. Alkynyl-Protected Au₂₃ Nanocluster: A 12-Electron System. *Angew. Chem. Int. Ed.* **2015**, *54*, 5977.

(101) Shan, J.; Tenhu, H. Recent advances in polymer protected gold nanoparticles: synthesis, properties and applications. *Chem. Commun.* **2007**, 4580.

(102) Wuelfing, W. P.; Gross, S. M.; Miles, D. T.; Murray, R. W. Nanometer Gold Clusters Protected by Surface-Bound Monolayers of Thiolated Poly(ethylene glycol) Polymer Electrolyte. *J. Am. Chem. Soc.* **1998**, *120*, 12696.

(103) Corbierre, M. K.; Cameron, N. S.; Lennox, R. B. Polymer-Stabilized Gold Nanoparticles with High Grafting Densities. *Langmuir* **2004**, *20*, 2867.

(104) Chiu, J. J.; Kim, B. J.; Kramer, E. J.; Pine, D. J. Control of Nanoparticle Location in Block Copolymers. *J. Am. Chem. Soc.* **2005**, *127*, 5036.

(105) Shan, J.; Nuopponen, M.; Jiang, H.; Viitala, T.; Kauppinen, E.; Kontturi, K.; Tenhu, H. Amphiphilic Gold Nanoparticles Grafted with Poly(N-isopropylacrylamide) and Polystyrene. *Macromolecules* **2005**, *38*, 2918.

(106) Higashi, N.; Kawahara, J.; Niwa, M. Preparation of helical peptide monolayer-coated

- gold nanoparticles. *J. Colloid Interface Sci.* **2005**, *288*, 83.
- (107) Hussain, I.; Graham, S.; Wang, Z.; Tan, B.; Sherrington, D. C.; Rannard, S. P.; Cooper, A. I.; Brust, M. Size-Controlled Synthesis of Near-Monodisperse Gold Nanoparticles in the 1–4 nm Range Using Polymeric Stabilizers. *J. Am. Chem. Soc.* **2005**, *127*, 16398.
- (108) Fustin, C.-A.; Colard, C.; Filali, M.; Guillet, P.; Duwez, A.-S.; Meier, M. A. R.; Schubert, U. S.; Gohy, J.-F. Tuning the Hydrophilicity of Gold Nanoparticles Templated in Star Block Copolymers. *Langmuir* **2006**, *22*, 6690.
- (109) Gentilini, C.; Evangelista, F.; Rudolf, P.; Franchi, P.; Lucarini, M.; Pasquato, L. Water-Soluble Gold Nanoparticles Protected by Fluorinated Amphiphilic Thiolates. *J. Am. Chem. Soc.* **2008**, *130*, 15678.
- (110) Huang, X.; Li, B.; Zhang, H.; Hussain, I.; Liang, L.; Tan, B. Facile preparation of size-controlled gold nanoparticles using versatile and end-functionalized thioether polymer ligands. *Nanoscale* **2011**, *3*, 1600.
- (111) Biondi, I.; Laurency, G.; Dyson, P. J. Synthesis of Gold Nanoparticle Catalysts Based on a New Water-Soluble Ionic Polymer. *Inorg. Chem.* **2011**, *50*, 8038.
- (112) Beija, M.; Marty, J.-D.; Destarac, M. Thermoresponsive poly(N-vinyl caprolactam)-coated gold nanoparticles: sharp reversible response and easy tunability. *Chem. Commun.* **2011**, *47*, 2826.
- (113) Bosman, A. W.; Janssen, H. M.; Meijer, E. W. About Dendrimers: Structure, Physical Properties, and Applications. *Chem. Rev.* **1999**, *99*, 1665.
- (114) Garcia, M. E.; Baker, L. A.; Crooks, R. M. Preparation and Characterization of Dendrimer–Gold Colloid Nanocomposites. *Anal. Chem.* **1998**, *71*, 256.
- (115) Hoffman, L. W.; Andersson, G. G.; Sharma, A.; Clarke, S. R.; Voelcker, N. H. New Insights into the Structure of PAMAM Dendrimer/Gold Nanoparticle Nanocomposites. *Langmuir* **2011**, *27*, 6759.
- (116) Love, C. S.; Chechik, V.; Smith, D. K.; Brennan, C. Dendron-stabilised gold nanoparticles: generation dependence of core size and thermal stability. *J. Mater. Chem.* **2004**, *14*, 919.
- (117) Kim, Y.-G.; Oh, S.-K.; Crooks, R. M. Preparation and Characterization of 1–2 nm Dendrimer-Encapsulated Gold Nanoparticles Having Very Narrow Size Distributions. *Chem. Mater.* **2003**, *16*, 167.
- (118) Chechik, V.; Crooks, R. M. Monolayers of Thiol-Terminated Dendrimers on the Surface of Planar and Colloidal Gold. *Langmuir* **1999**, *15*, 6364.

- (119) Endo, T.; Yoshimura, T.; Esumi, K. Synthesis and catalytic activity of gold–silver binary nanoparticles stabilized by PAMAM dendrimer. *J. Colloid Interface Sci.* **2005**, *286*, 602.
- (120) Jia, L.; Lv, L.-P.; Xu, J.-P.; Ji, J. Phosphorylcholine functionalized dendrimers for the formation of highly stable and reactive gold nanoparticles and their glucose conjugation for biosensing. *J. Nanopart. Res.* **2011**, *13*, 4075.
- (121) Taubert, A.; Wiesler, U.-M.; Mullen, K. Dendrimer-controlled one-pot synthesis of gold nanoparticles with a bimodal size distribution and their self-assembly in the solid state. *J. Mater. Chem.* **2003**, *13*, 1090.
- (122) Jiang, G.; Wang, L.; Chen, T.; Yu, H.; Chen, C. Preparation of gold nanoparticles in the presence of poly(benzyl ether) alcohol dendrons. *Mater. Chem. Phys.* **2006**, *98*, 76.
- (123) Wang, R.; Yang, J.; Zheng, Z.; Carducci, M. D.; Jiao, J.; Seraphin, S. Dendron-Controlled Nucleation and Growth of Gold Nanoparticles. *Angew. Chem. Int. Ed.* **2001**, *40*, 549.
- (124) Deng, S.; Fulghum, T. M.; Krueger, G.; Patton, D.; Park, J.-Y.; Advincula, R. C. Hybrid Gold-Nanoparticle-Cored Conjugated Thiophene Dendrimers: Synthesis, Characterization, and Energy-Transfer Studies. *Chem. Eur. J.* **2011**, *17*, 8929.
- (125) Hermes, J. P.; Sander, F.; Peterle, T.; Urbani, R.; Pfohl, T.; Thompson, D.; Mayor, M. Gold Nanoparticles Stabilized by Thioether Dendrimers. *Chem. Eur. J.* **2011**, *17*, 13473.
- (126) Namazi, H.; Fard, A. M. P. Preparation of gold nanoparticles in the presence of citric acid-based dendrimers containing periphery hydroxyl groups. *Mater. Chem. Phys.* **2011**, *129*, 189.
- (127) Boisselier, E.; Diallo, A. K.; Salmon, L.; Ruiz, J.; Astruc, D. Gold nanoparticles synthesis and stabilization via new "clicked" polyethyleneglycol dendrimers. *Chem. Commun.* **2008**, 4819.
- (128) Boisselier, E.; Diallo, A. K.; Salmon, L.; Ornelas, C.; Ruiz, J.; Astruc, D. Encapsulation and Stabilization of Gold Nanoparticles with "Click" Polyethyleneglycol Dendrimers. *J. Am. Chem. Soc.* **2010**, *132*, 2729.
- (129) Bourissou, D.; Guerret, O.; Gabbaï, F. P.; Bertrand, G. Stable Carbenes. *Chem. Rev.* **1999**, *100*, 39.
- (130) de Frémont, P.; Marion, N.; Nolan, S. P. Carbenes: Synthesis, properties, and organometallic chemistry. *Coord. Chem. Rev.* **2009**, *253*, 862.
- (131) Arduengo, A. J.; Harlow, R. L.; Kline, M. A stable crystalline carbene. *J. Am. Chem. Soc.* **1991**, *113*, 361.

- (132) Dröge, T.; Glorius, F. The Measure of All Rings—N-Heterocyclic Carbenes. *Angew. Chem. Int. Ed.* **2010**, *49*, 6940.
- (133) Kühl, O. Sterically induced differences in N-heterocyclic carbene transition metal complexes. *Coord. Chem. Rev.* **2009**, *253*, 2481.
- (134) Díez-González, S.; Nolan, S. P. Stereoelectronic parameters associated with N-heterocyclic carbene (NHC) ligands: A quest for understanding. *Coord. Chem. Rev.* **2007**, *251*, 874.
- (135) Glorius, F. In *N-Heterocyclic Carbenes in Transition Metal Catalysis*; Springer Berlin Heidelberg 2007, *21*, 1.
- (136) Mercks, L.; Albrecht, M. Beyond catalysis: N-heterocyclic carbene complexes as components for medicinal, luminescent, and functional materials applications. *Chem. Soc. Rev.* **2010**, *39*, 1903.
- (137) Tapu, D.; Dixon, D. A.; Roe, C. ¹³C NMR Spectroscopy of “Arduengo-type” Carbenes and Their Derivatives. *Chem. Rev.* **2009**, *109*, 3385.
- (138) Marion, N.; Nolan, S. P. Well-Defined N-Heterocyclic Carbenes–Palladium(II) Precatalysts for Cross-Coupling Reactions. *Acc. Chem. Res.* **2008**, *41*, 1440.
- (139) Díez-González, S.; Nolan, S. P. Copper, Silver, and Gold Complexes in Hydrosilylation Reactions. *Acc. Chem. Res.* **2008**, *41*, 349.
- (140) Herrmann, W. A. N-Heterocyclic Carbenes: A New Concept in Organometallic Catalysis. *Angew. Chem. Int. Ed.* **2002**, *41*, 1290.
- (141) Nair, V.; Vellalath, S.; Babu, B. P. Recent advances in carbon-carbon bond-forming reactions involving homoenolates generated by NHC catalysis. *Chem. Soc. Rev.* **2008**, *37*, 2691.
- (142) Marion, N.; Díez-González, S.; Nolan, S. P. N-Heterocyclic Carbenes as Organocatalysts. *Angew. Chem. Int. Ed.* **2007**, *46*, 2988.
- (143) Pyykkö, P.; Runeberg, N. Comparative Theoretical Study of N-Heterocyclic Carbenes and Other Ligands Bound to AuI. *Chem. Asian J.* **2006**, *1*, 623.
- (144) Crudden, C. M.; Horton, J. H.; Ebralidze, I. I.; Zenkina, O. V.; McLean, A. B.; Drevniok, B.; AU - She, Z.; Kraatz, H.-B.; Mosey, N. J.; Seki, T.; Keske, E. C.; Leake, J. D.; Rousina-Webb, A.; Wu, G. Ultra stable self-assembled monolayers of N-heterocyclic carbenes on gold. *Nat. Chem.* **2014**, *6*, 409.
- (145) Hurst, E. C.; Wilson, K.; Fairlamb, I. J. S.; Chechik, V. N-Heterocyclic carbene coated metal nanoparticles. *New J. Chem.* **2009**, *33*, 1837.

- (146) Richter, C.; Schaepe, K.; Glorius, F.; Ravoo, B. J. Tailor-made N-heterocyclic carbenes for nanoparticle stabilization. *Chem. Commun.* **2014**, *50*, 3204.
- (147) Rodriguez-Castillo, M.; Laurencin, D.; Tielens, F.; van der Lee, A.; Clement, S.; Guari, Y.; Richeter, S. Reactivity of gold nanoparticles towards N-heterocyclic carbenes. *Dalton Trans.* **2014**, *43*, 5978.
- (148) Vignolle, J.; Tilley, T. D. N-Heterocyclic carbene-stabilized gold nanoparticles and their assembly into 3D superlattices. *Chem. Commun.* **2009**, 7230.
- (149) Lara, P.; Rivada-Wheelaghan, O.; Conejero, S.; Poteau, R.; Philippot, K.; Chaudret, B. Ruthenium Nanoparticles Stabilized by N-Heterocyclic Carbenes: Ligand Location and Influence on Reactivity. *Angew. Chem. Int. Ed.* **2011**, *50*, 12080.
- (150) Gonzalez-Galvez, D.; Lara, P.; Rivada-Wheelaghan, O.; Conejero, S.; Chaudret, B.; Philippot, K.; van Leeuwen, P. W. N. M. NHC-stabilized ruthenium nanoparticles as new catalysts for the hydrogenation of aromatics. *Catal. Sci. Tech.* **2013**, *3*, 99.
- (151) Baquero, E. A.; Tricard, S.; Flores, J. C.; de Jesús, E.; Chaudret, B. Highly Stable Water-Soluble Platinum Nanoparticles Stabilized by Hydrophilic N-Heterocyclic Carbenes. *Angew. Chem. Int. Ed.* **2014**, *53*, 13220.
- (152) Crespo, J.; Guari, Y.; Ibarra, A.; Larionova, J.; Lasanta, T.; Laurencin, D.; Lopez-de-Luzuriaga, J. M.; Monge, M.; Olmos, M. E.; Richeter, S. Ultrasmall NHC-coated gold nanoparticles obtained through solvent free thermolysis of organometallic Au(i) complexes. *Dalton Trans.* **2014**, *43*, 15713.
- (153) Serpell, C. J.; Cookson, J.; Thompson, A. L.; Brown, C. M.; Beer, P. D. Haloaurate and halopalladate imidazolium salts: structures, properties, and use as precursors for catalytic metal nanoparticles. *Dalton Trans.* **2013**, *42*, 1385.
- (154) Song, S. G.; Satheeshkumar, C.; Park, J.; Ahn, J.; Premkumar, T.; Lee, Y.; Song, C. N-Heterocyclic Carbene-Based Conducting Polymer–Gold Nanoparticle Hybrids and Their Catalytic Application. *Macromolecules* **2014**, *47*, 6566.
- (155) Ranganath, K. V. S.; Kloesges, J.; Schäfer, A. H.; Glorius, F. Asymmetric Nanocatalysis: N-Heterocyclic Carbenes as Chiral Modifiers of Fe₃O₄/Pd nanoparticles. *Angew. Chem. Int. Ed.* **2010**, *49*, 7786.
- (156) Feng, L.; Tianjun, L.; Li, W. In *7th Asian-Pacific Conference on Medical and Biological Engineering*; Peng, Y., Weng, X., Eds.; Springer Berlin Heidelberg 2008, *19*, 186.
- (157) De Jong, W. H.; Borm, P. J. A. Drug delivery and nanoparticles: Applications and hazards. *Int. J. Nanomed.* **2008**, *3*, 133.

- (158) Chen, S.; Murray, R. W. Arenethiolate Monolayer-Protected Gold Clusters. *Langmuir* **1999**, *15*, 682.
- (159) J. Zhong, C.; X. Zhang, W.; L. Leibowitz, F.; H. Eichelberger, H. Size and shape evolution of core-shell nanocrystals. *Chem. Commun.* **1999**, 1211.
- (160) Maye, M. M.; Zheng, W.; Leibowitz, F. L.; Ly, N. K.; Zhong, C.-J. Heating-Induced Evolution of Thiolate-Encapsulated Gold Nanoparticles: A Strategy for Size and Shape Manipulations. *Langmuir* **2000**, *16*, 490.
- (161) Maye, M. M.; Zhong, C.-J. Manipulating core-shell reactivities for processing nanoparticle sizes and shapes. *J. Mater. Chem.* **2000**, *10*, 1895.
- (162) Teranishi, T.; Hasegawa, S.; Shimizu, T.; Miyake, M. Heat-Induced Size Evolution of Gold Nanoparticles in the Solid State. *Adv. Mater.* **2001**, *13*, 1699.
- (163) Shimizu, T.; Teranishi, T.; Hasegawa, S.; Miyake, M. Size Evolution of Alkanethiol-Protected Gold Nanoparticles by Heat Treatment in the Solid State. *J. Phy. Chem. B* **2003**, *107*, 2719.
- (164) Isaacs, S. R.; Choo, H.; Ko, W.-B.; Shon, Y.-S. Chemical, Thermal, and Ultrasonic Stability of Hybrid Nanoparticles and Nanoparticle Multilayer Films. *Chem. Mater.* **2006**, *18*, 107.
- (165) Agasti, S. S.; You, C.-C.; Arumugam, P.; Rotello, V. M. Structural control of the monolayer stability of water-soluble gold nanoparticles. *J. Mater. Chem.* **2008**, *18*, 70.
- (166) Srisombat, L.-o.; Zhang, S.; Lee, T. R. Thermal Stability of Mono-, Bis-, and Tris-Chelating Alkanethiol Films Assembled on Gold Nanoparticles and Evaporated “Flat” Gold. *Langmuir* **2010**, *26*, 41.
- (167) Klecha, E.; Inger, D.; Walls, M.; Pileni, M. P. Immunity of Coated Self-Ordered Silver Nanocrystals: A New Intrinsic Property Due to the Nanocrystal Ordering. *Langmuir* **2009**, *25*, 2824.
- (168) Winkler, K.; Wojciechowski, T.; Liszewska, M.; Gorecka, E.; Fialkowski, M. Morphological changes of gold nanoparticles due to adsorption onto silicon substrate and oxygen plasma treatment. *RSC Advances* **2014**, *4*, 12729.
- (169) Templeton, A. C.; Hostetler, M. J.; Kraft, C. T.; Murray, R. W. Reactivity of Monolayer-Protected Gold Cluster Molecules: Steric Effects. *J. Am. Chem. Soc.* **1998**, *120*, 1906.
- (170) Weisbecker, C. S.; Merritt, M. V.; Whitesides, G. M. Molecular Self-Assembly of Aliphatic Thiols on Gold Colloids. *Langmuir* **1996**, *12*, 3763.

- (171) Paulini, R.; Frankamp, B. L.; Rotello, V. M. Effects of Branched Ligands on the Structure and Stability of Monolayers on Gold Nanoparticles. *Langmuir* **2002**, *18*, 2368.
- (172) Isaacs, S. R.; Cutler, E. C.; Park, J.-S.; Lee, T. R.; Shon, Y.-S. Synthesis of Tetraoctylammonium-Protected Gold Nanoparticles with Improved Stability. *Langmuir* **2005**, *21*, 5689.
- (173) Mei, B. C.; Oh, E.; Susumu, K.; Farrell, D.; Mountziaris, T. J.; Mattoussi, H. Effects of Ligand Coordination Number and Surface Curvature on the Stability of Gold Nanoparticles in Aqueous Solutions. *Langmuir* **2009**, *25*, 10604.
- (174) Murray, C. B.; Kagan, C. R.; Bawendi, M. G. Self-Organization of CdSe Nanocrystallites into Three-Dimensional Quantum Dot Superlattices. *Science* **1995**, *270*, 1335.
- (175) Stowell, C.; Korgel, B. A. Self-Assembled Honeycomb Networks of Gold Nanocrystals. *Nano Lett.* **2001**, *1*, 595.
- (176) Dabbousi, B. O.; Murray, C. B.; Rubner, M. F.; Bawendi, M. G. Langmuir-Blodgett Manipulation of Size-Selected CdSe Nanocrystallites. *Chem. Mater.* **1994**, *6*, 216.
- (177) Salzemann, C.; Zhai, W.; Goubet, N.; Pileni, M.-P. How to Tune the Au Internanocrystal Distance in Two-Dimensional Self-Ordered Superlattices. *J. Phy. Chem. Lett.* **2010**, *1*, 149.
- (178) Dong, A.; Ye, X.; Chen, J.; Murray, C. B. Two-Dimensional Binary and Ternary Nanocrystal Superlattices: The Case of Monolayers and Bilayers. *Nano Lett.* **2011**, *11*, 1804.
- (179) Shenton, W.; Pum, D.; Sleytr, U. B.; Mann, S. Synthesis of cadmium sulphide superlattices using self-assembled bacterial S-layers. *Nature* **1997**, *389*, 585.
- (180) Legrand, J.; Petit, C.; Pileni, M. P. Domain Shapes and Superlattices Made of 8 nm Cobalt Nanocrystals: Fabrication and Magnetic Properties. *J. Phy. Chem. B* **2001**, *105*, 5643.
- (181) Lisiecki, I.; Albouy, P. A.; Pileni, M. P. Face-Centered-Cubic “Supracrystals” of Cobalt Nanocrystals. *Adv. Mater.* **2003**, *15*, 712.
- (182) Peng, Z. A.; Peng, X. Mechanisms of the Shape Evolution of CdSe Nanocrystals. *J. Am. Chem. Soc.* **2001**, *123*, 1389.
- (183) Talapin, D. V.; Shevchenko, E. V.; Kornowski, A.; Gaponik, N.; Haase, M.; Rogach, A. L.; Weller, H. A New Approach to Crystallization of CdSe Nanoparticles into Ordered Three-Dimensional Superlattices. *Adv. Mater.* **2001**, *13*, 1868.
- (184) Dong, A.; Chen, J.; Vora, P. M.; Kikkawa, J. M.; Murray, C. B. Binary nanocrystal superlattice membranes self-assembled at the liquid-air interface. *Nature* **2010**, *466*, 474.

List of publications

The publications during this thesis

I. “Nanocrystals: Why Do Silver and Gold N-Heterocyclic Carbene Precursors Behave Differently?”, Ling, X.; Schaeffer, N.; Roland, S.; Pileni, M.-P., *Langmuir* **2013**, *29*, 12647.

II. “Supracrystals of N-Heterocyclic Carbene-Coated Au Nanocrystals”, Ling, X.; Roland, S.; Pileni, M.-P., *Chem. Mater.* **2014**, *27*, 414.

III. “Superior oxygen stability of N-Heterocyclic Carbene-coated Au Nanocrystals - Comparison with Thiol-coated Analogues”, Ling, X.; Schaeffer, N.; Roland, S.; Pileni, M.-P., submitted.